Mechanistic Aspects in the Self-Assembly of Coordination Polymers Based on Rigidity and Flexibility of the Linkers: Synthesis, Structural Characterization and Magnetic Properties

Thesis Submitted for the Degree of
DOCTOR OF PHILOSOPHY

By

Bharat Kumar Tripuramallu

School of Chemistry
University of Hyderabad
Hyderabad 500 046
INDIA

July 2012

Dedicated to

My Parents and Teachers.....

CONTENTS

Statement

I hereby declare that the matter embodied in the thesis is the result of investigation carried out by me in the School of Chemistry, University of Hyderabad, Hyderabad, India, under the supervision of **Prof. Samar K. Das**.

In keeping with the general practice of reporting scientific observations, due acknowledgements have been made wherever the work described is based on the findings of other investigators. Any omission, which might have occurred by oversight or error, is regretted.

Bharat Kumar Tripuramallu

University of Hyderabad

July, 2012

Prof. Samar Kumar Das, F.A.Sc
School of chemistry
University of Hyderabad
Gachibowli, Hyderabad-500046, India
Work: +91-40-23011007
Residence: +91-40-23010536
Fax: +91-40-2301246
E-mail: skdsc@uohyd.ernet.in
http://chemistry.uohyd.ernet.in/~skd/

CERTIFICATE

Certified that the work contained in the thesis entitled "**Mechanistic Aspects in the Self-Assembly of Coordination Polymers Based on Rigidity and Flexibility of the Linkers: Synthesis, Structural Characterization and Magnetic Properties"** has been carried out by **Mr. Bharat Kumar Tripuramallu** under my supervision and the same has not been submitted elsewhere for a degree.

Prof. Samar K. Das

(Supervisor)

Dean

School of Chemistry

Acknowledgements

I take the opportunity of placing on record, my deep appreciation for all who have been instrumental in shaping up my research efforts

To begin with I express my deep sense of gratitude and profound thanks to my mentor ***Prof. Samar K. Das*** *for his valuable guidance, patience, encouragement, and for the freedom he gave me in carrying out research. His constant encouragement and meticulous workaholism inspired me to tackle problems whenever I got stuck during research activities and primed me to complete my work successfully. Throughout my Ph.D tenure, he is always approachable, helpful, friendly and extremely tolerant. I consider my association with him as a cherishable memory in my life.*

I take this opportunity to thank Prof. M. V. Rajasekharan, Dean, School of Chemistry for providing us the facilities needed for our research. I extend my sincere thank to former Deans Prof. D. Basavaiah and Prof. M. Periasamy, and all the faculty members, School of Chemistry for their co-operation on various aspects.

I would like to thank Prof. S.N. Kaul and his research group especially, Mr. Yugandhar, Mr. Pawan, Mr. Umashankar, Mr. Ravi for their tireless efforts in recording the magnetic susceptibility measurements. I thank Prof. P. S. Mukherjee (IISC Bangalore) and his student Mr. Sandip Mukherjee for helping me in analyzing the magnetic data. I thank Prof. S. Mahapatra and his student Mr. Naga Prasad for theoretical studies. I take this opportunity to thank Prof. K. Vidyasagar (IIT Madras) for introducing me to the field of research.

It is great pleasure to thank my lab seniors Dr. V. Shivaiah, Dr. S. Supriya, Dr. V. Madhu, Dr. P. Raghavaiah, Dr. Arumuganathan, and Dr. Tanmay for their help, and cooperation during my Ph.D. tenure. I am grateful to my beloved seniors Dr. B. Ramababu garu for initiating and guiding my work, Dr. A Srinivasa rao garu and G.D.P garu for their generous love towards me. I wish to thank my batchmates kishore, monima and my juniors Mrs. Sridevi garu, Mr. Veeranna, Mr. Praveen, Mr. Krishna for creating cheerful work atmosphere. A special token of thank to my junior Ms. Paulami for her support from the last two years. I thank to project students Bhuveneshwari, Nagaraju, Sujatha, Dayakar, Sirisha, Ashwathy, Sreenivas(ugc) to work with me and helping to complete my thesis work. I further thanks to project students Shivaiah, Ashok, Siva, Dr. Pratap, Pal, Lavanya, Upama, Arti, Olivia, Shruthi, M. Raju and Dhanabal for their pleasant presence.

I take this opportunity to thank Prof. Anjali patel and her student Mr. Ketal patel from M.S. University of Baroda, Vadodhara for their kind companion.

I also thank all the non-teaching staff of the School of Chemistry for their assistance on various occasions. I thank DST funded National Single Crystal X-ray Diffraction Facility, UGC / UPE for providing the basic requirements and UGC for the financial support.

I would like to acknowledge Prof. A.V. Prasada Rao, Prof. GNR and Dr. Vani Madam, and all my teachers during my Post graduation at Andhra University, Visakhapatnam. I take this opportunity to thank my teachers from my childhood Angeliena miss, Bhargavi miss and Sundari madam at my school level and KMD sir at my graduation level for shaping me in the right direction.

'If one wants an accounting of one's worth, count his/her friends' I am indeed fortunate to have friends like Kishore(pilli), Jami, Raja, Kishore (Natudu) who have been good friends over the years, and make my moments with them as a bunch of joyful memories throughout my life. I also thank my M.Sc friends especially Kiran, Giri and kalyan for their warmth of friendship towards me. I thank Raghu, pandu, vijaywardhan, Srirammurthy, sudheer, goutham, Sarithi, Uday Bhaskar, Divya, Indira and Rajgopal for offering memorable moments to share with them.

A Special note of thank to my friends Chandu, Kasi, Sowjanya, Sharma and Nagendra who have been with me for a long period to cherish the valuable and blissful occasions of my teenage.

I would like to acknowledge the NRS hostelmates especially GK (King) for his pleasant company, Naveen, chairman (phalgun) making the hostel life more memorable. It is pleasure to thank some of my friends Subrata for pleasant companion, Suresh in euridite coaching, gouse, kiran, rambabu in my schooling, Prashanth, Swagathika, Adarsh in france trip, Sreedhar, Malli, Srikanth, kalyan in my graduation.

I am lucky enough to have the support of many School of Chemistry friends and colleagues, Satish anna, DK anna, Chaitanya, M. Ramu, Vikram, Dr. Phani Pavan, Anjaneyalu, Ram Suresh, Dr. Venu Srinivas, Sanjeev, Ravi, Santhosh(AS lab), Balu, Narayana, Chandrsekhar, Ajay, Sunny, Nagarjuna(VB lab), Srinivas (Allu) Gupta, Hari, Srinivas(LGP lab), Karunakar, Ramu Yadav, Mallesh, Bhanu, Shesu, Rama Krishna, Venu, Suresh, Madhu, Anish, Sekhar Reddy, Ganesh, Vigensh, Praveen, Dr. Arindam, Dr. Arun Babu, Malakappa, Swami, Nagaraju, Satish, Krishna Chary, Mehboob. Dr. Bhargavi, Dr. Jagadish anna, Dr.Bipul, Dr. Ranjith, Dr. Naba, Dr.Palash, Suryanarayana, Geetha, Rajesh, Ashok, Chandu, Dr. J. P. anna, Dr. Abijit, Dr. Rajesh, Balaswamy, Tirupathi Reddy, Pavan, Yaseen, Sasi, Dr. Bhuvan anna, Sajna, Ramesh, Gangadhar, Nagarjuna reddy, Vijji, Ramaraju, Ramesh, RamKumar, Dr. Ramesh Reddy anna, Dr. Sekhar Reddy, Satpal, Santosh(DB lab), Mallikarjun, Guru Braham, Dr. Satish, Rajgopal Jr. Dr. Ramkumar, Narayana, Rumpa, Vijendhra Reddy, Chary, Bharani, Shivaprasad, Srinivas Reddy, Ganesh, Srinivas(RB lab), Raveendra Babu, Vanaja, Naveen, Vikaranth, Sandip, Tradib, Obaiah, Satish (PKP), Basik, Pramithi exceptionally generous in helping me at various occasions.

Undoubtedly great pleasure of thank to my mother for her indeed confidence on me. The greatest debt I owe is to my father, sister, brother-in-law, kavya and yagnesh for lending me an emotional boost for this arduous task. I feel fortunate to have an imperative support from my brother Mr.Kiran kumar. It is gratitude of token to thank my uncles Mr. Siva Prasad, Mr. Satya Prasad for giving me moral support to my educational career.

In all reverence, I dedicate this work to the loving memory of my mother. A strict disciplinarian with a tender heart, an astute teacher and a conscientious worker ---- That's how I can best describe her. Her blessings have always steered me onto the right track following which here I am.

Aryan Bharat

University of Hyderabad

July, 2012

SYNOPSIS

The thesis work entitled with **"Mechanistic Aspects in the Self-Assembly of Coordination Polymers Based on Rigidity and Flexibility of the Linkers: Synthesis, Structural Characterization and Magnetic Properties",** consists of six chapters followed by concluding remarks and future scopes: (**1**) A general overview on metal-organic frameworks and coordination polymers: introduction and motivation of the present work, (**2**) Mechanistic aspects in the formation of copper dimer bridged by phosphonic acid and extending its dimensionality by organic and inorganic linkers: synthesis, structural characterization, magnetic properties and theoretical studies, **(3)** Synthesis, structural characterization and properties of one-dimensional coordination polymers of cobalt (II)- and nickel(II)-phosphonate complexes: influential role of secondary ligand and biphenyl spacer, **(4)** Hydrothermal synthesis and characterization of novel metal oxide materials: role of polyanion and tetrazole molecule in the self-assembly, **(5)** Factors affecting the conformational modulation of flexible ligands in the self assembly process of coordination polymers: synthesis, structural characterization, magnetic properties and theoretical studies, **(6)** Synthesis, structural characterization and magnetic properties of a series of coordination polymers: importance of linker coordination angle in tuning the dimensionality.

Apart from the first chapter (introduction), each chapter is subdivided into three parts: (a) Introduction (literature survey), (b) Experimental Section and (c) Results and Discussion. The compounds obtained in the present study are generally characterized by IR, TGA techniques followed by elemental analyses and unambiguously characterized by X-ray crystallography. Variable temperature magnetic susceptibility measurements are taken for the compounds where magnetic exchange phenomenon is prominent. Theoretical calculations have been performed to establish the experimental results.

Chapter 1

A general overview on metal-organic frameworks and coordination polymers: introduction and motivation of the present work

This chapter begins with more basic knowledge about metal-organic frameworks and coordination polymers (CPs). The research progress in the field of MOFs and Cps has been presented under three sections: (1) Rational applications in the field of gas storage, polymerization reactions, catalysis, sensors, magnetic materials and industrial applications has been discussed with brief examples (2) Various synthetic approaches in the preparation of MOFs and CPs have been presented from the past to modern days (3) The plausible mechanistic aspects in the self-assembly of the coordination architectures emphasizing the designing strategy with different examples has been briefed. Finally, the motivation to explore the role of flexible ligands in the self-assembly of the coordination architectures and the main objectives in the thesis are conversed shortly.

Chapter 2

Mechanistic aspects in the formation of copper dimer bridged by phosphonic acid and extending its dimensionality by organic and inorganic linkers: synthesis, structural characterization, magnetic properties and theoretical studies

Chapter **2** describes the mechanistic aspects in the formation of copper dimer bridged by phosphonic acid and extending its dimensionality by organic and inorganic linkers. Six new copper metal complexes with formulae $[Cu(H_2O)(2,2'\text{-bpy})(H_2L)]_2 \cdot H_4L \cdot 4H_2O$ (**1**), $[\{Cu(H_2O)(2,2'\text{-bpy})(H_3L)\}_2(H_2L)] \cdot 2H_2O$ (**2**), $[Cu(H_2O)(1,10\text{-phen})(H_2L)]_2 \cdot 6H_2O$ (**3**), $[Cu(2,2'\text{-bpy})(H_2L)]_n \cdot nH_2O$ (**4**), $[Cu(1,10\text{-phen})(H_2L)]_n \cdot 3nH_2O$ (**5**) and $[\{Cu(2,2'\text{-bpy})(MoO_3)\}_2(L)]_n \cdot 2nH_2O$ (**6**) have been synthesized starting from the copper salts, *p*-xylylenediphosphonic acid (H_4L) and 2,2′-bipyridine (2,2′-bpy) or 1,10-phenanthroline (1,10-phen) as secondary linkers and characterized by single crystal X-ray diffraction analysis, IR spectroscopy and Thermogravimetric (TG) analysis. All the complexes were synthesized by hydrothermal methods. A dinuclear motif (Cu- dimer) bridged by phosphonic acid represents a new class of simple building unit (SBU) in construction of coordination architectures in metal phosphonate

chemistry (Figure 1). The initial pH of the reaction mixture induced by the secondary linker plays an important role in the formation of the molecular phosphonates **1**, **2** and **3**.

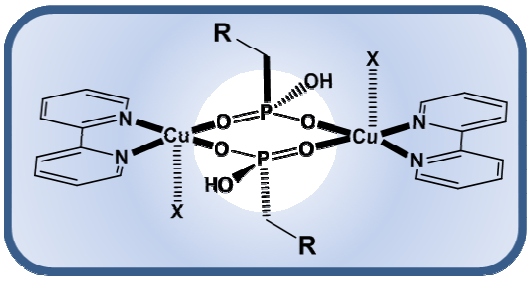

Figure 1. Schematic representation of the dinuclear motif Cu dimer bridged by phosphonic acid

Temperature dependent hydrothermal synthesis of the compounds **1**, **2** and **3** reveals the mechanism of the self-assembly of the compounds based on the solubility of the phosphonic acid H_4L. 2D coordination polymers **4**, **5** and **6**, that are formed by increasing the pH of the reaction mixture, comprise of Cu-dimers as nodes, organic (H_2L) and inorganic (Mo_4O_{12}) ligands as linkers (Figure 2). The void space-areas, created by the (4, 4) connected nets in compounds **4** and **5**, are occupied by lattice water molecules.

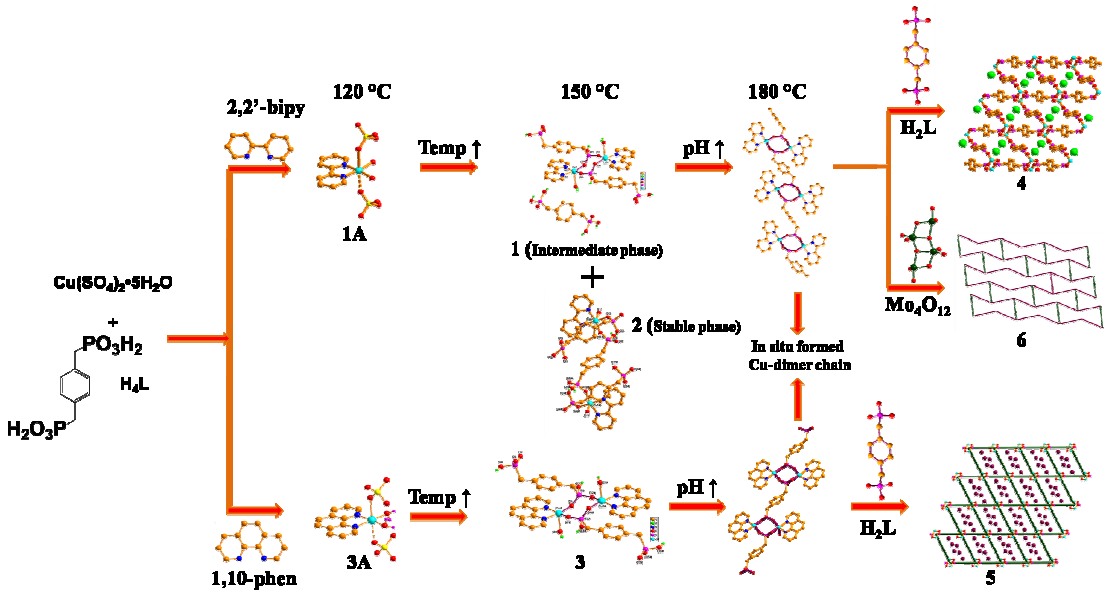

Figure 2. Mechanism of the formation of the compounds presented in the study

Thus compounds **4** and **5** have potential to accommodate guest species / molecules. Variable temperature magnetic studies of the compounds **3**, **4**, **5** and **6** reveal the antiferromagnetic

interactions between the two Cu(II) ions in the eight membered ring, observed in their crystal structures. A density functional theory (DFT) calculation correlates the conformation of the Cu-dimer ring with the magnitude of the exchange parameter based on the torsion angle of the conformation.

Chapter 3

Synthesis, structural characterization and properties of one-dimensional coordination polymers of cobalt (II)- and nickel(II)-phosphonate complexes: influential role of secondary ligand and biphenyl spacer

Chapter **3** describes the structural consequences in the metal phosphonate architectures by introducing secondary ligand, and explains the role of biphenyl spacer in modulating the dimensionalities. Two isomorphous cobalt and nickel phosphonates $[M^{II}(2,2´\text{-bipy})_2H_4pxp]_n[H_2pxp]_n$ M = Co (compound **1**), M = Ni (compound **2**) were synthesized from *p*-xylylenediphosphonic acid (H_4pxp) with 2,2´-bipyridine as secondary ligand component and the two other compounds [Co (2,2´-bipy) $(H_2dbp)]_n$ (**3**) and [Ni $(2,2´\text{-bipy})_2(H_2dbp)(H_2O)]\cdot H_2O$ (**4**) are synthesized from 4,4´-dimethylenebiphenyldiphosphonic acid (H_4dbp) with 2,2´-bipyridine as secondary ligand. All the compounds are characterized by routine elemental analyses, IR-, electronic-spectral analyses, thermogravimetric studies and unambiguously characterized by single crystal X-ray crystallography.

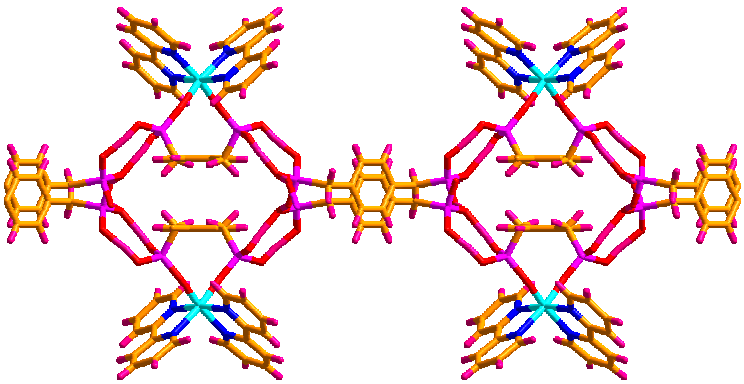

Figure 3. 2D supramolecular network formed due to hydrogen bonding between *cis* and *trans* conformations of the $H_x$pxp in compounds **1** and **2**

The crystal structure of compounds **1** and **2** consists of 1D $[M(2, 2´\text{-bipy})_2H_4pxp]^{2+}$ chains, and $[H_2pxp]^{2-}$ anions .The flexibility of non-rigid ligand *p*-xylylenediphosphonic acid (H_4pxp) tends

to adopt a rare *cis* conformation in the crystal structure to meet the coordination requirement of the metal centre from the usual *trans* conformation. The hydrogen bonding in the crystal structure leads to cylindrical tubes that extend *via p*-xylylenediphosphonic acid resulting in a 2D supramolecular sheet throughout the crystal (Figure 3). Compound **3** is a 1D extended coordination polymer constituted by the Co-dimer rings and H_2dbp ligands and **4** is a discrete molecular compound. A comparative study between the geometries of H_4dbp ligand and *p*-xylylenediphosphonic acid (H_4pxp) ligand demonstrate the effect of the twisting in the benzene rings in changing higher dimensional $H_x$pxp (x refers to number of protonated hydroxyl groups) compounds to lower dimensional $H_x$dbp compounds (Figure 4). The eight membered Co-dimer rings formed in compound **3** represents the simple and isolated Co-dimer, exhibiting weak antiferromagnetic exchange between metal centers through OPO bridges.

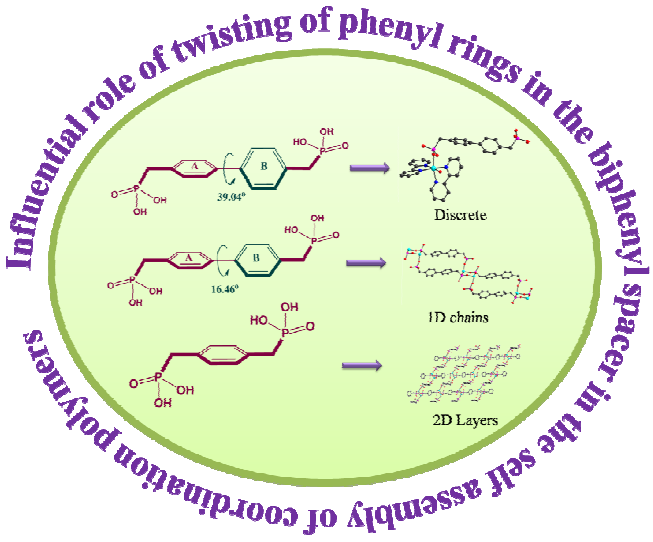

Figure 4. Figure demonstrating the influential role of biphenyl spacer in tuning the dimensionality.

Chapter 4

Hydrothermal synthesis and characterization of novel metal oxide materials: role of polyanion and tetrazole molecule in the self-assembly

Chapter 4 describes the synthesis and structural characterization of two different classes of metal oxide based materials based on metal organophosphonates and tetrazoles respectively.

In the first section two new metal organophosphonate oxide materials with formulae $[Cu^{II}_4Cu^{I}_2(L)_2(2,2'\text{-bpy})_6(HPW_{12}O_{40})]_n \cdot 4nH_2O$ (**1**) and $[Cu(2,2'\text{-bpy})VO_2(OH)(H_2L)]_n$ (**2**) have

been synthesized starting from the Cu(II) salts, 2,2′-bipyridine (2,2′-bpy), *p*-xylylenediphosphonic acid (H_4L), with sodium tungstate (for **1**) and ammonium metavanadate (for **2**) respectively. Compound **1** consists of 2D copper phosphonate layers connected by the polyanion keggin to form a 3D framework. The copper phosphonate layers in compound **1** are fabricated by the rare hexanuclear clusters in which the four terminal copper atoms form two eight membered Cu-dimer ($Cu_2P_2O_4$) rings (top and the bottom) that are connected to each other by the two central Cu atoms by a four membered Cu_2O_2 rings. These hexanuclear assemblies are connected to each other along the plane through the p-xylyl linkers to form a 2D layers. Compound **1** is a unique example in terms of existence of hexanuclear copper phosphonate cluster in the 3D coordination matrix. Compound **2** is a 2D structure in which the 1D $[Cu(2,2'\text{-}bpy)(H_2L)]_n$ chains are connected by the VO_2OH subunits to from a 2D layers. The formation of VO_2OH in compound **2** ceases the formation of eight membered Cu-dimer rings.

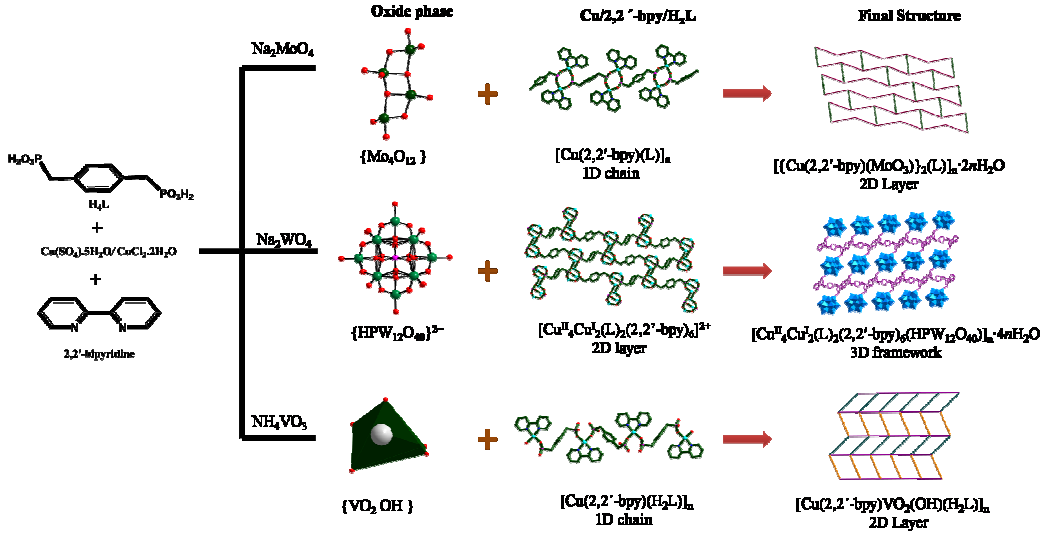

Figure 5. Schematic representation of the self-assembly of the metal oxide phases and metal organophosphonate phases

In the second section, the hydrothermal reaction of Cu(II) salt, ammonium heptamolybdate, and 4-ptz (5-(4-pyridyl) tetrazole) at different synthetic conditions yields two compounds $[Cu(4\text{-}Hptz)(Mo_2O_7)]$ (**3**) and $[Cu(4\text{-}Hptz)_2(H_2O)_3]_2[Mo_8O_{26}]$ (**4**). Compound **3** exhibits a 3D bimetallic oxide framework, constructed from the tetrazoles and $\{CuMo_2O_7\}$ oxide phase. The coordination ability of nitrogen atoms in the tetrazole ring makes the ring acting as a template in the formation of $\{Cu_4Mo_6O_{10}\}$ rings, made up of $[Mo_2O_7]^{2-}$ anions and Cu(II) octahedral; the

stacking of these $\{Cu_4Mo_6O_{10}\}$ rings along crystallographic *c* axis results in the formation of 3D bimetallic oxide framework. Compound **4** consists of infinite octamolybdate chains and Cu-tetrazolate complex cation. The present chapter discusses the self-assembly of metal oxide based materials with structure directing agents like metal organophosphonates and tetrazoles.

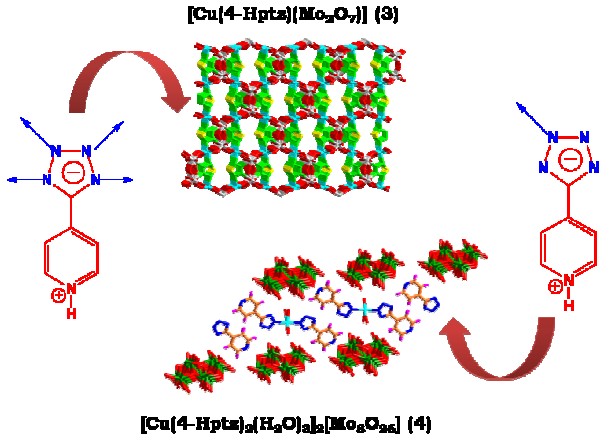

Figure 6. Assessing the influence of tetrazole molecule on the metal oxide based inorganic solids.

Chapter 5

Factors affecting the conformational modulation of flexible ligands in the self assembly process of coordination polymers: synthesis, structural characterization, magnetic properties and theoretical studies

In chapter 5, six new metal complexes with the formulae, $[Co(pda)(bix)]_n$(**1**), $[Ni(pda)(bix)(H_2O)]_n$ (**2**), $[Cu(pda)(bix)_2(H_2O)_2]_n \cdot 8nH_2O$ (**3**), $[Co_2(\mu\text{-}OH)(pda)(ptz)]_n \cdot nH_2O$ (**4**), $[Co(hfipbb)(bix)_{0.5}]_n$ (**5**), and $[Co(2,6\text{-}pydc)(bix)_{1.5}]_n \cdot 4nH_2O$ (**6**) have been synthesized by the reactions of Co(II) , Ni(II), and Cu(II) salts with two flexible ligands 1,4–phenylenediaceticacid (H_2pda), and 1,4-bis (imidazole-1-ylmethyl)-benzene (bix) in presence of co-ligands 5-(4-Pyridyl) tetrazole (4-ptz), 4,4′-(hexa-fluoroisopropylidene)bis(benzoicacid) (H_2hfipbb), and 2,6-pyridine dicarboxylic acid (2, 6–H_2pydc), and characterized by single crystal X-ray diffraction analysis, IR spectroscopy and thermogravimetric (TG) analysis. Because of the coordination geometry around the metal ions, and the diverse coordination modes of the flexible ligands in combination with the rigid and flexible co-ligands, the obtained complexes show diverse structures from one dimensional (1D) chain to three dimensional (3D) coordination

polymers. **1, 4, 5,** and **6** are Co(II) complexes in which Co(II) ions show tetrahedral coordination in **1,** trigonal bipyrimidal coordination in **4**, and octahedral coordination in **5** and **6.** Complexes **2** and **3** are respectively Ni(II) and Cu(II) complexes in which the metal ions present in octahedral coordination geometries. Factors affecting the conformational change of the flexible ligands in the self assembly process of coordination polymers, such as, coordination geometry around the metal ions, and geometry of the co-ligands have been systematically studied. The rotation of the bonds $C(sp^3)$—$C(sp^2)$ and $C(sp^3)$—$N(sp^3)$ in H_2pda and bix ligands causes different conformations (*cis, trans, gauche*); these conformations have been studied by measuring the torsion angle. A comparative study between the torsion angle of the particular conformation of the ligands and coordination geometry of metal ion/geometry of the co-ligand has been undertaken. All the possible *cis, trans,* and *gauche* conformations of the flexible ligands have been obtained / observed in our complexes. Theoretical calculations were performed to determine the energies of the different conformations of the flexible ligands. The electronic properties of these complexes have also been investigated in the solid state at room temperature. Finally the temperature dependent magnetic studies for compounds **4** and **5** are described.

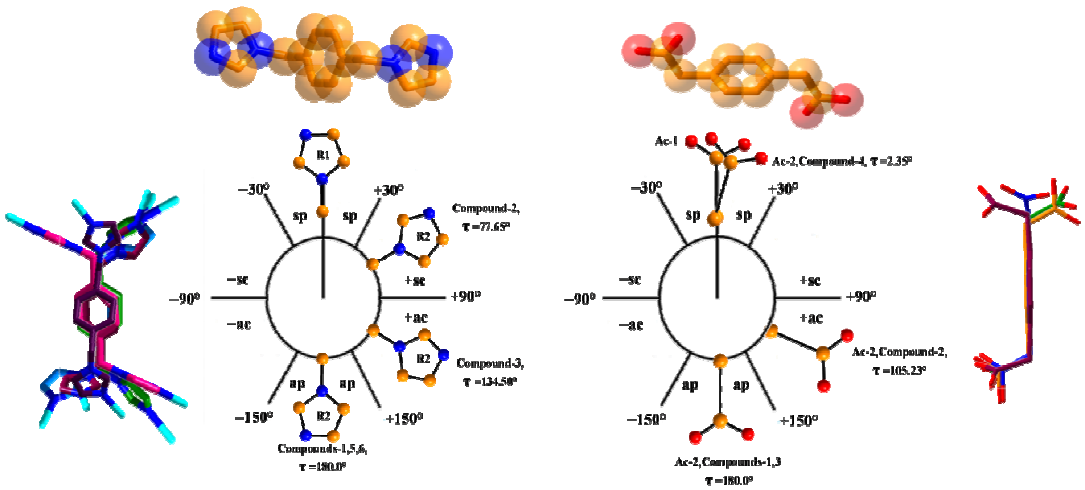

Figure 7. Figure illustrating the different conformations of the flexible ligands with the aid of torsion angle measurements.

Chapter 6

Synthesis, structural characterization and magnetic properties of a series of coordination polymers: importance of linker coordination angle in tuning the dimensionality

Chapter 6 describes the affect on the dimensionality of the mixed linker coordination networks by varying the linker coordination angles of the ligands. In this chapter, we have described six metal complexes $[Co(hfipbb)(1,2\text{-}bix)]_n$ (**1**), $[Co(hfipbb)(1,3\text{-}bix)_{0.5}]_n$ (**2**), $[Co(1,2\text{-}pda)(1,2\text{-}bix)]_n$ (**4**), $[Co_2(\mu\text{-}OH)(1,3\text{-}pda)(4\text{-}ptz)]_n$ (**7**) , $[Co(2\text{-}pztz)(1,4\text{-}pda)_2]_2[Co(H_2O)_6]\cdot 2nH_2O$ (**8**) and $[Mn(2\text{-}pztz)(1,4\text{-}pda)_2]_2[Mn(H_2O)_6]\cdot 2nH_2O$ (**9**) based on the flexible carboxylate ligands 1,2-phenylenediaceticacid (1,2-H_2pda), 1,3–phenylenediaceticacid (1,3-H_2pda), 4,4'(hexa-fluoroisopropylidene)bis(benzoicacid) (H_2hfipbb) and secondary N-donor ligands 1,3-bis (imidazole-1-ylmethyl)-benzene (1,3-bix), 1,2-bis (imidazole-1-ylmethyl)-benzene (1,2-bix), 5-(4-Pyridyl) tetrazole (4-ptz) and 2-(2H-tetrazol-5-yl)pyrazine (2-pztz). The positions of the coordinating groups in the linker are explained based on the linker coordination angles (LCA) as shown in Figure 8.

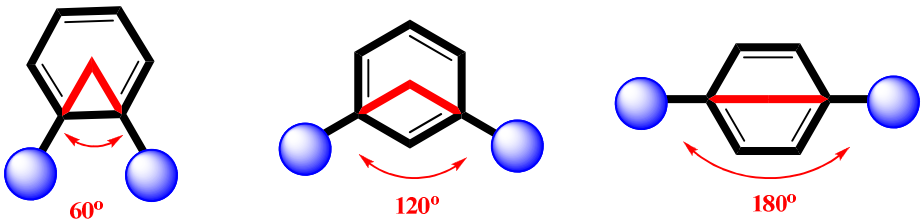

Figure 8. The possible linker coordination angles for the simple phenyl linker

Influential role of linker coordination angles in tuning the dimensionality of the coordination polymers based on flexible ligands have been systematically analyzed. A systematic comparison between the compounds **1**, **2**, **4** and **7**-**9** with the compounds described in the previous chapter $[Co(hfipbb)(1,4\text{-}bix)_{0.5}]_n$ $[Co(1,4\text{-}pda)(1,4\text{-}bix)]_n$ and $[Co_2(\mu\text{-}OH)(1,4\text{-}pda)(4\text{-}ptz)]_n\cdot nH_2O$ has been made to elucidate the role of LCA in tuning the dimensionality. Finally temperature dependent magnetic susceptibility measurements of compounds are described.

Introduction and Motivation of the Present Work: A General Overview on Metal–Organic Frameworks and Coordination Polymers

1

In the recent years, remarkable progress has made in the area of Metal-organic frameworks (MOFs) and coordination polymers (CPs). The synthesis and characterization of infinite one-, two- and three- dimensional networks have been an area of considerable interest. The key to this rapid growth of this research area is mainly due to tendency of these materials to meet the vast applications at the industrial level. This chapter gives a general view on the MOFs and CPs in terms of introduction, background, and research progress which deal with applications, synthetic procedures, and self-assembly process.

1.1. Introduction

Over the past two decades, much progress has been made in the development of organic-inorganic hybrid materials, namely, metal-organic materials (MOMs), metal-organic polyhedra (MOPs) and metal-organic frameworks (MOFs) or coordination polymers (CPs). These readily modular materials have introduced new possibilities in applications that have traditionally utilized the inorganic zeolites, e.g., in catalysis and separations,[1] in size- and shape-selective uptake[2] and gas storage[3] as well as novel applications.[4] MOMs have drawn considerable awareness because of the potential of exploiting properties of both organic and inorganic components within a single material, in addition to their modular nature and mild synthesis conditions.[5]

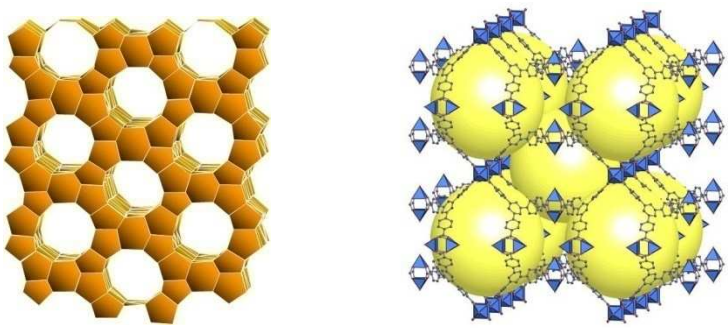

Figure 1.1. Topology of ZSM-5 structure (left) and MOF $Cu_3(BTB)_2(H_2O)_3 \cdot (DMF)_9(H_2O)_2$ (right)

Organic molecules offer tunable properties based on the shape (i.e., potential ligand coordination angles), size (i.e., expansion of a ligand) and functionality (i.e., decoration of a ligand). Inorganic elements provide the potential for similar properties to traditional zeolites, including thermal and mechanical stability, as well as many more optical,[6] and electronic properties.[7]

The attractive feature of these materials is the ability to target structures of particular topologies that may be desirable for certain applications by using the molecular building block (MBB) approach. This is a design strategy for the construction of solid-state materials, where the metal ions, coordination clusters, and organic ligands are pre-designed to have specific geometry and directionality upon coordination *in situ*.[8]

1.2. Background

MOMs have rich history, and there have been several efforts to design and synthesize functional porous structures containing compounds. Prior to the late 1980s, a variety of metal-organic coordination compounds were discovered (e.g., Werner complexes,[9] Hofmann clatharates,[10] Prussian blue[11]) and explored for their interesting properties including molecular inclusion and magnetism. Nevertheless, no systematic approach to the construction of this class of solid-state materials had been introduced until 1989. Hoskins and Robson proposed the design of open framework MOMs[12] based on a node-and-spacer approach, that is, tetrahedral nodes can be linked by linear molecular spacers to construct an open structure based on the extension of cubic diamond (assembly of the simple tetrahedral building blocks). Hoskin's and Robson's molecular node-and-spacer concept of design was realized in 1990 upon their synthesis of series of analogous MOFs with varied linkers and nodes (i.e., $Zn(CN)_2$, $Cd(CN)_2$, Cu^I[4,4′,4′′,4′′′-tetracyanotetraphenylmethane]$BF_4 \cdot x C_6H_5NO_2$ having skeletons that can be simplified as a net analogous to an extended cubic diamond lattice (*dia*).[13] In the latter, both the single-metal ion and central carbon of the ligand serve as the tetrahedral nodes or tetrahedral building units (TBUs) and the cyanophenyl moieties serve as the spacers.

1.3. Coordination Polymers versus Metal–Organic Frameworks.

The crystal engineering studies deal entirely with non-covalent interactions, such as hydrogen bonding interactions that have been termed as organic crystal engineering, while those with metal –coordination bonds have been called inorganic crystal engineering. The majority of the latter studies deals with the engineering of CPs or MOFs. Yet another term

hybrid inorganic and organic framework materials is also in use,[14] but this term was not so popular in terms of wider implications. Some other terminologies, which are popularized based on these materials, are metal organic materials (MOMs), Metal organic polyhedra (MOPs) etc., but most importantly, the CPs and MOFs are highly pronounced terms in inorganic crystal engineering.

The topic search using Sci-Finder Scholar for the term 'Coordination polymers' reveals that the term CP dates back to before 1950s, while the term MOFs dates to the late 1990s as shown in Table 1.1. The statistics clearly make known that the usage of these two terms has increased tremendously during the period 2001-2012 along with the expansion of the new areas of the research.

The term CP is defined in the Wikipedia[15] as "the term given in inorganic chemistry to a metal coordination compound where a ligand bridges between metal centers, where each metal centre binds to more than one ligand to create an infinite array of metal centers". The term "coordination polymer" was defined by J. C. Bailear in 1964, when he compared organic polymers with inorganic compounds that can be considered as polymeric species. In comparison, he established rules for the building and the required properties of new species involving metal ions and organic ligands.

Wikipedia defines MOFs as "crystalline compound consisting of metal ions or clusters coordinated to often rigid organic molecules to form one-, two-, or three-dimensional structures that can be porous". This definition seems to be very specific for crystallinity and dimensionality; the latter is restricted to only extend interactions through covalent or coordinate bonds and not to other nonbonding interactions.

Inorganic chemists probably prefer to use the term CPs, while solid-state chemists tend to prefer the term MOF. Multiple terminologies do exist in science and as long as we know the meaning of them, there should not be any confusion. Further, unanimous agreement will certainly eliminate confusion and frustration among the research community. The term coordination polymer very broadly encompasses all the extended structures based on metal ions linked into an infinite chain, sheet, or three-dimensional architecture by bridging ligands that usually contain carbon atom. Whereas the term MOF is very much appropriate to use for three-dimensional networks; it is inappropriate to use for extended one-dimensional or two-dimensional networks. Although the new terminologies, such as, porous coordination polymers (PCPs)[16] and metal-organic rotaxane frameworks

(MORFs)[17] have been introduced; they are primarily the extensions of the existing terminologies and add no confusion to the literature.

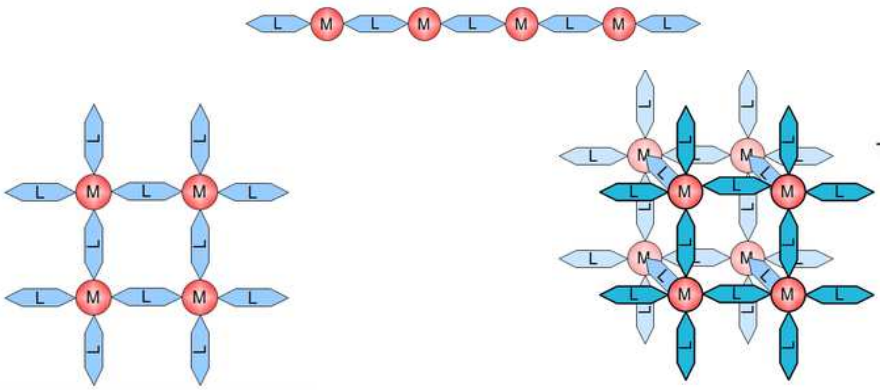

Scheme 1.1. An illustration of 1-, 2- and 3- dimensionality.

Table 1.1. Details of the Hits for CPs and MOFs in the literature using Sci-Finder Database search.[18]

Years	Coordination Polymers	Metal organic Frameworks
Up to 1950	1	0
1951-1960	12	0
1961-1970	174	0
1971-1980	129	1
1981-1990	154	3
1991-2000	531	39
2001-2010	5696	4127
2010-2012	1996	2337

1.4. Research Progress

The research in the MOFs and CPs is enormously growing in integrating all areas of science to meet the applications that are needed for the society. The challenge in this field is chemical and physical functionalization of these coordination architectures, through the porous properties of the frameworks. The current research in the field of MOFs and CPs triggers in designing a target structure with specific properties and functions which represent an eternal aspiration for materials scientists. In this aspect, as shown in the Figure 1.2, the major fields in the MOFs and CPs. where scientists progress, are mainly exploring the applications of the framework materials, developing the most reliable and

straight forward synthetic procedures and studying the mechanistic aspects of the self-assembly process to develop a thumb rules to obtain a desired topological frameworks containing materials.

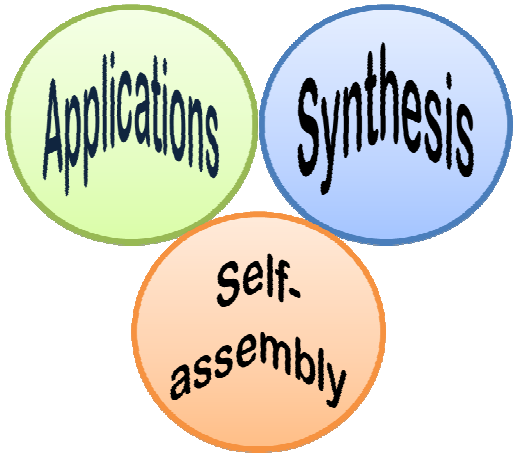

Figure 1.2. Figure showing the major areas of research in the field of MOFs and CPs.

1.4.1. Applications

1.4.1.1. Gas Storage

1.4.1.1.1. Hydrogen Storage

Decreasing stockpiles of fossil fuels and the increasing threat of global warming have prompted the global community to search for alternative energy carriers to supplement the currently used petroleum-based gasoline and diesel fuel in road vehicles such as automobiles, buses, and trucks. Among various alternatives, hydrogen stands at the forefront. Hydrogen is ubiquitous, and has an energy density much greater than gasoline and emits no carbon-dioxide after burning. On a weight basis, hydrogen has nearly three times higher energy content than gasoline: lower heating values are 33.3 kWh Kg^{-1} (123 MJ Kg^{-1}) for hydrogen and 11.1 kWh Kg^{-1} (47.2 MJ Kg^{-1}) for gasoline.

The successful commercialization of hydrogen fuel-cell powered vehicles, however, largely relies on the development of a safe, efficient, and economical on-board hydrogen storage system. To maintain a typical driving range of 300 miles, it is estimated that about 5 Kg of hydrogen would be needed. The U.S. Department of Energy (DOE) has set up the targets for on-board H_2 storage system with the concept that higher efficiency fuel-cell power sources will replace current carbon-based energy source in future vehicles. The year 2017 H_2 storage targets are 5.5 wt% in gravimetric capacity, 40 g L^{-1} of volumetric capacity at an operating temperature of −40 to −60 °C under a maximum

delivery pressure of 100 atm. The targets for complete system including all necessary components are set by the DOE.[19]

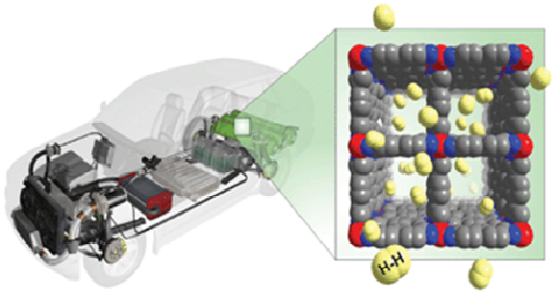

Storage Parameter	2005	2010	2015
Gravimetric Capacity (Specific energy)	1.5 kWh/kg 0.045 kg H_2/kg	2.0 kWh/kg 0.060 kg H_2/kg	3.0 kWh/kg 0.090 kg H_2/kg
System Weight:	*111 Kg*	*83 Kg*	*55.6 Kg*
Volumetric Capacity (Energy density)	1.2 kWh/L 0.036 kg H_2/L	1.5 kWh/L 0.045 kg H_2/L	2.7 kWh/L 0.081 kg H_2/L
System Volume:	*139 L*	*111 L*	*62 L*
Storage system cost	$6 /kWh	$4 /kWh	$2 /kWh
System Cost:	*$1000*	*$666*	*$333*
Refueling rate	.5 Kg H_2/min	1.5 Kg H_2/min	2.0 Kg H_2/min
Refueling Time:	*10 min*	*3.3 min*	*2.5 min*

Figure 1.3. Diagrammatic representation illustrating the usage of hydrogen filled cylinders in the automobiles and storage parameters issued by U. S DOE.

Table 1.2. Hydrogen storage capacities of some well known MOFs.[22a]

Material	**P(bar)**	**T(K)**	**Hydrogen storage capacity**	**Reference**
NU-100	70	77	164 mg g^{-1}	22b
	56	77	99.5 mg g^{-1}	
{[Zn_4O)T^2DC)($BTB)_{4/3}$]}	80	77	176 mg g^{-1}	22c
MOF-210	80	77	176 mg g^{-1}	22d
ZIF-8	30	77	3.3 wt %	22e
Co(BDP)·2DEF·H_2O	10	50	5.5 wt %	22f
	30	77	3.1 wt %	
$Mn_3[(Mn_4Cl)_3(BTT)_8(CH_3OH)_{10}]_2$	90	77	6.9 wt %	22g
MOF-177	70	77K	7.5 wt %	22h
MIL-101	80	77	6.1 wt %	22i

Porous MOFs or CPs have been recently deemed one of the most promising candidates to approach the DOE targets for on-board hydrogen storage, due to their high-specific surface areas, tunable pore sized, functionalizable pore wall and well defined framework-hydrogen interaction sites. Yaghi et al., reported the first measurements of hydrogen adsorption on an MOF: a remarkable 4.5 wt% at 77K and pressures less than 1 atm, and 1.0 wt % at room temperature at 20 bar on the material Zn_4O(bdc) (bdc= 1,4-benzenedicarboxylate) (also referred to as MOF-5 and IRMOF-1).[20] Later on, different materials have been reported with the increasing hydrogen adsorption capacities by

modifying the structural parameters.[21] The hydrogen adsorption capacities of some MOFs are shown in the Table 1.2.

1.4.1.1.2. Methane Storage

As with hydrogen, methane is considered as an ideal energy gas for future applications. Delivery of methane to the majority of homes and businesses in the United States and many other countries worldwide is already in progress. However, as in the case of hydrogen, current vehicles store the methane CNG (compressed natural gas) in high pressure tanks (greater than 200 atm), which are heavy and potentially explosive. To address the needs for methane storage technology, the U. S. DOE has set the targets for the methane storage systems at 180 V(STP)/ (STP equivalent of methane per volume of adsorbent material storage system).[23]

MOFs are a relatively newcomer to the field of methane adsorbants, while carbon materials have been extensively studied for methane storage since the early 1990s;[24] the first reported measurement of methane uptake by an MOF was demonstrated in 1991 by Kitagawa and coworkers.[25] The methane uptake of this pyrazine-based MOF was low, comparable to several zeolites.

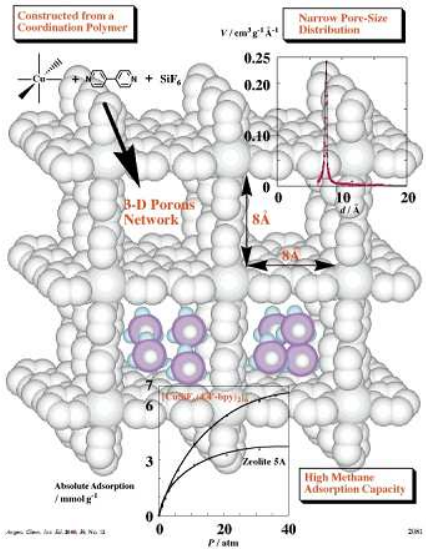

Figure 1.4. Figure representing the narrow pore-size distribution and high methane adsorption capacity coordination polymer reported by the kitagawa and coworkers.

A second MOF, reported by Kitagawa and coworkers in the next year, represented a serious effort in rationally synthesizing a material which would have a higher uptake of

methane; this material exceeded by nearly 100 % of the most adsorptive zeolites, zeolites 5A. The material IRMOF-6, constructed by the typical bdc ligand, was modified to generate 1,2-cyclobutane-3,6-benznedicarboxylate (Figure 1.4).[26] The resulting MOF was found to adsorb 155 v(STP)/ v methane at 298 K and 36 atm, which is considerably higher than any zeolites material or any other MOF at that time.

1.4.1.1.3. Carbon Dioxide capture

Carbon dioxide (CO_2) is a major green house gas that mainly contributes to the global warming causing climate changes, which is one of the greatest environmental challenges facing worldwide.[27] Human activities, mainly burning of fossil fuels are largely increasing the concentration of CO_2 in the atmosphere (Figure 1.5). Carbon capture and storage (CCS), where carbon dioxide is removed from industrial flue gases has attracted considerable attention as it is technologically feasible and could play a significant role in reducing green house gas emissions.[28] Separation of CO_2 from power plant flue gas containing water-saturated N_2 with some amount of O_2 and other gases is the key technical challenge. Currently, several methods like adsorption, amine scrubbing, and membrane separation are used in CCS technology to remove CO_2 from industrial flue gases.

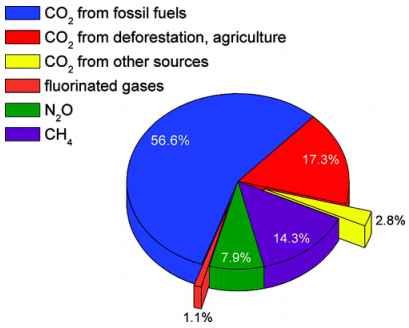

Figure.1.5. Global green house gas emission sources in 2004 of which approximately 77% are represented by CO_2 emissions.[29]

From the last two decades porous coordination polymers (PCPs) and metal-organic frameworks (MOFs) have been emerged as new type of porous materials and very promising candidates for CCS technology.[30] A large number of highly porous materials has been reported which can store a large amount of CO_2 and at the same time the separation of CO_2 from other gases viz. CO_2/N_2 (postcombustion), CO_2/H_2 (precombustion), CO_2/O_2 (air separation), and CO_2/CH_4 (natural gas purification), have high technological and industrial importance. Ghosh et al., reported a robust and water stable porous coordination polymer $[Cd\text{-}(NDC)_{0.5}(PCA)]\cdot G_x$ which has high selectivity in

uptake of CO_2 over the other gases (H_2, O_2, Ar, N_2,and CH_4).[31] Nevertheless, in the context of CO_2 capture, the ability to readily modify the surface chemistry of the MOFs of PCPs is of particular interest for installing the desired chemical features for enhancing the performance of the material. Such procedure has been demonstrated on the compounds IRMOF-3,[32] DMOF-1-NH_2,[33] UiO-66-Br,[34] MIL-101(Cr)[35] and the scope of reactions available is growing.

Table 1.3. CO_2 adsorption capacities of selected MOFs and CPs.

Material	Surface area (m^2/g) Langmuir	P(bar)	T(K)	Capacity (Wt%)	Ref.
MOF-210	10400	50	298	74.2	36a
Be-BTB	4400	40	313	58.5	36b
Mg-MOF	1733	1	298	27.5	36c
Co-MOF-74	1388	1	298	24.9	36d
SNU-5	2850	1	273	38.5	36e
Cu-EBTC	2844	1	273	25.9	36f

1.4.1.2. Polymerization reactions in porous coordination polymers

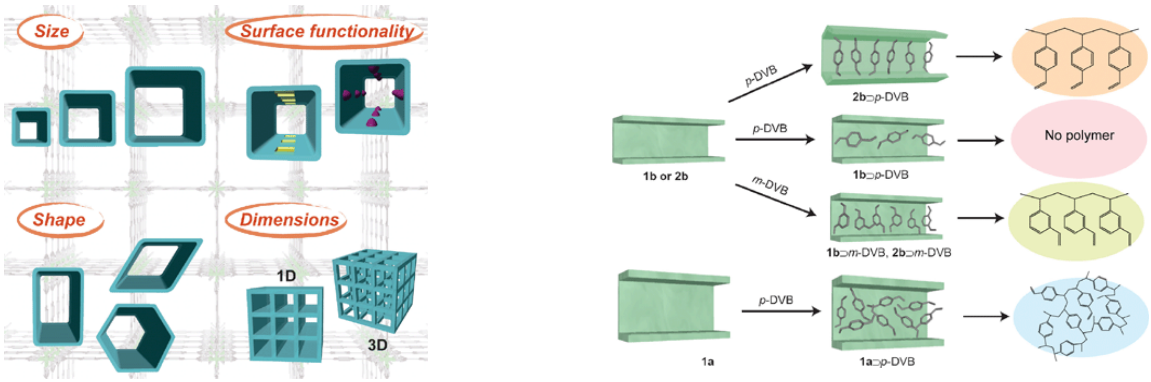

(a) **(b)**

Figure 1.6. (a) The designable channel features of PCPs from the view point of pore size, shape, dimensions and surface functionality, (b) schematic images for the inclusion and polymerization of DVBs in the coordination nanochannels.[37]

Compared to conventional porous coordination matrices, PCPs are of particular interest because of their designable framework structures; the size, shape, dimensions and surface functionality of the nano channels can be systematically tuned by changing the combination of organic ligands and metal ions.[38] The polymerization of monomer

encapsulated with in confined and designed nano spaces based on PCPs can lead to polymeric materials with desirable structures, which can be regarded as tailor-made polymerization systems.[39]

Kitagawa et al., reported the selective linear radical polymerization of DVBs (Divinyl-benzene) in the channels of $[M_2(1,4\text{-bdc})_2(ted)]_n$ (bdc = benzenedicarboxylate; ted = triethylenediamine; M =Zn^{2+} (1a), Cu^{2+} (1b)), which have regular and continuous one-dimensional nano-channels with a pore size of 7.8 X 7.8 $Å^2$ along their *c* axes.[40] The PCPs bearing active sites in or on nano channels have been used for fabricating π-conjugate polymers that show interesting optical and electrical properties. The regulated and tailor-made pore characteristics of PCPs play an important role for achieving unique polymer encapsulating systems.[41]

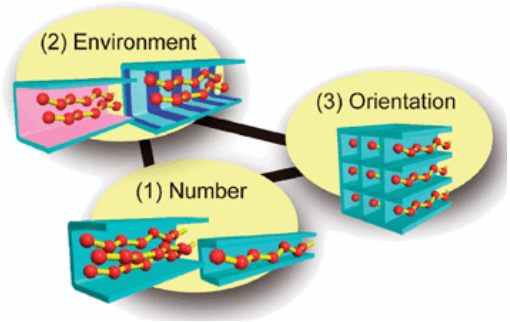

Figure 1.7. Precise control of polymer assemblies can be achieved in the designable nanochannels of PCPs.

1.4.1.3. Catalysis.

Heterogeneous catalysis was one of the earliest proposed applications of crystalline MOFs or PCPs, as well as one of the earliest demonstrated applications.[42] Although, the catalysis was proposed on these materials nearly 20 years ago and experimentally demonstrated 15 years ago, recently there has been extensive experimental exploration. Among the newly demonstrated concepts, important ones are: heterogenization of well defined homogeneous catalysts, framework-encapsulation of molecular catalysts,[43] coupling of catalysts to chemical seperations,[44] post synthesis incorporation of catalytic metal sites,[45] and substrate-size-selective catalysis.[46] In 1994, Fujita et al., first demonstrated the utility of crystalline porous coordination polymer as a heterogeneous Lewis acid catalyst which promoted the cyanosilylation of aldehydes with shape selectivity.[47] The acyl transfer reaction between *N*-acetylimidazole and various pyridyl carbinols has been propagated through the ZnPO-MOF, reported by the Shultz et al.[48] Various reactions catalyzed by MOFs are shown in Table 1.4.

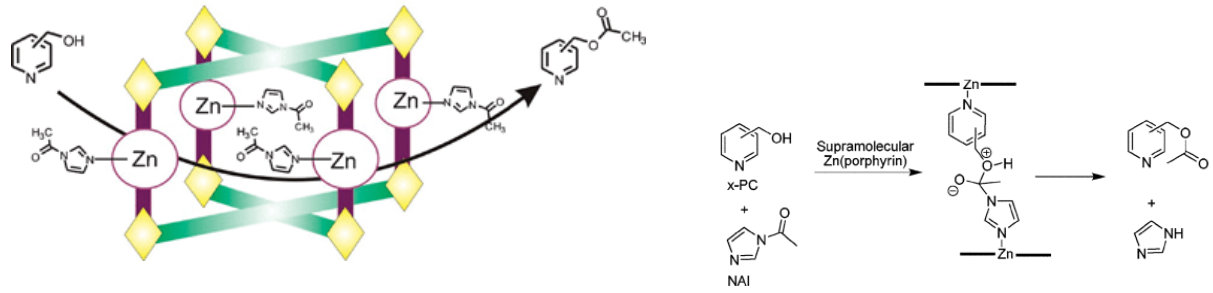

Figure 1.8. A schematic view showing a unit cell of ZnPO-MOF that effectively pre-concentrates and Lewis-acid activates *N*-acetylimidazole for catalytic acyl transfer to pyridyl carbinol species.[49]

Table 1.4. Catalogue of known catalytic MOFs and summary of reactions catalyzed.

Material	Substrate(s)	Reactions Catalyzed	Ref.
$[Cd(4\text{-btapa})_2(NO_3)_2]$	Benzaldehyde and malononitrile	Knoevenagel condensation	50a
$[Zn_4O(bdc)_3]$	tert-Butylchloride and toluene	Friedel–Crafts alkylation	50b
$[Cu(L2)_2(H_2O)_2]$	Linear and cyclic olefine	Epoxidation of olefine	50c
$[Cr_3F(H_2O)_2O(bdc)_3]$	Iodobenzene and acrylic acid	Heck coupling	50d
$[In_{48}(HImDC)_{96}]$	Cyclohexane	Oxidation of alkane	50e
$[Mn_3((Mn_4Cl)_3BTT_8(CH_3OH)_{10})]_2$	Benzaldehyde and methyltrimethylsilyldimethyl ketene acetal	Mukaiyama-aldol	50f
$[Cu(SO_4)(pbbm)]$	2,6-Dimethylphenol	Oxidative self -coupling	50g
$[Pd(2\text{-pymo})_2]$	Cinnamyl alcohol	Suzuki–Miyauracoupling	50h

Asymmetric Catalysis

The most remarkable development in the field of MOFs or PCPs is the development of asymmetric catalysis in an enantioselective manner. In the year 2000, Kim and co-workers reported the first homochiral MOF, POST-1 exhibiting catalytic activity for an asymmetric chemical reaction.[51] This seminal work triggered interests in rational design of chiral ligands and homochiral metal-organic systems for heterogeneous asymmetric catalysis.

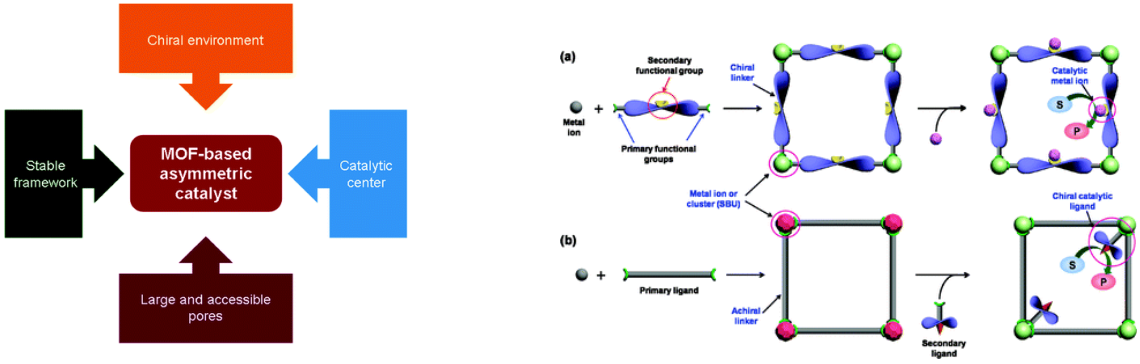

(a) (b)

Figure 1.9. (a) General requirements for MOF-based asymmetric catalysts (b) Representative strategies to construct of MOF-based asymmetric catalysts.[52]

Table 1.5. List of Chiral MOF-Based Asymmetric Catalysts

Catalytic MOF	Catalytic Reaction	Conversion (%)	ee(%)	Ref.
$[Sm(L_1{-}H_2)(L_1{-}H_3)(H_2O)_4]{\cdot}xH_2O$	Cyanosilylation of aldehydes	55-69	<5	53a
$Zn_3(ChirBTB\text{-}1)_2$	Mukaiyama aldol reaction	22-83	0-40	53b
$[Zn_2(bpdc)_2(L_{24})]{\cdot}10DMF{\cdot}8H_2O$	epoxidation	71	82	53c
Ce-MDIP-1	Cyanosilylation of aldehydes	>95	91-98	53d
$[Cu_2(L_{34})_2Cl_2]{\cdot}H_2O$	1,2-addition of α,β-unsaturated ketones	88-98	55-99	53e

1.4.1.4. Magnetism

One of the main attributes of MOFs or PCPs is magnetism.[54] It can be implemented by incorporating magnetic moment carriers such as paramagnetic metals or open-shell organic ligands or both.[55] The ligands, used in the development of magnetic MOF, are usually those having oxygen / oxide (rarely found for cobalt), water, hydroxide, alkoxide, alcohol and carboxylate or nitrogen (amine, pyridine, azide and azole) coordinating atoms and in few cases, sulfur (thiolate). The magnetic properties of MOFs have been generally explored and they illustrate the potential of producing magnets of many different long range ordered ground states, ferromagnet, ferrimagnet, antiferromagnet, canted antiferromagnet and most unusual metamagnets in addition to short-range ordered states, single-molecule magnets and single-chain magnets.

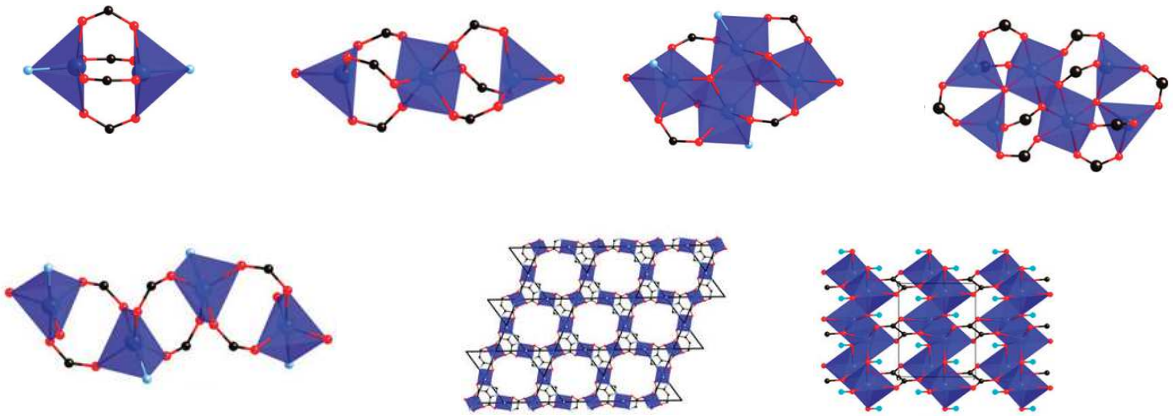

Figure 1.10. Structures of some magnetic SBUs observed in the MOFs: Dimer, Trimer, Tetramer, Hexamer, 1D chain, 2D layer, 3D framework (Top left to bottom right).[56]

1.4.1.5. Sensors

Recently several investigators have begun exploring the potential of MOFs and PCPs as chemical sensors,[57] although yet to be systematically exploited. The exceptional tunability of MOF structures and properties should constitute an important advantage over other candidate classes of chemo-sensory materials. Important elements to consider in optimizing the performance and utility of chemical sensors are sensitivity, selectivity, response time, materials stability, and reusability. The source of selectivity is chemically specific interactions of the adsorbate with the internal surface of the frameworks. For example, Zn(bptc) (bptc=4,4′-bipyridine-2,6,2′,6′ tetracarboxylate) was shown to preferentially adsorb polar molecules and those with conjugated π systems. These interactions were attributed to H-bond and π-π interactions, respectively, between the guests and MOF struts.[58] Lu et al. synthesized a copper MOF containing the ligand 3,6-di(pyridin-4-yl)-1,2,4,5-tetrazine (dptz), which shows solvatochromic behavior when immersed in solvents ranging in polarity from water to chloroform (shown in Figure 1.11).[59] Overall, the material shows a negative solvatochromic effect with the absorption band blue-shifting with increasing solvent polarity. Two distinct groupings were observed, one for hydroxylic and one for nonhydroxylic solvents, when the measured band gaps were plotted versus solvent polarity. Xie et al., incorporated phosphorescent complexes of iridium(III) into a MOF as struts and showed that emission is quenched by energy transfer to O_2.[60] The responsiveness of the porous material to dioxygen, and its absence of sensitivity to dinitrogen, is a consequence of the triplet electronic configuration of ground-state O_2 (versus singlet configurations for most other molecules).

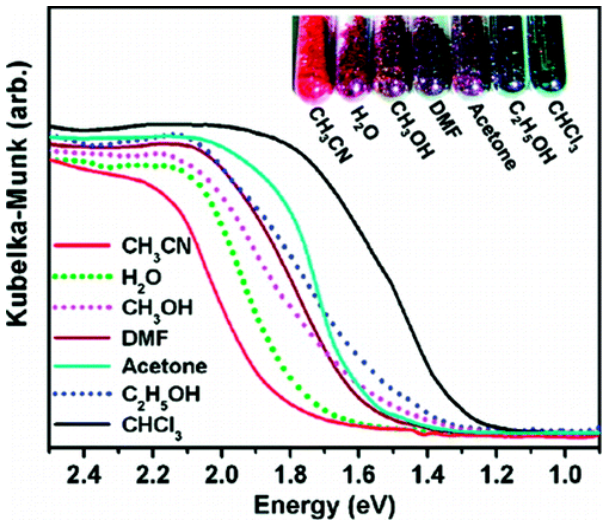

Figure 1.11. Visible spectra and photograph of MOF crystals containing solvents (condensed vapors). A negative vapochromic effect is observed for both hydroxylic and nonhydroxylic vapors (solvents).

Recently, Lan and co-workers have reported two fluorescent Zn-based MOFs capable of sensing nitro-containing molecules relevant to detection of explosives.[61] MOF sensors have shown excellent potential for detecting a range of organic molecules and ions (as well as detecting radiation), but there is much room for improvement. Literature reports are dominated by studies of luminescent MOFs fabricated by traditional methods.

1.4.1.6. Industrial Applications

The generation of MOFs and CPs enables the tailoring of novel solids with regular porosity from the micro to nanopore scale. Since the discovery of this new family of nanoporous materials and the concept of so called 'reticular design', nowadays several hundred different types of MOFs and CPs are known.[62] The self assembly of metal ions, which act as coordination centers, linked together with a variety of polyatomic organic bridging ligands, results in tailored nanoporous host materials as robust solids with high thermal and mechanical stability. The driving research in the field of MOFs and CPs turned to new dimensions in preparing these materials in the industrial scale, which discover the real industrial applications such as, removal of impurities in natural gas, pressure swing separation of rare gases, and storage of the gases.[63]

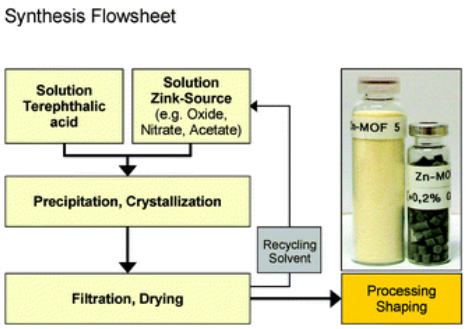

Figure 1.12. Principle flowsheet scheme of industrial MOF synthesis procedure. Cost efficiency and sustainability requires solvent recycling and zinc oxide rather than zinc nitrate.

Cu-BTC-MOF was used in the removal of sulfur odorant components from natural gas. In a fixed bed reactor vessel (inner diameter of 10 mm) about 10 g of granular Cu-MOF of a particle size fraction of 1–2 mm were thoroughly packed. At a temperature of 25 °C a gas stream of methane odorized with 13 ppm of tetrahydrothiophene (THT) was fed over the packing and analyzed in the reactor effluent by means of gas chromatography until breakthrough occurred. Taking the breakthrough curve of tetrahydrothiophene as depicted in Fig. 1.13, it can be clearly seen that the sulfur odorant is completely omitted from the natural gas in the effluent and even detection by smelling is not any longer indicative. The analysis of the used Cu-MOF after the test cycle reveals an volume specific uptake of 70 g THT L^{-1}_{MOF} which is considerably higher than 0.5 g THT L^{-1} for Norit-carbon or 6.5 g THT L^{-1} for the CarboTech sample.Interestingly, the colour of the Cu-MOF had changed from a deep blue into a light greenish one.[64]

Thus, storage of a gas in MOF-filled canisters can be used either way to enhance capacity in a given volume or to transport an equivalent amount of gas at a far lower pressure. Similarly, other gases like methane and hydrocarbons can be held at a denser state in the same manner.[66] The same finding holds for propane also. Fig. 1.13b depicts the curves for shaped MOF-5 pellets in gas containers over non-filled containers. The non-MOF-filled container represents the almost linear uptake behaviour, whereas the MOF-filled container is far higher and with a steeper increase at the beginning. Taking the pressure at about 10 bar it becomes clear that one MOF-filled container substitutes the amount of three state-of-art pressurized cylinders.[65]

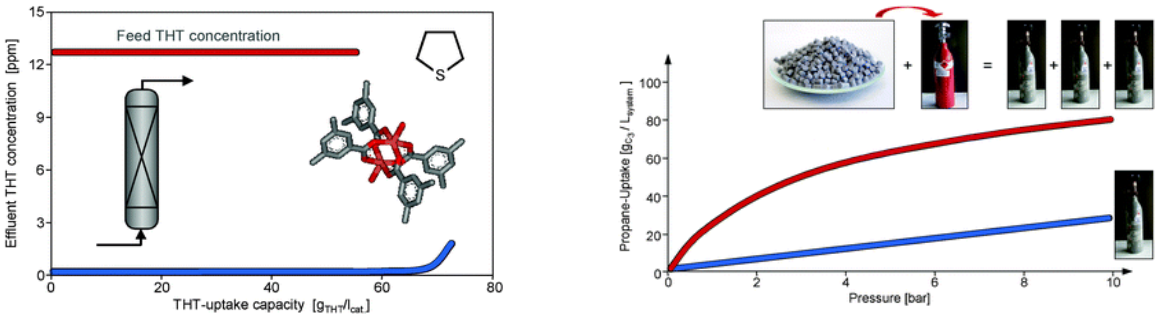

(a) **(b)**

Figure 1.13. (a) Breakthrough-curve of continuous tetrahydrothiophene-removal from natural gas using Cu-BTC-MOF out of electrochemical synthesis, (b) Compression of propane into gas container with and without MOF-filling (MOF-5 tablets in lecture bottles, room temperature).[65]

1.4.2. Synthesis

Synthetic methods used for the preparation of MOFs have been developed in three stages. At first, it is based on on slow evaporation of the solvents or their diffusion over time to create large single crystals in very small quantities over periods from weeks to months. Later, solvothermal approaches, borrowed from conventional zeolite synthesis, start to be implemented, allowing reaction times to be reduced to a few days.[67] Although microcrystalline powders are usually obtained under these conditions, the method can be finely tuned so as to lead to the isolation of single crystals. The present task facing crystal engineers is to reduce reaction times further to increase yields and produce functional materials in large amounts. Current research is mainly driven by the desire to develop industrial applications of MOFs as functional devices. In this context different methods, applied for synthesis of coordination architectures in the modern days, are discussed below.

1.4.2.1. Solvothermal Synthesis

In the 1940s, Barrer[68a] and Milton[68b] hydrothermally synthesized the first zeolites. Synthetic hydrothermal zeolite formation involves mixing the reagents, usually the tetrahedral atom source or sources, an organic structure-directing agent (SDA, often called the template), a mineralizer, and the solvent. The mixture is then heated (<220 °C) in a polytetrafluoroethylene (PTFE)-lined steel autoclave at high autogeneous pressure for a period of time. Hydrothermal or, more generally, solvothermal techniques involve heating a reaction mixture in a sealed vessel such that reaction temperatures greater than the boiling point of the solvent can be reached (typically between 100 and 250 °C in

hydrothermal chemistry), typically under autogenous pressure. The superheated solvents exhibit

(i) reduced viscosity (and therefore enhanced diffusion of chemical species) and

(ii) very different solubilizing properties (e.g. the dielectric constant of water decreases rapidly with increasing temperature)[7] compared to ambient conditions.

These factors can lead to very different chemistry. For example, (ii) it can lead to otherwise insoluble reagents being solubilised (which can be exploited to overcome solubility differences between metal salts and ligands), and (i) it can lead to enhanced crystal growth from reaction solutions. Furthermore, the temperature regime available in solvothermal techniques which is in intermediate between low-temperature solution chemistry and high-temperature solid-state chemistry, can favor the formation of metastable kinetic products rather than the thermodynamic products (e.g. metal oxides) favored at higher temperatures. All these features of hydrothermal chemistry have long been exploited in materials chemistry, e.g. in the preparation of zeolites, and there are several excellent reviews in this area.[69] These techniques have been employed extensively in the synthesis of coordination polymers (or metal-organic frameworks),[70] including magnetic materials.[71]

1.4.2.2. Ionothermal

Ionothermal synthesis, the use of ionic liquids as both solvent and template (structure-directing agent), has been used to prepare zeolites and inorganic–organic hybrids such as metal–organic frameworks. Ionic liquids[72] are a class of organic solvents with high polarity and a pre-organized solvent structure. Room-temperature (or near-room-temperature) ionic liquids are classically defined as liquids at ambient temperatures (or <100 °C) that consist only of ions.[73] They have excellent solvating properties, little measurable vapor pressure, and high thermal stability. In the area of materials science, there have been several reports of ionic liquids being used as solvents with very little or controlled amounts of water involved in the synthesis.[74]

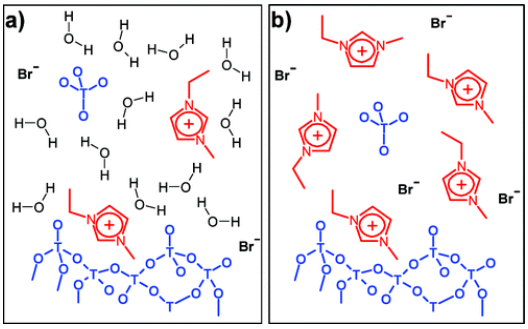

Figure 1.14. Schematic comparison between (a) hydrothermal and (b) ionothermal synthesis.

In panel (a) interactions between the excess solvent (water) and the template or framework dominate, while in panel b, the template–framework interactions dominate.[75] The first organic–inorganic hybrid material synthesized ionothermally by using $BMImBF_4$ as the solvent to synthesize $Cu(bpp)BF_4$ [bpp = 1,3-bis(4-pyridyl)propane].[76] The BF_4^- anions were incorporated into the extended one-dimensional coordination polymer as charge-compensating species, and the $BMIm^+$ remained in solution. The first three-dimensional MOF organic–inorganic hybrid material was synthesized with the same ionic liquid as the solvent and provider of the charge-compensating species, BF_4^-. The structure of $Cu_3(tpt)_4(BF_4)_3 \cdot (tpt)_{2/3} \cdot 5H_2O$ [tpt = 2,4,6-tris(4-pyridyl)-1,3,5-triazine] has large channels (~5 Å in diameter) which are filled with non coordinating free tpt, H_2O, and BF_4^-.[77] In contrast to the previously mentioned examples of organic–inorganic hybrids, synthesized in ionic liquids, these examples incorporate the ionic liquid cation as the SDA and charge-balancing species. Recently, it has been shown that the use of a chiral ionic liquid can induce chirality in the resulting solid (in this case, a coordination polymer), opening a great many possibilities in this area.[78]

1.4.2.3. Mechanochemical

Mechanochemistry can be as simple as grinding two reactants in a pestle and mortar, and this technique has been employed by several groups to demonstrate solvent-free synthesis of metal complexes.[79] Ball mills, however, have the advantage of requiring no physical effort, supplying greater power and being programmable, allowing more systematic studies of the process. The kinetic energy, supplied during grinding can have several effects on a crystalline solid[80] including: heating, reduction of particle size (with concomitant increase in surface area and the generation of fresh surfaces), formation of defects and dislocations in crystal lattices, local melting and even phase changes to

alternative polymorphs. Collisions between crystals during grinding can also lead to local deformations and potentially melting. Different methods in the mechanochemical synthesis involves neat grinding, grinding-annealing, liquid assisted grinding and kneading etc.

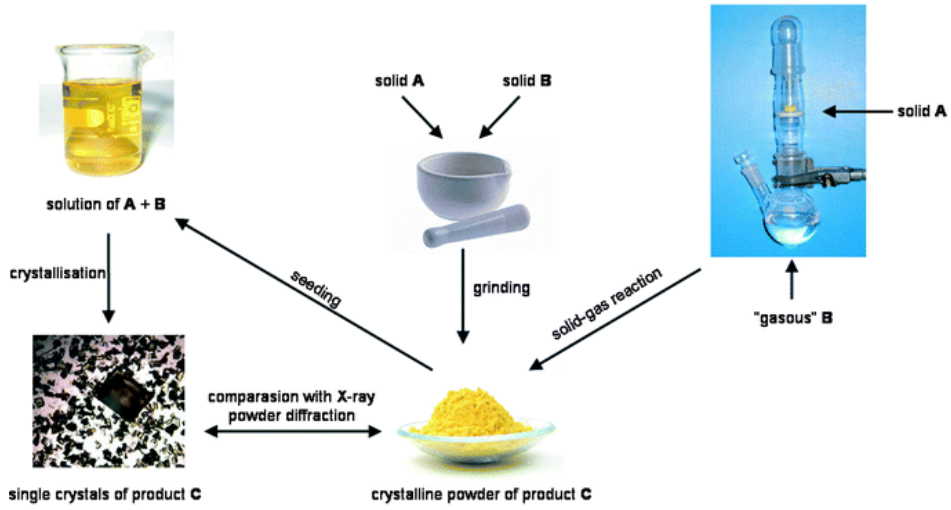

Figure 1.15. The solid–gas (right) and solid–solid (middle) processes and the strategy to obtain single crystals by recrystallization of the solid reaction product in the presence of seeds (left) of the desired crystals.

Furthermore solvent-free reactions often lead to very pure products and reduce the formation of solvate species and may thus be exploited in the quest for elusive crystal polymorphs.[81] These might be useful notions for crystal engineers and solid-state chemists.

1.4.2.4. Microwave-assisted Synthesis

Synthesis of MOFs proceeds *via* the self-assembly of primary building units through a self-recognition process. The vast majority of reported structures have been prepared by solvothermal synthesis which usually requires long reaction times (days to weeks), bulky equipment and heavy energy consumption. To overcome these limitations, new approaches have been developed, such as electrochemical essays[82] and solvothermal synthesis with immiscible solvents .[83] An even more promising route involves microwave-assisted synthesis.

Microwaves are normally generated by a magnetron, consisting of an oscillator converting high-voltage direct current into high-frequency radiation. In a typical laboratory instrument, waveguides transfer the generated energy from the magnetron to the sample

chamber (Fig. 1 – *left*). Many molecules, notably water, possess dielectric moments and rotate to align themselves with the alternating electric field of the microwaves. The heat generated by the molecular movement is dispersed as the molecules collide with other molecules. The sample chamber is a Faraday cage which prevents the microwaves escaping into the environment. The main advantage of microwave heating is its energy efficiency because power is only applied within the reactive mixture. Energy is generated directly throughout the bulk of the material instead of by conduction from the external surface (Fig. 1 – *right*). Microwave heating is almost instantaneous, takes place without heating the air or the container, and allows the use of temperatures above the boiling point of a solvent within pressurized vessels.[84] The heating is specific, with different materials responding differently to microwave energy. For example, pharmaceuticals can be sterilised without damaging the packaging.

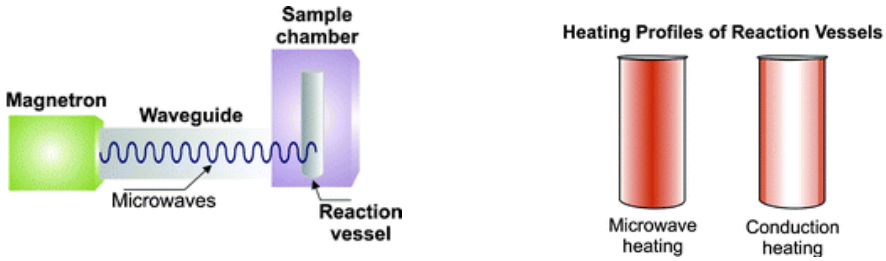

Figure 1.16. (left) Schematic representation of the basic components of a monomode microwave oven designed for scientific research. (right), comparison of heating profiles inside the reaction vessels for standard conductive and microwave heating.

The use of microwave assisted synthesis in the preparation of MOFs is still in its infancy; several interesting reports are available.[86] Microwave heating allows a considerable reduction of the reaction time,[87] enables phase selectivity[18] and the control of crystal morphology.[88]

Table 1.6. Reaction conditions for selected microwave-assisted syntheses of MOFs.

MOFs	Reaction conditions	Ref.
IRMOF1, IRMOF2, IRMOF3	25 s	**85a**
$[Ni_{20}(C_5H_6O_4)_{20}(H_2O)_8]\cdot 40H_2O$	150–220 °C within 1 min	**85b**
$[Mn_3(BTC)_2(H_2O)]_6$	120 °C, 10 min	**85c**
MOF-5	95–135 °C, 10–60 min	**85d**
$[Co_3(NDC)_3(DMF)_4]$	110 °C, 30 min	**85e**
Cr-MIL-101	210 °C, 1–40 min	**85f**
$[Cd(HIDC)(bbi)_{0.5}]$	2.0 Mpa, 20 min	**85g**
$[Zn_2(NDC)_2(DPNI)]$	120 °C, 1 h	**85h**

1.4.2.5. Post synthetic Modifications

The key limitation in the development of functional MOFs lies with the introduction of functionality, whilst maintaining the same ability to design and assemble overall framework without unfavorable effects from the presence of the "functional" components. Therefore two possible approaches involve (a) the self assembly of the MOF with the functionality already present, and (b) the postsynthetic modification of the MOF after self-assembly. In the latter approach, Gamez et al. have recently reported[89] the crystallographic observation of MOF-based postsynthetic covalent modification inside the pores of a new MOF, in which the amino functional groups oriented inside the pores have been covalently functionalized by reaction with other organic molecules in the cavities without modifying the original three-dimensional framework.

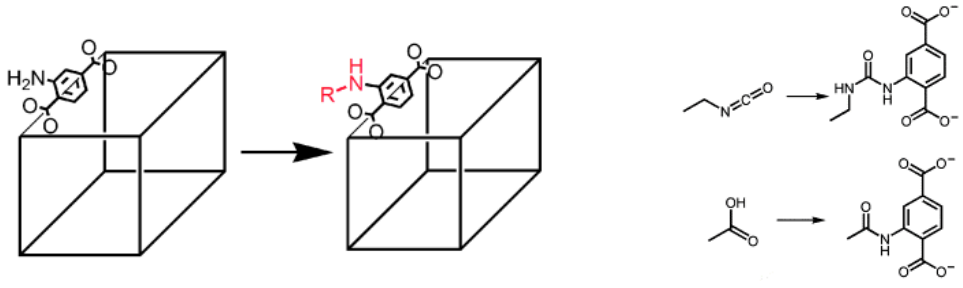

Figure 1.17. Schematic representation of postsynthetic modification.

It should be noted that chemical modification of MOFs in the porous channels was first reported in 2000 by Kim et al.,[90] in which the *N*-alkylation of all of the pyridyl groups in

the MOFs occurred by adding an excess amount of iodomethane to a suspension of crystalline porous MOF material at room temperature. The pore size was also modulated after *N*-alkylation of the pyridyl groups, with the pore volume of the MOF shrinking by 14 %. Postsynthetic modification of MOFs can be achieved under mild conditions, and this strategy facilitates the generation of new MOFs with new physical and chemical properties, which are not observable in robust original MOFs. Programming the architectures in the cavity of the porous material can result in the specific interaction of MOFs with guest molecules, such as hydrogen storage.

1.4.3. Mechanistic aspects in the Self-assembly process

The field of coordination frameworks brings together diverse scientific disciplines combining synthetic methodology and structural analysis with the preparation of new generations of multi-functional materials. The research area has developed apace from its origins in coordination and supramolecular chemistry, and now embraces materials in the fields of separation science, theory, electronics, magnetism, and catalysis. Underpinning all of this research is the primary requisite for the designed synthesis and understanding of new structural materials. The basic principles that lie at the heart of designing such materials are explored by study of mechanistic aspects in the self assembly process. The designing of coordination polymers with specified property remains intriguing challenge to the synthetic chemists, in terms of choosing both organic building units (OBUs) as well as metal ions. The synthesis of metal−organic frameworks can be influenced by many factors, such as, the nature of metal ions and organic linkers, conditions of reactions, counterions, as well as molecular interactions including hydrogen bonding etc. Employing appropriate bridging ligands can connect metal ions in different modes and provide possible ways to achieve more robust polymeric structures.

The study of the factors that influence the final architectures elutes the basic principles in the self-assembly process. Furthermore, the study can afford a good opportunity to investigate the details of a self-assembly process and provide more information for the directional synthesis of target CPs.

Table 1.7. Influential role of synthetic parameters.[91]

Factors influencing in the synthesis of the MOFs and CPs		
pH Temperature, Pressure, Time of the reaction, Concentration of reactants	**Synthetic Methods** **1.** Hydrothermal **2.** Ionothermal **3.** Microwave **4.** Mechanochemical **5.** Sonochemical **6.** Electrolysis.	Solvent, Template effect, Metal Source (nitrate, acetate, carbonate, sulfate, chloride), Mineralizer, Structure directing agents, In situ linkers, Precursors

Table 1.8. Influential role of nature of metal ions.

Nature of the metal ion						
C.NO.	**2**	**3**	**4**	**5**	**6**	**7**
Metal Polyhedra	Linear	Trigonal planar	Tetrahedral Square Planar	Square pyramidal Trigonal Bipyrimidal	Octahedral	Pentagonal Bipyrimidal

Table 1.9. Influential role of nature of organic ligands.

Nature of Organic ligand		
Coordinating groups Phosphonic acids (PO_3H_2) Carboxylic acids (COOH) Sulfonic acids (SO_3H) Azoles i. Imidazoles ii. Triazoles iii. Tetrazoles Pyridine derivatives Polyoxoanions	**Number of coordinating groups**. 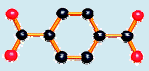 Dipodal 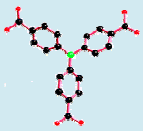 Tripodal 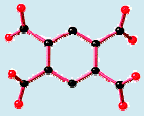 Tetrapodal Hexapodal, etc.	**Geometry** Rigid Flexible Long V-shaped S-shaped

The perspectives in the study of mechanistic aspects of self-assembly process are:

[1] Interpreting the topology of the architectures by changing the potential factors such as solvent, length and geometry of the spacer, type or coordination groups, varying synthetic parameters, position of the coordinating groups in the spacer etc (see Table 1.7-1.9).

[2] Adjusting the porosity and increasing the adsorption capacity by modification of the organic ligands etc.

[3] Analyzing the influential factors which tune the dimensionality of the frameworks etc.

Our group recently started the research in the coordination polymers, which gives us practical experience in studying the assembly coordination networks. Here we discuss some of the interesting aspects of the self assembly with examples reported by different groups.

1.4.3.1. Dimensionality of coordination polymers decided by the type of hybridization of the central carbon atom of the solvent molecule that coordinates to an alkali metal cation

Recently, it has been demonstrated the synthesis of sodium metal based coordination polymers of diverse dimensionality (from 1D to 2D through to 3D) based on a gold(III) dithiolene complex anion $[Au^{III}(btdt)_2]^-$ by changing the solvents of recrystallization . It is shown that dimensionality of a sodium coordination based polymer system, coupled with a gold(III) bis(dithiolene) complex, can be regulated by the type of hybridization of the central carbon atom of the solvent coordinating to the sodium ion. We have investigated the solvent coordination to the sodium ion more vigilantly. The following observations are noteworthy: during crystallization , the 1D coordination polymer **2** is obtained from MeOH and the hybridization of central carbon atom attached to the sodium -coordinated solvent atom (O) is sp^3; likewise, the sp^2 hybridized central carbon atom (of DMF solvent) attached to the coordinating atom (O) leads to the formation of 2D coordination polymer (crystallized from DMF). The 3D coordination polymer, crystallized from CH_3CN, includes N as coordinating solvent atom, which is attached to a sp hybridized central carbon atom. These three observations clearly reveal that the diverse hybridizations of the central carbon atoms of the solvents (MeOH, DMF and CH_3CN in the present study), attached to the coordinating atoms, have a wonderful relationship with the dimensional-topologies.[92]

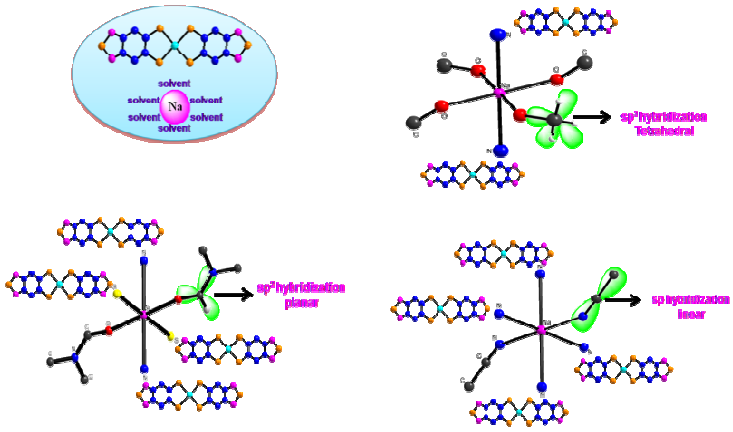

Figure 1.18. $[Na(solvent)_n][Au(btdt)_2]$ complexes present in solution state (left above); crystallization from MeOH (sp^3hybridized orbitals of central carbon) directs the formation of a 1D coordination polymer (right above); crystallizing in DMF (sp^2 hybridized orbitals of central carbon) influences the formation of a 2D coordination polymer (left below); crystallization from CH_3CN (sp hybridized orbitals of central carbon) directs the formation of a 3D coordination polymer (right below).

1.4.3.2. Structural Diversity Tuned by Apparently Innocent *o*-, *m*-, and *p*-Nitro Substituents of Benzoate in Their Complexes of Mn(II) with 4,4′-Bipyridine to form 1D Ladder, 2D Sheet, and 3D Framework

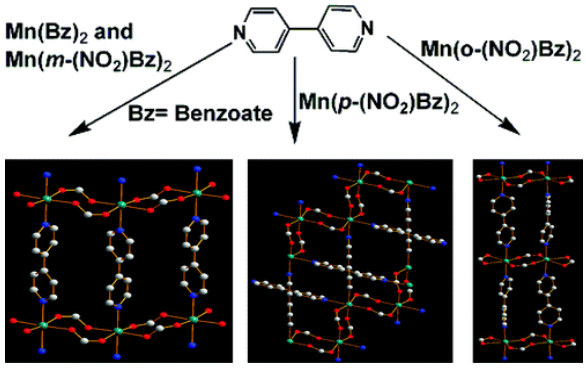

Figure 1.19. Schematic representation of change in dimensionality by altering the position of nitro group.

Ghosh *et al.*, successfully synthesized four coordination polymers by reacting 4,4′-bpy with MnX_2 where X = benzoate and isomeric *o*-, *m*-, and *p*-nitrobenzoates in a 1:1 molar ratio. The general formula of all four complexes are the same, $[Mn(4,4'\text{-bpy})(X)_2]_n$, but the topologies of the polymers are different. The species with benzoate and *m*-nitrobenzoate are 2D rectangular grid-like sheets; the complex with *o*-nitrobenzoate is a 1D molecular ladder, whereas the compound with *p*-nitrobenzoate is a unique 3D framework. This series of complexes clearly demonstrates that although the nitro group does not coordinate to the metal center its mere presence in the *o*-, *m*-, or *p*-position has a striking effect on the structure and dimensionality of the resulting coordination polymer. The participation of

nitro group in p···π and/or C–H···π interactions might be one of the probable reasons for the differences, but more complexes with various substituent's in the phenyl ring of benzoate are needed to be characterized structurally to establish a relationship between the position of apparently innocent substituent and the topology of the polymers. This would potentially be an effective approach of controlling the dimensionality of the coordination polymers, and we will pay attention to exploit this dimension of crystal engineering as a tool for tuning the crystalline solid architecture.[93]

1.4.3.3. Structural inter-conversion between a chain polymer and a two-dimensional network accompanied by tunable magnetic properties

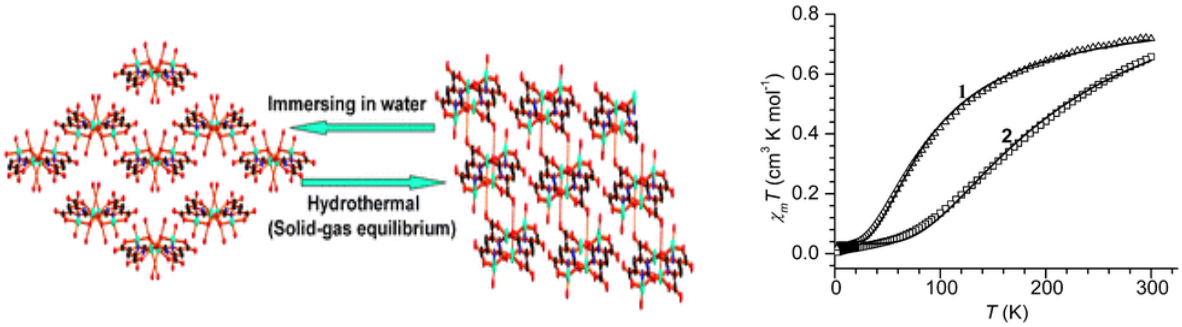

Figure 1.20. The packing patterns of 1D chains in $[Cu_2(hpdc)(OH)(H_2O)_4]\cdot H_2O$ and 2D layers in $[Cu_2(hpdc)(OH)(H_2O)]$ accompanying with significant difference in magnetic couplings.

Zhang et al., reported the two compounds by the reaction of 2-hydroxypyrimidine-4,6-dicarboxylic acid (H_3hpdc) with $CuCl_2$ under different temperatures to give a chain-like compound $[Cu_2(hpdc)(OH)(H_2O)_4]\cdot H_2O$ and a layer-like compound $[Cu_2(hpdc)(OH)(H_2O)]$, which exhibit structural inter-conversion and tunable magnetic properties upon dehydration and hydration. A reversible structural transformation from a 1D coordination polymer chain to a 2D layer-like network upon dehydration–hydration, which is associated with changes in coordination geometries and exhibits significant difference in magnetic coupling interaction, was observed in the compounds. The transformation from **1** to **2** can be viewed as an aggregation of the 1D chain into a 2D layer through the Cu–O (carboxylate) contacts after removing the axial water molecules. During this transformation, the basal planes between the nearest Cu(II) ions in **2** (the dihedral angle: 31.45°) become more tilted towards each other than those in **1** (the dihedral angle: 28.49°). Furthermore, the coordination geometries around Cu(II) ions change from the distorted octahedral and square pyramid in **1** to highly distorted square pyramid and square planar in **2**, accompanied by an increase of the Cu–O–Cu bond angle that is responsible for a larger antiferromagnetic coupling interaction.[94]

1.4.3.4. Adjusting the Porosity and Interpenetration of Cadmium (II) Coordination Polymers by Ligand Modification: Syntheses, Structures, and Adsorption Properties

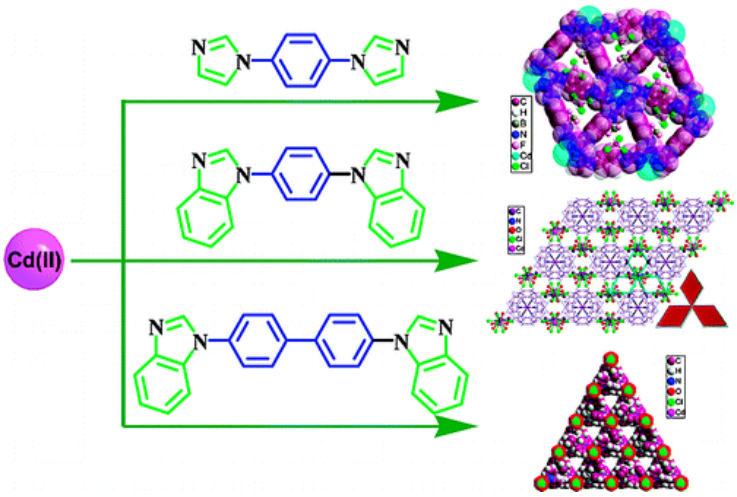

Figure 1.21. Figure illustrating the type of coordination architectures obtained by changing the backbones of the organic ligands.

Bu *et al.* prepared a series of cadmium based coordination polymers with structurally related rigid imidazole ligands, 1,4-bis(imidazol-1-yl)benzene 1,4-bis(benzoimidazol-1-yl)benzene and 4,4′-bis(benzoimidazol-1-yl)biphenyl. All the compounds are α-Po metal−organic frameworks (MOFs) based on six-connected Cd^{II} nodes which are octahedrally coordinated by six nitrogen atoms of ligand molecules. Quantum calculation shows that the volume of coordination sphere comprising of one Cd^{II} center and six imidazole rings is 334.6 cm^3/mol, whereas the volume of the Cd^{II} node consisting of one Cd^{II} center and six benzoimidazole molecules is 523.0 cm^3/mol. Therefore, bulky terminal groups usually result in a larger coordination sphere, and further bear a negative effect on the degree of interpenetration. The longer biphenyl spacer would greatly decrease the influence of bulky group to interpenetration, and a interpenetrating α-Po network is observed in compound with biphenyl spacer. Probably because the spacer has an obvious effect on interpenetration, which is enough to offset the negative effect from the bulky coordination sphere, the void volume is 4034.3 $Å^3$, that is, 52.4% of the cell volume. The degree of interpenetration is tunable by varying ligand backbones; therefore, the porosity of these complexes was also adjusted.[95]

1.4.3.5. Control of Channel Size for Selective Guest Inclusion with Inlaid Anionic Building Blocks in a Porous Cationic Metal–Organic Host Framework

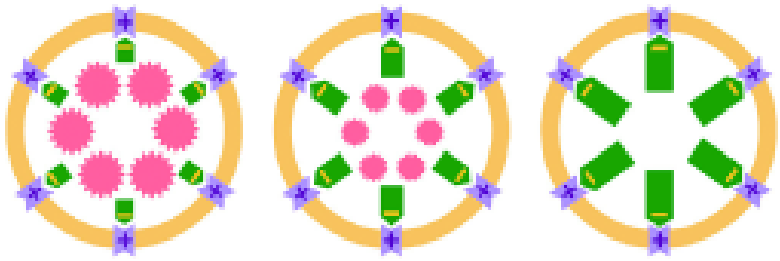

Figure 1.22. Schematic representation of controlling the pore size by the anionic building blocks.

Mak and co-workers prepared a series of isostructural porous metal–organic hybrid host frameworks and coordination polymers by employing silver(I) perfluorocarboxylates and the short flexible ligand di-3-pyridinylmethanone as starting materials. By attaching anionic building blocks of variable bulk to a cationic metal–organic framework, stepwise channel-size adjustment of the resulting porous three-dimensional host framework is achieved (see picture). This method is a new and viable approach for materials with predesigned nanopores for application in molecular recognition and selective guest inclusion. They demonstrated a workable approach to control the effective channel volume of a specific open framework without affecting its overall structure, which relates to the adjustment of a secondary building block that lines its inner surface. This strategy can be considered as a significant development of the traditional concept of connectors and linkers for building MOFs with predesigned nanopores for application in molecular recognition and selective guest inclusion, and it also points the way to the functionalization of a specific porous framework under favorable circumstances.

1.5. Motivation of the present work

The recent trend in the inorganic crystal engineering focuses on the extended frameworks, which promise us the real applications for the mankind. Omar M. Yaghi, Susumu Kitagawa, Jeffrey R. Long, Michael O'Keeffe and Joseph T. Hupp etc.[97] are prominent people in the field of MOFs and CPs; they explored the basic principles and the recent methodologies in terms of synthesis, design, self-assembly and applications. The specific design and synthesis of the framework material with desired topology to meet the required application was still remains as a top priority for the researchers. The study of mechanistic

aspects in the self-assembly process elutes some basic principles through which a synthetic path way and designing methods can be schemed for desired topology.

Choosing organic ligand is one of the most important concepts in the field of MOFs and CPs. As already mentioned, different types of organic ligands are available for coordination with the metal ions, among which flexible ligands are peculiar, unique and offers interesting aspects of the self-assembly process. Rong Cao et al.,[98] studied and reviewed the coordination polymers based on flexible ditopic carboxylates and nitrogen-donor ligands in 2010, which is the first review based on the flexible ligands. The review covers major aspects of the self-assembly process of the coordination polymers based on the flexible ligands. Several groups *viz*. Robert. L. Laduca, Yao-Yu Wang, and S. Kitagawa etc.[99] worked on the coordination polymers based on the flexible ligands.

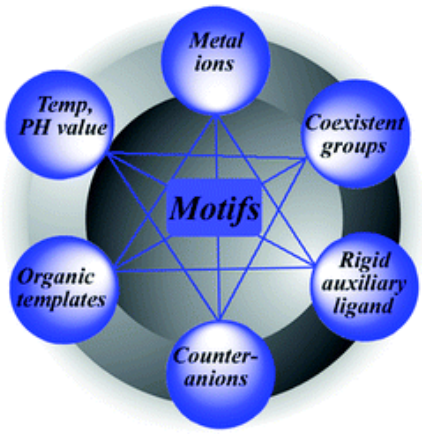

Figure 1.23.Schematic representation of subtle factors affecting the conformation of the flexible ligands.

A significant progress has been made in terms of rational prediction and design of CPs related to rigid and highly directional molecules. Compared to rigid ligands, the use of flexible ligands to construct CPs is more difficult and developing systematic methodologies via flexible ligands is still a great challenge due to the following reasons.

(a) The ligand itself can adopt different conformations and low symmetry as a consequence of rotations about single bonds. These can lead to a loss of control in the design and assembly of the aggregates.

(b) In comparison with rigid ligand, the final structures based on flexible ligands are more sensitive to many subtle factors and the synthesis and characterization are somewhat more difficult. However, the flexibility of ligands is essential to forming some particular properties and structures.[100]

1. Molecular switch derived from a conformational change,
2. Breathing ability in the solid state,
3. Adaptive recognition property for coexisting guests or counterions,
4. Flexible molecular clips, composed of prismatic coordination discrete molecules.

Furthermore, the flexibility of the ligand can afford a good opportunity to investigate the details of a self-assembly process and provide more information for the directional synthesis of target CPs. It is therefore an important aspect of considerable attention and has potential for erecting some signpost toward future research on predicted and pre-designed CPs. Some representative examples of flexible ligands are shown in the following Figure 1.24.

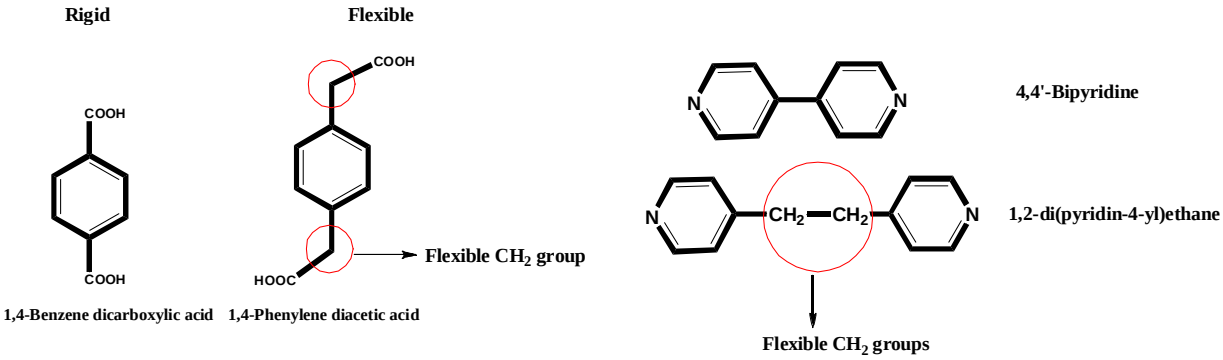

Figure 1.24. Rigid and flexible carboxylate and bipyridine ligands.

The above mentioned concept has prompted us to study the mechanistic aspects in the self-assembly of coordination polymers based on flexible ligands. In chapter-1, mechanistic aspects in formation of Cu-dimer bridged by the flexible phosphonate analogue and extending its dimensionality by organic and inorganic linkers have been studied. Influential role of the biphenyl spacer and secondary ligands in tuning the dimensionality of the coordination polymers involving flexible phosphonic acids has been systematically presented in the chapter-2. Role of polyoxometalates in the self-assembly process of metal-organoamine/organophosphonate systems has been analyzed in the chapter-3. Factors affecting the conformational modulation of flexible ligands in the self-assembly process have been discussed in the chapter-4. Finally the effects of linker coordination angles in tuning the dimensionalities have been studied in the chapter-5. Theoretical calculations have been performed to establish the stabilities of different

conformations of the flexible ligands and magnetic properties have been studied to understand the exchange phenomenon.

1.6. References

[1] (a) Mueller, U.; Schubert, M.; Teich, F.; Puetter, H.; Arndt, K. S.; Pastré, J. *J. Mater. Chem.* **2006**, *16*, 626. (b) Yoon, M.; Srirambalaji, R.; Kim, K. *Chem. Rev.* **2012**, *112*, 1196.

[2] Kosal, M. E.; Chou, J. H.; Wilson S. R.; Suslick, K. S. *Nature Materials* **2002,** 118.

[3] Rowsell, J. L.C.; Yaghi, O. M. *Angew. Chem. Int. Ed*. **2005**, *44*, 4670.

[4] (a) Horcajada, P.; Gref, R.; Baati, T.; Allan, P. K.; Maurin, G.; Couvreur, P.; Férey, G.; Morris, R. E.; Serre, C. *Chem. Rev.* **2012**, *112* , 1232. (b) Bétard, A.; Fischer, R. A.; *Chem. Rev.* **2012**, *112*, 1055.

[5] Eddaoudi, M.; Moler, D. B.; Li, H.; Chen, B.; Reineke, T. M.; O'Keeffe, M.; Yaghi, O. M. *Acc. Chem. Res.* **2001**, *34*, 319.

[6] Huang, Y. Q.; Ding, B.; Song, H. B.; Zhao, B.; Ren, P.; Cheng, P.; Wang, H. G.; Liao, D. Z.; Yan, S. P. *Chem. Commun.* **2006**, 4906.

[7] Bordiga, S.; Lamberti, C.; Ricchiardi, G.; Regli, L.; Bonino, F.; Damin, A.; Lillerud, K.-P.; Bjorgen, M.; Zecchina, A.; *Chem. Commun.* **2004**, 2300.

[8] Yaghi, O. M.; Li, H.; Davis, C.; Richardson, D.; Groy, T. L. *Acc. Chem. Res.* **1998**, *31*, 474.

[9] Lipowski, J. *Inclusion Compounds: Structural Aspects of Inclusion Compounds Formed by Inorganic and Organometallic Host Lattices:* In Atwood, J. L,; Davies, J. E. D.; MacNicol, D. D., Eds., Academic Press: London, 1984.

[10] Iwamoto, T.; Nakano, T.; Morita, M.; Miyosh, T.; Miyamoto, T.; Sasaki, Y. *Inorg. Chim. Acta* **196***8, 2,* 313.

[11] Dunbar, K. R.; Heintz, T. A. *Prog. Inorg. Chem.* **1997**, *45*, 283

[12] Hoskins, B. F.; Robson, R. *J. Am. Chem. Soc.* **1989**, *111*, 5962.

[13] Hoskins, B. F.; Robson, R. *J. Am. Chem. Soc.* **1990**, *112*, 1546.

[14] (a) Khan, M. I.; Lee, Y. S.; O'Connor, C. J.; Haushalter, R. C.; Zubieta, J. *Inorg. Chem.* **1994**, *33*, 3855. (b) Cheetham, A. K.; Rao, C. N. R.; Feller, R. K. *Chem. Commun.* **2006**, 4780.

[15] Coordination polymers. In *Wikipedia, The Free Encyclopedia*.http://en.wikipedia.org/wiki/Coordination_polymers

[16] Kitagawa, S.; Matsuda, R. *Coord. Chem. Rev.* **2007**, *251*, 2490.

[17] Loeb, S. J. *Chem. Commun.* **2005**, 1511.

[18] Biradha, K.; Ramanan, A.; Vittal, J. J. *Cryst. Growth Des.* **2009**, *9*, 2969.

[19] http://www1.eere.energy.gov/hydrogenandfuelcells/storage/current_technology.html.

[20] Rosi, N. L.; Eckert, J.; Eddaoudi, M.; Vodak, D. T.; Kim, J.; O'Keeffe, M.; Yaghi, O. M.*Science* **2003**, *300*, 1127.

[21] Rowsell, J. L. C.; Millward, A. R.; Park, K. S.; Yaghi, O. M. *J. Am. Chem. Soc.* **2004**, *126*, 5666.

[22] (a) Suh, M. P.; Park, H. J.; Prasad, T. K.; Lim, D. W.; *Chem. Rev.* **2012,** *112*, 782. (b) Farha, O. K.; Yazaydin, A. O.; Eryazici, I.; Malliakas, C. D.; Hauser, B. G.; Kanatzidis, M. G.; Nguyen, S. T.; Snurr, R. Q.; Hupp, J. T. *Nat. Chem.* **2010**, *2*, 944. (c) Furukawa, H.; Ko, N.; Go, Y. B.; Aratani, N.; Choi, S. B.; Choi, E.; Yazaydin, A. O.; Snurr, R. Q.; O'Keeffe, M.; Kim, J.; Yaghi, O. M. *Science* **2010**, *329*, 424. (d) Phan, A.; Doonan, C.; Uribe-Romo, F. J.; Knobler, C. B.; O'keeffe, M.; Yaghi, O. M. *Acc. Chem. Res.* **2009**, *43*, 58. (e) Choi, H. J.; Dincă, M.; Long, J. R. *J. Am. Chem. Soc.* **2008**, *130*, 7848 (f) Dincă, M.; Dailly, A.; Liu, Y.; Brown, C. M.; Neumann, D. A.; Long, J. R. *J. Am. Chem. Soc.* **2006**, *128*, 16876. (g) Wong-Foy, A. G.; Matzger, A. J.; Yaghi, O. M. *J. Am. Chem. Soc.* **2006**, *128*, 3494. (h) Férey, G.; Mellot-Draznieks, C.; Serre, C.; Millange, F.; Dutour, J.; Surble, S.; Margiolaki, I. *Science* **2005**, *309*, 2040.

[23] Burchell, T.; Judkins, R. R.; Rogers, M. *PCT Int. Appl*. **2000**.

[24] Muris, M.; Pavlovsky, N. D.; Bienfait, M.; Zeppenfeld, P. *Surf. Sci.* **2001**, *492*, 67.

[25] Kondo, M.; Okubo, T.; Asami, A.; Noro, S.; Yoshitomi, T.; Kitagawa, S.; Ishii, T.; Matsuzaka, H.; Seki, K. *Angew. Chem. Int. Ed.* **1999**, *38*, 140.

[26] Noro, S.; Kitagawa, S.; Kondo, M.; Seki, K.; *Angew. Chem. Int. Ed*. **2000,** *39*, 2081.

[27] (a) Jacobson, M. Z. *Energy Environ. Sci.* **2009**, *2*, 148. (b) IPCC. *IPCC Special Report on Carbon Dioxide Capture and Storage*; Cambridge University Press:Cambridge, UK, **2005**.

[28] (a) Kikkinides, E. S.; Yang, R. T.; Cho, S. H. Ind. Eng. Chem. Res. **1993**, *32*, 2714. (b) D'Allessandro, D. M.; Smit, B.; Long, J. R. *Angew. Chem., Int. Ed*. **2010**, *49*, 6058. (c) Keskin, S.; Heest, T.; van; Sholl, D. *ChemSusChem* **2010**, *3*, 879. (d) Choi, H. S.; Suh, M. P. *Angew. Chem., Int. Ed.* **2009**, *48*, 6865.

[29] Sumida, K.; Rogow, D. L.; Mason, J. A.; McDonald, T. M.; Bloch, E. D.; Herm, Z. R.; Bae, T. H.; Long, J. R. *Chem. Rev.* **2012**, *112*, 724.

[30] (a) Llewellyn, P. L.; Bourrelly, S.; Serre, C.; Vimont, A.; Daturi, M.; Hamon, L.; Weireld, G.; De, Chang, J. S.; Hong, D. Y.; Hwang, Y. K.; Jhung, S. H.; Ferey, G. *Langmuir* **2008**, *24*, 7245. (b) Gallo, M.; Glossnan-Mitnik, D. *J. Phys. Chem.C* **2009**, *113*, 6634.

[31] Nagarkar, S. S.; Chaudhari, A. K.; Ghosh, S. K.; *Inorg. Chem.*, **2012**, *51*, 572.

[32] Wang, Z.; Cohen, S. M. *J. Am. Chem. Soc.* **2007**, *129*, 12368.

[33] Wang, Z.; Cohen, S. M. *J. Am. Chem. Soc.* **2009**, *131*, 16675.

[34] Garibay, S. J.; Cohen, S. M. *Chem. Commun.* **2010**, *46*, 7700.

[35] Bernt, S.; Guillerm, V.; Serre, C.; Stock, N. *Chem. Commun.* **2011**, *47*, 2838.

[36] (a) Furukawa, H.; Ko, N.; Go, Y. B.; Aratani, N.; Choi, S. B.; Choi, E.; Yazaydin, A. O.; Snurr, R. Q.; O'Keefe, M.; Kim, J.; Yaghi, O. M. *Science* **2010**, *329*, 424. (b) Herm, Z. R.; Swisher, J. A.; Smit, B.; Krishna, R.; Long, J. R. *J. Am. Chem. Soc.* **2011**, *133*, 5664. (c) Bao, Z.; Yu, L.; Ren, Q.; Lu, X.; Deng, S. *J. Colloid Interface Sci.* **2011**, *353*, 549. (d) Yazaydin, A. Ö.; Snurr, R. Q.; Park, T.-H.; Koh, K.; Liu, J.; LeVan, M. D.; Benin, A. I.; Jakubczak, P.; Lanuza, M.; Galloway, D. B.; Low, J. L.; Willis, R. R. *J. Am. Chem. Soc.* **2009**, *131*,18198. (e) Lee, Y.-G.; Moon, H. R.; Cheon, Y. E.; Suh, M. P. *Angew. Chem., Int. Ed.* **2008**, *47*, 7741. (f) Hu, Y.; Xiang, S.; Zhang, W.; Zhang, Z.; Wang, L.; Bai, J.; Chen, B. *Chem. Commun.* **2009**, 7551.

[37] Uemura, T.; Yanai, N.; Kitagawa, S. *Chem. Soc. Rev.* **2009**, *38*, 1228.

[38] (a) Yaghi, O. M. ; O'Keeffe, M. ; Ockwig, N. W. ; Chae, H. K. ; Eddaoudi, M.; Kim, J. *Nature* **2003**, *423*, 705. (b) Kitagawa, S.; Kitaura, R.; Noro, S.-i. *Angew. Chem., Int. Ed.* **2004**, *43*, 2334.

[39] Uemura, T.; Horike, S.; Kitagawa, S. *Chem.–Asian J.* **2006**, *1*, 36.

[40] Uemura, T.; Hiramatsu, D.; Kubota, Y.; Takata, M.; Kitagawa, S. *Angew. Chem., Int. Ed.* **2007**, *46*, 4987.

[41] (a) Higuchi, M.; Horike, S.; Kitagawa, S. *Supramol. Chem.* **2007**, *19*, 175. (b) Lam, J. W. Y. Tang, B. Z. *Acc. Chem. Res.* **2005**, *38*, 745.

[42] Hoskins, B. Z.; Robson, R. *J. Am. Chem. Soc.* **1990**, *112*, 1546.

[43] Alkordi, M. H.; Liu, Y.; Larsen, R. W.; Eubank, J. F.; Eddaoudi, M. *J. Am. Chem. Soc.* **2008**, *130*, 12639.

[44] Nuzhdin, A. L.; Dybtsev, D. N.; Bryliakov, K. P.;. Talsi, E. P.; Fedin, V. P. *J. Am. Chem. Soc.* **2007**, *129*, 12958.

[45] (a) Wu, C. D.; Hu, A.; Zhang, L.; Lin, W. *J. Am. Chem. Soc.* **2005**, *127*, 8940. (b) Chui, S. S.; Lo, S. M.; Charmant, J. P.; Orpen, A. G.; Williams, I. D. *Science* **1999**, *283*, 1148.

[46] Horike, S.; Dinca, M.; Tamaki, K.; Long, J. R. *J. Am. Chem. Soc.* **2008**, *130*, 5854.

[47] Fujita, M.; Kwon, Y. J.; Washizu, S.; Ogura, K. *J. Am. Chem. Soc.* **1994**, *116*, 1151.

[48] Shultz, A. M.; Farha, O. K.; Hupp, J. T.; Nguyen, S. T. *J. Am. Chem. Soc.* **2009**, *131*,4204.

[49] Lee, J. Y.; Farha, O. K.; Roberts, J.; Scheidt, K. A.; Nguyen, S. T.; Hupp, J. T. *Chem. Soc. Rev.* **2009**, *38*, 1450.

[50] (a) Hasegawa, S.; Horike, S.; Matsuda, R.; Furukawa, S.; Mochizuki, K.; Kinoshita, Y.; Kitagawa, S. *J. Am. Chem. Soc.* **2007**, *129*, 2607. (b) Ravon, U.; Domine, M. E;. Gaudillere, C.; Desmartin-Chomel, A.; Farrusseng, D. *New J. Chem.* **2008**, *32*, 937. (c) Pramanik, A.; Abbina, S.; Das, G. *Polyhedron* **2007**, *26*, 5225. (d) Hwang, Y. K.; Hong, D.-Y.; Chang, J.-S.; Jhung, S. H.; Seo, Y.-K.; Kim, J.; Vimont, A.; Daturi, M.; Serre, C.; Férey, G. *Angew. Chem., Int. Ed.* **2008**, *47*, 4144. (e) Alkordi, M. H.; Liu, Y.; Larsen, R. W.; Eubank, J. F.; Eddaoudi, M. *J. Am. Chem. Soc.* **2008**, *130*, 12639. (f) Horike, S.; Dinca, M.; Tamaki, K.; Long, J. R. *J. Am. Chem. Soc.* **2008**, *130*, 5854. (g) Xiao, B.; Hou, H.; Fan, Y. *J. Organomet. Chem.* **2007**, *692*, 2014. (h) Llabrés i Xamena, F. X.; Abad, A.; Corma, A.; Garcia, H. *J. Catal.* **2007**, *250*, 294.

[51] Seo, J. S.; Whang, D.; Lee, H.; Jun, S. I.; Oh, J.; Jeon, Y.; Kim, K. *Nature* **2000**, *404*, 982.

[52] Yoon, M.; Srirambalaji, R.; Kim, K. *Chem. Rev.*, **2012**, *112*, 1196.

[53] (a) Evans, O. R.; Ngo, H. L.; Lin, W. *J. Am. Chem. Soc.* **2001**, *123*, 10395. (b) Gedrich, K.; Heitbaum, M.; Notzon, A.; Senkovska, I.; Frçhlich, R.; Getzschmann,

J.; Mueller, U.; Glorius, F.; Kaskel, S.*Chem.-Eur. J.* **2011**, *17*, 2099. (c) Cho, S.-H.; Ma, B.; Nguyen, S. T.; Hupp, J. T.; Albrecht-Schmitt, T. E. *Chem. Commun.* **2006**, 2563. (d) Dang, D.; Wu, P.; He, C.; Xie, Z.; Duan, C. *J. Am. Chem. Soc.* **2010**, *132*, 14321. (e) Wang, M.; Xie, M.-H.; Wu, C.-D.; Wang, Y.-G. *Chem. Commun.* **2009**, 2396.

[54] (a) Metal–Organic and Organic Molecular Magnets, *Spec. Publ. - R. Soc. Chem.*, ed. P. Day and A. E. Underhill, Cambridge, UK, **2000**, vol. 252. (b) Rao, C. N. R.; Cheetham, A. K.; Thirumurugan, A. *J. Phys.: Condens. Matter*, **2008**, *20*, 083202.

[55] (a) Blundell, S. J.; Pratt, F. L. *J. Phys.: Condens. Matter,* **2004**, 16, R771–R828. (b) *Molecular Magnetism, New Magnetic Materials*, ed. K. Itoh and M. Kinoshita, Gordon Breach-Kodansha, Tokyo, **2000**.

[56] Kurmoo, M. *Chem. Soc. Rev.* **2009**, *38*, 1353.

[57] Kreno, L. E.; Leong, K.; Farha, O. K.; Allendorf, M.; Duyne, R. P. V. D.; Hupp, J. T. *Chem. Rev.* **2012**, *112*, 1105.

[58] Lin, X.; Blake, A. J.; Wilson, C.; Sun, X. Z.; Champness, N. R.; George, M. W.; Hubberstey, P.; Mokaya, R.; Schröder, M. *J. Am. Chem. Soc.* **2006**, *128*, 10745.

[59] Lu, Z.-Z.; Zhang, R.; Li, Y.-Z.; Guo, Z.-J.; Zheng, H.-G. *J. Am. Chem. Soc.* **2011**, *133*, 4172.

[60] Xie, Z.; Ma, L.; deKrafft, K. E.; Jin, A.; Lin, W. *J. Am. Chem. Soc.* **2009**, *132*, 922.

[61] (a) Lan, A.; Li, K.; Wu, H.; Olson, D. H.; Emge, T. J.; Ki, W.; Hong, M.; Li, J. *Angew. Chem., Int. Ed.* **2009**, *48*, 2334. (b) Pramanik, S.; Zheng, C.; Zhang, X.; Emge, T. J.; Li, J. *J. Am. Chem. Soc.* **2011**, *133*, 4153.

[62] Kitagawa, S.; Kitaura. R.; Noro, S. *Angew. Chem., Int. Ed.*, **2004**, *43*, 2334.

[63] (a) Mueller, U.; Hesse, M.; Lobree, L.; Hoelzle, M.; Arndt, J. D.; Rudolf, P. *WO 2002/070526*, **2002**, BASF.

[64] (a) Schlichte, K.; Kratzke, T.; Kaskel, S. *Microporous Mesoporous Mater.* **2004**, *73*, 81. (b) Chui, S. S.-Y.; Lo, S. M.-F. ; Charmant, J. P. H.; Orpen, A. G.; Williams, I. D. *Science*, **1999**, *283*, 1148.

[65] Mueller, U.; Schubert, M.; Teich, F.; Puetter, H.; Schierle-Arndt, K.; and Pastré, J. *J. Mater. Chem.* **2006**, *16*, 626.

[66] (a) Seki, K.; Mori, W. *J. Phys. Chem. B*, 2002, *106*, 1380. (b) Mueller, U.; Harth, K.; Hoelzle, M.; Hesse, M.; Lobree, L.; Harder, W.; Yaghi, O. M. *WO 2003/064030*, 07.08.2003.

[67] Xu, R.; Pang, W.; Yu, J.; Huo, Q.; Chen, J. *Chemistry of Zeolites and Related Porous Materials: Synthesis and Structure*; John Wiley and Sons, Inc.: Singapore, **2007**.

[68] (a) Barrer, R. M. *J. Chem. Soc*. **1948**, *127*, 132. (b) Breck, D. W.; Eversole, W. G.; Milton, R. M.; Reed, T. B.; Thomas, T. L *Phys. Inorg. Chem.* **1956,** *78*, 971.

[69] (a) Rabenau, A.; *Angew. Chem. Int. Ed. Engl.* **1985**, *24*, 1026. (b) Demazeau, G. *J. Mater. Chem.* **1999,** *9*, 15. (c) Gopalakrishnan, J. *Chem. Mater.* **1995**, *7*, 1265.

[70] (a) Haushlater, R. C.; Strohmaier, K. G.; Lai, F. W. *Science* **1989**, *246*, 1289. (b) Yaghi, G. M.; Li, H. *J. Am. Chem. Soc*. **1995**, *117*, 10401. (c) Doran, M. B.; Norquist, A. J.; O'Hare, D. *Inorg. Chem.* **2003**, *42*, 6968.

[71] (a) Gutschke, S. O. H.; Price, D. J.; Powell, A. K.; Wood, P. T. *Angew. Chem. Int. Ed.* **2001**, *40*, 1920. (b) Rujiwatra, A.; Kepert, C. J.; Rossiensky, M. J. *Chem. Commun.* **1999**, 2307. (c) Kuhlman, R.; Schimek, G. L.; Kolis, J. L. *Inorg. Chem.* **1998**, *38*, 194.

[72] Del Popolo, M. G.; Voth, G. A. *J. Phys. Chem. B* **2004**, *108*, 1744.

[73] Wasserscheid, P.; Keim, W. *Angew. Chem., Int. Ed.* **2000,** *39*, 3773.

[74] Antonietti, M.; Kuang, D.; Smarsly, B.; Zhou, Y. *Angew. Chem., Int. Ed.* **2004,** *43*, 4988.

[75] Cooper, E. R.; Andrews, C. D.; Wheatley, P. S.; Webb, P. B.; Wormald, P.; Morris, R. E. A *Stud. Surf. Sci. Catal., A* **2005**, *158*, 247.

[76] Jin, K.; Huang, X.; Pang, L.; Li, J.; Appel, A.; Wherland, S. *Chem. Commun.* **2002**, 2872.

[77] Dybtsev, D. N.; Chun, H.; Kim, K. *Chem. Commun*. **2004**, 1594.

[78] Lin, Z.; Slawin, A. M. Z.; Morris, R. E. *J. Am. Chem. Soc.* **2007**, *129*, 4880.

[79] Garay, A. L.; Pichon, A.; James, S. L. *Chem. Soc. Rev.* **2007**, *36*, 846.

[80] Suryanarayana, C. *Prog. Mater. Sci.* **2001**, *46*, 1.

[81] (a) Tanaka, K.; Toda, F. *Chem. Rev.* **2000**, *100*, 1025. (b) Tanaka, K.; Toda, F. *Solvent-Free Organic Synthesis*, Wiley-VCH, London, **2003**. (c) Cave, G. W. V.; Raston, C. L.; Scott, J. L. *Chem. Commun.* **2001**, 2159.

[82] (a) Rowsell, J. L. C.; Yaghi, O. M. *Microporous Mesoporous Mater.* **2004**, 73, 3. (b) Férey, G. *Chem. Soc. Rev.* **2008**, *37*, 191.

[83] Forster, P. M.; Thomas, P. M.; Cheetham, A. K. *Chem. Mater.* **2002**, *14*, 17.

[84] Foster, B. L.; Cournoyer, M. E. *Chem. Health Saf.* **2005**, *12*, 27.

[85] (a) Ni, Z.; Masel, R. I. *J. Am. Chem. Soc.* **2006**, *128*, 12394. (b) Jhung, S. H.; Lee, J. H.; Forster, P. M.; Férey, G.; Cheetham, A. K.; Chang, J. S. *Chem.–Eur. J.* **2006**, *12*, 7899. (c) Taylor, K. M. L.; Rieter, Lin, W. B. *J. Am. Chem. Soc.* **2008**, *130*, 14358. (d) Vondrova, M.; Burgess, C. M.; Bocarsly, A. B. *Chem. Mater.* **2007**, *19*, 2203. (e) Liu, B.; Zou, R. Q.; Zhong, R. Q.; Han, S.; Shioyama, H.; Yamada, T.; Maruta, G.; Takeda, S.; Xu, Q. *Microporous Mesoporous Mater.* **2008**, *111*, 470. (f) Jhung, S. H.; Lee, J. H.; Yoon, J. W.; Serre, C.; Férey, G.; Chang, J. S. *Adv. Mater.* **2007**, *19*, 121. (g) Liu, W. L.; Ye, L. H.; Liu, X. F.; Yuan, L. M.; Lu, X. L.; Jiang, J. X. *Inorg. Chem. Commun.* **2008**, *11*, 1250. (h) Bae, Y. S.; Mulfort, K. L.; Frost, H.; Ryan, P.; Punnathanam, S.; Broadbelt, L. J.; Hupp, J. T.; Snurr, R. Q. *Langmuir* **2008**, *24*, 8592.

[86] Vondrova, M.; Majsztrik, P. W.; Gould, S.; Bocarsly, A. B. *Chem. Mater.* **2005**, *17*, 4755.

[87] Jhung, S. H.; Yoon, J. W.; Hwang, J. S.; Cheetham, A. K.; Chang, J. S. *Chem. Mater.* **2005**, *17*, 4455.

[88] Hwang, Y. K.; Chang, J. S.; Park, S. E.; Kim, D. S.; Kwon, Y. U.; Jhung, S. H.; Hwang, J. S.; Park, M. S. *Angew. Chem., Int. Ed.* **2005**, *44*, 556.

[89] Costa, J. S.; Gamez, P.; Black, C. A.; Roubeau, O.; Teat, S. J.; Reedijk, J. *Eur. J. Inorg. Chem.* **2008**, 1551.

[90] Seo, J.S.; Wand, D.; Lee, H.; Jun, S.I.; Oh, J.; Jeon, Y.; Kim, K. *Nature* **2000**, *404*, 982.

[91] Stock, N; Biswas, S. *Chem. Rev.* **2012**, *112*, 933.

[92] Bolligarla, R.; Das, S. K. *CrystEngComm*, **2010**, *12*, 3409.

[93] Kar, P.; Biswas, R.; Ida, Y.; Ishida, T.; Ghosh, A. *Cryst. Growth Des.* **2011**, *11*, 5305.

[94] Chen, C.; Sun, J.-K.; Li, W.; Chen, C.-N.; Zhang, J. *Chem. Commun.* **2011**, *47*, 6683.

[95] Li, Z.-X.; Hu, T.-L.; Ma, H.; Zeng, Y.-F.; Li, C.-J.; Tong, M.-L.; Bu, X.-H. *Cryst. Growth Des.*, **2010**, *10*, 1138.

[96] Chen, X.-D.; Wan, C.-Q.; Sung, H. H.-Y.; Williams, I. D.; Mak, T. C. W. *Chem. Eur. J.* **2009**, *15*, 6518.

[97] (a) O'Keeffe, M.; Yaghi, O. M. *Chem. Rev.* **2012**, *112*, 675. (b) Kitagawa, S.; Kitaura, R.; Noro, S. *Angew.Chem.Int.Ed.* **2004**, *43*, 2334. (c) Murray, L. J.; Dincă,

M.; Long, J. R. *Chem. Soc. Rev.* **2009**, *38*, 1294. (d) Lee, J. Y.; Farha, O. K.; Roberts, J.; Scheidt, K. A.; Nguyen, S. T.; Hupp, J. T. *Chem. Soc. Rev*. **2009**, *38*, 1450.

[98] Liu,T.-F.; Lu, J.; Cao, R. *CrystEngComm*, **2010**, *12*, 660.

[99] (a) Karyn M. Blake, K. M.; Gregory A. Farnum, G. A.; Lindsey L. Johnston, L. L.; Robert L. LaDuca, R. L. *Inorganica Chimica Acta* **2010**, *363*, 88. (b) Yang, G. P.; Wang, Y. Y.; Zhang, W. H.; Fu, A. Y.; Liu, R. T.; Lermontava, E.; Shi, Q. Z. *CrystEngComm*, **2010**, *12*, 1509.

[100] (a) Chen, C.; Zhang, J.; Su, C. *Eur. J. Inorg. Chem.* **2007**, 2997. (b) Hong, M.; Zhao, Y.; Su, W.; Cao, R.; Fujita, M.; Zhou, Z.; Chan, A. S. C. *Angew. Chem., Int. Ed.* **2000**, *39*, 2468.

Mechanistic Aspects in the Formation of Copper Dimer Bridged by Phosphonic Acid and Extending its Dimensionality by Organic and Inorganic Linkers: Synthesis, Structural Characterization, Magnetic Properties and Theoretical Calculations

2

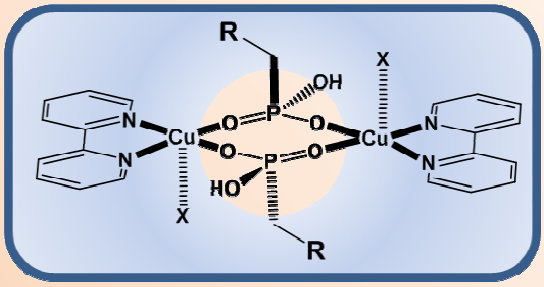

*Six new copper metal complexes with formulae $[Cu(H_2O)(2,2'\text{-bpy})(H_2L)]_2 \cdot H_4L \cdot 4H_2O$ (**1**), $[\{Cu(H_2O)(2,2'\text{-bpy})(H_3L)\}_2(H_2L)] \cdot 2H_2O$ (**2**), $[Cu(H_2O)(1,10\text{-phen})(H_2L)]_2 \cdot 6H_2O$ (**3**), $[Cu(2,2'\text{-bpy})(H_2L)]_n \cdot nH_2O$ (**4**), $[Cu(1,10\text{-phen})(H_2L)]_n \cdot 3nH_2O$ (**5**) and $[\{Cu(2,2'\text{-bpy})(MoO_3)\}_2(L)]_n \cdot 2nH_2O$ (**6**) have been synthesized starting from the p-xylylenediphosphonic acid (H_4L) and 2,2′-bipyridine (2,2′-bpy) or 1,10-phenanthroline (1,10-phen) as secondary linkers and characterized by single crystal X-ray diffraction analysis, IR spectroscopy and Thermogravimetric (TG) analysis. All the complexes were synthesized by hydrothermal methods. A dinuclear motif (Cu- dimer) bridged by phosphonic acid represents a new class of simple building unit (SBU) in construction of coordination architectures in metal phosphonate chemistry. The initial pH of the reaction mixture induced by the secondary linker plays an important role in the formation of the molecular phosphonates **1**, **2** and **3**. Temperature dependent hydrothermal synthesis of the compounds **1**, **2** and **3** reveals the mechanism of the self-assembly of the compounds based on the solubility of the phosphonic acid H_4L. 2D coordination polymers **4**, **5** and **6**, that are formed by increasing the pH of the reaction mixture, comprise of Cu-dimers as nodes, organic (H_2L) and inorganic (Mo_4O_{12}) ligands as linkers. The void space-areas, created by the (4, 4) connected nets in compounds **4** and **5**, are occupied by lattice water molecules. Thus compounds **4** and **5** have potential to accommodate guest species / molecules. Variable temperature magnetic studies of the compounds **3**, **4**, **5** and **6** reveal the antiferromagnetic interactions between the two Cu(II) ions in the eight membered ring, observed in their crystal structures. A density functional theory (DFT) calculation correlates the conformation of the Cu-dimer ring with the magnitude of the exchange parameter based on the torsion angle of the conformation.*

2.1. Introduction

Over the past few decades, structural inorganic chemistry has provided a firm relationship between the aesthetics of crystalline architectures and their potential functions, in which the ultimate goal is to obtain the desired tailor made materials with intriguing functional properties.[1] In order to model the functional crystalline solids with desired properties, considerable efforts have been devoted to understand the self assembly process of the coordination networks.[2] In this context, numerous coordination polymers have been reported by utilizing the multitopic building blocks such as carboxylates,[3] phosphonates,[4] sulfonates,[5] organonitrogen bridging ligands and terminal aromatic chelating ligands[6] etc. The majority of metal organic framework (MOF) structures rely on carboxylate derivatives, as the concerned bidentate ligands have regular coordination modes.[7] In contrast, metal organophosphonates are also among the earliest and extensively studied examples of coordination polymers / metal organic frameworks, that are important because of their potential applications in the areas of sorption, ion exchange, sensing, and catalysis.[8] Additionally, metal phosphonates have offered great opportunities to understand fundamental magnetic phenomena, such as spin canting, anisotropy, relaxation dynamics and field induced magnetic transitions.[9] Shimzu et al. reviewed the recent progress in phosphonate MOFs with an emphasis of open frameworks.[10] Due to availability of more possible ligating modes and three possible protonation states of PO_3H_2 groups, the controlled formation of geometrically well-defined structures has not been succeeded. The self assembly of metal phosphonate coordination polymers is dependent upon many factors, such as, specific metal incorporation, degree of protonation, geometry of the phosphonic acid and geometry of secondary linker as well as synthetic parameters under solvothermal conditions, e.g., temperature, pressure, vessel fill volume, time, pH and the presence or absence of any mineralizing agent in the reaction mixture.[11] In order to understand the structural consequences of some of the aforementioned factors, systematic studies are needed to evaluate the basic principles in the mechanisms of the self assembly process of metal phosphonates. Our interests lie in the study of the factors that influence the self assembly process of the coordination networks.[12] Recently, we discuss about the factors affecting the conformational modulation of flexible ligands in the self assembly process of coordination polymers of carboxylic acids.[13] Due to availability of more number of ligating sites, phosphonic acids (PO_3H_2 groups) coordinate to more number of metal sites there by forming a layered structures and the bisphosphonic acids form a

pillared-layered structures.[14] A control over the protonation states and introduction of secondary chelating ligands result in the formation of clusters with different nuclearities.[15] This approach results in the stabilization of molecular phosphonates with interesting magnetic properties because O–P–O bridge is known to be efficient in transmitting weak to moderately strong antiferromagnetic and ferromagnetic interactions.[16] In the recent era, the research progresses on metal phosphonates lead to the evolution of 2D and 3D coordination networks.[17] In these extended networks, metal clusters act as nodes and organic parts act as linkers similar to carboxylic acids.[17e] Generally, the growth of single crystals with phosphonates is difficult as they often precipitate rapidly (as less ordered insoluble phases). Hydro(solvo)thermal techniques have been extensively employed in the synthesis of metal phosphonates to overcome this problem that hinders the formation of crystalline solids.[18] The investigation of self assembly process under the hydrothermal conditions by varying synthetic parameters reveals the mechanism of the formation of the crystalline solids. Among molecular phosphonates, two copper atoms connected by O–P–O bridges forming a 8-membered ring represent the simplest dinuclear model. Based on the torsion angles in the 8-membered ring, ten symmetrical conformations have been established.[19] The magnetic exchange interactions of this dinuclear copper complex were reported with different peripheral subunits but still it can be considered as a rare subunit to extend its dimensionality.[20] In this contribution, we have chosen a *p*-xylylenediphosphonic acid (H_4L) as a organic linker and 2,2′-bpy or 1,10-phen as chelated secondary linkers with copper metal to construct the dinuclear copper systems. Recently we have reported both *cis* and *trans* conformations of the flexible *p*-xylylenediphosphonic acid with cobalt ion.[4g] Copper(II) compounds are of particularly interest from the theoretical point of view, because they are the simplest paradigms of magnetic interactions that involve only two unpaired electrons.[21] Here we present syntheses and structural characterizations of six dinuclear copper complexes [Cu(H_2O) (2,2′-bpy)(H_2L)]$_2$·H_4L·4H_2O (**1**), [{Cu(H_2O)(2,2′-bpy)(H_3L)}$_2$(H_2L)]·2H_2O (**2**), [Cu (H_2O)(1,10-phen)(H_2L)]$_2$· 6H_2O (**3**), [Cu(2,2′-bpy)(H_2L)]$_n$·*n*H_2O (**4**), [Cu(1,10-phen)(H_2L)]$_n$·3*n*H_2O (**5**) and [{Cu(2,2′-bpy)(MoO_3)}$_2$(L)]$_n$·2*n*H_2O (**6**). The mechanism for the formation dinuclear copper complex by varying the secondary linker at variant temperatures has been studied under hydrothermal conditions. The dimensionality of the Cu-dimers has been extended to 2D polymers by employing the organic and inorganic linkers. Temperature dependent magnetic measurements have been performed and the

magnitudes of the exchange interactions have been calculated in the dimers. The relevant results are compared with theoretical values, calculated by DFT. The reversible dehydration and rehydration of lattice water molecules have been studied on compounds **4** and **5** demonstrating the host–guest properties.

2.2. Experimental

2.2.1. Materials and Methods

All the chemicals were received as reagent grade and used without any further purification. The ligands *p*-xylylenediphosphonic acid (H_4L) was prepared according to the literature procedure.[22] Elemental analyses were determined by FLASH EA series 1112 CHNS analyzer. Infrared spectra of solid samples obtained as KBr pellets on a JASCO – 5300 FT – IR spectrophotometer. Thermogravimetric analyses were carried out on a STA 409 PC analyzer and corresponding masses were analyzed by QMS 403 C mass analyzer, under flow of N_2 gas with a heating rate of 5 ^oC min^{-1}, in the temperature range of 30–1000 ^oC. Powder X-ray diffraction patterns were recorded on a Bruker D8-Advance diffractometer using graphite monochromated $CuK_{\alpha1}$ (1.5406 Å) and $K_{\alpha2}$ (1.54439 Å) radiations. Magnetic susceptibilities were measured in the temperature range 2–300 K on a Quantum Design VSM-SQUID. All the compounds were synthesized in 23 mL Teflon-lined stainless vessels (Thermocon, India).

The following computational methodology was used to calculate the exchange coupling constants in the reported complexes.[23] The phenomenological Heisenberg Hamiltonian $H = -\Sigma_{(i>j)}J_{ij}S_iS_j$ (where where S_i and S_j are the spin operators of the paramagnetic metal centers *i* and *j;* and the J_{ij} parameters are the exchange-coupling constants for the different pair-wise interactions between the paramagnetic metal centers of the molecule) can be used to describe the exchange coupling between each pair of transition-metal ions present in the polynuclear complex to construct the full Hamiltonian matrix for the entire system.

To calculate the exchange coupling constants for any polynuclear complex with *n* different exchange constants, at least the energy of (*n* + 1) spin configurations must be calculated. For example, in the case of the studied dinuclear complexes, the exchange coupling value *J* can be obtained by taking into account the energy of two different spin distributions: triplet with $S = 1$, and singlet with $S = 0$.

The hybrid B3LYP functional[24] has been used in all calculations as implemented in *Gaussian 03* package,[25-28] The We have used the LanL2DZ basis set for Cu atoms and 6-

31g(d) basis set for the lighter atoms.[29] The calculations were performed on the complexes built from the experimental geometries.

2.2.2. Synthesis

Synthesis of $[Cu(H_2O)$ (2,2′-bpy)$(H_2L)]_2 \cdot H_4L \cdot 4H_2O$ (1) and $[\{Cu(H_2O)($ 2,2′-bpy$)(H_3L)\}_2(H_2L)] \cdot 2H_2O$ (2)

Compounds **1** and **2** are isolated from the same reaction mixture. To the mixture of $CuSO_4.5H_2O$ (0.086 g, 0.348 mmol), 2,2′-bpy (0.050 g, 0.320 mmol) and H_4L (0.109 g, 0.407 mmol), 10.0 mL of distilled water was added. The resulting reaction mixture was stirred for 3 h and transferred to 23 mL Teflon lined stainless vessel, sealed and heated at 150 °C for 72 h followed by cooling to room temperature over 48 h to obtain blue color needle shaped crystals of **1** and blue block crystals of **2** in the same reaction mixture. (Initial and final pH values are 1.9 and 2.1) Yield: ~10% for **1** and 40 % for **2** (based on Cu) Anal. Calcd. (%) for $C_{44}H_{60}Cu_2N_4O_{24}P_6$ (**1**) : C, 39.38; H, 4.50; N, 4.17. Found: C, 39.22; H, 4.03; N, 3.98 Anal. Calcd. (%) for $C_{44}H_{56}Cu_2N_4O_{22}P_6$ (**2**): C, 40.47; H, 4.32; N, 4.29. Found: C, 40.22; H, 4.05; N, 4.16. IR (KBr pellet, cm^{-1}) for compound **1**: 3414, 3250, 3423, 3059, 2341, 1660, 1604, 1510, 1473, 1448, 1267, 1143, 1033, 920, 765, 565, 420. IR (KBr pellet, cm^{-1}) for compound **2**: 3429, 2920, 1660, 1608, 1504, 1450, 1257, 1032, 765, 549, 470.

Synthesis of $[Cu(H_2O)$(1,10-phen)$(H_2L)]_2 \cdot 6H_2O$ (3)

The above mentioned synthetic procedure has been used to synthesize compound **3** using 1,10-phenanthroline (0.063 g, 0.318 mmol) instead of 2,2′-bpy to obtain blue block crystals (Initial and final pH values are 2.5 and 2.4. Yield: 65% (based on Cu). Anal. Calcd. (%) for $C_{40}H_{52}Cu_2N_4O_{20}P_4$: C, 41.42; H, 4.51; N, 4.83. Found: C, 41.22; H, 4.02; N, 4.38. IR (KBr pellet, cm^{-1}): 3470, 3080, 2918, 2361, 1655, 1581, 1518, 1429, 1261, 1147, 1047, 939, 852, 723, 561, 474, 424.

Synthesis of $[Cu(2,2'$-bpy$)(H_2L)]_n \cdot nH_2O$ (4)

A mixture of $CuSO_4 \cdot 5H_2O$ (0.088 g, 0.353 mmol), H_4L (0.110 g, 0.413 mmol) and 2,2'-bpy (0.038 0.248 mmol) was dissolved in 10.0 mL of distilled water. The pH of the reaction mixture was adjusted to 3.0 by addition of 5M NaOH solution. Consequently the resulting mixture was stirred for 30 min and transferred to a 23mL Teflon-lined stainless vessel, which was sealed and heated at 180 °C for 72 h and the reaction system was cooled to room temperature over 48 h to obtain green colored block crystals. Yield: 49% (based

on Cu) Anal. Calcd. (%) for $C_{18}H_{20}CuN_2O_7P_2$: C, 43.08; H, 4.01; N, 5.58. Found: C, 42.91; H, 3.22; N, 5.22. IR (KBr pellet, cm^{-1}): 3398, 2916, 2851, 1579, 1518, 1429, 1257, 1134, 1049, 939, 902, 854, 723, 553.

Synthesis of $[Cu(1,10\text{-phen})(H_2L)]_n \cdot 3nH_2O$ (5)

The same synthetic procedure as that of compound **4** was used to synthesize compound **5** using 1,10-phenanthroline (0.063 g, 0.318 mmol) instead of 2,2′-bpy and the pH of the reaction mixture was maintained 4.0. Yield: 69% (based on Cu) Anal. Calcd. (%) for $C_{20}H_{24}CuN_2O_9P_2$: C, 42.75; H, 4.30; N, 4.98. Found: C, 42.40; H, 3.83; N, 4.84 IR (KBr pellet, cm^{-1}): 3470, 3080, 2918, 2361, 1655, 1581, 1518, 1429, 1261, 1147, 1047, 939, 852, 723, 561, 474, 424

Synthesis of $[\{Cu(2,2'\text{-bpy})(MoO_3)\}_2(L)]_n \cdot 2nH_2O$ (6)

A Mixture of $CuSO_4 \cdot 5H_2O$ (0.087 g ,0.349 mmol), 2,2′-bpy (0.051 g, 0.320 mmol), $Na_2MoO_4 \cdot 2H_2O$ (0.105 g, 0.438 mmol) , H_4L (0.109 g, 0.407 mmol) and water (11.0 g , 612 mmol) were taken in 23ml Teflon lined autoclave , and the pH was adjusted to 6.10 by 5M HCl. The resulting mixture was stirred at room temperature for 60 min and heated at 180 ^oC for 72 h followed by cooling to room temperature over 48 h to obtain green block crystals (52 % yield based on Mo). Anal. Calcd. for (%) $C_{28}H_{28}Cu_2Mo_2N_4O_{14}P_2$: C, 32.79; H, 2.75; N, 5.46. Found: C, 32.42; H, 2.42; N, 5.27. IR (KBr pellet, cm^{-1}): 3454, 1643, 1601, 1493, 1469, 1444, 1309, 1165, 1051, 976, 883, 763, 729, 652, 551, 488, 410.

2.2.3. Single crystal X-ray structure determination of the compounds 1–6

Single-crystals suitable for structural determination of all the compounds (**1–6**) were mounted on a three circle Bruker SMARTAPEX CCD area detector system under Mo-Kα (λ=0.71073A) graphite monochromated X-ray beam, crystal to detector distance 60mm, and a collimator of 0.5 mm. The scans were recorded with an ω scan width of 0.3º. Data reduction performed by SAINTPLUS,[30a] empirical absorption corrections using equivalent reflections performed by program SADABS,[30b] structure solution using SHELXS-97[30c] and full-matrix least-squares refinement using SHELXL-97[30d] for above compounds. All the non-hydrogen atoms were refined anisotropically. Hydrogen atoms on the C atoms were introduced on calculated positions and were included in the refinement riding on their respective parent atoms. Attempts to locate the hydrogen atoms for the solvent water molecules in the crystal structure of compounds through Fourier electron density were failed. However, no attempts were made to fix these atoms on their parents. The hydrogen

atoms on some of the P–OH groups in the compounds are fixed by the proper HFIX commands and some are located by the Fourier electron density map. The oxygen atoms O6 and O5 of the terminal PO_3H groups in the compound **2** suffer significant disorder problem and they have been splitted over two positions after fixing their occupancies to 0.5 for each oxygen atom. Crystal data, structure refinement parameters for all the compounds (**1–6**) are summarized in Table 2.4.

2.3. Results and discussion

2.3.1. Synthesis

The title compounds **1**–**6** were synthesized by conventional hydrothermal technique. A systematic approach has been attempted by employing organic and inorganic ligands to understand the formation of Cu-dimer and extending its dimensionality. The reaction mixture of $CuSO_4 \cdot 5H_2O$ (0.349 mmol), 2,2′-bpy (0.320 mmol), H_4L (0.109 g, 0.407 mmol) in the ratio 1.09 : 1 : 1.16 with pH 1.90 at 150 °C results in the formation of compounds **1** and **2** in the product mixture. The yield of compound **1** is very low compared to that of **2** in the product mixture. Both the compounds **1** and **2** have identical chemical composition as far stoichiometric is concerned. The importance of copper-dimer formed in the **1** and the ambiguity in the formation of two compounds in the same reaction mixture leads us to carry out further reactions to understand the mechanism. H_4L can exists in different protonation states depending upon the pH of the reaction mixture (Scheme 2.1)

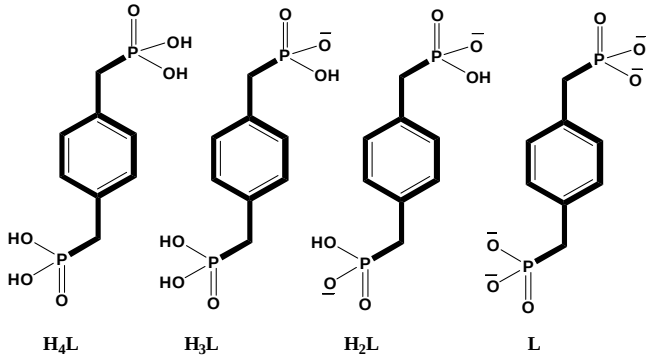

Scheme 2.1. Different protonation states of H_4L.

Different sets of reactions have been performed to obtain compound **1** as a major product in the product mixture. Initially, the temperature has been varied from 120 °C to 200 °C keeping concentration and time of reaction constant. At 120 °C, compound **1A** has been formed with composition $[Cu(2,2'\text{-bpy})(H_2O)_2(SO_4)]_n$, and in the temperature range 150

°C to 160 °C, we observe both the compounds **1** (minor product) and **2** (major product). The product mixture in this temperature range consists of blue needle shaped crystals of **1** and blue block crystals of **2** along with some unidentified blue powder. In the temperature range 160 °C to 200 °C, a pure crystalline form of compound **2** (in the form of large blue block crystals) was obtained. An attempt in obtaining compound **1** without neutral phosphonic acid (H_4L) as lattice component by decreasing the concentration of H_4L in the relevant synthesis, always result in the formation of **2** with low yield. By changing the concentration of the reactants and time of the reaction, the product mixture favors the formation of either **1A** or **2** in all the cases.

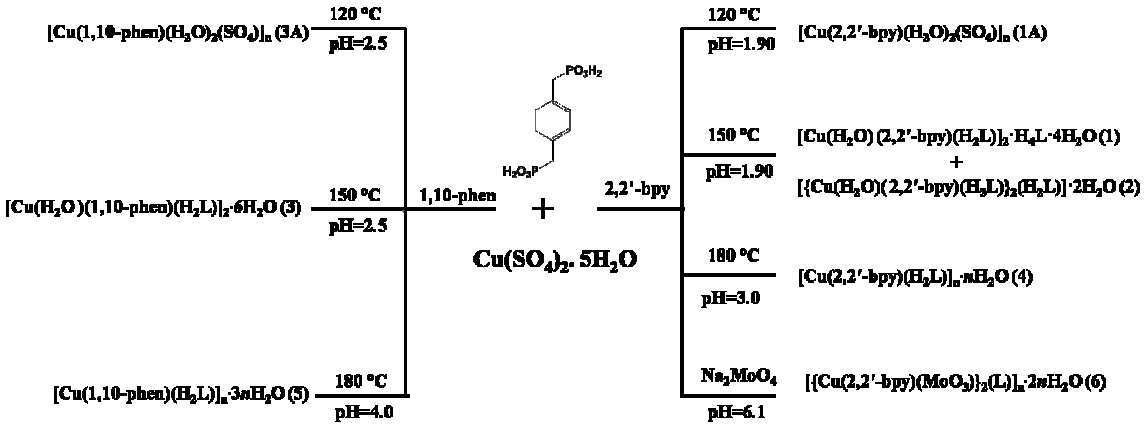

Scheme 2.2. Synthetic route for the formation of compounds presented in the study.

The results indicate that compound **1** is thermodynamically less stable than compound **2**; the detailed mechanism is discussed in the later sections. In order to stabilize the Cu-dimer core in **1**, a different set of reactions was performed by changing the pH of the reaction mixture and adding secondary reactants. Due to different possible degree of deprotonation, pH of the reaction mixture plays an important role in the self assembly process. The presence of H_4L, H_3L and H_2L ligands (see Scheme 2.1) in the crystal structures of compounds **1** and **2** indicates the partial deprotonation of the ligand at the pH 1.90. Increasing the pH of the reaction mixture from 1.90 to 3.0 by adding 5M NaOH and heating the reaction mixture at 180 °C results in the formation of 2D coordination polymer **4**. By adding sodium molybdate in the reaction mixture and adjusting the pH to 6.10 followed by heating the reaction mixture at 180 °C results in the 2D coordination polymer **6** with Cu-dimers extended by tetramolybdate subunits. Replacing the 2,2′-bpy with 1,10-phen in the reaction mixture, with initial pH 2.50 results in the formation of **3A** at 120 °C

and **3** at 150 °C and with higher pH (4.0) at 180 °C, affords a 2D coordination polymer **5**. The detailed synthesis has been described in the Scheme 2.2.

2.3.2. Description of crystal structures

Structural description of $[Cu(2,2'\text{-bpy})(H_2O)_2(SO_4)]_n$ (1A) and $[Cu(1,10\text{-phen})(H_2O)_2(SO_4)]_n$ (3A)

Both the compounds $[Cu(2,2'\text{-bpy})(H_2O)_2(SO_4)]_n$ (**1A**) and $[Cu(1,10\text{-phen})(H_2O)_2(SO_4)]_n$ (**3A**) are isostructural and crystallize in monoclinic space group *C*2/*c*. Both the compounds are synthesized by heating the reaction mixture of $CuSO_4{\cdot}5H_2O$, 2,2′-bpy or 1,10-phen, and H_4L in the ratio 1.09 : 1 : 1.16 at pH 1.90 and heated at 120 °C for 72 h. These two compounds are obtained in the process of studying the mechanism of formation of Cu-dimers. The coordination environment of metal center in both the compounds is octahedral in which two equatorial sites are occupied by the nitrogen atoms of the 2,2′-bipyridine and1,10-phenanthroline rings (respectively in **1A** and **3A**) and the remaining two sites are occupied by the water molecules, and the apical sites are occupied by the sulfate anion SO_4^{2-} (Figure 2.1a) .

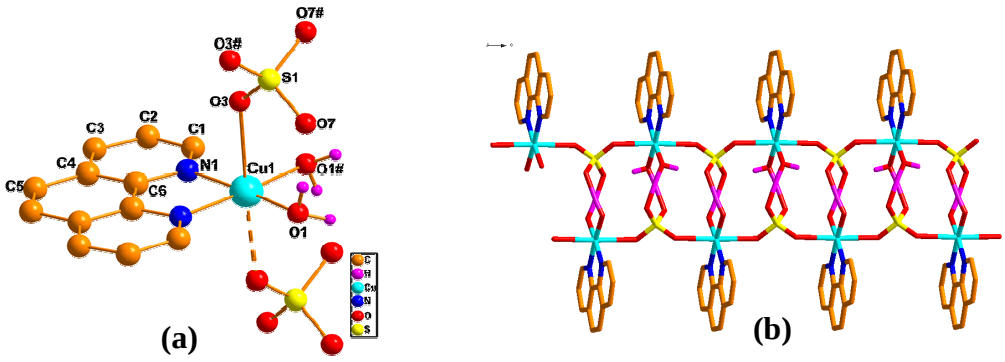

Figure 2.1. (a) Molecular diagram of the compound **3A**, (b) 1D tube formed through hydrogen bonding between two 1D chains by the coordinated aqua molecules.

The sulfate anion coordinates to the another adjacent $Cu(2,2'\text{-bpy})(H_2O)_2$ unit thereby forming a 1D coordination polymer. Two adjacent such chains are connected to each other by non covalent interactions involving the coordinated water molecules and sulfate anions to form 1D tube structure (Figure 2.1b). Compounds **1A** and **3A** are reported earlier in the literature.[31] But the compounds obtained by us crystallizes in different space groups apart from the reported. Crystallographic details of these compounds **1A** and **3A** are presented in the Supporting Information.

Structural description of $[Cu(H_2O)\ (2,2'\text{-bpy})(H_2L)]_2 \cdot H_4L \cdot 4H_2O$ (1)

Compound **1** is discrete copper dimer that crystallizes in triclinic space group *P*-1. The molecular structure consists of two square planar copper(II) ions bridged by two phosphonate oxygens (O2, O4) from two H_2L^{2-} ligands in the basal plane to form dimer; the rest coordination sites of each copper ion in the basal plane are occupied by two nitrogen atoms from 2,2′-bpy molecule. The apical position of each copper is accommodated by one aqua ligand. One neutral phosphonic acid (H_4L) and two water molecules remain in the lattice void per formula unit (Figure 2.2a). In the bridging region, one arm of each H_2L bridges two Cu ions through P=O and P–O^- groups to form a dimer leaving P–OH group in the interstitial position and the other arm remains uncoordinated to form a discrete compound. The distance between two copper metal centers in the dimer is 5.123 Å. The eight membered Cu-dimer can exist in ten canonical conformations, among which the dimer formed in this crystal structure (compound **1**) is confined to chair conformation. The assignment of P=O, P–O^- and P–OH bonds are consistent with the literature.[32]

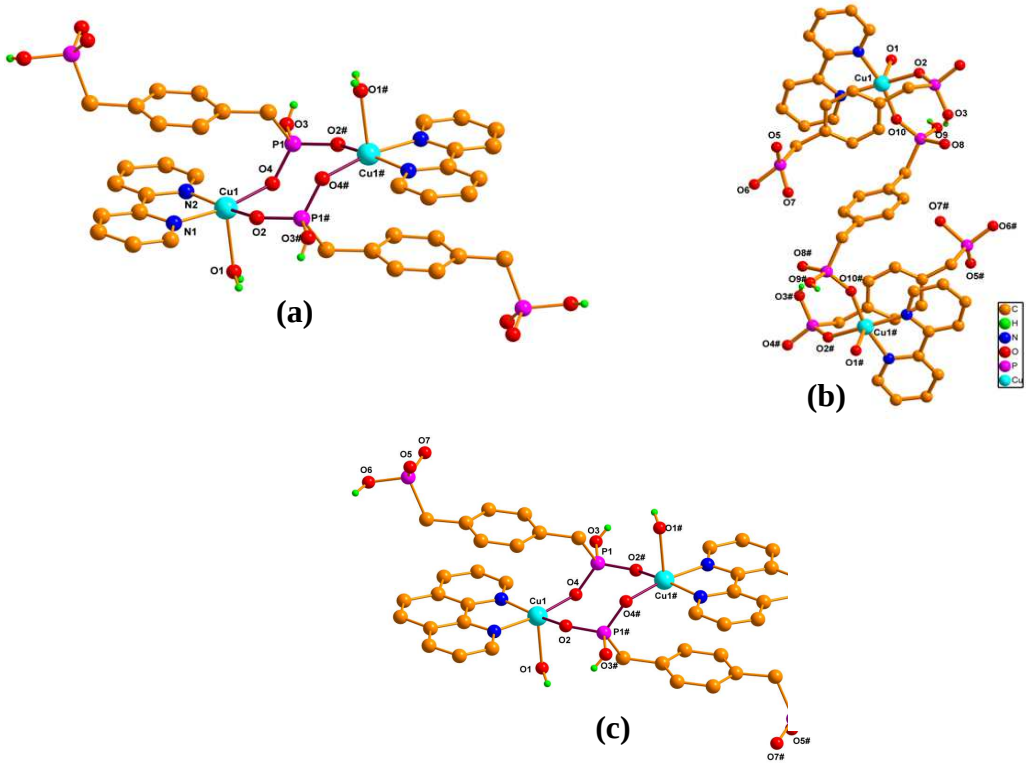

Figure 2.2. (a) Molecular diagram of the compound **1**; lattice H_4L component, has been removed for the clarity, (b) Molecular diagram of the compound **2**, (c) Molecular diagram of the compound **3**; Hydrogen atoms on the carbon atoms and lattice water molecules are removed for the clarity in all the molecular diagrams.

All these lattice phosphonic acids are present in *trans* conformation with antiperiplanar torsion angle of 180°. As anticipated, classical hydrogen bonding between lattice phosphonic acid P–OH group and dimer phosphonic acid P–OH group are observed with O···O separations varying from 2.474(4) to 3.024(6)Å. A 2D supramolecular network has been constructed by considering the interactions from the dimer in two directions. In this 2D arrangement, each dimer is linked to another dimer in the crystallographic *b* axis through the apical water molecule O1 and coordinated phosphonate oxygen atom O4 to form a ring $R^2_2(8)$ and extended to one dimensional chain. In another direction, each Cu-dimer is connected to another dimer through the P–OH groups of lattice H_4L ligand, lattice aqua ligand O12 and phosphonate oxygen atom O6 of H_2L in the crystallographic *a* axis to form a 10 membered ring $R^3_3(10)$. These two chains thread into each other to form a 2D supramolecular sheet as shown in the Figure 2.3a. The main focus of the article deals with the formation and stability of the Cu-dimer mentioned and extending its dimensionality (vide infra).

Table 2.1 Assignment of P–O bond lengths in the compounds **1** and **2.**

Coordination mode	**Compound 1 Cu dimer (Å)**	**Compound 2 Linear Cu chain (Å)**
	H_2L	**H_3L**
P1-O2	1.500(P=O)	1.517(P=O)
P1-O3	1.559(P−OH)	1.528(P−OH)
P1-O4	1.510($P-O^-$)	1.532(P−OH)
	H_2L	**H_3L**
P2-O5	1.513($P-O^-$)	
P2-O6	1.573(P−OH)	
P2-O7	1.496(P=O)	1.474(P=O)
	H_4L	**H_2L**
P3-O8	1.546(P−OH)	1.526($P-O^-$)
P3-O9	1.552(P−OH)	1.556(P−OH)
P3-O10	1.483(P=O)	1.492(P=O)

Structural description of $[\{Cu(H_2O)(2,2'\text{-bpy})(H_3L)\}_2(H_2L)]\cdot 2H_2O$ (2)

Compound **2** is a discrete linear copper dimer crystallizes in the monoclinic space group $P2_1/n$. The full molecule consists of two copper atoms chelated by two 2,2′-bpy rings coordinated to H_3L ligands and linked by the phosphonate oxygen atoms of H_2L ligand. The square pyramidal geometry of each Cu(II) in the dimer is furnished by the two

nitrogen atoms from the 2,2′-bpy ring, and two oxygen atoms (O10, O2) from the two different acid groups, one from the H_2L and other from the H_3L ligands respectively in the basal plane and one aqua ligand in the apical position. H_2L ligand links two $\{Cu(H_2O)($ 2,2′-bpy**)**$(H_3L)\}^+$ groups by using P=O coordination to the metal centre leaving two P–OH and $P–O^-$ groups in to the interstitial positions, with both arms of the ligand (Figure 2.2b). H_2L in the compound exists in μ_1-η_1, η_0, η_0 coordination mode on the both sides. In the same way two H_3L ligands attached to the metal polyhedra through P=O group with μ_1-η_1, η_0, η_0 coordination mode through the $–PO_3H_2$ arm and the $–PO_3H$ arm on other side remains uncoordinated. The assignment of the P–OH, $P–O^-$ and P=O bonds for the different protonation states of the H_4L are shown in the Table 2.1, that are consistent with the literature values.[32] A structural comparison between the compounds **1** and **2** reveals that the compound **1** is a eight membered dimer with H_4L as lattice component and **2** is a linear dimer and can be viewed as inclusion of lattice H_4L to the coordination matrix as H_2L.

Structural description of $[Cu(H_2O)(1,10\text{-phen})(H_2L)]_2\cdot 6H_2O$ (3)

Compound **3** is a discrete copper dimer crystallizing in triclinic space group *P*-1. The structure of copper dimer in the compound **3** is same as that in the compound **1** except that 2,2′-bipyridine is replaced by the 1,10-phenanthroline (Figure 2.2c). In compound **1** along with the dimer, a neutral H_4L ligand also present in the crystal structure which is absent in the case of compound **3.** The transformation of Cu-dimer to the linear chain is not observed in the case of **3** probably due to the absence of H_4L as a lattice component**.**

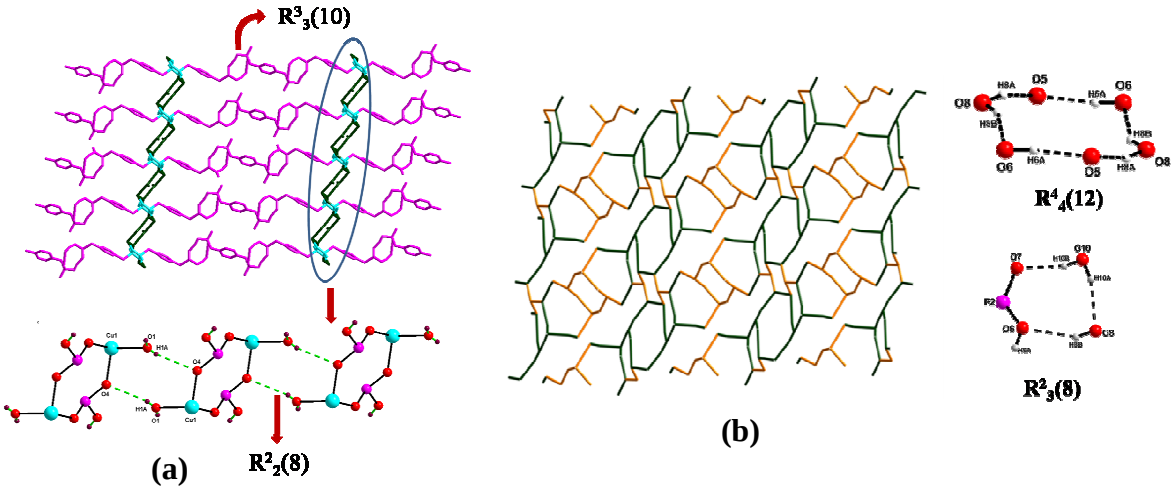

Figure 2.3. (a) 2D supramolecular network formed due to non covalent interactions between the P–OH groups of lattice H_4L, coordinated H_4L ligands and lattice aqua molecules in compound **1**, (b) 2D supramolecular network formed between six water molecules and P–OH groups of the coordinated H_4L ligands in compound **3**.

The presence of six lattice water molecules per formula unit of compound **3**, extensive non covalent interactions are observed in the crystal structure. The hydrogen bonding interactions between the lattice water molecules and the P–OH groups result in a 1D chainlike arrangement and these chains with aid of the copper dimers form a 2D supramolecular network as shown in the Figure 2.3b.

Structural description of $[Cu(2,2'\text{-bpy})(H_2L)]_n \cdot nH_2O$ (4)

Compound **4** is a two dimensional coordination polymer constructed from the copper dimers and crystallizes in triclinic space group *P*-1.

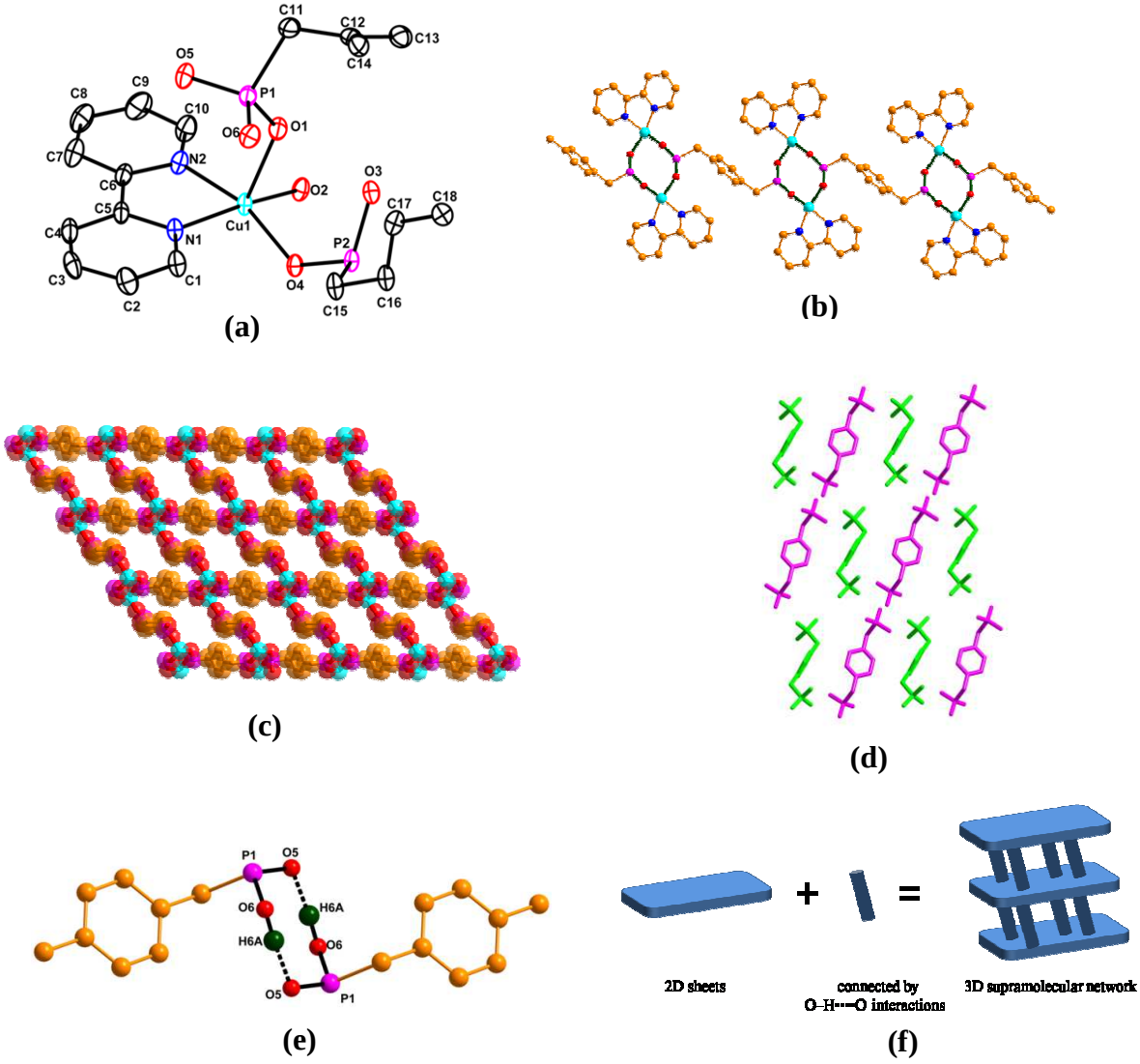

Figure 2.4. (a) ORTEP view of the basic unit of **4**. Hydrogen atoms and lattice water molecules have been removed for clarity. Thermal ellipsoids are at the 30% probability level, (b) One dimensional Cu-dimer chain running the crystallographic *c* axis, (c) (4, 4) connected 2D coordination polymer of **4**; Lattice water molecules in the void space are removed for clarity, (d) Packing diagram of the linking and bridging phosphonic acids; Green color represents bridging ligands and purple color represents linking ligands, (e) Non covalent interactions connecting the two layers, (f) Scheme representing the formation of 3D supramolecular network from the 2D sheets through O–H···O interactions.

The relevant asymmetric unit consists of one copper metal centre in square pyramidal geometry, chelated by 2,2′-bipyridine ring nitrogen atoms and coordinated to oxygen atoms of three different H_2L ligands (Figure 2.4a). The structure of copper dimer is same as explained in the compound **1** except the apical water molecule in the square pyramidal geometry is replaced by the oxygen atom of the H_2L ligand in compound **4**. Compound **4** can be described as the uncoordinated phosphonate arm ($–PO_3H$) of the copper dimer in the compound **1** coordinated to another dimer in the μ_2-η_1, η_1, η_0 coordination mode to form a one dimensional chain constituted by Cu-dimers bridged by H_2L ligands along crystallographic *c* axis (Figure 2.4b). These chains are linked by another H_2L ligand in μ_1-η_1, η_0, η_0 coordination mode resulting in the formation of a two-dimensional coordination polymer as shown in the Figure 2.4c.

In compound **4** two types of phosphonic acids which differs in the mode of the connectivity are involved *i.e* μ_2–H_2L bridges two Cu(II) ions to form 1D Cu-dimer chains and these chains are linked by the μ_1–H_2L ligand, the packing diagram of bridging and linking phosphonic acids is shown in the Figure 2.4d. Topologically the structure can be viewed as (4, 4) connected net with Cu-dimers as vertices and μ_2–H_2L, μ_1–H_2L as sides forming rectangular boxes with dimensions 11.73 x 11.30 Å, in which lattice water molecules are accommodated. Two lattice water molecules per one Cu-dimer are present in the crystal structure. These two lattice water molecules are situated in the middle of the rectangular box and exactly in the plane of two dimensional sheets. The distance between two layers viewed through the plane of phenyl group is 9.976 Å. Non covalent interactions between the lattice water molecules (O7, O7#) of one layer to another layer are absent in the crystal structure. But the two layers are connected to each other with non covalent interactions between the P–OH groups of the phosphonate arm in μ_1– H_2L ligand to form a 8-membered $R^2_2(8)$ ring thereby forming a 3D supramolecular network as shown in the Figures 2.4e & 2.4f.

Structural description of $[Cu(1,10\text{-phen})(H_2L)]_n \cdot 3nH_2O$ (5)

Compounds **4** and **5** are isostructural except 2,2′-bipyridine in compound **4** is replaced by 1,10-phenanthroline. Compound **5** also crystallizes in triclinic space group *P*-1 (Figure 2.5a). The coordination network and topological view of the **5** are similar to those explained in the compound **4**. The major difference between compounds **4** and **5** is number of lattice water molecules and their arrangement in respective void spaces. In compound **5,** six water molecules per Cu-dimer are presented in the void spaces created by the (4, 4)

connected layers (Figure 2.5b). An intricate hydrogen bonded network is formed between the lattice water molecules and deprotonated P–OH groups of the layers. To explain this hydrogen bonding, we consider six lattice water molecules in the rectangular void as a single domain (O7, O8, O9, O9#, O8#, O7#). The intramolecular hydrogen bonding in the domains are constituted between four lattice water molecules O8, O9, O9#, and O8# to form short chains. These chains with terminus O8 and O8# are connected to remaining lattice water molecules O7 and O7# in the domain through the phosphonate oxygen atoms O5 and O6 of the layer to form a long chain (Figure 2.5c). The long chains of the adjacent domains are connected to each other to form a one dimensional chain running through the crystallographic *c* axis. When viewed through the crystallographic *b* axis, the distance between two domains of different layers is 10.89 Å. Total number of lattice water molecules for one Cu-dimer are same in both discrete compound **3** and 2D coordination polymer **5**.

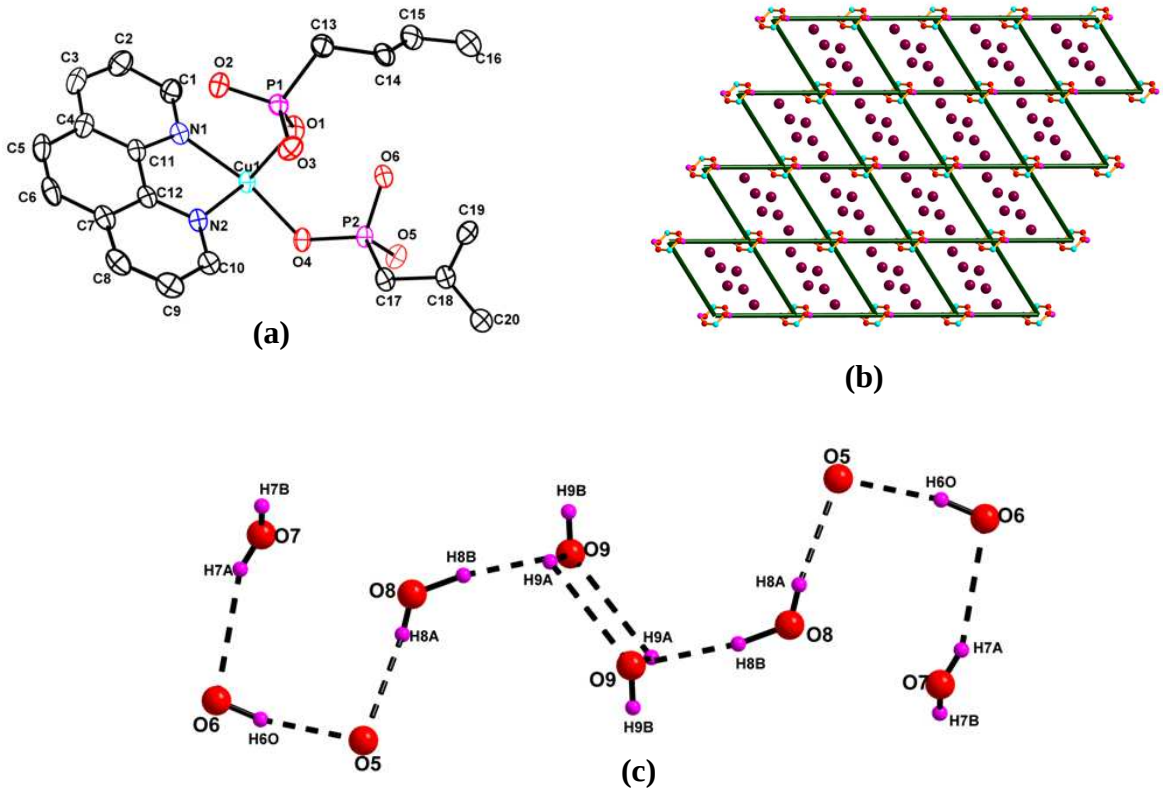

Figure 2.5. (a) ORTEP view of the basic unit of **5**. Hydrogen atoms and lattice water molecules have been removed for clarity. Thermal ellipsoids are at the 30% probability level, (b) (4,4) connected 2D coordination polymer of **5** representing the dimers as nodes and H_2L ligands as linkers and lattice water molecules in the void space, (c) Non covalent interactions between the lattice water molecules in the single layer.

As mentioned in the compound **4**, noncovalent interactions between the lattice water molecules of the two layers are absent, due to the large separation between the layers. But

these layers are connected by the P–OH groups of the phosphonate arm in μ_1–H_2L ligand to form a 8-membered $R^2_2(8)$ ring resulting in the formation of 3D supramolecular network.

Structural description of [{Cu(2,2′-bpy)(MoO_3)}$_2$(L)]$_n$·2*n*H_2O (6)

Compound **6** is a two dimensional coordination polymer constructed from the Cu dimers bridged by the ligand L and linked by Mo_4O_{12} subunits.

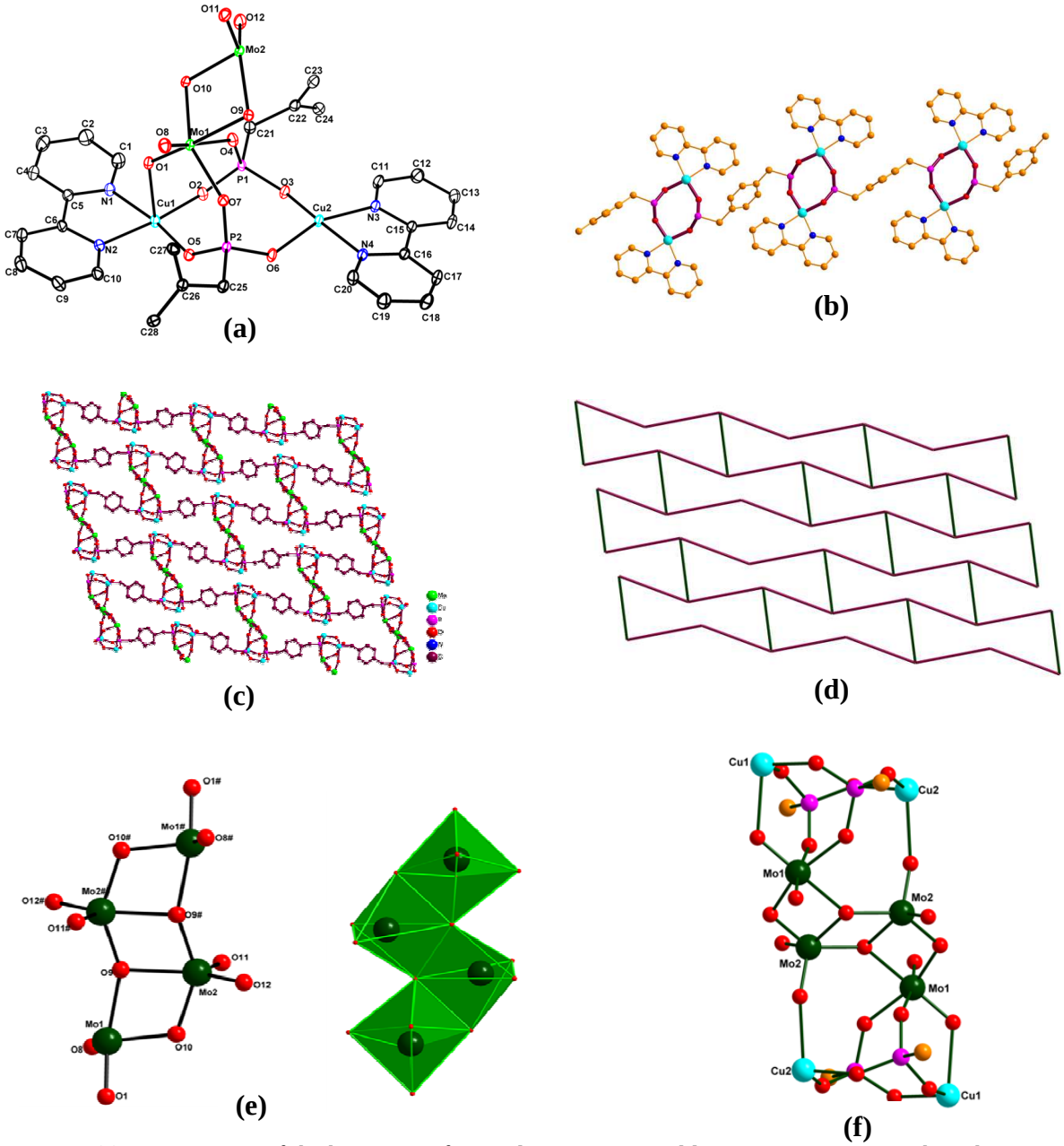

Figure 2.6. (a) ORTEP view of the basic unit of **6**. Hydrogen atoms and lattice water molecules have been removed for clarity. Thermal ellipsoids are at the 30% probability level, (b) 1D Cu-dimer chains formed by bridging H_2L ligand, (c) 2D coordination polymer of the compound **6** and its topological representation (green color line indicates the Mo_4O_{12} subunit), (d) Ball and stick and polyhedral representation of the Mo_4O_{12} subunit, (e) Figure showing the sandwiching of tetramolybdate between two Cu-dimers.

The asymmetric unit consists of two copper atoms chelated by two 2,2′-bipyridine rings, Mo_2O_3 subunit and one ligand L^{4-} bridging the Cu atoms and Mo_2O_3 subunit (Figure 2.6a) . The ligand H_4L is completely deprotonated and the three oxygen atoms of the each arm ($–CH_2–PO_3^{2-}$) connected to metal centers in $\mu_3–\eta_1$, η_1, η_1 bridging mode in which two oxygen atoms bridges two Cu metal centers and the remaining one oxygen atom connected to Mo metal center. Two L^{4-} ligands bridges the two Cu metal centers to form 8-membered ring and these rings are extended through the *p*-xylyl linkers to form a 1D Cu-dimer chain as shown in the Figure 2.6b. These 1D chains are linked by the inorganic linker Mo_4O_{12} to form (4, 4) connected 2D coordination polymer as shown in the Figure 2.6c, unlike in compounds **4** and **5**, in which 1D chains are linked by organic linker H_2L. Mo_4O_{12} subunit comprises of edge sharing two MoO_6 and two MoO_5 polyhedra with four μ_2–bridging oxygen atoms and eight terminal oxygen atoms (Figure 2.6d).

Each Mo_4O_{12} subunit is connected to two Cu-dimers from the opposite 1D chain by coordinating to the apical site of the Cu–metal polyhedra through terminal oxygen atoms with a separation of 12.54 Å between the two 1D chains. Also the oxygen atom which remains left in the phosphonate group after forming the Cu-dimer is coordinated to the Mo–polyhedra. The μ_3 coordination of the phosphonate groups apart from the classical μ_2 coordination (which was observed in the compounds **1**, **3**, **4** and **5**) results in the crown conformation of the 8–membered ring apart from the chair conformation. The neutral tetramolybdate is sandwiched between the two 1D Cu-dimer chains with Cu–O and Mo–O bonds as pillars to form a 2D coordination polymer as shown in the Figure 2.6e. Two lattice water molecules per Cu-dimer are located in the void spaces in the (4,4) connected network. Jubieta et al. reported a 3D compound $[\{Cu(bpy)\}_2Mo_4O_{10}(O_3PCH_2C_6H_4CH_2PO_3)_2]$ starting from the molybdenum oxide in which $\{Mo_4O_{10}(O_3PR)_4\}_n^{4n-}$ chains decorated with$\{Cu(bpy)\}^{2+}$subunits and linked through the *p*-xylyl tethers of the diphosphonate ligand into a framework architecture.[33]

2.3.3. Understanding the formation of copper dimer and extending its dimensionality by organic and inorganic linkers

As discussed in the section of synthesis, the serendipitous identification of compound **1** as minor product along with compound **2** has prompted us to study the mechanism of formation of the dimer and its stability in the coordination matrix. Temperature plays an important role in the nucleation process under hydrothermal conditions. In the reaction mixture of $CuSO_4{\cdot}5H_2O$, 2,2′-bpy and H_4L, copper sulfate pentahydrate remains

presumably in the form of $[Cu(H_2O)_n]^{2+}$ counter balanced by sulfate anion. At low temperature, 2,2′-bipyridine ligand chelates the Cu metal centre to form $[Cu(2,2'\text{-}bpy)(H_2O)_{n-2}]^{2+}$ complex by replacing the two water molecules in the equatorial positions. The apical water molecule of the Cu metal polyhedron are replaced by the sulfate anion to form a one dimensional coordination polymer $[Cu(2,2'\text{-}bpy)(H_2O)_2(SO_4)]_n$ (**1A**). Due to 1:1 ratio of $CuSO_4{\cdot}5H_2O$ and 2,2′-bpy, only two equatorial coordination sites are chelated by the bipyridine ring. The non participation of the H_4L in the complex **1A** is probably due to low solubility of phosphonic acid at a low temperature. As the temperature increases the solubility of the phosphonic acid increases and participate in the nucleation process and in the temperature region 150 °C to 160 °C, it gives two compounds **1** and **2**, among which in compound **1** phosphonic acid (H_2L) bridges the two $[Cu(2,2'\text{-}bpy)]^{2+}$ units to form a dimer $[Cu(H_2O)(2,2'\text{-}bpy)(H_2L)]_2$ (**1**) along with one neutral H_4L ligand as a lattice component. In compound **2**, H_2L links two $[Cu(2,2'\text{-}bpy)(H_3L)]^{1+}$ units to form a linear chain of composition $[\{Cu(H_2O)(2,2'\text{-}bpy)(H_3L)\}_2(H_2L)]{\cdot}2H_2O$ (**2**). The yield of the dimeric compound **1** is very less in comparison to compound **2**. The attempts to isolate the compound **1** as a single product were unsuccessful, even by varying all the possible parameters (see synthesis section). These reactions suggest that the chainlike form in the compound **2** is thermodynamically more stable compared to the dimeric form along with lattice H_4L in compound **1**. When the temperature is increased from 150 °C to 200 °C, the yield of **2** increases and in the temperature in region 170 °C to 200 °C only compound **2** is formed as pure block crystals. The crystallization of compound **1** was observed in the temperature range 150 °C to 160 °C.

Table 2.2. Protonation states of the H_4L with pH value of the reaction mixture and secondary linker in the compounds **1**–**6**.

C.No.	Secondary Linker	pH	State of Phosphonic acid
1	2,2′-bpy	1.90	H_4L,H_2L
2	2,2′-bpy	1.90	H_3L, H_2L
3	1,10-phen	2.5	H_2L
4	2,2′-bpy	3.0	H_2L
5	1,10-phen	4.0	H_2L
6	2,2′-bpy	6.1	L

The initial acidic pH (1.90) of the reaction mixture is responsible for the existence of protonated form (H_4L) of the ligand as a lattice component. As shown in scheme 2.3, the phosphonic acid H_4L (shown in red), that remains as a lattice component in **1**, undergoes deprotonation resulting in H_2L which bridges two copper centers in compound **2**. The coordinated / deprotonated H_2L, present in compound **1**, gets protonated to H_3L in the formation of **2**. The compound **1** can be considered as an intermediate in the formation of compound **2** since both have identical chemical compositions and also compound **1** could not be isolated at higher temperature indicating it to be thermodynamically a less stable phase at higher temperature. Detailed mechanisms for the formation of compounds **1** and **2** are given in the following equations.

$$CuSO_4.5H_2O + 2,2'\text{-bpy} + H_4L \xrightarrow[pH=1.90]{180\ ^oC} [Cu(2,2'\text{-bpy})(H_3L)(H_2L)]_2\cdot 2H_2O \quad (2)$$

$$CuSO_4.5H_2O \xrightarrow{H_2O} [Cu(H_2O)_6]^{2+}\ SO_4^{2-}$$

$$[Cu(H_2O)_6]^{2+}\ SO_4^{2-} + 2,2'\text{-bpy} \xrightarrow{120\ ^oC} [Cu(2,2'\text{-bpy})(H_2O)_2SO_4]_n \quad (1A)$$

$$[Cu(2,2'\text{-bpy})(H_2O)_2SO_4]_n + H_4L \xrightarrow[pH=1.90]{150\ ^oC} [Cu(2,2'\text{-bpy})(H_2L)]_2\cdot H_4L\cdot 4H_2O \quad (1) + [Cu(2,2'\text{-bpy})(H_3L)(H_2L)]_2\cdot 2H_2O \quad (2)$$

$$[Cu(2,2'\text{-bpy})(H_2O)_2SO_4]_n + H_4L \xrightarrow[pH=1.90]{180\ ^oC} [Cu(2,2'\text{-bpy})(H_3L)(H_2L)]_2\cdot 2H_2O \quad (2)$$

The compound **3** was isolated by employing 1,10-phenanthroline as co-ligand and the single crystal X-ray analysis of compound **3** reveals the presence of Cu-dimeric unit similar to that found in compound **1**. The compound **3** was obtained as single major product in the temperature region of 150 °C to 180 °C. Compound **3** was also formed starting from the **3A** as explained in the case of **1**.

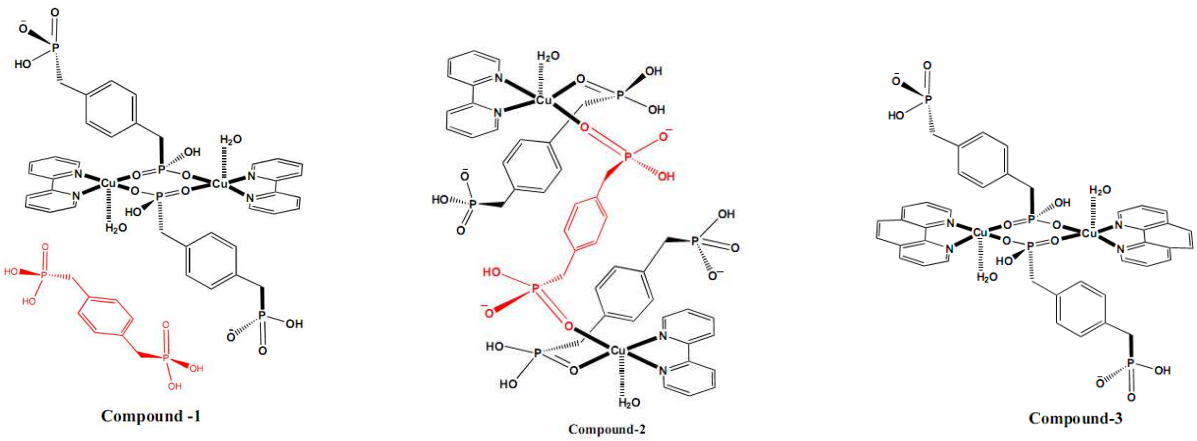

Scheme 2.3. Schematic representation of molecular compounds **1**-**3**.

The stability of compound **3** in comparison to compound **1** can be attributed to the absence of lattice H_4L ligand**.** The initial pH of the reaction mixture in the formation of compound **3** was 2.50 in comparison to the pH of 1.90 in the synthesis of 2,2′-bpy system. The relatively higher pH of the reaction mixture in the synthesis of phenanthroline system might not favor the stabilization of H_4L and H_3L that are found in compounds **1** and **2**. The pH variation caused by the replacement of 2,2′-bpy with 1,10-phenanthroline co-ligand limits the deprotonation to H_2L thereby forming the dimeric compound **3**.

$$[Cu(H_2O)_6]^{2+}SO_4^{2-} + \text{1,10-phen} \xrightarrow[pH=2.5]{120\ ^oC} [Cu(\text{1,10-phen})(H_2O)_2SO_4]_n \quad (3A)$$

$$[Cu(\text{1,10phen})(H_2O)_2SO_4]_n + H_4L \xrightarrow[pH=2.5]{150\ ^oC} [Cu(H_2O)(\text{1,10-phen})(H_2L)]_2\cdot 6H_2O \quad (3)$$

The O–P–O bridging in Cu-dimeric unit in compounds **1** and **3** is known to transmit weak to moderately strong anti-ferromagnetic and ferromagnetic exchange interactions efficiently between the two copper (II) ions. The extended structures with higher dimensionality, based on copper phosphonic acid dimeric systems, have been isolated at relatively higher pH as compounds **4** and **5** (shown below). These two compounds represent the extension of the Cu-dimers by organic linkers. A temperature dependent hydrothermal synthesis reveals

$$CuSO_4.5H_2O + \text{2,2'-bpy} + H_4L \xrightarrow[pH=3.0]{180\ ^oC} [Cu(\text{2,2'-bpy})H_2L]_n\cdot nH_2O \ (4)$$

$$CuSO_4.5H_2O + \text{1,10-phen} + H_4L \xrightarrow[pH=4.0]{180\ ^oC} [Cu(\text{1,10-phen})H_2L]_n\cdot 3nH_2O \ (5)$$

that compounds **4** and **5** are also formed starting from the **1A** and **3A** respectively. Further investigations to obtain higher dimensional Cu-dimer systems, we have employed molybdate based inorganic linker. Sodium molybdate undergoes hydrolysis to form molybdates of different nuclearities such as MoO_4^{2-}, $Mo_2O_7^{2-}$, Mo_2O_3, Mo_4O_{12}, $Mo_8O_{26}^{4-}$ etc.[34] depending on the pH of the reaction mixture and geometry of available coordination sites of the secondary metal etc. The tetramolybdate Mo_4O_{12}, formed from the MoO_4^{2-}, extends the dimensionality of Cu-dimer to 2D coordination polymer. The Cu···Cu separation is found to be 12.54 Å in compound **6** (tetramolybdate is the linker) and that found in compounds **4** and **5** is 12.93 Å (H_2L as a linker) (Figure 2.7).

$$CuSO_4.5H_2O + 2,2'\text{-bpy} + Na_2MoO_4 + H_4L \xrightarrow[pH=6.1]{180\ ^oC} [\{Cu(2,2'\text{-bpy})(MoO_3)\}_2(L)]_n \cdot 2nH_2O\ (6)$$

$$Na_2MoO_4 \xrightarrow{H_2O} MoO_4^{2-} + 2Na^+$$

$$4MoO_4^{2-} + 8H^+ \longrightarrow Mo_4O_{12} + 4H_2O$$

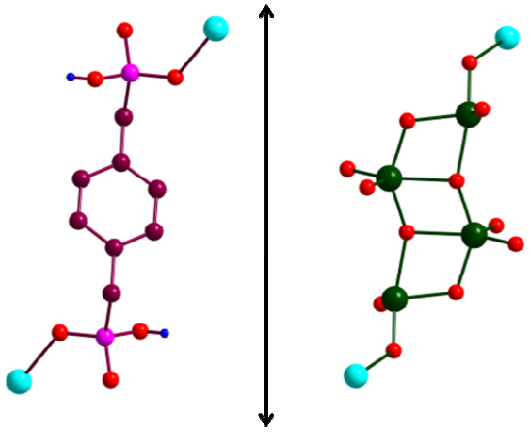

Figure 2.7. Length of the H_2L and Mo_4O_{12} subunits connecting the Cu-dimer chains.

The overall synthetic procedures for the formation compounds **1**–**6** representing the reaction parameters and conditions are shown in the Scheme 2.4. The detailed protonation states of the phosphonic acid along with the secondary linkers are shown in the Table 2.2.

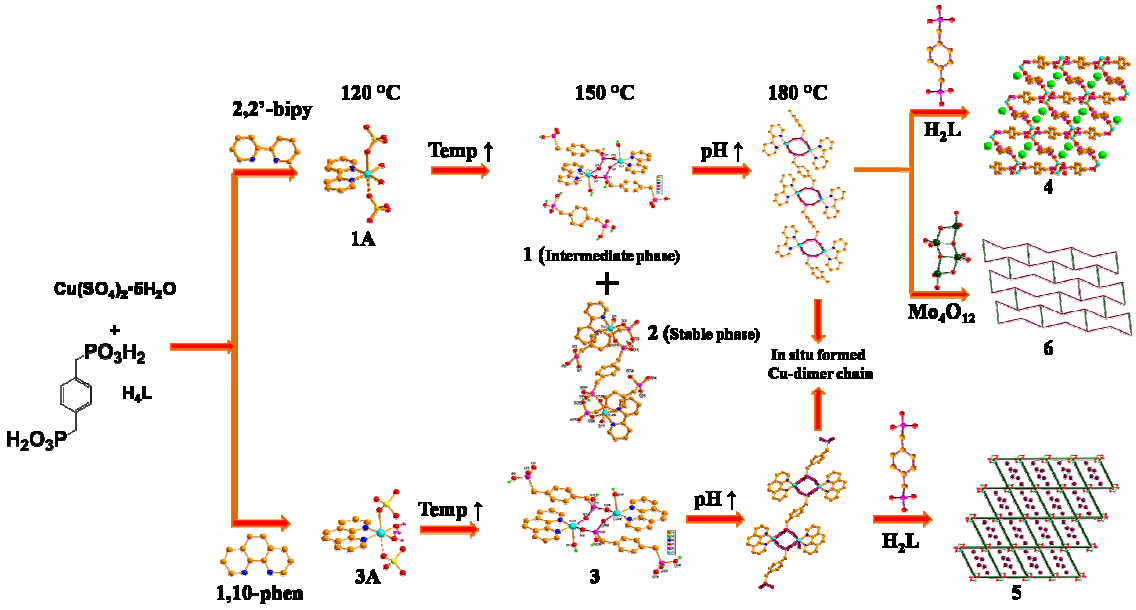

Scheme 2.4. Systematic schematic representation of formation of compounds **1**−**6**.

2.3.4. Thermogravimetric studies

TGA studies were carried out under flow of N_2 for crystalline compounds **2–6** in the temperature range 30–1000 °C. Compound **2** shows a continuous weight loss of 4.92 % (calcd, 5.5%) from the room temperature to 190 °C followed by decomposition in two steps with a residual mass of 32 %. Compound **3** shows a weight loss of 10.21% at 170 °C corresponding to the loss of six water molecules (calcd, 12.41%) and the dimeric components remains stable up to 270 °C. Compound **3** decomposes in two steps at the temperatures greater than 270 °C leaving behind the final residue of 40%. Compound **4** remains exceptionally stable up to 330 °C with weight loss 4.02 % (calcd, 3.5 %) corresponding to the two lattice water molecules and decomposition took place in two steps leaving residue of 27.4 %. The compound **5** contains six lattice water molecules and these water molecules lost at 120 °C with weight loss of 8.02% (calcd, 9.62 %) and the relevant structure remains stable up to 325 °C. In the first step of its decomposition, the xylylene moieties come out with weight loss of 19.84 % (calcd, 18.89 %) in the temperature range of 326 °C to 512 °C. In the second step, 1,10-phenanthroline moieties are eliminated in the temperature range of 520 °C to 1050 °C leaving a residue of 37.3%.

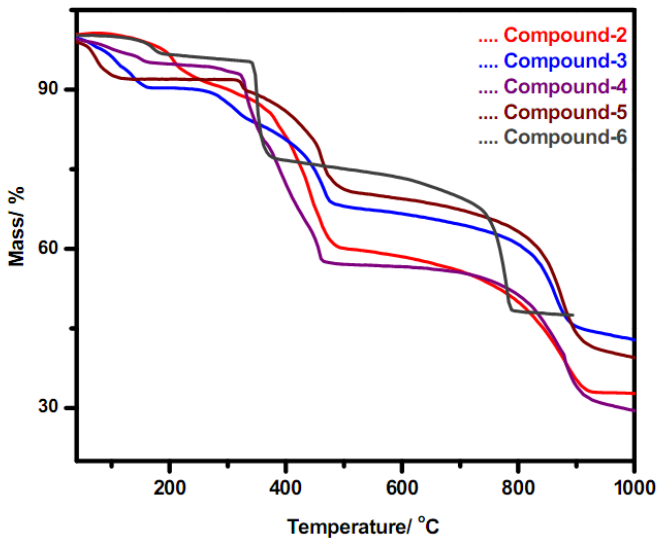

Figure 2.8. Thermogravimetric curves of the compounds **2–6.**

The final product is estimated to be $Cu(PO_3)_2$ with formula weight of 221.49 (39.2 %). The thermogravimetric study of compound **5** reveals that the decomposition pattern follows the initial dehydration of lattice water molecules followed by the pyrolysis of organic units, leaving end product $Cu(PO_3)_2$. Compound **6** shows thermal stability up to

340 °C with initial dehydration of two water molecules of crystallization. The pyrolysis of organic units starts in the region of 350 °C to 800 °C leaving the final residue of 47.40 % which is supposed to be $CuMoO_4$, MoO_3, P_2O_5.[35] The overall process of decomposition of **6** is consistent with the following equations. Thermogravimetric curves of the compounds are shown in the Figure 2.8.

$$[\{Cu(2,2'\text{-bpy})(MoO_3)\}_2(L)]\cdot 2H_2O \xrightarrow{30-180\ ^oC} [\{Cu(2,2'\text{-bpy})(MoO_3)\}_2(L)] + 2H_2O$$

$$[\{Cu(2,2'\text{-bpy})(MoO_3)\}_2(L)] + 44\ O_2 \xrightarrow{350-800\ ^oC} CuMoO_4 + MoO_3 + P_2O_5 + 28CO_2 + 4NO_2 + 12\ H_2O$$

2.3.5. PXRD Studies

To ensure the phase purity of the products, X-ray powder diffraction studies for all the compounds have been performed and compared to the simulated diffraction patterns obtained from single crystal X-ray analysis.

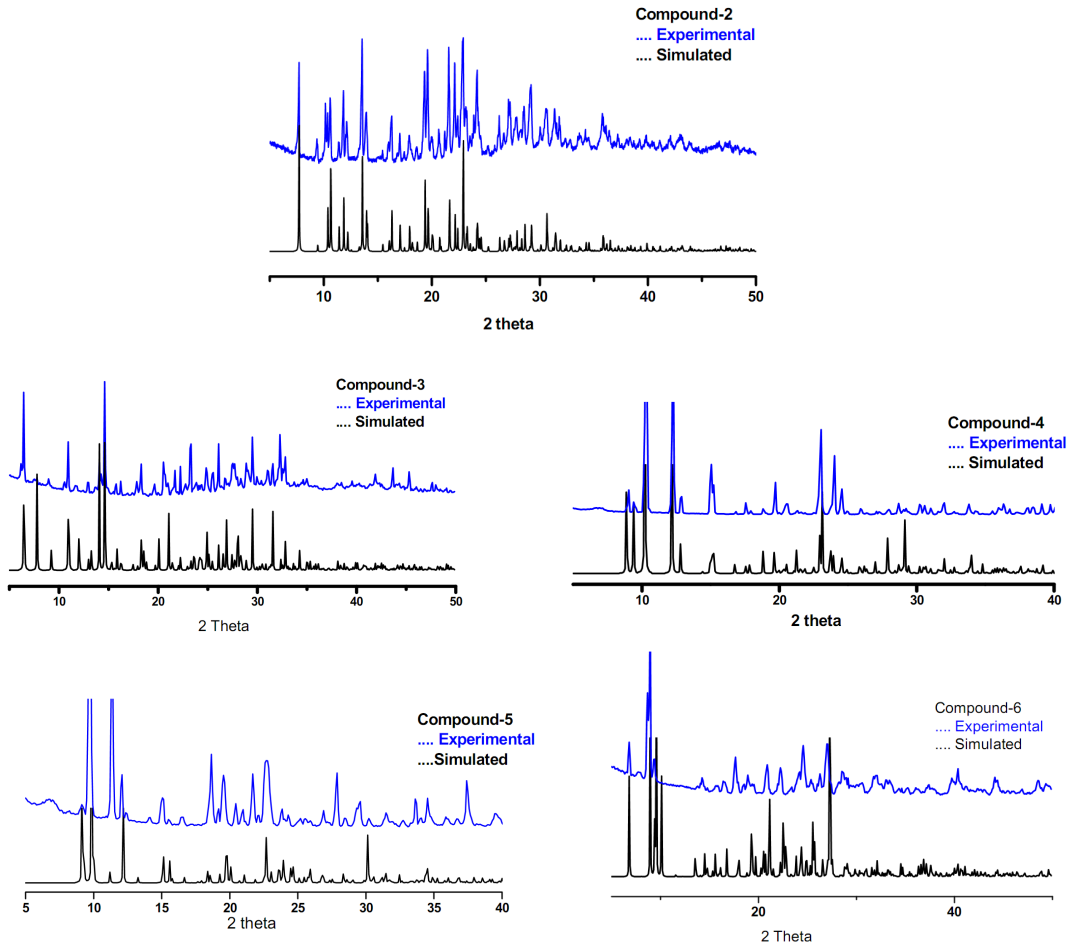

Figure 2.9. Powder X-ray patterns of the compounds **2**–**6**.

The similarity between observed and simulated patterns proves the bulk homogeneity of the crystalline solids (Figure 2.9). Although the experimental patterns have a very few un-indexed diffraction peaks and some are slightly broadened and shifted in comparison to those simulated from the single-crystal data, it can still be regarded that the bulk synthesized materials have homogenous phase.

2.3.6. Variable temperature PXRD studies

The TGA studies show that all the compounds are stable up to 300 to 350 °C. Variable temperature PXRD studies have been performed to ensure the stability of the frameworks of compounds **4** and **5** after the removal of lattice water molecules. The PXRD patterns of the dehydrated frameworks at different temperatures show sharp peaks with almost same Bragg intensity. Some differences in the intensities of the reflections are observed at relatively higher temperatures due to the gradual loss of solvent water molecules. The TGA curve of compound **4** shows loss of lattice water molecules taking place at 170 °C. The VT-PXRD graphs of compound **4** are similar to the simulated pattern up to 130 °C and at 150 °C a new peak is observed in the region of 11.46° along with all the peaks displayed in simulated pattern. At 170 °C, the intensity of the peak at 11.46° increases and the intensity of the peak corresponding to the reflection (1–10) at 12.35° is decreased and at 190 °C there is no peak corresponding to the (1-10) reflection. The slight shifting of the peak corresponding to the reflection (1-10) from 12.35° to 11.46° in the temperature region 150 °C to 190 °C indicates the expansion of the coordination network after losing the lattice water molecules. The powder pattern displayed at 190 °C is stable up to temperature 310 °C. This data indicates that crystals of coordination polymer **4** exhibit breathing-like behavior and the breathing starts at 150 °C. The dehydrated form of compound **4**, obtained by heating up to 170 °C, on exposure to the open atmosphere / water vapor at room temperature for 48 hrs results in the regeneration of original compound **4**. The regenerated PXRD pattern of the compound **4** shows similar peaks but the broadening of the peaks indicates the loss of crystallinity at higher temperatures (Figure 2.10).

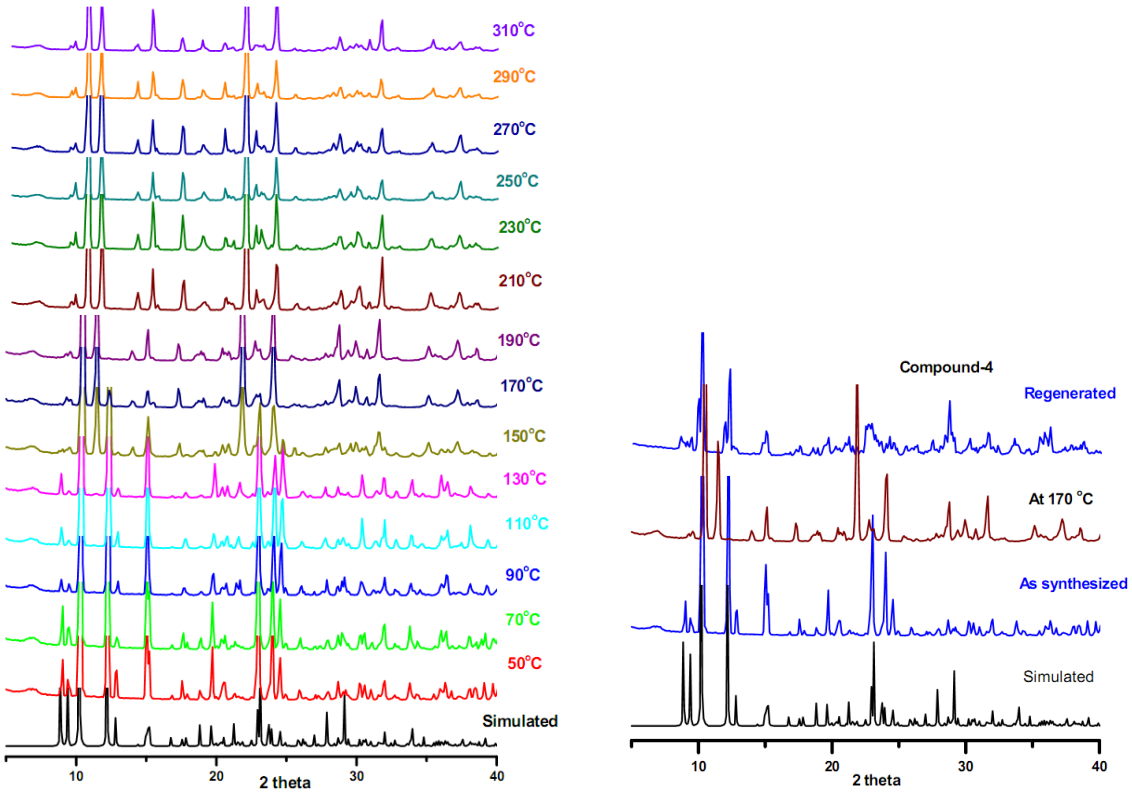

Figure 2.10. Variable temperature and regenerated PXRD patterns of compound **4**.

In compound **5**, lattice water molecules depart from the crystal in the temperature range of room temperature to 100 °C. The VT–PXRD pattern shows similar peaks displayed in the simulated pattern up to 310 °C with slight broadening of peak positions and difference in the intensity of the peaks is due to loosely held water molecules in the lattice voids. The only major difference is the intensity of the peak corresponding to the reflection (1-10), which is decreased to a little extent at 50 °C and not at all appeared in the temperature range 70 °C to 310 °C. Unlike in compound **4,** no major shift of the peaks to the lower 2θ values are not observed in compound **5**. But when the dehydrated sample (obtained by heating at 70 °C) is taken and exposed to open atmosphere/water vapor at room temperature, it results in the incorporation of the lattice water molecules into the void spaces. An attempt to study the dehydration-rehydration cycle through single crystal to single crystal transformation was not successful due to the cracking of the crystals on heating. The results indicate that the compounds **4** and **5** have potential to perform host-guest chemistry in the lattice voids. The relevant PXRD patterns (dehydration / rehydration) for compound **5** is shown in Figure 2.11.

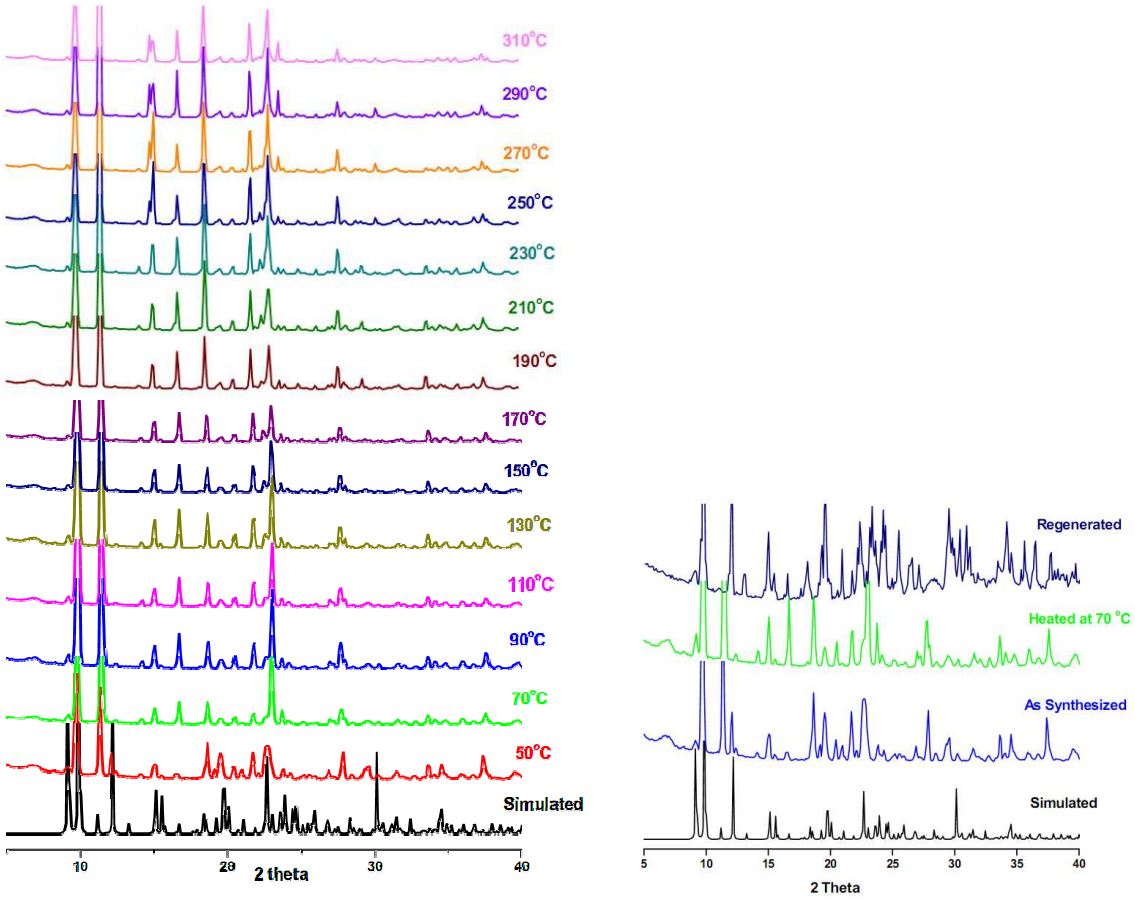

Figure 2.11. Variable temperature and regenerated PXRD patterns of compound **5**.

2.3.7. Magnetic Behavior

Compound 3

Variable temperature magnetic susceptibility measurements of a polycrystalline sample **3** have been performed at 2000 Oe between 2 K and 300 K. The data are presented as a χ_M *vs T* and $\chi_M T$ *vs T* plots in Figure 2.12a (where χ_M is the molar magnetic susceptibility per Cu^{II}_2 unit). The room temperature (300K) $\chi_M T$ product amounts to 0.78 cm^3 K mol^{-1}, which is in agreement with two uncoupled *S*=1/2 Cu(II) spins with unquenched orbital momentum ($\chi_M T$ = 0.375 cm^3 K mol^{-1} for a *S* = 1/2 ion). As the temperature is lowered, the $\chi_M T$ value continuously decreases to 0.68 cm^3 K mol^{-1} at 65 K and then sharply decreases up to 2 K reaching a minimum value of 0.01 cm^3 K $mol^{-1.}$ The $1/\chi_M$ *vs T* plot above the 50 K follows the Curie-Weiss law with negative Weiss constant θ = –16.7 K. This magnetic behavior is generally observed for complexes that possess an intra-complex antiferromagnetic interaction. The magnetic interaction through the –O–P–O– bridges between two Cu(II) centers leads to a *S*=0 ground state. A simple reasonable fit can be

obtained for interacting dinuclear unit with conventional Hamiltonian: $H=-JS_1 \bullet S_2$ (where S_1 and S_2 are the spin operators with $S_1=S_2=1/2$). Introducing an inter-cluster zJ' term, the analysis of experimental values has been performed by the following expression:

$$\chi_M = \chi_M'/\{1-\chi_M'(2zJ'/Ng^2\beta^2)\}$$

$$\text{where } \chi_M' = 2Ng^2\beta^2/kT[3+exp(-J/kT)]$$

The values giving the best fit are J= –36.44(1) cm^{-1}, zJ'=+3.99(3) cm^{-1} and g=2.100(4) [R= 3.2 X 10^{-4}].

Compound 4

Compound **4** is 2D coordination polymer constituted by Cu dimers bridged by phosphonic acid as the nodes and *p*-xylylenediphosphonic acid as linker. The main structural difference between the discrete dimer (e.g., compounds **1** and 3) and the dimer present in coordination polymer **4** can be described by the apical site, which, in the discrete dimer, is occupied by the oxygen atom from the aqua ligand and in coordination (polymer) dimer, is coordinated by phosphonate oxygen. Figure 2.12b shows the temperature dependence of χM and $\chi_M T$ values for compound **4.** The room temperature $\chi_M T$= 1.03 cm^3 K mol^{-1} is higher than the expected value for two uncoupled Cu^{II} ions. The $\chi_M T$ value gradually decreases upon cooling and reaches a minimum value 0.63 cm^3 K mol^{-1} at 18 K and sharply decreases to 0.27 cm^3 K mol^{-1} at 2 K. The $1/\chi_M$ *vs T* plot above the 30 K follows the Curie–Weiss law with negative Weiss constant with θ= –18.1 K. The nature of the $\chi_M T$ *vs T* plot and the negative Weiss constant suggest a dominant antiferromagnetic exchange between the two Cu^{II} ions through the –O–P–O– bridges. The susceptibility data analyzed by the expression, described above, gives the best fit parameters, J= –3.03(2) cm^{-1}, zJ'= –0.88(5) cm^{-1} and g=1.961(5) with an agreement factor R= 7.2 X 10^{-6}, where $R=\Sigma[(\chi_M T)_{exp}-(\chi_M T)_{cal}]^2/\ \Sigma(\chi_M T)_{exp}^2$. From the values, obtained, the magnitude of exchange has been decreased in the case of dimer found in coordination polymer compared to that in discrete dimer.

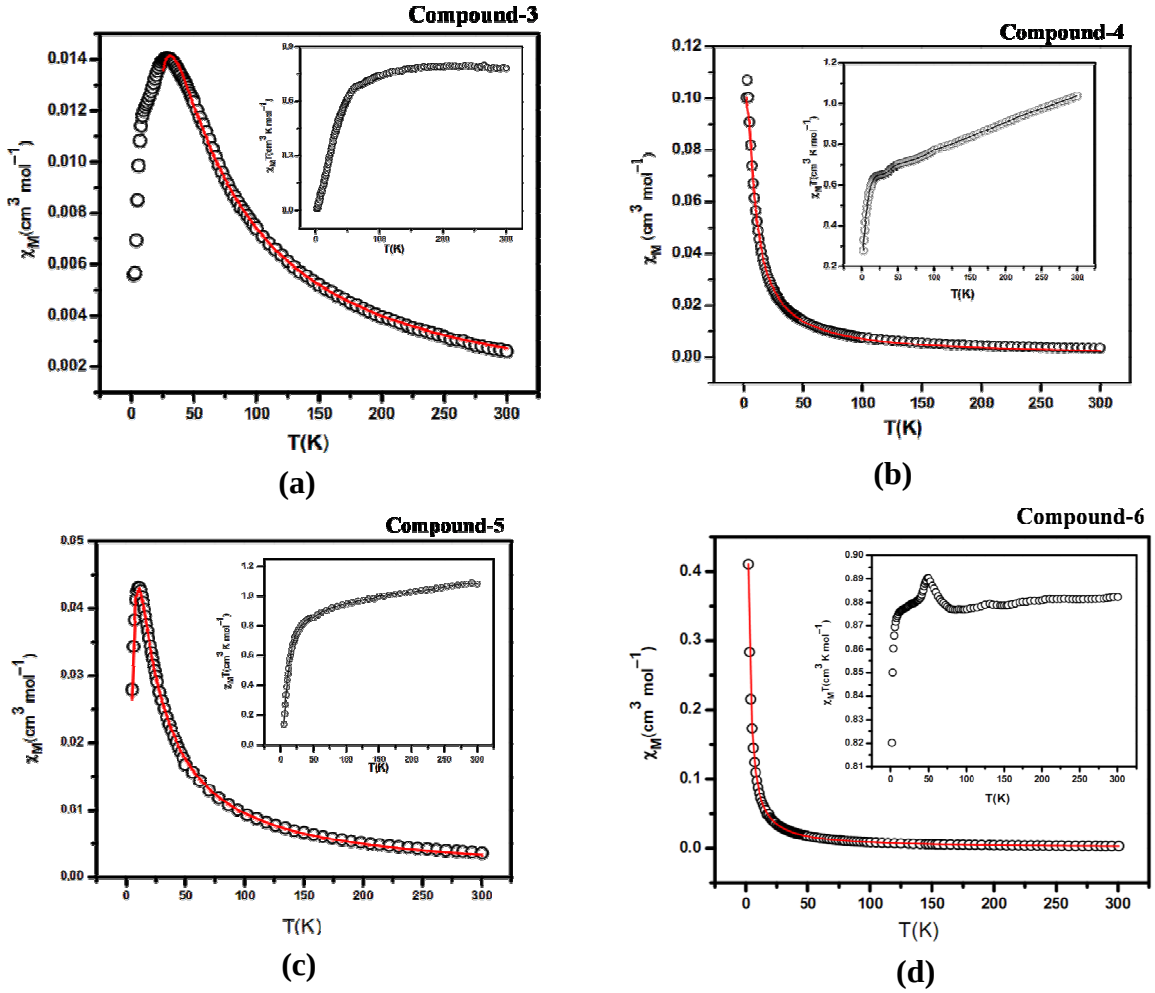

Figure 2.12. Plots of χ_M *vs T* and $\chi_M T$ *vs T* (inset) for the compounds **3**, **4**, **5**, and **6** in the temperature range of 2–300K.The red line indicates the fitting using theoretical model (see text).

Compound 5

Compound **5** is an extended coordination polymer of compound **3** in which 1,10-phenanthroline chelates the metal atoms. The plots of both χ_M *vs T* and $\chi_M T$ *vs T* per Cu^{II}_2 unit for compound 5 are shown in Figure 2.12c. Room temperature (300 K) $\chi_M T$ value of 1.08 cm^3 K mol^{-1} is higher than the expected value for two uncoupled Cu^{II} ions ($\chi_M T$ = 0.375 cm^3 K mol^{-1} for a S=1/2 ion). As the temperature is lowered, the $\chi_M T$ decreases gradually to 0.80 cm^3 K mol^{-1} at 30K and then sharply decreases to minimum value of 0.13 cm^3 K mol^{-1} at 5 K. $1/\chi_M$ *vs T* plot above the 30 K follows the Curie–Weiss law with negative Weiss constant θ= –19.2 K. The negative Weiss constant indicates the dominant antiferromagnetic exchange in intra-dimer through –O–P–O– bridges. The experimental susceptibility values are analyzed by the theoretical expression, described above, to give the best fit parameters. The obtained parameters are J= –11.18(3) cm^{-1}, zJ'= –2.58(1) cm^{-1}

and g=2.340(5) with an agreement factor of R= 1.9 X 10^{-5}. The exchange magnitude in the coordination polymer dimer increases by replacing 2,2′-bipyridine with 1,10-phenanthroline.

Compound 6

Compound **6** is an extended coordination polymer of the discrete Cu-dimer which extends by the Mo_4O_{12} subunit. The apical coordination site of the copper metal atom in this polymer is occupied by the oxygen atom from the Mo_4O_{12} subunit. The plots of both χ_M *vs* T and $\chi_M T$ *vs* T for **5** per Cu^{II}_2 unit are shown in Figure 2.12d. The $\chi_M T$ value at the room temperature is 0.88 cm^3 K mol^{-1} which is slightly higher than the expected value of two uncoupled Cu^{II} ions. Interestingly the decrease in the $\chi_M T$ value by lowering the temperature is very low. The $\chi_M T$ value is almost constant up to 70 K and then slightly increases to 0.89 cm^3 K mol^{-1} and then decreases to minimum value of 0.82 cm^3 K mol^{-1}. $1/\chi_M$ *vs* T plot above the 30K follows the Curie–Weiss law with negligible negative Weiss constant θ= –0.1 K. This value indicates that there is no significant exchange between the two Cu^{II} ions. To determine the magnitude of the exchange, the experimental susceptibilities are analyzed by the theoretical expression described above. The best fit parameters obtained were J= –0.79(3) cm^{-1}, zJ'= –0.16(1) cm^{-1} and g=2.167 (1) with an agreement factor R= 6.7 X 10^{-7}. By replacing the aqua ligand (in compounds **1** and **3**) and organic linker (compounds **4** and **5**) with the inorganic linker Mo_4O_{12}, the exchange through the –O–P–O– bridges was decreased drastically.

2.3.8. Magnetostructural correlations and DFT studies

To better understand the magnetic exchange mechanism in the reported complexes spin-unrestricted DFT calculations are performed on the complexes taking the geometries of the models from the crystal data (Figure 2.13). In the field of coordination polymers, the exchange interactions are generally calculated by using model structures that nearly resembles the basic repeating unit of the actual compound. We have considered dinuclear units for the compounds **3**, **4**, **5** and **6** with slight variations from the actual ones as the model structures. Only the equatorial bonds are taken as bridges, as they interact directly to the magnetic orbitals on the Cu atoms $d(x^2–y^2)$. From Table 2.3, it is evident that the calculated J values match with the experimental values only qualitatively (which is expected because in the actual complexes there are intercluster interactions), but the predicted sign of the exchange parameters is more important here (as the magnitudes are

quite low), and matches satisfactorily. The variations in the *J* values in the compounds are explained based on the two possible reasons.

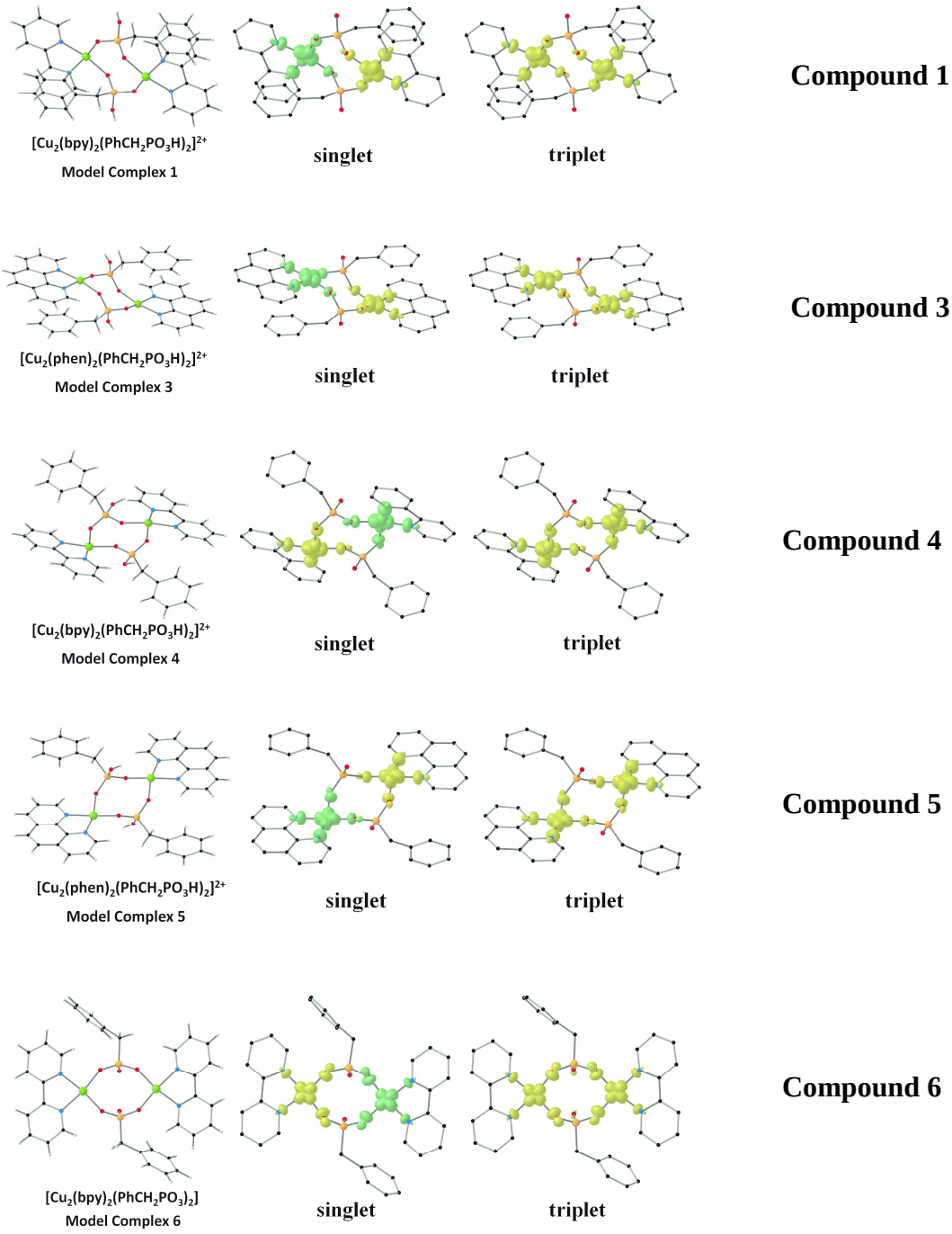

Figure 2.13. Spin density maps calculated for the two spin states of the Model Complexes at B3LYP level. Positive and negative spin populations are represented as yellow and green surfaces. The isodensity surfaces correspond to a value of 0.01 e/b^3. Color Code: green = Cu, orange = P, red = O, blue = N, black = C and light gray = H.

2.3.8.1. Conformation of the eight membered Cu-dimer rings

The eight membered Cu-dimer ring, formed in the compounds, can exist in ten canonical conformations based on the torsion angles between the Cu–O–P–O atoms. The conformation of the ring has a vital role in the magnitude of the exchange between the two Cu(II) ions. In all the compounds, the bridging ligand occupies equatorial position at both Cu(II) ions (O_{eq}–P– O_{eq}). In the compounds **2, 3, 4**, the ring exists in chair conformation and in the compound **6** the ring exists in the crown conformation as shown in the Figure 2.14.

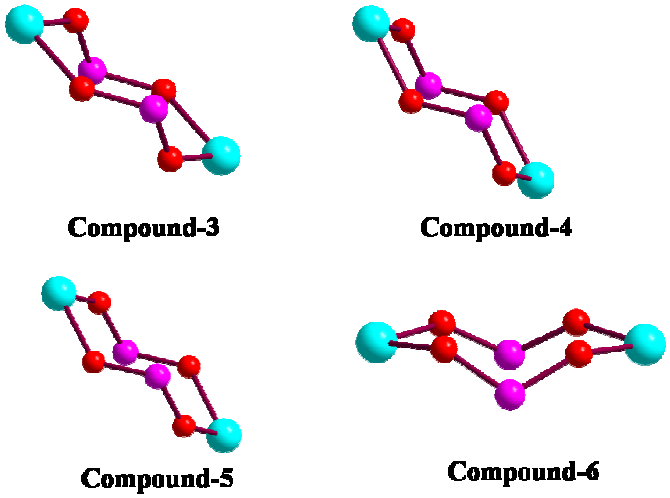

Figure 2.14. Conformations of the Cu-dimer rings present in the compounds **3**, **4**, **5**, and **6**.

The Cu atoms in the dimers have a square pyramidal geometry in which the unpaired electron in the magnetic orbital on each copper atom is predominantly d(x^2–y^2), the *x* and *y* axis being roughly defined by the copper to phosphonate oxygen bonds. These orbitals on Cu atoms are delocalized toward the 2p oxygen orbitals of the O–P–O bridge and the exchange coupling through the phosphonate groups become operative. The overlap between the magnetic orbitals of the Cu(II) ion and the bridging oxygen atoms defines the pathway for the delocalization of the electron density between the metal centers. The conformation of the dimer ring can be explained based on the torsion angles between the Cu–O–P–O atoms. The eight membered Cu-dimer can be explained by considering four types of torsion angle as shown in the Scheme 2.5. The average of the torsion angles along the same bridges are represented by τ_{avg1} τ_{avg2}. In symmetrical Cu-dimers τ_{avg1}= τ_{avg2} and in unsymmetrical Cu-dimers these values are not equal to each other. Torsion angle explains the deviation of the phosphonate group from the mean Cu–O plane in the Cu–O–P–O–Cu

skeleton, which accounts for the electron density delocalization pathways between the metal centers. Doyel et al. reported a series of copper complexes with pyrophosphate bridges in which the slight structural differences concerning the Cu–O–P–O–Cu skeleton are measured by the angles P–O–Cu angle α and the angle δ between the O–P–O plane and Cu–O axis.[36] For the large δ values the main delocalization from the metal ion to the bridge occurs through a π pathway leading to strong antiferromagnetic contributions. A simple discrete Cu-dimer bridged by the pyrophosphate unit was reported by the kruger in which the overlap between the magnetic orbitals of the two Cu (II) ions are predicted to be σ exchange pathways as a result weak magnetic coupling, that is expected with the *J* values –20 cm^{-1}.[37] As shown in the Table 2.3, τ_{avg} values for the chair conformations are more when compared to the crown conformation. A linear relationship is observed between the J_{DFT} values and τ_{avg} values in the compounds **1**, **3**, **4**, **5**, and **6**. It is also interesting to note that for compound **6**, which has the crown conformation the predicted *J* value is very low and positive,

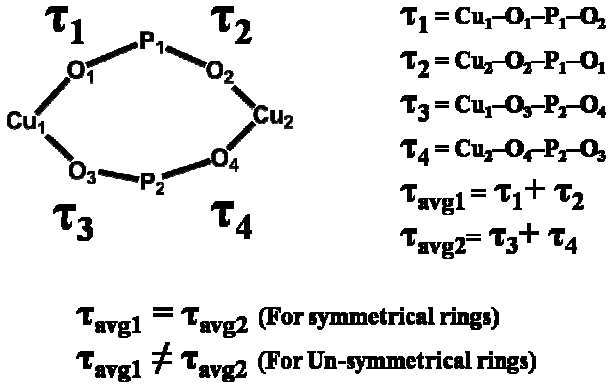

Scheme 2.5. Torsion angle measurement of the symmetrical and unsymmetrical Cu dimers

matching nicely with the experimental results. In compound **6**, the two Cu atoms are bridged differently by the O–P–O moieties in the crown conformation which enables the τ_{avg} to go below the critical limit stabilizing the triplet state making the exchange parameter positive. Only a few three atom phosphonate bridged Cu(II) complexes are available for comparison. Chandrasekhar et al. reported simple discrete phosphonate bridged copper complex[20a] $[Cu_2(\mu_2\text{-}C_3H_7PO_3)_2(bpya)_2(H_2O)_2]\bullet(H_2O)_2$ in which the *J* value is –1.53 cm^{-1} with τ_{avg} value 100.5°. In contrast Zurowska found a weak ferromagnetic interaction between the two metal centers in the compound Cu_2(2-mpmpe)$_2(H_2O)_2(NO_3)_2$ with J = 1.86 cm^{-1} in which τ_{avg} is 72.5°.[20b] Also Chandrasekhar

reported a series of hexanuclear compounds[16e] in which the Cu-dimers bridged by phosphonic acids are linked by the oxo-bridged Cu-dimer. The magnetic exchange in these compounds is mainly due to Cu(II) ions bridged by oxo groups only.

Table 2.3. Magnetostructural Correlations (See also Scheme 2.4)*

C.No.	$d_{Cu\text{-}Cu}$(Å)	Confomation	τ_{avg1}/ τ_{avg2} (°)	J (cm^{-1})	J_{DFT} (cm^{-1})	*Ref.*
1	5.12	Chair	98.70/98.70	----	–13	
3	5.15	Chair	99.32/99.32	– 36.44	– 51	This Work
4	5.14	Chair	102.4/102.4	– 3.03	– 68	
5	5.11	Chair	99.18/99.18	–11.8	–45	
6	5.08	Crown	95.31/99.74	+1.14	+ 4	
2	5.17	Chair	100.79/100.79	–1.53		20a
	4.69	Chair	73.02/73.02	1.86		20b
1	4.73	Crown	57.35/82.38	–2.35		16e
3	4.91	Crown	72.06/91.76	–0.23		16e

***Sign of the torsion angle was not considered when the values are averaged*

The weak antiferromagnetic exchange is observed between the Cu(II) ions bridged by the phosphonic acid group with J values in the range of –0.23 to –2.35 cm^{-1} in which the τ_{avg} values are in the range of 50° to 85°. In the phosphonate bridged Cu (II) complexes, if the τ_{avg} values are below 90° then weak antiferromagnetic and ferromagnetic interactions are observed between Cu(II) ions; if τ_{avg} value is more than 90^{o}, then a moderate to strong antiferromagnetic interactions are observed between the Cu(II) ions. Even though this factor is important in determining the magnitude of the exchange parameter, additional factors are also needed to fully account the variations in the exchange parameters, e.g., electronic effect induced by the atoms connected to the oxygen atom which are not part of the dimer.

2.3.8.2. Electronic effect induced by the peripheral subunits.

In the phosphonate bridge, the oxygen atom which is protonated and non coordinated in the compounds **3**, **4**, and **5** and it is deprotonated and coordinated to the large electron withdrawing group Mo_4O_{12} in the compound **6**, which exerts the electron withdrawing effect on the bridging atoms, thereby decreasing the electron density on the oxygen atoms. This causes a small overlap between the metal magnetic orbitals through the bridge resulting in the exchange to be very weak. Doyel shows the effect of protonation of non

coordinated oxygen atom on the exchange parameter in the pyrophosphate mediated magnetic interactions in Cu(II) coordination complexes.[36]

2.4. Conclusion

In summary we report here the six new coordination polymers (**1**–**6**) based on the simple building unit Cu-dimer bridged by *p*-xylylenediphosphonic acid and secondary chelated linkers (2,2′-bpy,1,10-phen). We have explored the coordination chemistry of eight membered Cu-dimer ring, in which the terminal sites are chelated by secondary linkers, as SBU in construction of multi-dimensional coordination architectures. The mechanisms for the formation of Cu-dimer starting from the **1A** to **1** and **2, 3A** to **3** have been investigated with varying the temperature. Compounds **1–3** represents the classical example in which the pH, induced by the secondary linker, changes composition of the structure. The compounds **4** and **5** represent the 2D architectures of the Cu-dimer extended by the organic linker H_2L in which the dimer acts as node and H_2L ligands as linkers. The large void spaces in the (4, 4) connected nets of **4** and **5** can be potentially used for the host–guest phenomenon which has been proved by the dehydration-rehydration of the lattice water molecules. Compound **6** represents the 2D coordination polymer of the dimer which is extended by the inorganic linker Mo_4O_{12}. All the compounds are thermally stable up to the temperature region 350 °C. The OPO bridges in the 8 membered Cu-dimer rings show net antiferromagnetic interactions between the Cu(II) ions in the compounds **3**, **4**, **5** and **6**. DFT calculations correlates the magnitude of the exchange parameter with the conformation of the 8–membered ring based on the torsion angles of the conformation that reveals the electron density delocalization pathways between the two Cu^{II} ions through OPO bridges. By changing the linkers (organic and inorganic), the conformation can be tuned which enhances the magnetic exchange between the metal centers. In short this article gives comprehensive study of the new class of SBU (Cu-dimer bridged by phosphonic acid) in metal phosphonate chemistry in prospects of formation and stabilization in coordination matrix, which gives opportunity to construct the coordination polymers with potential void spaces and finally temperature dependent magnetic exchange phenomenon through phosphonate bridges. We are presently working on exploration of this SBU with various linkers to design the materials with functional applications.

Table 2.4. Crystal data and structural refinement parameters for compounds **1–6**

	1	**2**	**3**
Empirical formula	$C_{44}H_{60}Cu_2N_4O_{24}P_6$	$C_{44}H_{56}Cu_2N_4O_{22}P_6$	$C_{40}H_{52}Cu\ N_4O_{20}P_4$
Formula weight	1341.86	1305.83	1159.82
T(K) / λ(Å)	298(2) /0.71073	298(2) /0.71073	298(2) /0.71073
Crystal system	Triclinic	Monoclinic	Triclinic
Space group	*P*-1	$P2_1/n$	*P*-1
a (Å)	7.506(4)	9.9084(17)	7.4340(8)
b (Å)	11.972(7)	17.024(3)	11.6079(13)
c (Å)	15.631(9)	16.134(3)	13.8609(16)
α (°)	86.158(10)	90	99.406(2)
β (°)	79.073(10)	106.403(2)	92.522(2)
γ (°)	81.553(10)	90	97.815(2)
Volume ($Å^3$)	1363.1(13)	2610.7(8)	1166.4(2)
Z, ρ_{calcd} (g cm^{-3})	1, 1.635	2, 1.661	1, 1.651
μ (mm^{-1}), *F*(000)	1.043, 692	1.084, 1344	1.134, 598
goodness-of-fit on F^2	1.052	1.029	1.048
R1/ wR2 [I > 2σ (I)]	0.0533/0.1170	0.0322/0.0895	0.0296/0.0832
R1/ wR2 (all data)	0.0701/0.1252	0.0347/0.0913	0.0316/0.0847
Largest diff peak/ hole (e $Å^{-3}$)	0.567/-0.409	0.471/-0.568	0.423/-0.250
	4	**5**	**6**
Empirical formula	$C_{18}H_{20}CuN_2O_7P_2$	$C_{20}H_{24}CuN_2O_9P_2$	$C_{28}H_{28}Cu_2Mo_2N_4O_{14}P_2$
Formula weight	501.84	561.89	1025.46
T(K) / λ(Å)	298(2)/0.71073	298(2)/0.71073	298(2)/0.71073
Crystal system	Triclinic	Triclinic	Triclinic
Space group	*P*-1	*P*-1	*P*-1
a (Å)	9.9763(11)	10.725(4)	11.130(6)
b (Å)	10.1710(11)	10.896(4)	12.406(7)
c (Å)	11.3001(13)	11.456(4)	13.926(7)
α (°)	110.125(2)	66.984(6)	71.952(8)
β (°)	108.317(2)	64.714(5)	72.257(8)
γ (°)	92.168(2)	84.486(6)	64.876(7)
Volume ($Å^3$)	1008.26(19)	1110.1(7)	1621.5(15)
Z, ρ_{calcd} (g cm^{-3})	2, 1.653	2, 1.681	2, 2.100
μ (mm^{-1}), *F*(000)	1.287, 514	1.185, 578	2.227, 1016
goodness-of-fit on F^2	1.047	1.056	1.065
R1/ wR2 [I > 2σ (I)]	0.0342/0.0892	0.0607/ 0.1521	0.0291/ 0.0704
R1/ wR2 (all data)	0.0420/0.0925	0.0786/ 0.1628	0.0333/ 0.0726
Largest diff peak/ hole (e $Å^{-3}$)	0.453/-0.374	1.737/ -0.887	0.764/ -0.475

Table 2.5. Geometrical parameters of the O–H···O hydrogen bonds (Å,°) involved in supramolecular networks of compounds **1**, **3, 4** and **5**.[a] D=donor; A=acceptor.[*]

D-H···A	d(D-H)	d(H···A)	d(D···A)	<(DHA)
		Compound-1		
O(14)-H(11C)...O(9)#3	0.76(5)	2.23(5)	2.964(5)	161(5)
O(4)-H(9A)...O(5)#4	1.02(7)	1.47(7)	2.474(4)	166(6)
O(10)-H(6A)...O(10)#5	0.85(6)	1.66(6)	2.511(5)	171(6)
O(5)-H(1A)...O(4)#6	0.58(5)	2.46(5)	3.024(6)	165(7)
O(3)-H(3A)…O(7)#7	0.74(4)	1.85(5)	2.584(4)	172(5)
		Compound-3		
O(10)-H(10B)...O(7)#2	0.92(5)	1.93(3)	2.783(3)	153(4)
O(10)-H(10A)...O(8)#3	0.86(4)	2.12(4)	2.928(7)	156(3)
O(8)-H(8B)...O(6)#4	0.88(5)	2.26(5)	3.083(3)	154(4)
O(8)-H(8A)...O(5)#5	0.95(5)	1.91(5)	2.825(3)	163(4)
O(6)-H(6A)...O(5)#5	0.84(4)	1.74(4)	2.580(2)	173(4)
O(3)-H(3A)...O(7)#6	0.70(3)	1.89(3)	2.580(2)	173(3)
		Compound-4		
O(6)-H(6)...O(5)#4	0.82	1.78	2.598(3)	174.2
		Compound-5		
O(6)-H(6O)...O(5)# 4	0.82	1.83	2.613(5)	160.5
O(7)-H(7B)...O(7)# 5	0.72(12)	2.21(11)	2.859(15)	132(15)
O(7)-H(7A)...O(6)# 4	0.64(7)	2.37(8)	2.964(9)	156(9)
O(9)-H(9B)...O(2)# 6	0.94(11)	2.35(11)	3.199(8)	150(9)

[*] ***(1)*** *#3 -x,-y+1,-z+1; #4 -x+1,-y+2,-z+1; #5 -x,-y+2,-z+1; #6 -x,-y+1,-z; #7 -x+1,-y+2,-z*
(3) *#2 x,y-1,z; #3 -x+1,-y+1,-z+1; #4 -x+1,-y+2,-z+1; #5 -x,-y+2,-z+1; #6 -x,-y+2,-z+2*
(4) *#4 -x+1,-y+1,-z+1 (5) #4 -x+1,-y+1,-z+2; #5 -x,-y+1,-z+2 ; #6 x-1,y,z*

2.5. References

[1] (a) Wang, B.; Cote, A. P.; Furukawa, H.; O'Keeffe, M.; Yaghi, O. M. *Nature* **2008**, *453* , 207. (b) Kitagawa, S.; Kitaura, R.; Noro, S. *Angew.Chem. Int. Ed.* **2004**, *43*, 2334. (c) Chen, X.-M.; Tong, M.-L. *Acc. Chem. Res.* **2007**, *40*, 162. (d) Zheng, B.; Dong, H.; Bai, J.; Li, Y.; Li, S.; Scheer, M. *J. Am. Chem. Soc.* **2008**, *130* , 7778. (e) Wang, X.-L.; Qin, C.; Wang, E.-B.; Xu, L.; Su, Z.-M.; Hu, C.-W. *Angew. Chem. Int. Ed.* **2004**, *43*, 5036. (f) Robson, R. *Dalton Trans.* **2008**, 5113. (g) Jiang, L.; Zhang, X.-B.; Han, S.; Xu, Q. *Inorg. Chem.* **2008**, *47*, 4826.

[2] (a) Kitura, R.; Fujimoto, K.; Noro, S.; Kondo, M; Kitagawo, S. *Angew. Chem. Int. Ed*. **2002**, *41*, 133. (b) Shin, D. M.; Lee, I. S.; Chung, Y. K. *Inorg. Chem*. **2003**, *42*, 8838. (c) Ayappan, P; Evans, O, R.; Cui, Y.; Wheeler, K. A.; Lin, W. B. *Inorg. Chem*. **2002**, *41*, 4978. (d) Dinca, M.; Long, J. R. *J. Am. Chem. Soc*. **2005**, *127*, 9376. (e) Yoon, J. W.; Jung, S. H; Hwang, Y. K.; Humphrey, S. M.; Wood, P.T.; Chang, J. S. *Adv. Mater*. **2007**, *19*, 1830. (f) Han, S. S.; Deng, W, Q.; Goddard, W. A. *Angew. Chem. Int. Ed*. **2007**, *46*, 6289. (g) Bar, A. K.; Chakrabarty, R.; Chi, K-W.; Batten, S. R.; Mukherjee, P. S. *Dalton Trans*. **2009**, 3222.

[3] (a) Li, H.; Eddaoudi, M.; Groy, T. L.; Yaghi, O. M. *J. Am .Chem. Soc*. **1998**, *120*, 8571. (b) Chen, B.; Eddaoudi, M.; Hyde, S. T.; O'Keeffe, M.; Yaghi, O. M. *Science* **2001**, *291*, 1021. (c) Eddaoudi, M.; Kim, J.; Rosi, N.; Vodak, D.; Wachter, J.; O'Keeffe, M.; Yaghi, O. M. *Science* **2002**, *43*, 2334. (d) Yaghi, O. M.; O'Keeffe, M.; Ockwig, N.; Chae, H.; Eddaoudi, M.; Kim, J. *Nature* **2003**, *423*, 705.

[4] (a) Zhang, B.; Clearfield, A. *J. Am. Chem. Soc.* **1997,** *119*, 2751. (b) Alberti, G.; Lehn, J. M.; *Comprehensive Supramolecular Chemistry*, Vol. 7, Pergamon, Elsevier Science Ltd., Oxford, UK, **1996**. (c) Cao, G.; Hong, H.; Mallouk, T. E. *Acc. Chem. Res.* **1992,** *25*, 420. (d) Maillet, C.; Janvier, P.; Pipelier, M.; Praveen, T.; Andres, Y.; Bujoli, B. *Chem. Mater*. **2001**, *13*, 2879. (e) Gomez, R.; Segura, J. L.; Martin, N. *J. Org. Chem.* **2000**, *65*, 7566. (f) Ungashe, S. B.; Wilson, W. L.; Katz, H. E.; Scheller, G. R.; Putvinski, T. M. *J. Am. Chem. Soc.* **1992,** *114*, 8717. (g) Tripuramallu, B. K.; Kishore, R.; Das, S. K. *Polyhedron* **2010**, *29*, 2985.

[5] (a) Mietrach, A.; Muesmann, T. W. T.; Christoffers, J.; Wickleder, M. S. *Eur. J. Inorg. Chem.* **2009**, 5328. (b) Yi, F. Y.; Lin, Q. P.; Zhou, T. H; Mao, J. G. *Cryst. Growth. Des.* **2010**, *10*, 1788.

[6] (a) Lin, P.; Clegg, W.; Harrington, R. W.; Henderson, R. A. *Dalton trans*. **2005**, 2388. (b) Dinca, M.; Long, J. R. *J. Am. Chem. Soc.* **2007**, *129*, 11172. (c) Pachfule, P.; Das, R.; Poddar, P.; Banerjee, R. *Cryst. Growth Des*. **2010**, *10*, 2475 (d) Li, Z. X.; Zeng, Y. F.; Ma, H.; Bu, X. H. *Chem. Commun*. **2010**, *46*, 8540. (e) Fan, J.; Yee. G. T.; Wang, G.; Hanson, B. E. *Inorg. Chem.* **2006**, *45*, 599. (f) Li, Z. X.; Xu, Y.; Zuo, Y.; Li, L.; Pan, Q.; Hu, T. L.; Bu, X. H. *Cryst. Growth Des*. **2009**, *9*, 3904. (g) Imaz, I. Maspoch, D.; Blanco, C. R.; Falcon, J. M. P.; Campo, J.; Molina, D. R. *Angew. Chem. Int. Ed.* **2008**, *47*, 1857. (h) Yang, J.; Ma, J. F.; Batten, S. R.; Su, Z. M. *Chem.Commun*. **2008**, 2233. (i) Sathiyendiran, M.; Wu, J. Y.; Velayudham, M.; Lee, G. H.; Peng, S. M.; Lu, K. L. *Chem. Commun*. **2009**, 3795. (j) Su, C. Y.; Cai, Y. P.; Chen, C. L.; Smith, M. D.; Kaim, W.; ZurLoye, H. C. *J. Am. Chem. Soc.* **2003**, *125*, 8595.

[7] (a) Collins, D. J.; Zhou, H.-C. *J. Mater. Chem*. **2007**, 17, 3154. (b) James, S. L. *Chem. Soc. Rev*. **2003**, *32*, 705. (c) Millward, A. R.; Yaghi, O. M. *J. Am .Chem. Soc*. **2003**, *125*, 11490.

[8] (a) Maeda, K.; Kiyozumi, Y.; Mizukami, F. *J. Phys. Chem. B.* **1997**, *101*, 4402. (b) Odobel, F.; Bujoli, B.; Massiot, D. *Chem. Mater*. **2001**, *13*, 163. (c) Alberti, G.; Casciola, M.; Costantino, U.; Peraio, A.; Montoneri, E. *Solid State Ionics* **1992**, *50*, 315. (d) Alberti, G.; Casciola, M. *Solid State Ionics* **1997**, *97*, 177. (e) Vermeulen, L. A.; Thompson, M. E. *Nature* **1992**, *358*, 656. (f) Deniaud, D.; Schollorn, B.; Mansuy, D.; Rouxel, J.; Battioni, P.; Bujoli, B. *Chem. Mater*. **1995**, *7*, 995.

[9] (a) Yin,P.; Gao, S.; Wang, Z -M.; Yan, C-H.; Zheng, L-M.; Xin, X-Q. *Inorg. Chem.* **2005**, *44*, 2761. (b) Chandrasekhar, V.; Senapati, T.; Dey, A; Sanudo, E. C. *Inorg. Chem*. **2011**, *50*, 1420. (c) Hou, S-Z.; Cao, D-K; Li, Y-Z.; Zheng, L-M. *Inorg. Chem*. **2008**, *47*, 10211. (d) Papoutsakis, D.; Jackson, J. E.; Nocera, D. G. *Inorg. Chem*. **1996**, *35*, 800.

[10] Shimizu, G. K. H.; Vaidhyanathan, R.; Taylor, J. M. *Chem. Soc .Rev*. **2009**, *38*, 1430.

[11] (a) Quellette, W.; Yu, M. H.; O'Connor, C. J.; Zubieta, *J. Inorg. Chem*. **2006**, *45*, 3224. (b) Quellette, W.; Yu, M. H.; O'Connor, C. J.; Zubieta, *J. Inorg. Chem.* **2006**, *45*, 7628.

[12] (a) Bolligarla, R.; Das, S. K. *CrystEngComm* **2010**, 3409. (b) Tripuramallu, B. K.; Kishore, R.; Das, S. K. *Inorg. Chim. Acta* **2011**, *368*, 132.

[13] Tripuramallu, B. K.; Manna, P.; Reddy, S. N.; Das, S. K. *Cryst. Growth Des.* **2012**, *12*, 777.

[14] (a) Bakhmutova, E. V.; Ouyang, X.; Medvedev, D. G.; Clearfield, A. *Inorg. Chem.* **2003**, *42*, 7046. (b) Drumel, S.; Janvier, P.; Barboux, P.; Doeuff, M. B.; Bujoli, B. *Inorg. Chem*. **1995**, *34*, 148. (c) Bideau, J. L.; Payen, C.; Palvadeau, P.; Bujoli, B. *Inorg. Chem.* **1994**, *33*, 4885. (d) Song, S. Y.; Ma, J. F.; Yang, J.; Cao, M. H.; Zhang, H. J.; Wang, H. S.; Yang, K. Y. *Inorg. Chem.* **2006**, *45*, 1201. (e) Cao,G.; Lee, H.; Lynch, V. M.; Mallouk, T. E. *Inorg. Chem.* **1988**, *27*, 2781. (f) Clearfield, A.; Wang, Z. *J. Chem. Soc., Dalton Trans.* **2002**, 2937.

[15] (a) Mehring, M.; Schurmann, M. *Chem. Commun.* **2001**, 2354. (b) Baskar, V.; Shanmugam, M.; Sanudo,E. C.; Shanmugam, M.; Collison, D.; McInnes, E. J. L.; Wei, Q.; Winpenny, R. E. P. *Chem. Commun*. **2007**, 37. (c) Samanamu, C. R.; Olmstead, M. M.; Montchamp, J. L.; Richards, A. F. *Inorg. Chem.* **2008,** *47*, 3879. (d) Murugavel, R.; Shanmugan, S. *Chem. Commun.* **2007**, 1257.

[16] (a) Chandrasekhar, V.; Azhakar, R.; Senapati, T.; Thilagar, P.; Ghosh, S.; Verma, S.; Boomishankar, R.; Steiner, A.; K¨ogerle, P. *Dalton Trans*. **2008**, 1150. (b) Chandrasekhar, V.; Nagarajan, L.; Cle´rac, R.; Ghosh, S.; Verma, S. *Inorg. Chem.* **2008**, *47*, 1067. (c) Doyle, R. P.; Kruger, P. E.; Moubaraki, B.; Murray, K. S.; Nieuwenhuyzen, M. *Dalton Trans.* **2003**, 4230. (e) Chandrasekhar, V.; Senapati, T.; Sanudo, E. C. *Inorg. Chem*. **2008**, *47*, 9553.

[17] (a) Taylor, J. M.; Mahmoudkhani, A. M.; Shimizu, G. K. H. *Angew. Chem. Int. Ed.* **2007**, *46*, 795. (b) Kong, D.; Zon, J.; Clearfield, J. M. A. *Inorg. Chem*. **2006**, *45*, 977. (c) Vaidhyanathan, R.; Mahmoudkhani, A. H.; Shimizu, G. K. H. *Can. J. Chem*. **2009**, *87*, 247. (d) Evans, O. R.; Ngo, H. L.; Lin, W. *J. Am. Chem. Soc.* **2001**, *123*, 10395.(e) Liang, J.; Shimizu, G. K. H. *Inorg. Chem*. **2007**, *46*, 10449

[18] (a) Almeida Paz, F. A.; Rocha, J.; Klinowski, J.; Trindade, T.; Shi, F-N.; Mafra, L. *Prog. Solid State Chem*. **2005**, *33*,113. (b) Lu, J.Y. *Coord. Chem. Rev*. **2003**, *246*, 327.

[19] (a) Perez, J.; Garcia, L.; Kessler, M.; Nolse, K.; Perez, E.; Serrano, J. L.; Martinez, J. F.; Carrascosa, R. *Inorg. Chim. Acta* **2005**, *358*, 2432. (b) Deng-Ke, C.; Jing, X.; Zhi, Y. L.; Modesto, C. J. J.; Eugenio, C.; Li-Min, Z. *Eur. J. Inorg. Chem.* **2006**, *9*, 1830. (c) Ling, S. J.; Gao, M. J. *Solid State Chem.*, **2005**, *178*, 3514. (d) Gao, M. J.; Zhike, W.; Abraham, C. *Inorg. Chem*. **2002**, *41*, 3713. (e) Krassimira, G.; Rita, D.; Luis, L.; Michael, D.; Vitor, F. *Dalton Trans.* **2004**, *12*, 1812.

[20] (a) Chandrasekhar, V.; Senapati, T.; Clérac, R. *Eur. J. Inorg. Chem.* **2009**, 1640. (b) Zurowska, B.; Brzuszkiewicz, A.; Ochocki. J. *Polyhedron* **2008**, *27* 1721.

[21] (a) Willet, R. D.; Gattesdhi, D.; Kahn(Eds.), O.; Magneto-Structural Correlation in Exchange Coupled Systems, Reidel, Dordrecht, **1985**. (b) Carlin, R. L.; vanDuyneveldt, A. J.; Magnetic Properties of Transition Metal Compounds, Springer, Berlin, **1997**.

[22] Mayer, C. R.; Herve, M.; Lavanant, H.; Blais, J. C.; Secheresse, F. *Eur. J. Inorg. Chem.* **2004**, *5*, 973.

[23] (a) Ruiz, E.; Alemany, P.; Alvarez, S.; Cano, J. *J. Am. Chem. Soc.* **1997**, *119*, 1297. (b) Ruiz, E.; Rodríguez-Fortea, A.; Cano, J.; Alvarez, S.; Alemany, P. *J. Comput. Chem.* **2003**, *24*, 982. (c) Ruiz, E.; Cano, J.; Alvarez, S.; Alemany, P. *J. Comput. Chem.* **1999**, *20*, 1391.(d) Ruiz, E. *Struct. Bonding* **2004**, *113*, 71.

[24] Becke, A. D. *J. Chem. Phys.* **1993**, *98*, 5648.

[25] Frisch, M. J.; Trucks, G. W.; Schlegel, H. B.; Scuseria, G. E.; Robb, M. A.; Cheeseman, J. R.; Montgomery, J. A.; Vreven, T.; Kudin, K. N.; Burant, J. C.; Millam, J. M.; Iyengar, S. S.; Tomasi, J.; Barone, V.; Mennucci, B.; Cossi, M.; Scalmani, G.; Rega, N.; Petersson, G. A.; Nakatsuji, H.; Hada, M.; Ehara, M.; Toyota, K.; Fukuda, R.; Hasegawa, J.; Ishida, H.; Nakajima, T.; Honda, Y.; Kitao, O.; Nakai, H.; Klene, M.; Li, X.; Knox, J. E.; Hratchian, H. P.; Cross, J. B.; Adamo, C.; Jaramillo, J.; Gomperts, R.; Stratmann, R. E.; Yazyev, O.; Austin, A. J.; Cammi, R.; Pomelli, C.; Ochterski, J.; Ayala, P. Y.; Morokuma, K.; Voth, G. A.; Salvador, P.; Dannenberg, J. J.; Zakrzewski, V. G.; Dapprich, S.; Daniels, A. D.; Strain, M. C.; Farkas, O.; Malick, D. K.; Rabuck, A. D.; Raghavachari, K.; Foresman, J. B.; Ortiz, J. V.; Cui, Q.; Baboul, A. G.; Clifford, S.; Cioslowski, J.; Stefanov, B. B.; Liu, G.; Liashenko, A.; Piskorz, P.; Komaromi, I.; Martin, R. L.; Fox, D. J.; Keith, T.; Al-Laham, M. A.; Peng, C. Y.; Nanayakkara,A.; Challacombe, M.; Gill, P. M. W.; Johnson, B.; Chen, W.; Wong, M. W.; Gonzalez, C.; Pople, J. A. *Gaussian 03*, revision B.4; Gaussian Inc.: Pittsburgh, PA, **2003**.

[26] Becke, A. D. *Phys. Re*v. *A* **1988**, *38*, 3098.

[27] Lee, C.; Yang, W.; Parr, R. G. *Phys. Re*v. *B* **1988**, *37*, 785.

[28] Ruiz, E.; Alvarez, S.; Cano, J.; Polo, V. *J. Chem. Phys.* **2005**, *123*, 164110.

[29] (a) Mukherjee, S.; Gole, B.; Chakrabarty, R.; Mukherjee, P. S. *Inorg. Chem.* **2009**, *48*, 11325. (b) Mukherjee, S.; Gole, B.; Song, Y.; Mukherjee, P. S. *Inorg. Chem.* **2011**, *50*, 3621. (c) Mukherjee, S.; Patil, Y. P.; Mukherjee, P. S. *Dalton Trans.* **2012**, *41*, 54.

[30] (a) *SAINT: Software for the CCD Detector System*; Bruker Analytical X-ray Systems, Inc.: Madison, WI, **1998** (b) *SADABS: Program for Absorption Correction;* G. M. Sheldrick University of Gottingen: Gottingen, Germany, **1997**. (c) *SHELXS-97: Program for Structure Solution;* G. M. Sheldrick, University of Gottingen: Gottingen, Germany, **1997**. (d) *SHELXL-97: Program for Crystal Structure Analysis;* G. M. Sheldrick University of Gottingen: Gottingen, Germany, **1997.**

[31] (a) Chattopadhyay, S. K.; Mak, T. C. W. *Inorg. Chem. Commun*. **2000**, *3*, 111. (b) Hu, X.; Guo, J.; Liu, C.; Zen, H.; Wang, Y.; Du, W. *Inorg. Chim. Acta* **2009**, *362*, 3421.

[32] Cabeza, A.; Ouyang, X.; Sharma, C. V. K.; Aranda, M. A. G.; Bruque, S.; Clearfield, A. *Inorg. Chem*. **2002,** *41*, 2325.

[33] Jones, S.; Liu, H.; Schmidtke, K.; O'Connor, C. C.; Zubieta. J. *Inorg. Chem. Commun*. **2010**, *13*, 298

[34] Pavani, K.; Ramanan, A. *Eur. J. Inorg. Chem*. **2005**, 3080.

[35] Armatas, N. G.; Allis, D. G.; Prosvirin, A.; Carnutu, G.; O'Connor, C. J.; Dunbar, K.; Zubieta, J. *Inorg. Chem*., **2008**, *47*, 832.

[36] Marino, N.; Ikotun, O. F.; Julve, M.; Lloret, F.; Cano, J.; Doyle, R. P. *Inorg Chem.* **2011**, *50*, 378.

[37] Kruger, P. E.; Doyle, R. P.; Julve, M.; Lloret, F.; Nieuwenhuyzen, M. *Inorg Chem.* **2001**, *40*, 1726.

Synthesis, Structural Characterization and Properties of One-Dimensional Coordination Polymers of Cobalt(II)- and Nickel(II)-Phosphonate Complexes: Influential Role of Secondary Ligand and Biphenyl Spacer

3

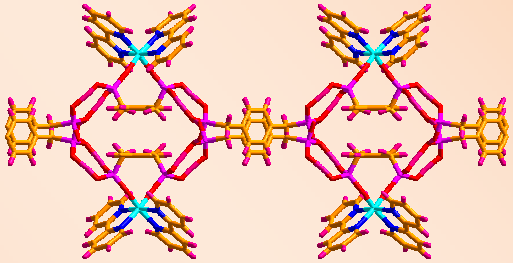

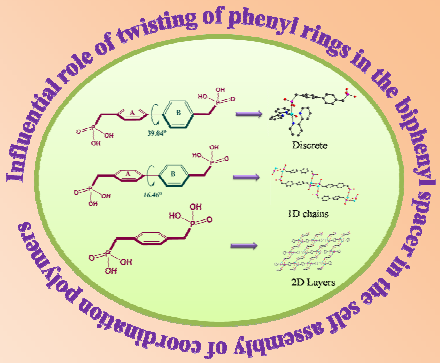

*Chapter **3** describes the structural consequences in the metal phosphonate architectures by introducing secondary ligand, and explains the role of biphenyl spacer in modulating the dimensionalities. Two isomorphous cobalt and nickel phosphonates $[M^{II}(2,2'\text{-bipy})_2H_4pxp]_n[H_2pxp]_n$ M = Co (compound **1**), M = Ni (compound **2**) were synthesized from p-xylylenediphosphonic acid (H_4pxp) with 2,2´-bipyridine as secondary ligand component and the two other compounds [Co (2,2´-bipy) $(H_2dbp)]_n$ (**3**) and [Ni $(2,2'\text{-bipy})_2(H_2dbp)(H_2O)]\cdot H_2O$ (**4**) were synthesized from 4,4'-dimethylenebiphenyldiphosphonic acid (H_4dbp) with 2,2´-bipyridine as secondary ligand. All the compounds are characterized by routine elemental analyses, IR-, electronic-spectral analyses, thermogravimetric studies and unambiguously characterized by single crystal X-ray crystallography. The crystal structure of compounds **1** and **2** consists of 1D $[M(2, 2'\text{-bipy})_2H_4pxp]^{2+}$ chains, and $[H_2pxp]^{2-}$ anions. The flexibility of non-rigid ligand p-xylylenediphosphonic acid (H_4pxp) tends to adopt a rare cis conformation in the crystal structure to meet the coordination requirement of the metal centre from the usual trans conformation. The hydrogen bonding in the crystal structure of compounds **1** and **2** leads to cylindrical tubes that extends via p-xylylenediphosphonic acid resulting in a 2D supramolecular sheet. Compound **3** is a 1D extended coordination polymer constituted by the Co-dimer rings and H_2dbp ligands and **4** is a discrete molecular compound. A comparative study between the geometries of H_4dbp ligand and H_4pxp ligand demonstrate the effect of the twisting in the benzene rings in changing higher dimensional H_xpxp (x refers to number of protonated hydroxyl groups) compounds to lower dimensional H_xdbp compounds. The eight membered Co-dimer rings formed in compound **3** represents the simple and isolated Co-dimer, exhibiting weak antiferromagnetic exchange between metal centers through OPO bridges.*

3.1. Introduction

Metal organic frameworks or coordination polymers are the class of materials that subject to enormous interest in the recent years in prospects of potential applications, such as, storage materials for gases, hi-capacity adsorbents, catalysis, bio-medical imaging.[1] Carboxylates constitute the major part of these functional materials to show high surface areas and uniform pore size distributions.[2] On the other hand, metal organophosphonates are among the earliest and most extensively studied examples of extended coordination architectures.[3] Clearfield et al. reported several metal phosphonates and explored the structural chemistry relevant to functional applications.[4] In contrast to carboxylates, phosphonates have strong tendency to coordinate with the metal centers, but the major problem in preparing crystalline phosphonate based MOFs is the less solubility of these materials.[5] The solubility of the metal phosphonates decreases as the valency of the metal atom increases. Usually phosphonates are having a propensity to form dense packed layered structures with general formula $M_x[O_3P(\text{organic spacer})PO_3]_y$ which are not porous in nature.[6] The layered structures can be modified by introducing secondary ligands, such as, 2,2´-bipyridine, 1,10-phenanthroline etc. It is worth mentioning that, the introduction of secondary ligands leads to formation of not only extended coordination structures with well defined channels but also increases the solubility which often hinders in formation of crystalline materials.[7]

Different types of organic spacers, such as, aromatic,[8] alkyl,[9] heterocyclic,[10] etc. are used in obtaining metal phosphonates. Rigid aromatic spacers, such as, 1,4-benzene bisphosphonic acid and 4,4'-biphenyl bisphosphonic acid are used widely to obtain several compounds that feature layered structures. Some of the metal phosphonates, obtained by using these phosphonic acids, have less solubility and are characterized by powder X-ray diffraction instead of single crystal methods.[11] The attachment of flexible groups *i.e.* CH_2 groups to these rigid ligands results in the flexible ligands that can also form a layered structure as shown by rigid ligands. But introduction of secondary ligands along with flexible ligands offers us to study the different conformations of the ligands which enable us to design the desirable frameworks and also increases the solubility of the compounds formed. *P*-xylylenediphosphonic acid (H_4pxp) is a well defined flexible ditopic ligand which was studied elaborately with and without secondary ligands.[12]

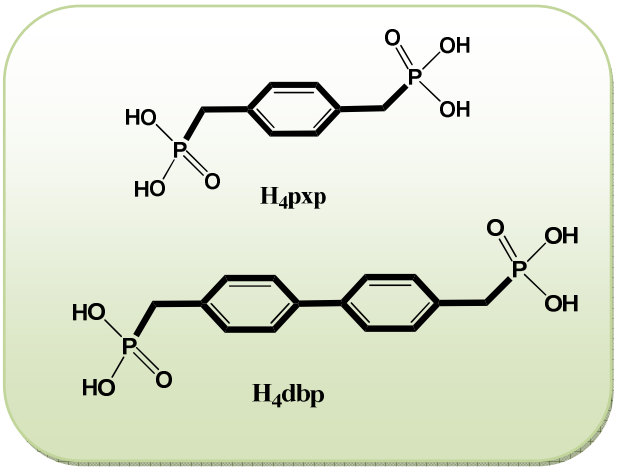

Scheme 3.1. Ligands used in this work

By introducing the flexible CH_2 groups to the 4,4′-biphenyl bisphosphonic acid, it results in the formation of versatile ligand 4,4′-dimethylenebiphenyldiphosphonic acid (H_4dbp). The versatility of this ligand is, the twisting of the benzene rings in the biphenyl spacer changes the orientation of the flexible CH_2 groups that has impact on the coordination modes of the PO_3H_2 groups. Here, we report four compounds [Co(2,2′-bipy)$_2$H$_4$pxp]$_n$[H$_2$pxp]$_n$ (**1**) [Ni(2,2′-bipy)$_2$H$_4$pxp]$_n$[H$_2$pxp]$_n$ (**2**) based on H_4pxp and [Co (2,2′-bipy) (H$_2$dbp)]$_n$ (**3**) and [Ni (2,2′-bipy)$_2$(H$_2$dbp)(H$_2$O)]·H$_2$O (**4**), based on H_4dbp with secondary ligand 2,2′-bipyridine.

In compounds **1** and **2**, the neutral ligand LH_4 acts as the linker in *cis* conformation *via* its coordination to the metal ion M^{2+} through P=O resulting in $[M^{II}(2,2'\text{-bipy})_2LH_4]^{2+}$ as a di-positive cation, which, in turn, is stabilized by the deprotonated anion LH_2^{2-}in *trans* conformation. To our knowledge, this is the first instance of a metal- *p*-xylylenediphosphonate compound that is isolated with a secondary ligand component (here it is 2,2′-bipyridine) in its both *cis* and *trans* conformations. Compounds **3** and **4** demonstrate the influence of the benzene ring twisting in the biphenyl spacer of H_4dbp ligand. The effect was discussed in detail in comparison with the H_4pxp ligand Variable temperature magnetic susceptibility measurements of the compound **1** have been performed and the results are fitted through the theoretical equations to obtain the magnitude of the exchange parameter.

3.2. Experimental Section

3.2.1. Materials and Methods

All the chemicals were received as reagent grade and used without any further purification. H_4pxp and H_4dbp were prepared according to the reported procedure.[13] Elemental analyses were determined by FLASH EA series 1112 CHNS analyzer. Infra red spectra of solid samples obtained as KBr pellets on a JASCO – 5300 FT – IR spectrophotometer. Thermogravimetric analyses were carried out on a STA 409 PC analyzer and corresponding masses were analyzed by QMS 403 C mass analyzer, under the flow of N_2 gas with a heating rate of 5 ^oC min^{-1}, in the temperature range of 30-1000 ^oC. The electronic absorption spectra have been recorded on a Cary 100 Bio UV-visible spectrophotometer at room temperature. Magnetic susceptibilities were measured in the temperature range 2–300 K on a Quantum Design VSM-SQUID. The compounds were synthesized in 23 mL Teflon-lined stainless vessels (Thermocon, India).

3.2.2. Synthesis

Synthesis of $[Co(2,2´\text{-bipy})_2(H_4pxp)]_n[H_2pxp]_n$ (1)

A mixture of $Na_2MoO_4 \cdot 2H_2O$ (0.038 g, 0.158 mmol), 2,2´-bipyridine (0.034 g, 0.221 mmol), $H_2PO_3(C_8H_8)PO_3H_2$ (0.115 g, 0.436 mmol), $CoSO_4 \cdot 7H_2O$ (0.123 g, 0.440 mmol), H_20 (10 g, 555 mmol), and concentrated HF (0.125 g) in mole ratio 1:1.3:2.75:2.78:3512 were stirred under air atmosphere for few hours. The solution was transferred into teflon-lined stainless steel vessel (25 mL), sealed and heated up to 200 °C for 96 h. By slow cooling of the reaction mixture to room temperature over two days red block crystals were obtained. Yield: (0.18 g, 45%). CHN analysis: Anal. calcd. for $C_{36}H_{38}N_4P_4O_{12}Co$: C, 47.96; H, 4.24; N, 6.21. Found C, 48.12; H, 4.19; N, 6.29. IR (KBr pellet) (υ/cm^{-1}) for **1**: 3425, 3088, 2744, 2648, 2334, 1658, 1597, 1512, 1469, 1440, 1255, 1141, 1097, 979, 927, 810, 771, 733, 684, 567, 507.

Synthesis of $[Ni(2,2´\text{-bipy})_2(H_4pxp)]_n[H_2pxp]_n$ (2)

The same synthetic procedure was used to synthesize **2** as that for **1** except $NiSO_4 \cdot 7H_2O$ was used instead of $CoSO_4 \cdot 7H_2O$. Yield: (0.10 g, 25%) CHN analysis: Anal. calcd. for $C_{36}H_{38}N_4P_4O_{12}Ni$: C, 47.97; H, 4.24; N, 6.21. Found C, 47.88; H, 4.28; N, 6.15. IR (KBr pellet)(υ/cm^{-1}) for **2**: 3425, 3097, 3003, 2627, 2361, 1649, 1599, 1510, 1469, 1440, 1255, 1141, 1093, 978, 927, 771, 736, 684, 569, 511.

Synthesis of [Co (2,2´-bipy) (H_2dbp)]$_n$ (3)

A mixture of $CoSO_4 \cdot 7H_2O$ (0.097 g, 0.348 mmol), 2,2´-bipyridine (0.05 g, 0.320 mmol), H_4dbp (0.149 g, 0.436 mmol), H_2O (10.0 g, 555 mmol) in mole ratio 1.08:1:1.3:1735 were stirred under air atmosphere for few hours. The solution was transferred into Teflon-lined stainless steel vessel (23 mL), sealed and heated up to 180 °C for 72 h. By slow cooling of the reaction mixture to room temperature over 48 h red block crystals were obtained. Yield: 72%. CHN analysis: Anal. calcd. for $C_{24}H_{22}CoN_2O_6P_2$ (555.31): C 51.91, H 3.99, N 5.04; Found C 52.09, H 4.19, N 5.58. IR (KBr pellet) (υ/cm^{-1}): 2905, 1597, 1496, 1473, 1439, 1408, 1205, 1130, 1080, 1020, 922, 835, 765, 734, 592, 526, 474.

[Ni (2,2´-bipy)$_2$(H_2dbp)(H_2O)]$\cdot H_2O$ (4)

The same synthetic procedure was used to synthesize **4** as that for **3** except $NiSO_4 \cdot 7H_2O$ was used instead of $CoSO_4 \cdot 7H_2O$. Yield: 66.3%. CHN analysis: Anal. calcd. for $C_{34}H_{34}N_4NiO_8P_2$ (747.30): C 54.65, H 4.58, N 7.49; Found C 55.39, H 4.09, N 7.99. IR (KBr pellet) (υ/cm^{-1}): 3477, 3354, 3059, 1658, 1599, 1568, 1494, 1440, 1317, 1248, 1161, 1068, 1022, 885, 765, 734, 590, 536, 470.

3.2.3. Single crystal X-ray structure determination of the compounds 1-4

Single-crystals suitable for structural determination of all the compounds (**1–4**) were mounted on a three circle Bruker SMARTAPEX CCD area detector system under Mo-Kα (λ=0.71073 Å) graphite monochromated X-ray beam, crystal to detector distance 60 mm, and a collimator of 0.5 mm. The scans were recorded with an ω scan width of 0.3º. Data reduction performed by SAINTPLUS,[14a] empirical absorption corrections using equivalent reflections performed by program SADABS,[14b] structure solution using SHELXS-97[14c] and full-matrix least-squares refinement using SHELXL-97[14d] for above compounds. All the non-hydrogen atoms were refined anisotropically. Hydrogen atoms on the C atoms were introduced on calculated positions and were included in the refinement riding on their respective parent atoms. Some of the hydrogen atoms of the hydroxyl groups were identified by the Fourier electron density and refined freely and some of the hydrogen atoms on the P–OH groups in the compounds are fixed by the proper HFIX commands. Attempts to locate the hydrogen atoms for the solvent water molecule in compound **4** through Fourier electron density were failed. However, no attempts were made to fix these atoms on their parents. Due to tiny crystals of compound **4**, we obtain slightly poor quality data which reflects in R factor and R_{int} values slightly greater than the expected limits.

Table 3.1 summarizes the structural data and refinement parameters of the studied crystals. The selected bond lengths, bond angles and hydrogen bonding parameters are presented in the Table 3.2 and Table 3.3 respectively.

3.3. Results and discussion

3.3.1. Synthesis

Compounds **1** and **2** have been synthesized by a direct one pot reaction of $MSO_4 \cdot 7H_2O$ (M= Co^{2+} and Ni^{2+}) with phosphonic acid H_4pxp, 2, 2´-bipyridine and sodium molybdate under hydrothermal conditions in the presence of hydrofluoric acid. Compounds **3** and **4** have also been synthesized by a direct one pot reaction of $MSO_4 \cdot 7H_2O$ (M= Co^{2+} and Ni^{2+}) with H_4dbp and 2, 2´-bipyridine under hydrothermal conditions. All the compounds were obtained as well-formed blocks. All the compounds are non-hygroscopic and stable in air and insoluble in common organic solvents and in water. Sodium molybdate, used in this synthesis, is not the part of the isolated compounds **1** and **2**. We believe that sodium molybdate plays an important role in this synthesis because the crystals of compounds **1** and **2** cannot be obtained, if we do not use sodium molybdate in the relevant synthesis. The ratio of the reactants is optimized by doing several experiments to obtain compounds with moderate yield. Also the ratio of the reactants is primarily responsible for forming the simple building unit (SBU) of eight membered dimer rings in compound **3**

3.3.2. Description of crystal structures

Structural description of $[Co(2,2´\text{-bipy})_2\ (H_4pxp)]_n[H_2pxp]_n$ (1) and $[Ni(2,2´\text{-bipy})_2\ (H_4pxp)]_n[H_2pxp]_n$ (2)

Both compounds **1** and **2** that crystallize in a monoclinic *C*2/c space group are isomorphous. The structural details for compound **2** are described herewith. The thermal ellipsoidal plot of the molecular structure of compound **2** is shown in Figure 3.1. As shown in Figure 3.1, the nickel ion is in NiO_2N_4 octahedron constructed by four nitrogen atoms from two bipyridine molecules and two oxygen atoms from two phosphonic acids. The phosphonic acid is coordinated to the metal atoms with P=O groups on both sides which is in good accordance with the P–O bond length of 1.476 **Å** and thereby the charge is balanced by the uncoordinated phosphonic acid which is deprotonated from LH_4 to LH_2^{2-}.

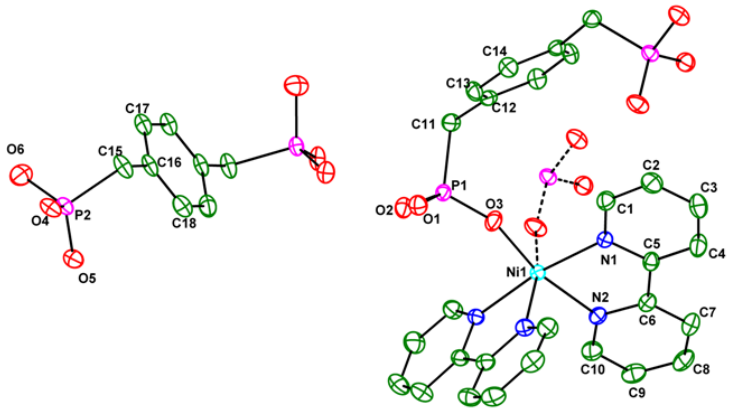

Figure 3.1. Thermal ellipsoidal plot of the molecular structure of compound $[Ni(2,2'\text{-bipy})_2(H_4pxp)]_n[H_2pxp]_n$ (**2**); hydrogen atoms are not shown for clarity (30% probability). H_4pxp = $(HO)_2O{=}PCH_2C_6H_4CH_2P{=}O(OH)_2$, cis conformation; H_2pxp^{2-} = $(HO)(O^-)O{=}PCH_2C_6H_4CH_2P{=}O(O^-)(OH)$, Trans conformation

In the crystal structure, an extended nickel coordination complex $\{NiO_2N_4\}$ (chain like) polymer is formed by the use of LH_4 (*p*-xylylenediphosphonic acid) as a linker. Along the chain, the nickel (II) ion has a coordination number of six (6) and is in the centre of a distorted octahedron formed by four nitrogen donors from two bipyridine ligands and two terminal oxygen atoms (P=O) from two different linkers. The formation of chain is schematically shown in Scheme 3.2. *p*-xylylenediphosphonic acid (in its neutral form) adopts a *cis* conformation by coordinating with the transition metal ion and *trans* conformation in its anionic form (uncoordinated) as shown in Scheme 3.3.

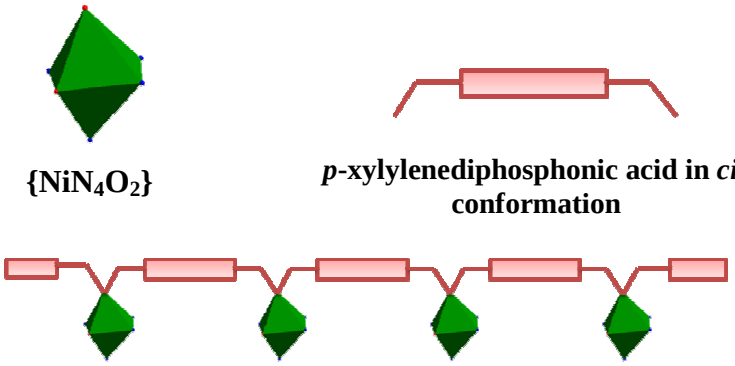

Scheme 3.2. Schematic representation of formation of 1D chain.

By introducing a secondary ligand component (2,2´-bipyridine in the present studies) blocks four coordination sites i.e. three equatorial and one apical positions of metal octahedron, leaving one equatorial and one apical sites available for coordination with LH_4. In order to meet this coordination requirement (i.e., to satisfy the coordination sites: one equatorial and one apical sites) a flexible non-rigid ligand (*p*-xylylenediphosphonic

acid in the present case) has to adopt a rare *cis* conformation. This conformational freedom of LH_4 allows the existence of both *cis* and *trans* conformations in the same crystal structure, which may not be observed / possible for the similar rigid system like $((HO)_2O=P–C_6H_4–P=O(OH)_2$.

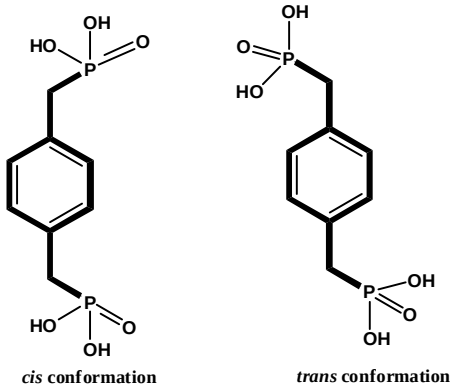

Scheme 3.3. *cis* and *trans* conformation of H_4pxp ligand.

The existence of *p*-xylylenediphosphonic acid in its *cis* conformation in the present study is first paradigm of its kind; the literatures related to crystal structures of *p*-xylylenediphosphonic acid-associated compounds do not say anything about its *cis* conformation. The arrangement of coordinated neutral LH_4 in its *cis* conformation and uncoordinated anionic LH_2^{2-} in its *trans* conformation in the packing diagram is shown in Figure 3.2.

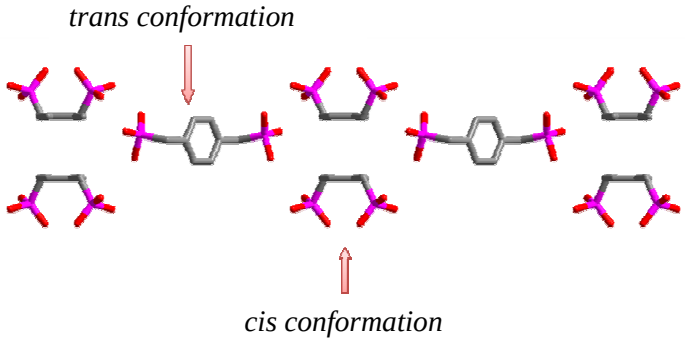

Figure 3.2. Arrangement of *cis* and *trans* conformations of *p*-xylylenediphosphonic acid in the packing diagram of compound **2**.

As shown in Scheme 3.2, the linker (*p*-xylylenediphosphonic acid) is attached to the two different metal centers on its both ends *via* its terminal oxygen atoms (P=O) and thereby extends the structure in one dimensional running parallel to the crystallographic *c* axis. The structure of compound **1** has not been shown here, because both compounds **1** and **2** are isomorphous and crystallize in *C2/c* space group.

In both the complexes **1** and **2**, the metals are present in +2 oxidation state. As mentioned above, the phosphonic acid is coordinated to the metal atoms with P=O group on both sides which is in good accordance with the P–O bond length of 1.476 Å (Table 3.4) and thereby the charge of overall complex is +2, which is counter-balanced by the deprotonated phosphonic acid (LH_2). So the resulting ion paired compounds can be termed as clathrated complexes.[15] The fact, that the coordinated *cis p*-xylylenediphosphonic acid is neutral and the uncoordinated *trans p*-xylylenediphosphonic acid is ionic, is supported by the observed phosphorous–oxygen bond lengths present in compound **2** as described in Table 3.4.

From Table 3.4, it is clearly evident that neutral phosphonic acid is coordinated to metal and the charge is balanced by the deprotonated phosphonic acid which is uncoordinated. The assignment of P–O bonds according to the bond lengths are in good accordance with the relevant reported values.[16] Use of secondary ligand component, 2,2´-bipyridine blocks the four coordination sites of the metal centre, thereby preventing the spatial expansion into 3-D as reported for *p*-xylylenediphosphonic acid-associated compound in the literature.[17] Thus the careful selection of the secondary ligand components allows us to direct the dimensionality of the coordination polymers.

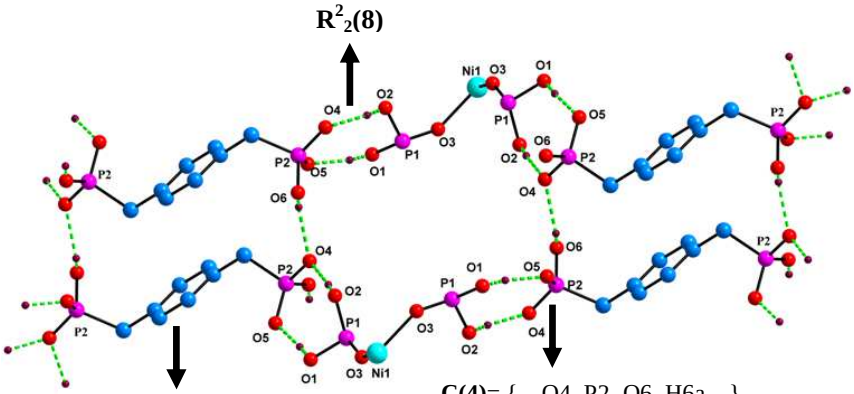

Scheme 3.4. Hydrogen bonding situation involving both *cis* and *trans p*-xylylenediphosphonic acid and *p*-xylylenediphosphonate anion respectively: 2,2´-bipyridine and *cis p*-xylylene moiety are not shown for clarity, dotted lines indicate hydrogen bonding, $R_2^2(8)$, C(4) are the graph set notations for the hydrogen bondings.

In the crystal structure, there are four protons, located on P–O bonds, resulting in four P–OH groups (two in the coordinated *cis* LH_4 and two in uncoordinated *trans* LH_2) and thereby an extended hydrogen bonding situation is expected. The oxygen atoms (O1 & O2) of the metal coordinated *cis* phosphonic acid are strongly hydrogen bonded to oxygen

atoms of uncoordinated *trans* phosphonic acid (O4 & O5) with in a distance of 2.49 and 2.52 Å respectively**.** The values are in good accordance for strong hydrogen bonding. The oxygen atom (O6) of the *trans* phosphonic acid is strongly hydrogen bonded to another *trans* phosphonic acid oxygen atom O4 with in a distance of 2.57 Å and so on resulting in a one-dimensional chain like arrangement that runs parallel to the crystallographic *c* axis with notation C(4) **{**---O4–P2–O6–H6a---**}.** Each metal center of a coordination polymer (for example chain A) is hydrogen bonded to its two adjacent *trans* phosphonate anions (LH_2) from opposite sides involving two hydrogen bonds (O(1)–H···O(4) and O(2)–H···O(5)) to form a rings of notation $R_2^2(8)$. Each of these LH_2 phosphonate anions, in turn, is hydrogen bonded to another *trans* LH_2 phosphonate anion by O(6)–H···O(4) hydrogen bond[C(4)] (Scheme 3.4). Each of these second generation LH_2 is again hydrogen bonded to a second coordination polymer (for example chain B) by using O(1)–H···O(4) and O(2)–H···O(5) hydrogen bonds to form a rings with notation $R_2^2(8)$. These chains A and B constitute a cylinder-like arrangement with the assistance of four *trans* LH_2 components (Scheme 3.4). These cylindrical arrangements are, consecutively, linked with another set of cylindrical arrangements as the linker is ($–CH_2$-C_6H_4-$CH_2–$) as shown in Figure 3.3. The relevant hydrogen bonding distances and angles with symmetry operations of both the compounds are listed in Table 3.3.

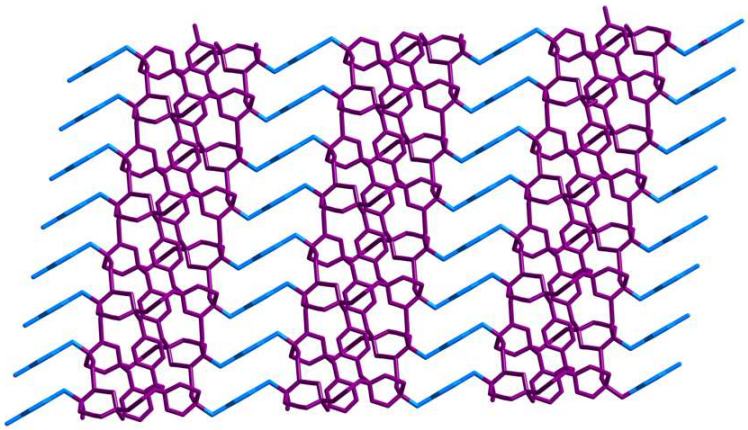

Figure 3.3. The molecular packing diagram of **2**, characterized by hydrogen bonding when viewed down to the crystallographic *b* axis; 2, 2′-bipyridine moieties are removed for clarity.

Structural Description of [Co (2,2′-bipy) (H_2dbp)]$_n$ (3)

Compound **3** crystallizes in triclinic space group *P*-1. As shown in the Figure 3.4a, Co(II) ion is present in square pyramidal CoN_2O_3 geometry constituted by the two nitrogen atoms from 2,2′-bipy ring and three oxygen atoms from three H_2dbp^{2-} ligands**.** The ligand

H_2dbp^{2-} coordinates to the two Co(II) centers on either sides with different coordination modes (Figure 3.4b). The PO_3H group on the arm C24–P2 of two H_2dbp^{2-} ligands bridges the two Co(II) ions in a typical μ_2 bridging mode to form a eight membered Co–$(OPO)_2$–Co ring leaving P–OH groups into the interstitial positions as shown in the Figure 3.4c. The PO_3H group on the other arm C11–P1 of the same two H_2dbp^{2-} ligands connects the Co atoms of two eight membered rings through P=O group in μ_1 coordination mode at the apical positions leaving P–OH and P–O^- into the interstitial positions.

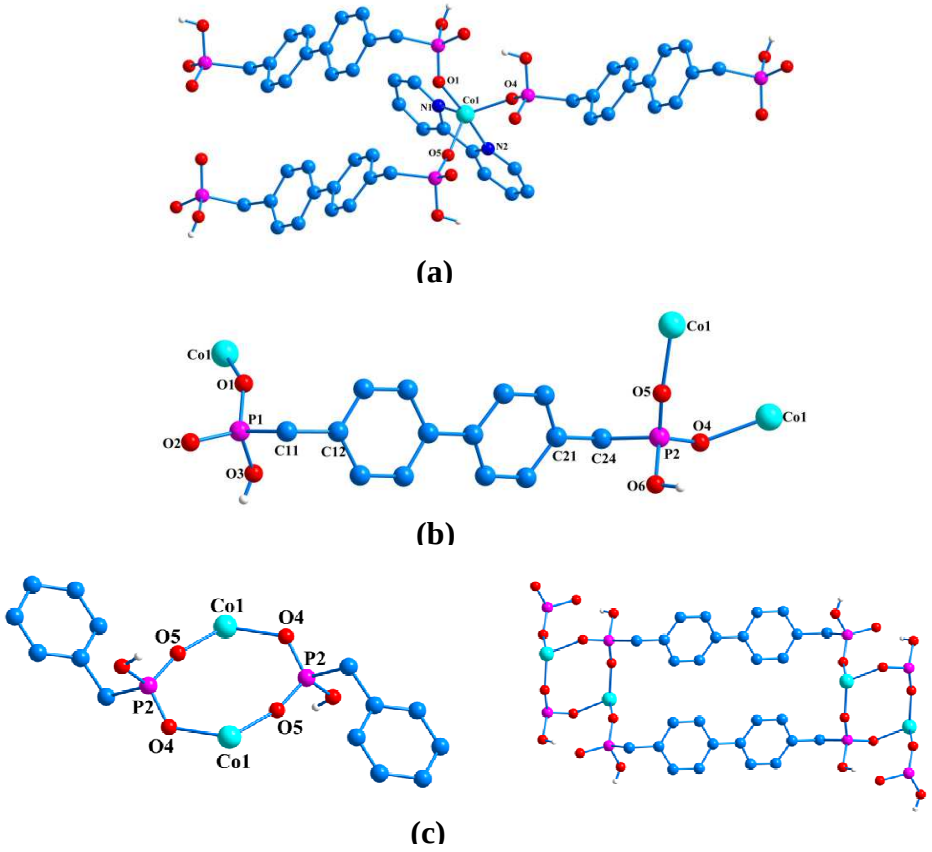

Figure 3.4. (a) Molecular diagram of compound **3** with metal polyhedra labeling, (b) Coordination modes of PO_3H groups in H_2dbp^{2-} of compound **3**, (c) Eight membered Co-dimer ring formed in compound **3** (left), pair of Co-dimers connected by the pair of H_2dbp^{2-} ligands to form a closed loop (Right).

The P–O bonds are assigned based on the bond lengths that are in good agreement with the literature [20]. Two such types of H_2dbp^{2-} ligands with μ_1 and μ_2 coordination modes link the four Co atoms to form a closed loop as shown in the Figure 3.4c. These loops are extended by other set of loops to form a 1D extended double chain as shown in the Figure 3.5. The ligand H_2dbp^{2-} anion exists in a typical *trans* conformation with antiperiplanar torsion angle of 177.7° between two phosphonic acid groups (viewed through P1–C11–

C24–P2) and creates a separation of 14.91 Å between two metal centers. In the biphenyl skeleton of H_2dbp^{2-} ligand, the phenyl group connected to μ_1–PO_3H group twists from the phenyl group connected to the μ_2–PO_3H by an angle of 16.46° (Scheme 3.5).

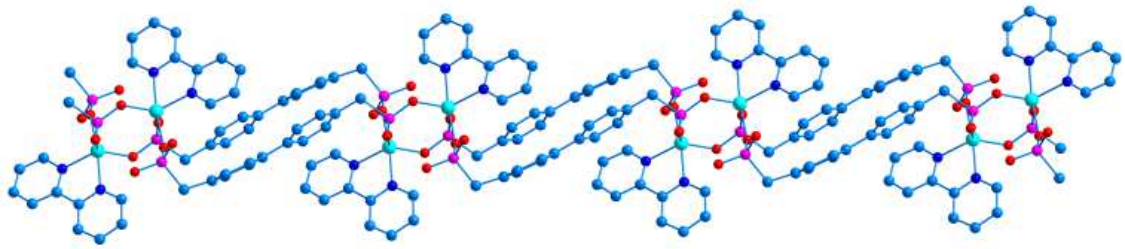

Figure 3.5. 1D extended double chain formed in the compound **3.**

Usually in the flexible ligands, if the ligand exists in *trans* conformation it leads to formation of higher dimensional structures but in compound **1** the *trans* conformation of the H_2dbp^{2-} ligand forms a 1D chain with $Co_2(H_2dbp)_2$ loops as shown by generally *cis* conformation. This is probably due to availability of more number of oxygen atoms on the phosphonate groups (PO_3H) and also the minor twist in the benzene rings of the biphenyl spacer that tends to form a closed loops rather than extended structures. As anticipated, the classical hydrogen bonding is observed between the P–OH groups of two adjacent 1D chains. The P–OH groups present on the arm in which PO_3H group exhibits μ_1 coordination mode are involved in the strong hydrogen bonding between two adjacent 1D chains to from a 2D supramolecular sheet (Figure 3.6).

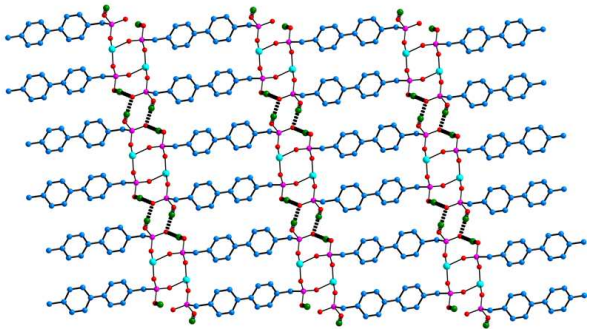

Figure 3.6. 2D supramolecular network formed due to hydrogen bonding between the P–OH groups of the adjacent chains in compound **3**.

Structural description of [Ni (2,2´-bipy)$_2$(H_2dbp)(H_2O)]·H_2O (4)

Compound **4** is a discrete compound that crystallizes in triclinic space group *P*-1. The relevant crystal structure consists of dipositive Ni ion in distorted NiN_4O_2 octahedral environment constituted by two bipyridine ligands; H_2dbp^{2-} ligand, one coordinated aqua ligand and one lattice aqua ligand (Figure 3.7a). Two bipyridine ligands block the three

equatorial coordination sites and one apical coordination site of the Ni(II) octahedron leaving one equatorial and one apical sites for coordination with the phosphonic acid. The Ni–N bond distances are in the range of 2.071Å to 2.082 Å. The residual equatorial site is coordinated by the phosphonic acid H_4dbp in the dianionic form H_4dbp^{2-} through the P=O group and the remaining apical site is coordinated by the aqua ligand with Ni–O distance of 2.077 Å. One arm of the H_2dbp^{2-} ligand is coordinated to the metal polyhedra through P=O group, with μ_1 coordination mode leaving P–OH and P–O^- groups into interstitial positions and the other arm (PO_3H) remains uncoordinated resulting in a discrete molecular structure rather than coordination polymer.

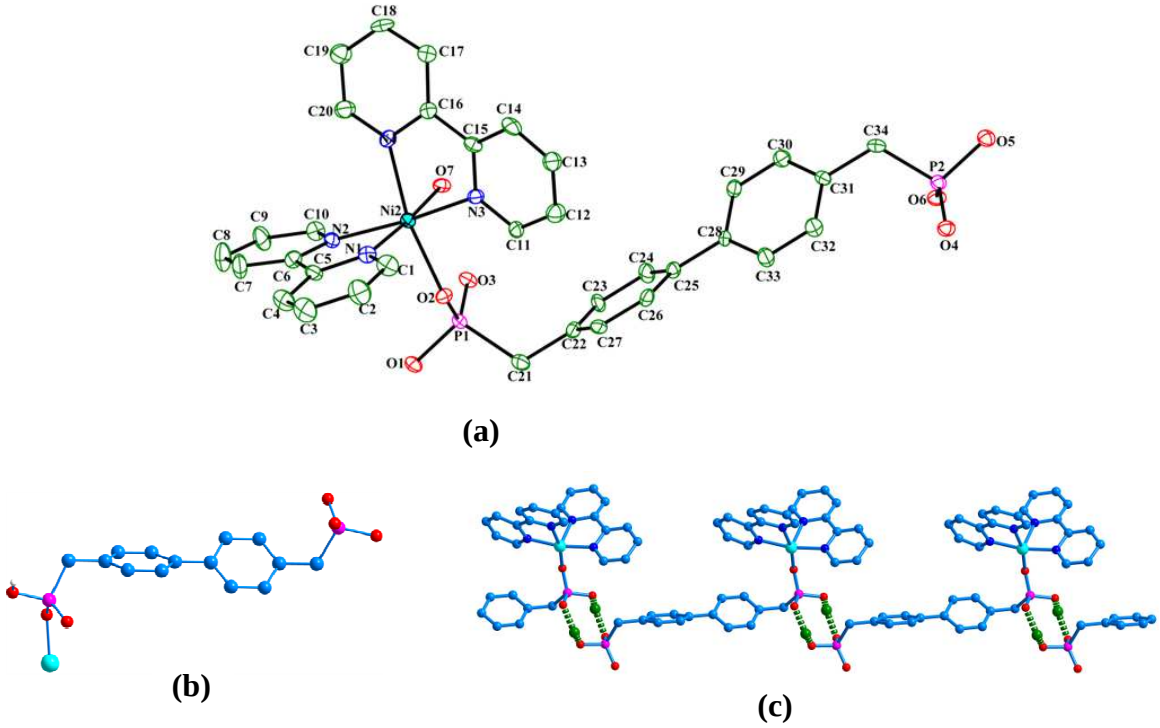

Figure 3.7. (a) ORTEP diagram of compound **4** at 30% probability level (Hydrogen atoms are omitted for clarity), (b) Conformation of H_2dbp^{2-} ligand in compound **4**, (c) 1D supramolecular chain formed due to hydrogen bonding between the adjacent molecular units.

In the biphenyl skeleton of H_2dbp^{2-} ligand, the phenyl ring connected to the non-coordinated PO_3H arm is twisted from the phenyl ring connected to the coordinated PO_3H arm by a large angle of 39.04° (Scheme 3.5); consequently the orientation of CH_2–PO_3H group of the twisted phenyl ring completely deviates from the mean position as shown in the Figure 3.7b. Further the two CH_2–PO_3H groups of H_2dbp^{2-} ligand are twisted with respect to each other by an antiperiplanar torsion angle of 157.51°. The formation of discrete structure apart from the extended coordination structure is mainly attributed to the large twisting of the phenyl ring in the biphenyl skeleton from the mean position.

Due to presence of P–OH groups, classical hydrogen bonding was observed between the molecular structures. The P–OH group on the non-coordinated PO_3H arm of one molecular compound is strongly connected to the $P–O^-$ group of the coordinated PO_3H arm of other molecular compound and vice versa through hydrogen bonding to form an eight membered $R^2_2(8)$ ring (Table 3.3). This type of connectivity leads to form a 1D supramolecular chain along the crystallographic *b* axis as shown in the Figure 3.7c.

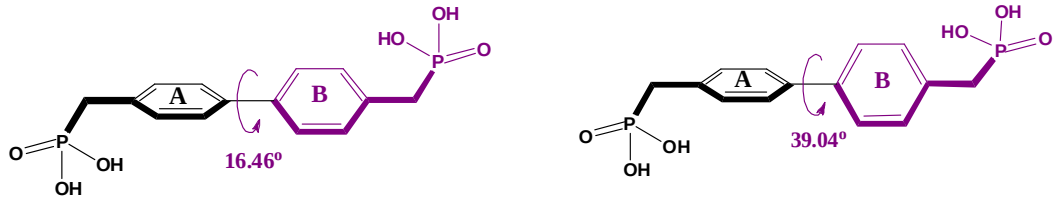

Scheme 3.5. Scheme representing the twisting of the benzene rings in the biphenyl spacer of the H_2dbp^{2-} in compounds **3** (Left) and **4** (Right).

3.3.3. Effect of length of the bisphosphonic acid

Compounds **1** and **2** are two isomorphous structures of general formula $[M(2,2´\text{-bipy})_2H_4pxp]_n[H_2pxp]_n$ (M=Co(II) and Ni(II)) with p-xylylene bisphosphonic acid and 2,2´-bipy as secondary ligand. 2,2´-bipy blocks the four coordination sites at the metal polyhedra and allows only two sites for the H_xpxp (x refers to protonated hydroxyl groups) to coordinate with the metal center. In order to meet this coordination requirement (*i.e.* to satisfy the coordination sites: one equatorial and one apical sites) a flexible non-rigid ligand H_xpxp has adopted a rare *cis* conformation in neutral form and thereby the charge is neutralized by the *trans* conformation of H_xpxp in anionic form. These two compounds are classical examples that feature the flexibility of the ligand to exist in both *cis* and *trans* conformations to meet the coordination geometry at the metal centre. In the present study, we also extend the length of the phosphonic acid by increasing one phenyl ring (H_4dbp) to investigate the effect on the final structures. Thus by introducing the other phenyl ring into the spacer, the twisting of two phenyl rings with respect to each other in the biphenyl moiety plays an important role in the self assembly process. The coordination environment of the metals is different in both the compounds *i.e.*, square pyramidal in compound **3** and octahedral in compound **4**.

In compound **3**, Co(II) ion is present in square pyramidal geometry in which two sites are blocked by the 2,2´-bipy ring and the remaining three coordination sites are occupied by the oxygen atoms from the three H_2dbp^{2-} ligands. Compound **3** is stoichiometrically

related to compound [Cu(2,2´-bipy)(H_2pxp)]·2H_2O (**1A**) reported in the previous chapter in which the spacer in the phosphonic acid is mono phenyl ring. The coordination environment and the protonation state of the phosphonic acids is same in both the compounds but **3** is 1D double chain whereas **1A** is a 2D layer. The difference in the dimensionality of these two compounds is mainly due to increase in the length of the spacer in the phosphonic acid by one phenyl ring (present study) which creates a twisting in the biphenyl group thereby the flexible arm adopt different orientations.

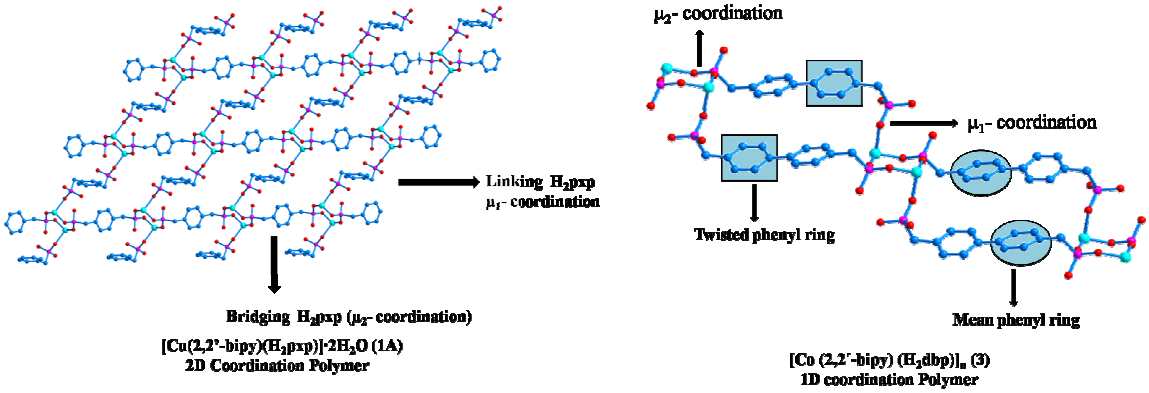

Figure 3.8. 2D packing diagram of Compound **1A** showing the coordination modes of the H_2pxp^{2-} ligand (left); 1D chain of compound **3** viewing the conformation and coordination modes of the H_2dbp^{2-} ligand (Right).

As shown in the Figure 3.8, in compound **1A**, two types of phosphonic acids are present in the crystal structure which differs in terms of coordination mode. The bridging H_2pxp bridges the Cu(II) atoms in μ_2 coordination mode to form a eight membered Cu-dimer rings and extended by the p-xylyl linkers to form a 1D chain and these chains are linked by the linking H_2pxp^{2-} ligand in μ_1 coordination mode to form a 2D network. But interestingly in compound **3**, the PO_3H groups in the phosphonic acid H_2dbp^{2-} adopt different coordination modes on either arms (*i.e.*, μ_1 on one arm and μ_2 on another arm). As shown in the Figure 3.8, one arm of H_2dbp^{2-} adopts μ_2 coordination mode and expected to adopt same coordination mode on other side. However, due to twisting of the phenyl ring B from the phenyl ring A by an angle of 16.46° (See Scheme 3.5) it changes the orientation of the PO_3H groups on the phenyl ring B that tends to adopt μ_1 coordination mode rather than μ_2 to meet the coordination geometry of the metal ion. This minor twist of the phenyl ring in the biphenyl skeleton changes the orientation of the CH_2–PO_3H groups on the phenyl ring B to adopt a different coordination mode as a result 1D double chains are formed in the compound **3** (Figure 3.8). Wang et al., also reported a 1D compound $[Cu_2(phen)_2(H_3dbp)_2(H_2dbp)]_n$ based on biphenyl bisphosphonic acid in which

two types of $H_x$dbp ligands are present in the crystal structure which differs mainly in the protonation states and adopts same coordination mode.[18] In which, two Cu(II) ions are linked by a pair of H_3dbp^{1-} ligands to form a molecular boxes and these boxes are linked by the H_2dbp^{2-} ligand to form a 1D extended chains.

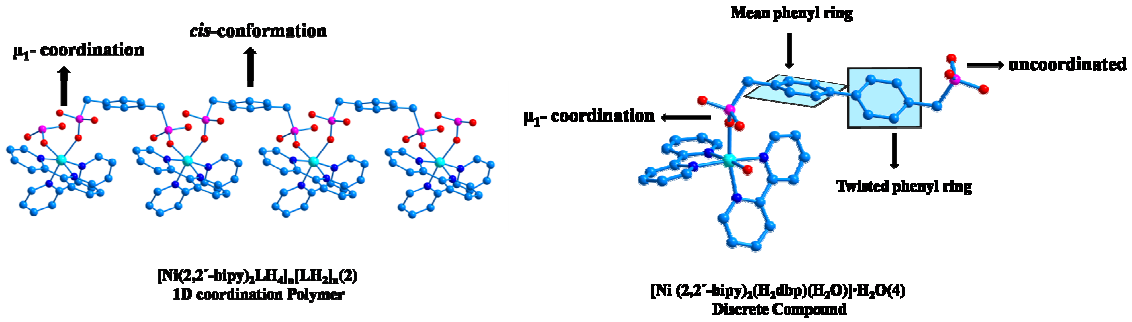

Figure 3.9. 1D cationic chain formed in the compound **2** viewing the conformation and coordination of the H_2pxp^{2-} ligand (left); Discrete compound **4** showing the mean and twisted phenyl rings in the H_2dbp^{2-} ligand (Right).

Compound **4** elaborately explains the effect of the twisting of the phenyl ring in the biphenyl skeleton in forming the low dimensional structures. The situation in compound **4** can be explained by the compound $[Ni(2,2´\text{-bipy})_2H_4pxp]_n[H_2pxp]_n$ (**2**). In both the compounds, the Ni ion is present in octahedral environment, in which three equatorial and one apical coordination sites are blocked by the two 2,2´-bipy rings to form $[Ni(□)_{eq}(□)_{ap}(2,2´\text{-bipy})_2]^{2+}$ cation. In compound **2**, H_4pxp adopts the rare *cis* conformation to meet the coordination geometry created by the 2,2´-bipy rings at the metal center (i.e one equatorial and one apical) resulting in a 1D chain $[Ni((2,2´\text{-bipy})_2$ *cis*-$H_4pxp]_n^{2+}$ and the charge is neutralized by the ligand H_2pxp^{2-} as lattice component in *trans* from. In the complex cation $[M(□)_{eq}(□)_{ap}(2,2´\text{-bipy})_2]^{2+}$ the linker phosphonic acid has only possibility to exist in the *cis* conformation to link the two cations. Recently Sun et al., also reported a compound similar to **2** with cadmium[19] which supports that only *cis* conformation of the flexible phosphonic acid has tendency to link this type of complex cations to form an extended 1D chains. In a similar way in compound **4**, the phosphonic acid H_4dbp in its neutral from or anionic form (H_2dbp^{2-}) has to adopt *cis* conformation to meet the coordination vacancies in the complex cation $[Ni(□)_{eq}(□)_{ap}(2,2´\text{-bipy})_2]^{2+}$. In compound **4**, the residual equatorial site is coordinated by the H_2dbp^{2-} through P=O group and the other end should be coordinated to the apical site by adopting the *cis* conformation. But due to biphenyl spacer in the phosphonic acid the phenyl ring B twists from the mean plane by an large angle of 39.04° and changes the orientation of the PO_3H groups on the flexible arm

as a result it does not meet the coordination geometry at the metal center and does not link the complex cations (Figure 3.9). The twisting of the phenyl ring B to a large extent completely changes the direction of the PO_3H groups, as a result, it does not meet the required conformation (*i.e., cis*) to act as a linker; consequently the molecular complex does not extend to the 1D polymer and remains as a discrete compound. The resulting complex $[Ni(2,2´\text{-bipy})_2(H_2dbp)]$ accommodates the water molecule into the apical site to furnish the octahedral geometry.

Based on the aforementioned discussion, the attachment of rigid biphenyl spacer to the flexible phosphonate groups have an accountable role in directing the dimensionality of the final products. The combination of both the twisting in benzene rings and the flexible nature of the CH_2 groups changes the orientation of the phosphonate groups. Due to this multiple effect, the two fold axis of symmetry in H_2dbp^{2-} is absent in both the compounds and the CH_2–PO_3H groups are twisted with respect to each other by a torsion angle of 177.79° and 157.49° in the compounds **3** and **4** respectively instead of 180.0°. The similar type of spacers (CH_2–C_6H_4–C_6H_4–CH_2) were also reported with imidazoles (4,4'-bis(imidazol-l-ylmethyl)biphenyl)[20] and triazoles (4,4'-bis(1,2,4-triazol-1-ylmethyl)biphenyl)[21]. But this effect does not show any influence in the dimensionality of the final compounds, because these ligands are only monodentate with μ_1 coordination mode. Metal carboxylates based on this ligand are not reported in the literature. As the number of coordinating atoms in the coordinating group increases, the coordination modes also increases, as result even a small twist in the phenyl rings of biphenyl spacer shows a major difference in the dimensionality as in the case of the phosphonates discussed here.

3.3.4. Thermal Properties

The TGA curve of compound $[Ni^{II}(2, 2´\text{-bipy})_2LH_4]_n[LH_2]_n$ (**2**) exhibits a thermal stability up to 320 °C. There are several weight loses in the region from 320 °C to 900 °C which are attributed to condensation of the hydroxyl groups in both the phosphonate ligands and combustion of bipyridine and organic ligands with the observed weight loss of 60% (theoretical values of 61.3%). The final end product is supposed to be $Ni(PO_3)_2$ with a formula weight of 216.0 (23%) but the observed weight remained is 333.0 (37%); this increase in weight may be due to the retention of some P_2O_5 at this temperature as shown by the continuous weight loss from 900 °C to 1100 °C. Compound $[Co^{II}(2,2´\text{-bipy})_2LH_4]_n[LH_2]_n$ (**1**) also exhibits a comparable TG curve that shows thermal stability

up to 315 °C. The TGA curve shows similar weight loses as shown in the TG curve of compound **2**. The final end product is supposed to be $Co(PO_3)_2$ with a formula weight of 216.0 (23%) but the observed weight remained is 180.2 (20%); this may be due to some loss of P_2O_5. Both TG curves are shown in Figure 3.10.

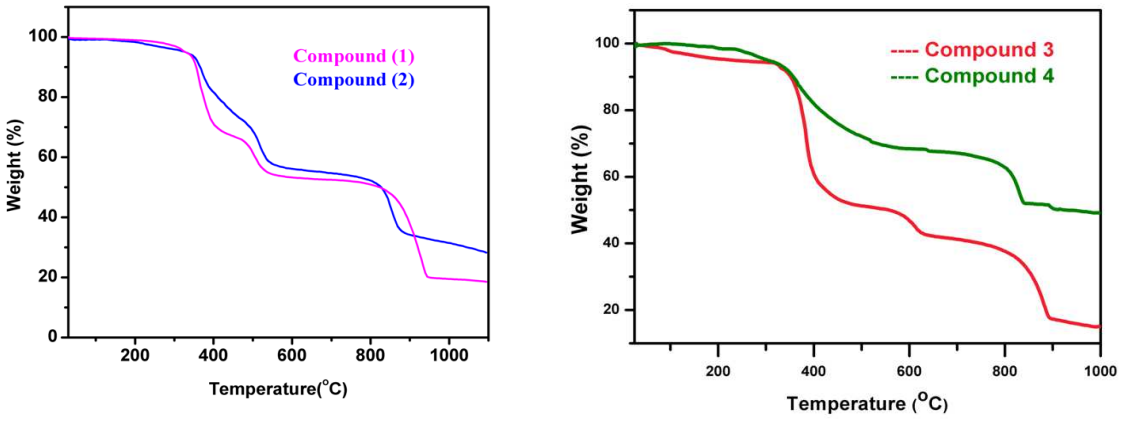

Figure 3.10. Thermogravimetric curves for compounds **1, 2** and **3**, **4.**

TGA curves are made under flowing N_2 for the compounds **3** and **4** in the temperature range 30–1000 °C (Figure 3.10). Compound **3** shows thermal stability up to 320 °C with weight loss of 6.2 % attributed to condensation of hydroxyl groups of the phosphonate ligands (theoretical values of 6.48%). From 320 °C to 900 °C, compound **3** undergoes continues weight losses in three steps due to combustion of organic groups 2,2′-bipyridine and biphenyl rings. The final end product is supposed to be $Co(PO_3)_2$ with a formula weight of 216.0 (38%) but the observed weight remained at 1000 °C is 83.25 (15%) . The difference in the weight, observed, is due to initial loss of water molecules due to condensation and loss of P_2O_5 from the residual mass. The overall decomposition and stability of the compound **3** follows the normal pathway as described for the metal phosphonates. Compound **4** is discrete compound and shows stability up to 290 °C with weight loss of 4.2% attributed to one coordinated and one lattice molecule (theoretical values of 4.8%) and undergoes continues weight losses up to 850 °C due to combustion of organic groups and shows constant residual mass of 366.3 (49.2%) up to 1000 °C. The final end product is supposed to be $Ni(PO_3)_2$ with a formula weight of 216.0 (38%) but the increase in the residual mass at 1000 °C is due to retention of some P_2O_5.

3.3.5. Electronic Properties

Compounds **1** and **2** are additionally characterized by solid state electronic absorption spectroscopy. The relevant diffuse reflectance spectra are shown in the Figure 3.11. Both compounds have almost identical electronic absorption spectral features except there is a well defined d-d band for compound **1**.

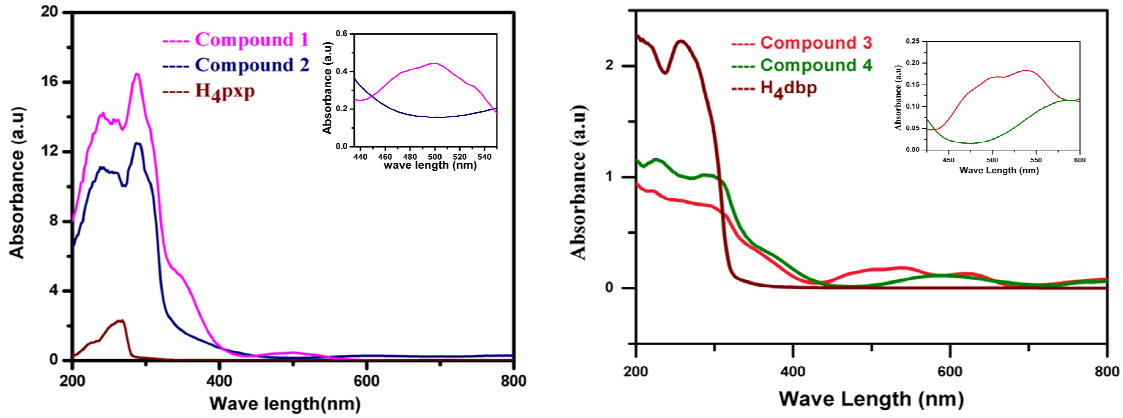

Figure 3.11. Diffuse reflectance electronic spectra for compounds **1, 2** and **3, 4.**

The compounds **3** and **4** are also characterized by the solid state electronic absorption spectroscopy. The relevant electronic spectra of both compounds compared with the phosphonic acid H_4dbp is shown in the Figure 3.11. Both the compounds show similar absorption peaks as displayed by the H_4dbp ligand. But there is a well defined d-d transition in the compound **3** in the region 450−555 nm which contains Co(II) ion.

3.3.6. Magnetic Properties

A variable temperature magnetic susceptibility measurement of the compound **4** was performed in the temperature region of 2– 300 K in an applied dc field of 1 K Oe. Both χ_M Vs T and χ_MT Vs T plots were shown in the Figure 3.12. (where χ_M is the magnetic susceptibility per Co^{II}_2 unit). The room temperature (300 K) $\chi_M T$ product amounts to 5.48 cm^3 K mol^{-1}, which is higher than the expected value of 3.75 cm^3 K mol^{-1} for two isolated high-spin Co(II) ions (g = 2 and S = 3/2). As the temperature is lowered, the $\chi_M T$ value continuously decreases to 4.27 cm^3 K mol^{-1} at 22 K and then sharply decreases up to 2 K reaching a minimum value of 1.34 cm^3 K $mol^{-1.}$ The $1/\chi_M$ *vs* T plot follows the Curie-Weiss law with negative Weiss constant Θ = –8.7 K. The decrease in $\chi_M T$ value with temperature and negative Weiss constant suggest antiferromagnetic interactions between the two Co(II) centers.

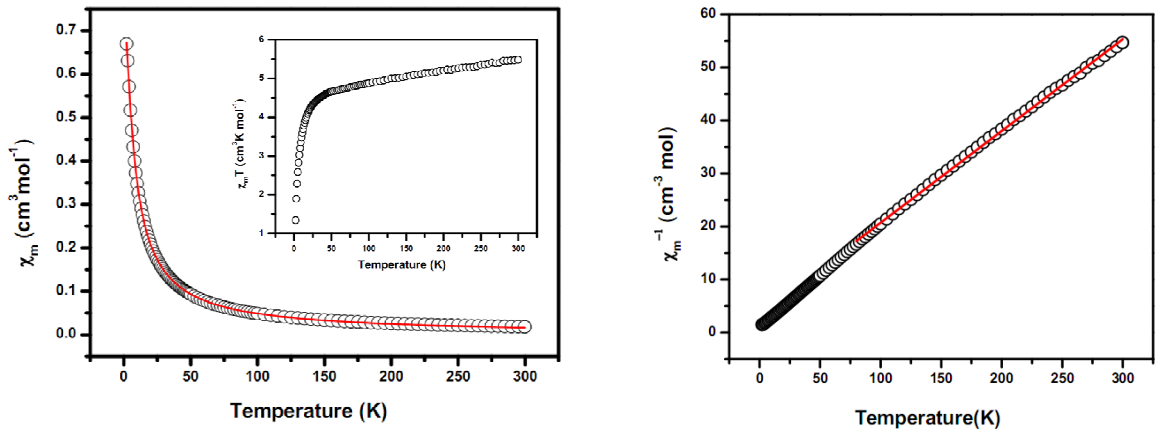

Figure 3.12. χ_M Vs T in the temperature range of 2–300 K (Inset graph shows χ_MT Vs T) of compound **4**. The red line indicates the fitting using theoretical model (see text) and $1/\chi_M$ *vs T* plot of compound **4**.

The magnetic data were fitted assuming the phosphonate bridges of the two Co(II) ions form a isolated spin dimer. By introducing inter-dimer magnetic coupling constant *zJ′* the magnetic susceptibility data from 2–300 K was fitted from the following equation which was deduced from the spin Hamiltonian.[22]

$$H = -JS_1 \bullet S$$

(where S_1 and S_2 are the spin operators with $S_1=S_2=3/2$)

$$E(S_T) = -JS_T(S_T+1)$$

$$S_T = 0, 1, 2, 3.$$

$$E(S_T) = 0, -J, -3J, -6J$$

$$\chi_M = \chi_M'/\{1-\chi_M'(2zJ'/Ng^2\beta^2)\}$$

$$\chi_M' = (2Ng^2\beta^2/KT)[A/B]$$

$$Where\ A=[exp(J/KT) +5exp(3J/KT) +14exp(6J/KT)]\ and$$

$$B=[1+ 3exp(J/KT) +5exp(3J/KT) +7exp(6J/KT)]$$

*The parameters **N**, β and K have their normal meanings. The best fit of the theoretical equation to the experimental data leads to the g= 2.332 (2) J= –0.685 (2) cm^{-1} and zJ′= –0.038 (4) with agreement factor of 8.4 X 10^{-8} (where $R=\Sigma[(\chi_MT)_{exp}-(\chi_MT)_{cal}]^2/\Sigma(\chi_MT)_{exp}^2$).*

The studies on magnetic behaviour of isolated Co(II)-dimers bridged by the phosphonate bridges are very rare when compared to the carboxylate bridges. But the magnetic behaviour of Co(II) ions bridged the phosphonate bridges to form a extended metal oxide coordination architectures are well studied. Clearfield et al., reported a compound $[Co_2(pxp)(H_2O)_2]$ in which the Co atoms are bridged by the phosphonate oxygen's to form a 2D metal oxide layers and the Co(II) ions shows a net antiferromagnetic interactions in

these layers.[12b] But till to the date, an isolated Co-dimer bridged by the phosphonate bridges is not reported and compound **4** represents a classical example of such system. From the crystal structure of the compound **4**, the only possible path way for spin exchanges between two Co(II) ions is phosphonate bridges; no other pathways (either through hydrogen bonding or through short inter dimer separation) are not possible. The magnitude of exchange parameter obtained through exchange between the Co(II) ions through the phosphonate bridges in the eight membered ring is very less indicating the weak σ pathway.

3.4. Conclusion

In conclusion, in this chapter, we report four novel structures in which, two are isomorphous one dimensional metal phosphonates of general formula $[M(2,2´\text{-bipy})_2(H_4pxp)]_n[H_2pxp]_n$ (M=Co (**1**), Ni (**2**)) and two are $[Co(2,2´\text{-bipy})(H_2dbp)]_n$ (**3**) and $[Ni(2,2´\text{-bipy})_2(H_2dbp)(H_2O)]\cdot H_2O$ (**4**). Compounds **1** and **2** are based on *p*-xylylenediphosphonic (H_4pxp) acid where 2, 2´-bipyridine used as secondary ligand component. The use of secondary ligand component prevents the spatial expansion into 3-D by blocking the coordination sites of the metal centre. The conformational freedom of the flexible non-rigid *p*-xylylenediphosphonic acid allows tending to be in *cis* conformation to meet the coordination geometry of the metal centre, as some of the coordination sites are already blocked by the secondary ligand components. This is the rare example in which *p*-xylylenediphosphonic acid adopts both *cis* and *trans* conformation during its coordination. Multiple hydrogen bonding interactions between the 1-D polymeric chains result in the formation of 2-D network consisting of cylindrical channels. The two compounds $[Co(2,2´\text{-bipy})(H_2dbp)]_n$ (**3**) and $[Ni(2,2´\text{-bipy})_2(H_2dbp)(H_2O)]\cdot H_2O$ (**4**) are based on rigid spacered flexible ligand H_4dbp with secondary linker 2,2´-bipyridine. Compound **3** is a extended double chain in which Co(II) ion is in square pyramidal geometry and H_2dbp^{2-} adopts a regular *trans* conformation to form a closed loops. Compound **4** is a discrete compound in which Ni(II) ion exists in octahedral geometry and H_2dbp^{2-} also exists in regular *trans* conformation. The twisting of benzene rings in the biphenyl spacer changes the orientation of the PO_3H groups of the H_2dbp^{2-} in compound **3** thereby the ligand adopt different coordination modes by the PO_3H groups on both ends resulting in the formation of 1D chains rather that 2D layers as obtained in case of H_4pxp ligand with same empirical formula. In a similar way in

compound **4** the benzene rings in the biphenyl spacer of the H_2dbp^{2-} ligand twist by a large angle of 39.04° as a result the conformation of the H_2dbp^{2-} ligand changes, due to which the ligand does not meet the coordination requirements at the metal center to link the metal polyhedra thereby form a discrete compound. The comparison of compounds **3** and **4** with the compounds based on the H_4pxp ligand reveals that twisting in the benzene rings of the biphenyl spacer is accountable for obtaining low dimensional compounds. The effect is primarily pronounced in the multidentate ligands rather than monodentate ligands. The systems presented in the chapter proves to be a good example to investigate self assembly process and provides more information of the directional synthesis of the targeted coordination polymers.Compound **3** is a first example to report the simplest and isolated Co-dimer bridged by the three membered OPO bridges. Analysis of variable temperature magnetic susceptibility measurement curves of compound **3** shows weak antiferromagnetic interactions between the metal ions through these OPO bridges.

Table 3.1. Crystallographic details of compounds **1**−**4**.

	1	**2**
Formula	$C_{36}H_{38}N_4O_{12}P_4Co$	$C_{36}H_{38}N_4O_{12}P_4Ni$
FW	901.51	901.29
Crystal system	Monoclinic	Monoclinic
Space group	*C*2/*c*	*C*2/*c*
a/Å	18.113(3)	18.051(4)
b/Å	24.451(3)	24.356(4)
c/Å	8.778(13)	8.776(16)
α [°]	90.00	90.00
β [°]	102.996(3)	103.119(4)
γ [°]	90.00	90.00
Z	4	4
ρ_{cal}/ Mg m^{-3}	1.581	1.593
Goodness-of-fit on F^2	1.093	1.128
$R_1(F^2_0)$ [I > 2 σ(I)]	0.0357	0.0532
wR_2 (F^2_0) [I > 2 σ(I)]	0.0832	0.1155
$R_1(F^2_0)$ (all data)	0.0403	0.0617
wR_2 (F^2_0) (all data)	0.0855	0.1199
Largest diff. peak and hole [e.$Å^{-3}$]	0.317 and -0.250	0.861 and -0.336
	3	**4**
Formula	$C_{24}H_{22}CoN_2O_6P_2$	$C_{34}H_{34}N_4NiO_8P_2$
FW	555.31	747.30
T(K) / *λ*(Å)	298/0.71073	298/0.71073
Crystal system	Triclinic	Triclinic
Space group	*P*-1	*P*-1
a/Å	10.959(2)	10.670(2)
b/Å	11.028(2)	11.900(2)
c/Å	11.353(2)	14.080(3)
α [°]	75.62(3)	77.80(3)
β [°]	83.96(3)	68.46(3)
γ [°]	62.63(3)	82.23(3)
Volume ($Å^3$)	1180.2(4)	1622.1(5)
Z, ρ_{cal}/ Mg m^{-3}	2, 1.563	2, 1.530
Goodness-of-fit on F^2	1.035	1.059
R1/ wR2 [I > 2σ (I)]	0.0505/0.1067	0.1087/0.1503
R1/ wR2 (all data)	0.0813/0.1209	0.1981/0.1936
Largest diff. peak and hole [e.$Å^{-3}$]	0.629 and -0.369	1.006 and -0.476

Table 3.2. Selected bond lengths (Å) and bond angles (°) of compounds **1**−**4**

Distances	Bond lengths	Angles	Bond angles
	$[Co^{II}(2,2´\text{-bipy})_2LH_4]_n[LH_2]_n$(1)		
Co(1)-N(1)	2.145(19)	N(1)-Co(1)-N(1) #1	169.18(11)
Co(1)-N(2)	2.140(2)	O(3) #1-Co(1)-N(2)	164.41(7)
Co(1)-O(3)	2.045(17)	O(3)-Co(1)-N(1)	98.79(7)
P(1)-O(1)	1.543(18)	N(2)-Co(1)-N(2) #1	92.49(11)
P(1)-O(2)	1.554(19)	N(1)#1-Co(1)-N(2)#1	76.01(8)
P(1)-O(3)	1.478(17)	O(3)#1-Co(1)-O(3)	96.16(11)
P(2)-O(4)	1.513(17)	O(3)#1-Co(1)-N(1)	88.46(7)
P(2)-O(5)	1.500(17)	N(1)#1-Co(1)-N(2)	96.39(11)
P(2)-O(6)	1.552(2)		
	$[Ni^{II}(2,2´\text{-bipy})_2LH_4]_n[LH_2]_n$(2)		
Ni(1)-N(1)#2	2.083(3)	N(1)-Ni(1)-N(1) #2	171.01(16)
Ni(1)-N(2)#2	2.087(3)	O(3) #2-Ni(1)-N(2)	166.43(11)
Ni(1)-O(3)	2.040(3)	O(3)-Ni(1)-N(1)	97.76(11)
P(1)-O(1)	1.549(3)	N(2)-Ni(1)-N(2) #2	94.61(16)
P(1)-O(2)	1.555(3)	N(1)#2-Ni(1)-N(2)#2	78.04(11)
P(1)-O(3)	1.475(3)	O(3)#2-Ni(1)-O(3)	93.67(17)
P(2)-O(4)	1.516(2)	O(3)#2-Ni(1)-N(1)	88.40(11)
P(2)-O(5)	1.498(3)	N(1)#2-Ni(1)-N(2)	95.79(11)
P(2)-O(6)	1.556(4)		
	[Co (2,2´-bipy) $(H_2dbp)]_n$ (3)		
Co(1)-O(5)#1	1.968(3)	O(5)#1-Co(1)-O(4)#2	118.46(12)
Co(1)-O(4)#2	1.997(2)	O(5)#1-Co(1)-O(1)	94.79(12)
Co(1)-O(1)	2.041(2)	O(5)#1-Co(1)-O(1)	94.79(12)
Co(1)-N(1)	2.111(3)	O(4)#2-Co(1)-O(1)	98.61(10)
Co(1)-N(2)	2.160(3)	O(5)#1-Co(1)-N(1)	109.75(11)
P(1)-O(1)	1.497(2)	O(4)#2-Co(1)-N(1)	127.04(11)
P(1)-O(2)	1.515(2)	O(1)-Co(1)-N(1)	97.92(11)
P(1)-O(3)	1.562(3)	O(5)#1-Co(1)-N(2)	84.70(12)
P(2)-O(5)	1.469(3)	O(4)#2-Co(1)-N(2)	87.50(11)
P(2)-O(4)	1.498(2)	O(1)-Co(1)-N(2)	173.27(10)
P(2)-O(6)	1.567(3)	N(1)-Co(1)-N(2)	76.01(11)
	[Ni $(2,2´\text{-bipy})_2(H_2dbp)(H_2O)]\cdot H_2O$ (4)		
Ni(2)-N(2)	2.069(7)	N(2)-Ni(2)-N(3)	169.4(3)
Ni(2)-N(3)	2.072(7)	N(2)-Ni(2)-O(2)	94.4(3)
Ni(2)-O(2)	2.076(6)	N(3)-Ni(2)-O(2)	92.2(3)
Ni(2)-O(7)	2.077(6)	N(2)-Ni(2)-O(7)	96.4(3)
Ni(2)-N(4)	2.080(8)	N(3)-Ni(2)-O(7)	91.8(2)
Ni(2)-N(1)	2.082(7)	O(2)-Ni(2)-O(7)	90.6(2)
P(1)-O(2)	1.509(6)	N(2)-Ni(2)-N(4)	95.7(3)
P(1)-O(3)	1.510(6)	N(3)-Ni(2)-N(4)	78.5(3)
P(1)-O(1)	1.567(5)	O(2)-Ni(2)-N(4)	168.8(2)
P(1)-C(21)	1.788(10)	O(7)-Ni(2)-N(4)	83.5(3)
P(2)-O(6)	1.480(6)	N(2)-Ni(2)-N(1)	78.7(3)
P(2)-O(4)	1.517(6)	N(3)-Ni(2)-N(1)	92.9(3)
P(2)-O(5)	1.586(5)	O(2)-Ni(2)-N(1)	91.2(3)

Symmetry transformations used to generate equivalent atoms:
#1 -x,y,-z+3/2, #2 -x,y,-z+1/2 #1 -x+1,-y+1,-z+1 #2 x-1,y+1,z-1 #3 x+1,y-1,z+1.

Table 3.3. Hydrogen bonding table for compounds **1**−**4**

D-H···A	D-H(Å)	H··· A(Å)	D··· A(Å)	D-H···A (°)
		$[Co^{II}(2,2´\text{-bipy})_2LH_4]_n[LH_2]_n$(1)		
O(1)-H(1A) ···O(5)#1	0.96(4)	1.52(5)	2.482(2)	176(4)
O(2)-H(2A) ···O(4)#2	0.79(3)	1.75(3)	2.535(3)	174(3)
O(6)-H(6A) ···O(4)#3	0.80(4)	1.78(4)	2.580(3)	171(4)
		$[Ni^{II}(2,2´\text{-bipy})_2LH_4]_n[LH_2]_n$(2)		
O(1)-H(1A)...O(5)#3	0.94(7)	1.57(7)	2.494(4)	169(7)
O(2)-H(2A)...O(4)#4	0.80(6)	1.73(6)	2.528(4)	173(6)
O(6)-H(6A)...O(4)#4	0.82	1.80	2.572(4)	155.2
		$[Co\ (2,2´\text{-bipy})\ (H_2dbp)]_n$ (3)		
O(6)-H(6A)...O(2)#1	0.89(5)	1.77(5)	2.638(4)	165(5)
O(3)-H(3A)...O(2)#2	0.77(5)	1.87(5)	2.643(4)	174(6)
		$[Ni\ (2,2´\text{-bipy})_2(H_2dbp)(H_2O)]\cdot H_2O$ (4)		
O(5)-H(5A)...O(3)#3	0.82	1.82	2.639(8)	175.8
O(1)-H(1A)...O(4)#4	0.82	1.82	2.609(8)	159.8
O(7)-H(70)...O(6)#5	0.94(8)	1.81(8)	2.747(8)	170(7)

#1 –x+1, y, -z+1.5, #2 x, -y+1, z+0.5
#3 –x+1, y, -z+0.5 #4 –x, -y+1, z+0.5.
#1 x+1,y-1,z+1 #2 -x,-y+1,-z
#3 x,y,z-1 #4 x,y,z+1 #5 -x,-y+1,-z

Table 3.4. Phosphorus−oxygen bond lengths in compound **2**

Coordinated *cis* neutral phosphonic acid LH_4 (in Å)		Uncoordinated *trans* ionic phosphonic acid LH_2^{2-} (in Å)	
P1-O1 **(P-OH)**	1.549 (3)	P2-O4 **(P-O)**	1.516 (2)
P1-O2 **(P-OH)**	1.555 (3)	P2-O5 **(P=O)**	1.498(3)
P1-O3 **(P=O)**	1.475 (3)	P2-O6 **(P-OH)**	1.556(4)

3.5. References

[1] (a) Halper, S. R.; Do, L.; Stork, J. R.; Cohen, S. M. *J. Am. Chem. Soc.* **2006,** *128*, 15255. (b) Hasegawa, S.; Horike, S.; Matsuda, R.; Furukawa, S.; Mochizuki, K.; Kinoshita, Y.; Kitagawa, S. *J. Am. Chem. Soc.* **2007**, *129*, 2607. (c) Kitagawa, S.; Matsuda, R. *Coord. Chem. Rev.* **2007**, *251*, 2490.(d) Yaghi, O. M.; O'Keeffe, M.; Ockwig, N. W.; Chae, H. K. Eddaoudi, M.; Kim, J. *Nature* **2003**, *423*, 705.

[2] Collins, D. J.; Zhou, H.-C.; *J. Mater. Chem.* **2007,** *17*, 3154.

[3] (a) Maeda, K.; Kiyozumi, Y.; Mizukami, F. *J. Phys. Chem. B.* **1997**, *101*, 4402. (b) Odobel, F.; Bujoli, B.; Massiot, D. *Chem. Mater.* **2001**, *13*, 163. (c) Alberti, G.; Casciola, M.; Costantino, U.; Peraio, A.; Montoneri, E. *Solid State Ionics* **1992**, *50*, 315. (d) Alberti, G.; Casciola, M. *Solid State Ionics* **1997**, *97*, 177. (e) Vermeulen, L. A.; Thompson, M. E. *Nature* **1992**, *358*, 656. (f) Deniaud, D.; Schollorn, B.; Mansuy, D.; Rouxel, J.; Battioni, P.; Bujoli, B. *Chem. Mater.* **1995**, *7*, 995.

[4] (a) Gagnon, K. J.; Perry, H. P.; Clearfield, A. *Chem. Rev.* **2012,** *112*, 1034 (b) Bakhmutova, E. V.; Ouyang, X.; Medvedev, D. G.; Clearfield, A. *Inorg. Chem.* **2003**, *42*, 7046.

[5] (a) Dines, M. B.; Cooksey, R. E.; Griffith, P. C.; Lane, R. H. *Inorg. Chem.***1983,** *22*, 1003 (b) Clearfield, A. *Dalton Trans.* **2008,** *44*, 6089.

[6] (a) Drumel, S.; Janvier, P.; Barboux, P.; Doeuff, M. B.; Bujoli, B. *Inorg. Chem.* **1995**, *34*, 148. (c) Bideau, J. L.; Payen, C.; Palvadeau, P.; Bujoli, B. *Inorg. Chem.* **1994**, *33*, 4885. (c) Clearfield, A.; Wang, Z. *J. Chem. Soc., Dalton Trans.* **2002**, 2937.

[7] (a) Mehring, M.; Schurmann, M. *Chem. Commun.* **2001**, 2354.(b) Murugavel, R.; Shanmugan, S. *Chem. Commun.* **2007**, 1257.

[8] (a) Song, S. Y.; Ma, J. F.; Yang, J.; Cao, M. H.; Zhang, H. J.; Wang, H. S.; Yang, K. Y. *Inorg. Chem.* **2006**, *45*, 1201. (b) Wang, Z.; Heising, J. M.; Clearfield, A. *J. Am .Chem. Soc.* **2003**, *125*, 10375.

[9] (a) Quellette, W.; YU, M. H.; O'Connor, C. J.; Zubieta, *J. Inorg. Chem.* **2006**, *45*, 7628. (b) Fu, R.; Xiang, S.; Zhang, H.; Zhang, J.; Wu, X. *Cryst.Growth. Des.* **2005,** *5*, 1795.

[10] (a) Yang, B. -P.; Mao, J. -G.; Sun, Y. -Q.; Zhao, H. -H.; Clearfield, A. *Eur. J. Inorg. Chem.*, **2003,** 4211. (b) Du, Z.-Y,; Xu, H.-B.; Mao, J.-G. *Inorg.Chem.***2006,** *45*, 9780.

[11] (a) Poojary, D. M.; Zhang, B.; Bellinghausen, P.; Clearfield, A. *Inorg. Chem.***1996**, *35*, 5254. (b) Poojary, D. M.; Zhang, B.; Bellinghausen, P.; Clearfield, A. *Inorg. Chem*. **1996**, *35*, 4942

[12] (a) Stock, N.; Bein, T. *J. Solid State Chem.* **2002**, *167*, 330. (b) konar, S.; Zon, J.; Prosvirin, A. V.; Dunbar, K. R.; Clearfield, A. *Inorg. Chem.* **2007**, *46*, 5229. (c) Shi, F.-N.; Trindade, T.; Rocha, J.; Paz, F. A. A. *Cryst.Growth.Des*. **2008,** *8*, 3917. (d) Hu, J.; Zhang, H. H.; Cao, Y. N.; Zhang, C. G.; Zhang, S. A.; Chen, Y. P.; Sun, R. Q. *Chin. J. Struct. Chem.* **2009**, *28*, 939.

[13] Mayer, C. R.; Herve, M.; Lavanant, H.; Blais, J. C.; Secheresse, F. *Eur. J. Inorg. Chem.* **2004**, *5*, 973.

[14] (a) *SAINT: Software for the CCD Detector System*; Bruker Analytical X-ray Systems, Inc.: Madison, WI, **1998.** (b) *SADABS: Program for Absorption Correction;* G. M. Sheldrick University of Gottingen: Gottingen, Germany, **1997.** (c) *SHELXS-97: Program for Structure Solution;* G. M. Sheldrick, University of Gottingen: Gottingen, Germany, **1997.** (d) *SHELXL-97: Program for Crystal Structure Analysis;* G. M. Sheldrick University of Gottingen: Gottingen, Germany, **1997**.

[15] Bakhmutova, E. V.; Ouyang, X.; Medvedev, D. G.; Clearfield, A. *Inorg. Chem.* **2003**, *42*, 7046.

[16] Cabeza, A.; Ouyang, X.; Sharma, C. V. K.; Aranda, M. A. G.; Bruque, S.; Clearfield, A. *Inorg. Chem*. **2002,** *41*, 2325.

[17] konar, S.; Zon, J.; Prosvirin, A. V.; Dunbar, K. R.; Clearfield, A. *Inorg. Chem.* **2007**, *46*, 5229.

[18] Fu, R.-B.; Wu, X.-T.; Hu, S.-M.; Wang, L.-S. *Jiegou Huaxue*. **2004,** *23*, 1107.

[19] Sun, Y.-Q.; Hu, J.; Zhang, H.-H.; Chen, Y.-P.; *J. Solid State Chem.* **2012**, *186*, 189.

[20] (a) Carlucci, L.; Ciani, G.; Maggini, S.; Proserpio, D. M. *CrystEngComm*. **2008**, 1191 (b) Ji, C.-C.; Qin, L.; Li, Y.-Z.; Guo, Z.-J.; Zheng, H.-G. *Cryst. Growth Des.* **2011**, *11*, 480.

[21] (a) Ren, C.; Liu, P.; Wang, Y.-Y.; Huang, W.-H.; Shi, Q.-Z. *Eur. J. Inorg. Chem.* **2010,** *35*, 5545. (b) Wang, X.-L.; Qin, C.; Wang, E.-B.; Su, Z.-M. *Chem. Commun*. **2007,** *41*, 4245.

[22] Kahn, O. Molecular Magnetism; VCH Publishers: NewYork, **1993**.

Hydrothermal Synthesis and Characterization of Novel Metal Oxide Materials: Role of Polyanion and Tetrazole Molecule in the Self-Assembly

4

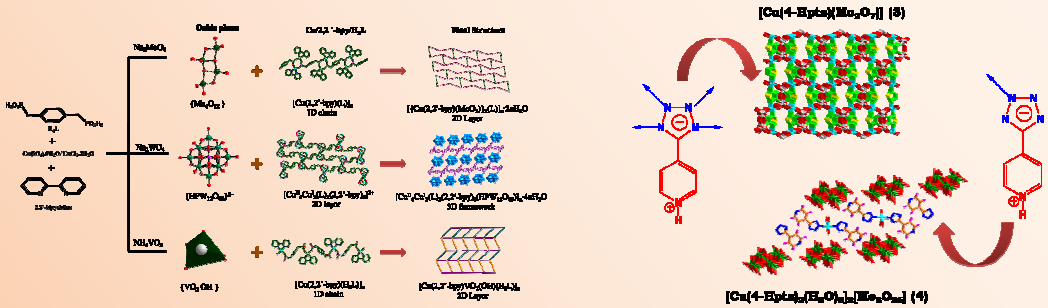

Chapter 4 describes the synthesis and structural characterization of two different classes of metal oxide based materials based on metal organophosphonates and tetrazoles respectively under two different sections.

Two new metal organophosphonate oxide materials with formulae $[Cu^{II}_4Cu^{I}_2(L)_2(2,2'\text{-}bpy)_6(HPW_{12}O_{40})]_n{\cdot}4nH_2O$ (***1***) *and* $[Cu(2,2'\text{-}bpy)VO_2(OH)(H_2L)]_n$ (***2***) *have been synthesized starting from the Cu(II) salts, 2,2'-bipyridine (2,2'-bpy), p-xylylenediphosphonic acid* (H_4L)*, with sodium tungstate (for* ***1****) and ammonium metavanadate (for* ***2****) respectively. Compound* ***1*** *consist 2D copper phosphonate layers connected by the polyanion keggin to form a 3D framework. The copper phosphonate layers in compound* ***1*** *are fabricated by the rare hexanuclear clusters in which the four terminal copper atoms form two eight membered Cu-dimer* ($Cu_2P_2O_4$) *rings (top and the bottom) that are connected to each other by the two central Cu atoms by a four membered* Cu_2O_2 *rings. These hexanuclear assemblies are connected to each other along the plane through the p-xylyl linkers to form a 2D layers. Compound* ***1*** *is a unique example in terms of existence of hexanuclear copper phosphonate cluster in the 3D coordination matrix. Compound* ***2*** *is a 2D structure in which the 1D* $[Cu(2,2'\text{-}bpy)(H_2L)]_n$ *chains are connected by the* VO_2OH *subunits to from a 2D layers. The formation of* VO_2OH *in compound* ***2*** *ceases the formation of eight membered Cu-dimer rings.*

The hydrothermal reaction of Cu(II) salt, ammonium heptamolybdate, and 4-ptz (5-(4-pyridyl) tetrazole) at different synthetic conditions yields two compounds $[Cu(4\text{-}Hptz)(Mo_2O_7)]$ (**3**) and $[Cu(4\text{-}Hptz)_2(H_2O)_3]_2[Mo_8O_{26}]$ (**4**). Compound **3** exhibits a 3D bimetallic oxide framework, constructed from the tetrazoles and $\{CuMo_2O_7\}$ oxide phase. The coordination ability of nitrogen atoms in the tetrazole ring makes the ring acting as a template in the formation of $\{Cu_4Mo_6O_{10}\}$ rings, made up of $[Mo_2O_7]^{2-}$ anions and Cu(II) octahedral; the stacking of these $\{Cu_4Mo_6O_{10}\}$ rings along crystallographic *c* axis results in the formation of 3D bimetallic oxide framework. Compound **4** consists of infinite octamolybdate chains and Cu-tetrazolate complex cation. The present chapter discusses the self-assembly of metal oxide based materials with structure directing agents like metal organophosphonates and tetrazoles.

4.1. Hydrothermal Synthesis and Characterizations of Novel Metal Organophosphonate Oxide Materials: Role of Hetero- polyanion in the Self Assembly of Metal Phosphonate Architectures

4.1.1. Introduction

Metal oxide-based solids belong to an important class of materials showing their promising applications in the contemporary research areas during past several years. A significant research in this area has been directed partly due to interest in their basic chemistry as well as their applications in the fields of separations, molecular electronics, energy storage and catalysis.[1-6] In general, there is a correlation between the complexity of the structure and functionality of the material.[7] The constant evolution of complexity of metal oxides in terms of functionality requires more knowledge on synthetic strategies to understand the oxide structures.[8] Polyoxometalates refer to vast family of metal oxides in the molecular level with diverse nuclearities, different sizes and oxidation states.[9] One such strategy for the modification of oxide structures (in terms of linking the metal oxide building blocks) involves introduction of organic molecules or secondary metal complexes as structure directors. Zubieta et al. reported a vast number of compounds based on this approach, and exploited the structural chemistry of metal oxide based inorganic-organic hybrid materials in the domain of secondary metals, binucleating ligands, tether lengths etc.[10] Among the ligand bridges, which are used to tether the metal oxides, organophosphonic acids are known to be efficient in terms of charge compensation due to more number of coordinating atom. Moreover, organophosphonic acids are considered as structure directing components owing to their flexibility in altering the organic groups.[11a-d] Organoamines, such as, pyridine derivatives, imidazoles, tetrazoles are also used to link the metal oxides.[11e-g]

Metal organophosphonates are among the earliest and extensively studied examples of coordination polymers / metal organic frameworks, that are important because of their potential applications in the areas of sorption, ion exchange, sensing, and catalysis.[12] Additionally, metal phosphonates have offered great opportunities to understand fundamental magnetic phenomena, such as spin canting, anisotropy, relaxation dynamics and field induced magnetic transitions.[13] Due to availability of more ligating sites, phosphonic acids (PO_3H_2 groups) coordinate to more number of metal sites there by forming a layered structures and the bisphosphonic acids form a pillared-layered structures.[14]

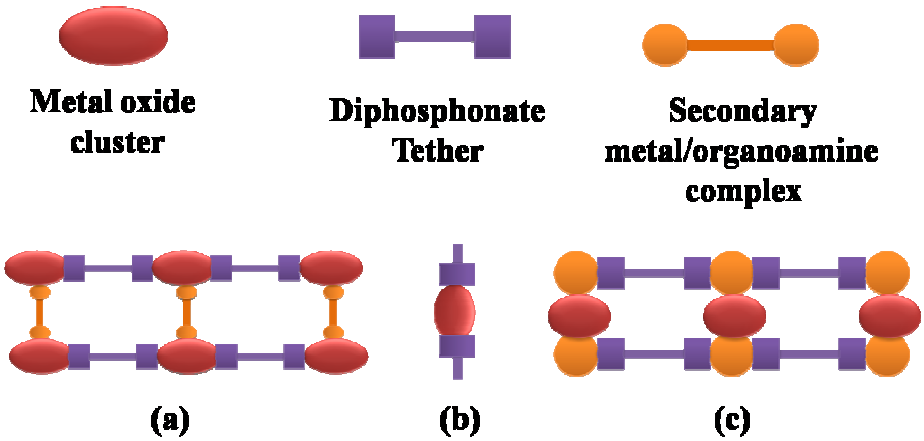

Scheme 4.1. Scheme representing the different types of self assembly process in the MOP oxide materials

A control over the protonation states and introduction of secondary chelating ligands result in the formation of clusters with different nuclearities.[15] This approach results in the stabilization of molecular phosphonates with interesting magnetic properties because O–P–O bridge is known to be efficient in transmitting weak to moderately strong antiferromagnetic and ferromagnetic interactions.[16] In the recent era, the research progresses on metal phosphonates lead to the evolution of 2D and 3D coordination networks.[17]

Metal organophosphonate (MOP) oxide materials are the combination of the metal oxides and metal organophosphonates architectures in such a way that it can be exploited as functional materials having applications from both the phases. Typically, hydrothermal methods have been commonly used to synthesize the metal organophosphonate oxide-based materials; the technique offers an excellent route to isolate metastable phases and stabilizes the reliability of the structure.[18] In the MOP oxides, both the polyoxometalate oxygen atoms and phosphonate oxygen atoms are involved in the formation of a oxide microstructures to which secondary metal/ligand components are attached to the peripherals of these oxide microstructures (Scheme 4.1). Zubieta et al. reported a class of compounds Mo_xO_y/diphosphonate/M(II) organo nitrogen families of bimetallic oxides in which the PO_3H_2 groups are directly coordinated to the Mo(VI) atoms to form a oxides of type $\{Mo_xO_y(O_3PR)\}^{n-}$ and these phases are linked with the aid of tethers attached to the phosphonic groups and metal organonitrogen cations.[19] Different classes of MOP oxides of type oxomolybdate-organodiphosphonates,[20] vanadium oxides with di- and tri-phosphonates[21] are well studied with metal organoimine cationic complex subunits.

Another class of MOP oxide materials involves the functionalization of polyoxometalates with mono- and di- phosphonate anions.[22] Kortz et. al. functionalized the heteropolymolybdates with amino acids through the phosphate, phosphonate and phosphate groups.[23] However, polyoxometalate anionic clusters with the secondary metal cationic complexes containing both the organonitrogen and organo phosphonic acids are very rare in the literature.[24]

We have chosen *p*-xylylenediphosphonic acid (H_4L) as a phosphonate source to study the effect on the oxide phases Na_2WO_4 and NH_4VO_3 with Cu as secondary metal and 2,2´-bipyridine as organoimine under hydrothermal conditions. Recently we have studied the mechanistic aspects in the formation of Cu-dimer with H_4L ligand and extended its dimensionality with organic and inorganic linkers including different conformation of the H_4L ligand in the presence of secondary ligand component.[25] In this article, we describe the synthesis and structural characterization of two new compounds $[Cu^{II}_4Cu^{I}_2(L)_2(2,2´\text{-}bpy)_6(HPW_{12}O_{40})]_n \cdot 4nH_2O$ (**1**) and $[Cu(2,2´\text{-}bpy)VO_2(OH)(H_2L)]_n$ (**2**). Compound **1** is a peculiar example, in which the Keggin-type hetero-polyanion acts as a linker in connecting the metal organoimine phosphonate layers to form a 3D architecture and in compound **2**, VO_2OH connects the metal phosphonate chains to form a 2D layers.

4.1.2. Experimental Section

4.1.2.1. Materials and Methods

All the chemicals were received as reagent grade and used without any further purification. H_4L was prepared according to the reported procedure.[27] Elemental analyses were determined by FLASH EA series 1112 CHNS analyzer. Infrared spectra of solid samples obtained as KBr pellets on a JASCO – 5300 FT – IR spectrophotometer. Thermo gravimetric analyses were carried out on a STA 409 PC analyzer and corresponding masses were analyzed by QMS 403 C mass analyzer, under the flow of N_2 gas with a heating rate of 5 °C min^{-1}, in the temperature range of 30–900 ^oC.

4.1.2.2. Synthesis

Synthesis of the compound $[Cu^{II}_4Cu^{I}_2(L)_2(2,2´\text{-}bpy)_6(HPW_{12}O_{40})]_n \cdot 4nH_2O$ (1)

A mixture of copper sulfate pentahydrate (0.2 mmol, 0.49 g), 2,2´-bpy (0.2 mmol, 0.031 g), sodium tungstate (0.5 mmol, 0.165g), H_4L (0.1 mmol, 0.26 g) and water (555.5 mmol 10.0 g) in the mole ratio 2:2:1:5:5555 was taken; to this reaction mixture, H_3PO_4 (0.1 mL) was added and the pH was adjusted to 4.20 by 5M HCl and then it was stirred for 30 min.

The resulting solution was then transferred to 23 mL Teflon lined autoclave in the stainless steel vessel and heated at 180 °C for 72 h followed by cooling to room temperature over two days resulting in the formation of tiny crystals of **1** in about 10 % yield (based on Cu) Anal. Calc. for $C_{76}H_{73}Cu_6N_{12}O_{56}P_5W_{12}$ (4792.69): C, 19.04; H, 1.53; N, 3.50. Found: C, 19.20; H, 1.12; N, 3.78. IR (KBr pellet) (υ/cm^{-1}): 3437, 3084, 1602, 1572, 1512, 1494, 1468,1444, 1311, 1251, 1201, 1157, 1130, 1097, 1060, 1030, 976, 958, 887, 817, 769, 729, 661, 561, 513.

Synthesis of the compound $[Cu(2,2´\text{-bpy})VO_2(OH)(H_2L)]_n$ (2)

A mixture of copper sulfate pentahydrate (0.34 mmol, 0.087 g), 2,2´-bpy (0.32 mmol, 0.051 g), ammonium metavanadate (0.43 mmol, 0.050 g), H_4L (0.407, 0.109 g) and water (555.5 mmol 10.0 g) in the mole ratio 1.08:1:1.36:1.27:1735 was taken; and the resulting reaction mixture with initial pH 2.70 were stirred for 30 min. The solution was then transferred to 23 mL teflon lined autoclave in the stainless steel vessel and heated at 180 °C for 72 h and cooled to room temperature over two days to give blue block crystals of **2**. Yield: 32% (based on copper) Anal. Calc. for $C_{18}H_{19}CuN_2O_9P_2V$ (583.78): C, 37.03; H, 3.28; N, 4.79. Found: C, 37.64; H, 3.01; N, 4.99. IR (KBr pellet) (υ/cm^{-1}): 3354, 3099, 2096, 1637, 1520, 1385, 1199, 1047, 956, 906, 841, 814, 754, 707, 596, 516, 480.

4.1.2.3. X-ray Crystallography

Single-crystals, suitable for structural determination of the compounds **1** and **2**, were mounted on a three circle Bruker SMARTAPEX CCD area detector system under Mo-Kα (λ=0.71073A) graphite monochromated X-ray beam, crystal to detector distance 60mm, and a collimator of 0.5 mm. The scans were recorded with an ω scan width of 0.3º. Data reduction performed by SAINTPLUS,[28a] empirical absorption corrections using equivalent reflections performed by program SADABS,[28b] structure solution using SHELXS-97[28c] and full-matrix least-squares refinement using SHELXL-97[28d] for above compounds. All the non-hydrogen atoms were refined anisotropically. Hydrogen atoms on the C atoms were introduced on calculated positions and were included in the refinement riding on their respective parent atoms. Attempts to locate the hydrogen atoms for the solvent water molecules in the crystal structure of compounds through Fourier electron density were failed. However, no attempts were made to fix these atoms on their parents. The hydrogen atoms on some of the P–OH groups in the compounds are fixed by the proper HFIX commands and some are located by the Fourier electron density map.

Compound **1** suffers a significant disorder problem due to disorder in the central PO_4 oxygen atoms in the keggin anion. The oxygen atoms O19 and O20 were splitted over two positions (O19A, O19B and O20A, O20B) after fixing their occupancies 0.5 to each atom. Due to this disorder problem, the central PO_4 group is changed to PO_8; as a result of this, the Keggin anion experiences an unresolved disorder problem.The maximum and minimum main axis ADP ratio of the oxygen atom O16, and carbon atoms C11, C25, C32, are more than 5.0 indicating the unresolved disorder. However, no proper model (by applying restraints ISOR or SIMU to displacement parameters) was used to resolve this problem. α- disordered keggin ions are known to show this type of unresolved disorder problems, that are very common in the literature.[29] In compound **2**, the oxygen atoms, connected to vanadium atom O1 and O8, also suffer from a significant disorder problem, which has been resolved by splitting oxygen atoms into two positions in the refined ratio 0.5 : 0.5. Crystal data, structure refinement parameters for both the compounds are summarized in Table 4.1 and selected bond lengths in Table 4.2.

4.1.3. Results and Discussion

4.1.3.1. Synthesis

The reactions of Cu(II) salts ($Cu(SO_4)_2 \cdot 5H_2O$ for **1** and $CuCl_2 \cdot 2H_2O$ for **2**), with organoamine ligand 2,2′-bipyridine, phosphonic acid H_4L and Na_2WO_4 for **1** and NH_4VO_3 for **2** at 180 °C under hydrothermal conditions for 72 h afford crystalline compounds **1** and **2** in the modest yields. Compound **1** is formed in the pH range 4.0 to 4.5 and its formation is purely pH dependent. The initial pH of the reaction mixture before the addition of H_3PO_4 is 7.32; by addition of 0.1ml H_3PO_4, the initial pH decreases to 6.27, finally the pH was adjusted to 4.20 with 5M HCl to obtain compound **1** in a very low yield in pure crystalline form. The further decrease in pH result in the formation of two different phases i.e. $[Cu(2,2'\text{-bpy})(H_2L)]_n \cdot nH_2O$ (pH 2.5−3.5) and $[\{Cu(H_2O)(2,2'\text{-bpy})(H_3L)\}_2(H_2L)] \cdot 2H_2O$ (pH below 2.0).[25] Even by increasing the pH above 4.5 results in the formation of amorphous blue colored powder, but does not increase the yield of the compound.

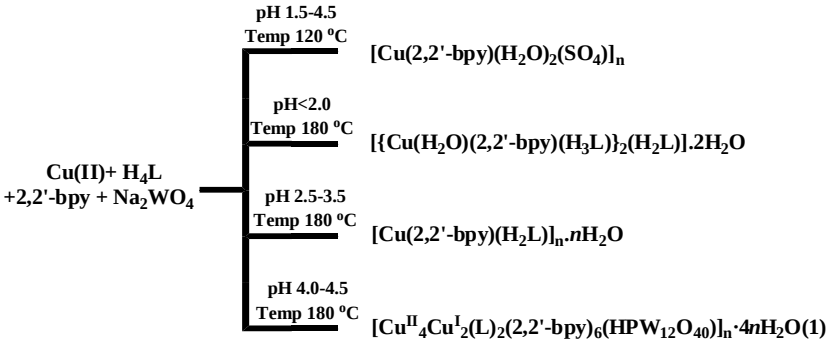

Scheme 4.2. Different phases formed in the synthesis of compound **1**.

When we use $H_3PW_{12}O_{40}$ instead of Na_2WO_4 in stiochiometric ratio, the initial pH of the reaction mixture drastically decreases to 1.80 and in this pH range, the hydroxyl groups in the H_4L do not deprotonate and the reaction mixture favors the formation of more thermodynamically and kinetically stable phase $[\{Cu(H_2O)(2,2'\text{-}bpy)(H_3L)\}_2(H_2L)]\cdot 2H_2O$.[25] The observations in the synthetic procedure imply that the thermodynamic equilibrium in the formation of the compound **1** is very less and pertained to particular pH range and the concentration of the reactants (See Scheme 4.2). The initial pH of the reaction mixture in case of compound **2** is 2.70; in this pH range, H_4L exists in doubly deprotonated form H_2L. The formation of compound **2** is straight forward and does not require much stringent synthetic conditions to obtain in the modest yields unlike compound **1**.

4.1.3.2. Description of the Crystal Structures

Structural description of $[Cu^{II}_4Cu^{I}_2(L)_2(2,2'\text{-}bpy)_6(HPW_{12}O_{40})]_n\cdot 4nH_2O$ (1)

Compound **1** is a 3D structure, that crystallizes in triclinic space group *P*-1; the relevant crystal data and structural refinement parameter are presented in Table 4.1. The relevant molecular structure consists of α-disordered classical keggin polyanion connected to a hexa-nuclear copper phosphonate complex; there are four solvent water molecules per formula unit in the crystal lattice (Figure 4.1a). The 3D structure is composed of 2D hexa-nuclear copper phosphonate layers connected by the α disordered classical Keggin hetero-polyanions $[HPW_{12}O_{40}]^{2-}$. The well-known Keggin anion structure is constituted by the central PO_4 tetrahedron, that shares its oxygen atoms with four W_3O_{13} groups which are made up of three edge sharing WO_6 octahedra. Each W_3O_{13} subunits are joined to each other by a corner sharing mode. The central phosphorous atom is disordered and surrounded by a cube of eight oxygen

atoms PO_8 with each oxygen site half occupied apart from the regular PO_4 tetrahedron (Figure 4.1b).

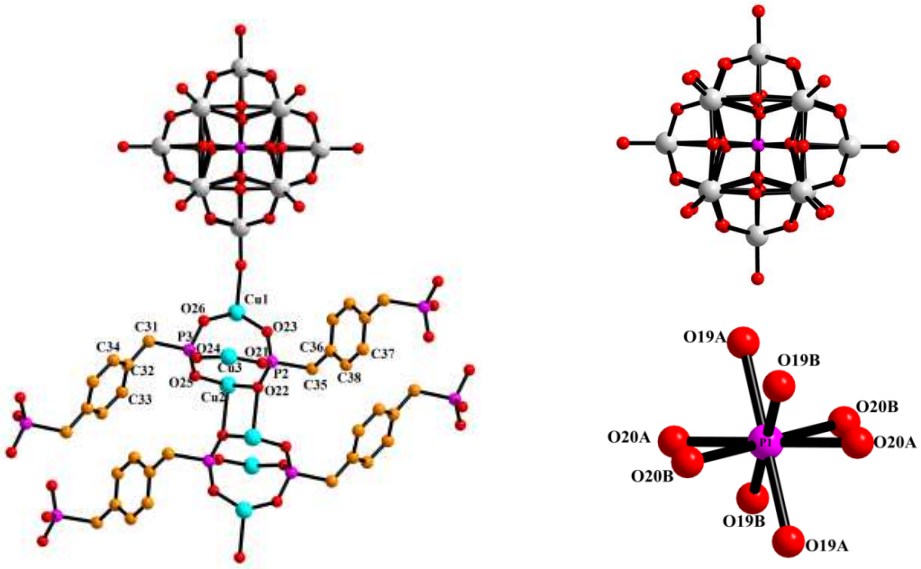

(a) **(b)**

Figure 4.1. (a) Molecular diagram of compound **1** (2,2′-bpy moieties, lattice water molecules, are removed for clarity), (b) pictorial representation of classical keggin ion and disordered PO_4 group.

The W−O bond distances in the polyanion $[HPW_{12}O_{40}]^{2-}$ are in the range of 1.673−1.686 Å for terminal oxygen atoms, 1.847−1.913 Å for μ_2−bridging oxygen atoms and 2.285−2.542 Å for μ_3−bridging oxygen atoms respectively. The P−O bond distances vary in the range of 1.524−1.683 Å with mean value of 1.614 Å. The disorder in the oxygen atoms connected to central atom reflects in the slight deviation of W−O bond distances in case of μ_2 and μ_3 bridging oxygen atoms from the predicted distances.[30] Bond valence sum calculations show that all the tungsten sites exhibit +VI oxidation state in the PW_{12} polyanion.[31] The coordination environment and W−O distances of the all the tungsten atoms are almost similar, which ruled out the +V oxidation states of the W atoms (i.e. $\{PW^{VI}_{11}W^{V}\}^{4-}$ and $\{PW^{VI}_{10}W^{V}_{2}\}^{5-}$). Usually the W−O distances around the W^{V} centers (av. 1.810 for terminal oxygen atoms) are slightly longer than those around the W^{VI} centers (av. 1.680 for terminal oxygen atoms in compound **1**).[32] Based on the bond valence sum calculations and W−O distances, the polyanion was formulated as $[HPW_{12}O_{40}]^{2-}$,[33] proton was added to balance the charge of the compound. The PW_{12} polyanions coordinate to two Cu ions (Cu1 and Cu1#) in a bidentate para coordination mode. The most striking structural feature of the compound **1** is presence 2D layers constituted by the mixed valent hexa-nuclear copper phosphonate clusters $[Cu^{II}_{4}Cu^{I}_{2}(L)_2(2,2'\text{-bpy})_6]^{2+}$. The hexa-nuclear cluster is an

assembly of four Cu atoms (Cu1, Cu2, Cu1*, Cu2*) in dipositive state which are in $\{CuN_2O_3\}$square pyramidal geometry and two Cu atoms (Cu3, Cu3*) in +I oxidation state and exist in $\{CuN_2O_2\}$ square planar geometry.

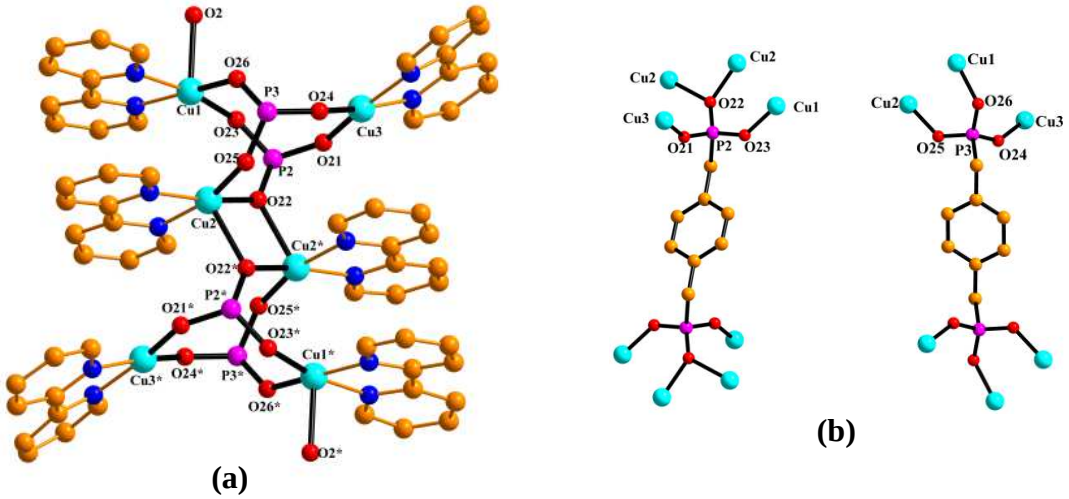

Figure 4.2. (a) Cu-hexamer presented in the compound with atom labelling, (b) Different coordination modes of the L^{4-} ligand (4.211− left and 3.111−right).

The oxidation states of the Cu atoms are conformed by the bond-valence sum calculations and particular coordination geometries of Cu. Two coordination sites of all the Cu atoms are blocked by the 2,2′-bpy ligands to form a $[Cu(bpy)]^{n+}$ subunits and these units are connected by the coordination of four L^{4-} ligands to form a hexanuclear cluster (Figure 4.2a). Among the two pairs of terminal Cu atoms (Cu1, Cu3 and Cu1*, Cu3*), each pair is connected by the OPO bridges from two L^{4-} ligands to form a eight membered $\{Cu1(OPO)_2Cu3\}$rings. The central Cu atoms Cu2 and Cu2* are bridged by the two oxygen atoms from two L^{4-} ligands to form a four membered Cu_2O_2 ring which is sandwiched between the two eight membered rings to form a hexa nuclear assembly as shown in the Figure 4.2a. The four phosphonate ligands (L^{4-}), used for coordination of six Cu atoms, are classified into two types (P2, P2* and P3, P3*) which differ mainly in terms of their coordination mode. The ligands, namely, P2 and P2* coordinate to the four Cu atoms in 4.211 coordination mode by bridging the terminal Cu atoms through the phosphonate oxygen atoms (O21 ,O23 and O21*,O23*) and the residual oxygen atoms O22 and O22* of the phosphonate groups bridge the two central Cu atoms as shown in the Figure 4.2b. On the other hand, the ligands P3 and P3* coordinate to three Cu atoms in 3.211 coordination mode by bridging the terminal Cu atoms through the phosphonate oxygen atoms (O24,O26 and O24*,O26*)

but the residual oxygen atoms O25 and O25* are just connected to central Cu atoms of the four membered ring Cu_2O_2 as shown in the Figure 4.2b. Each hexanuclear cluster connects to four other clusters through a pair of phosphonate ligands to form 2D layer as shown in the Figure 4.3a. These 2D layers are connected to PW_{12} polyanions through terminal oxygen atoms O2, O2* to form a 3D framework as shown in the Figure 4.3b. The hexa-nuclear cluster, reported in the compound, is structurally related to the hexanuclear complexes reported in the literature.[26] But, in the reported compounds, all the Cu atoms in the cluster are present in +II oxidation state and in square pyramidal geometry. It is noteworthy to mention that the hexanuclear cluster in compound **1** is comprised of two different coordination geometries and two different valence states of copper atoms. This exclusive feature distincts the hexanuclear cluster in compound **1** from the other reported hexanuclear clusters.

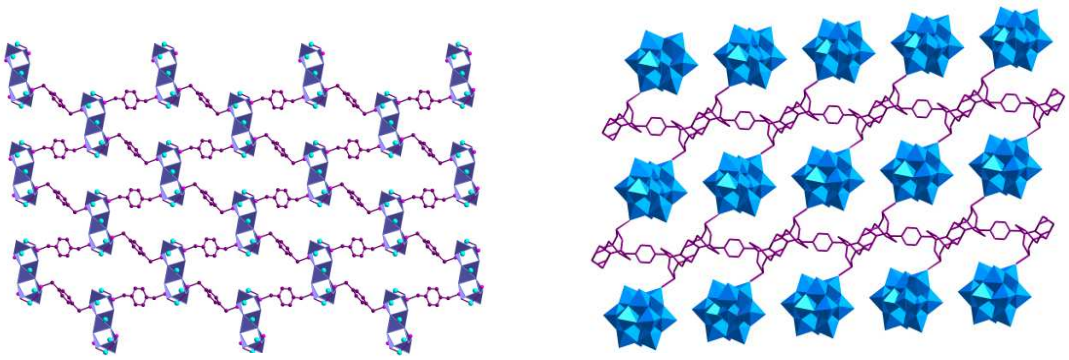

Figure 4.3. (a) 2D metal phosphonate layers in the compound **1**; Blue polyhedron represents the hexameric units, (b) 3D frame work formed due to connectivity of metal phosphonate layers with keggin ions. (2,2′-bpy units are removed for clarity).

Compound **1** represents a unique example in which the dimensionality of the Cu_6 cluster is extended in the layer through the p-xylyl linkers and the layers are connected to each other by the inorganic PW_{12} linkers. The distance between two layers along the length of the PW_{12} is 14.69 Å. In the reported compounds, only monophosphonic acid was used and thereby the dimensionality of the Cu_6 is extended by the terminal Cu atoms through the apically connected linkers like 4,4′-bpy etc. which results in the formation of only 1D chains. But in the present study, the use of a bisphosphonic acid and inorganic linker result in the formation of novel 3D framework based on the Cu_6 cluster and Keggin type polyoxometalate (POM) anion.

Structural description of $[Cu(2,2'\text{-bpy})VO_2(OH)(H_2L)]_n$ (2)

Compound **2** is two dimensional coordination polymer, that crystallizes in triclinic space group *P*-1. The relevant asymmetric unit contains the Cu atom in dipositive state, one 2,2′-bipyridine, two H_2L ligands, VO_2 group and one hydroxyl group. Bond valance sum calculations show that the Cu atoms are present in +II and vanadium atoms in +V oxidation states. As shown in the Figure 4.4, the square pyramidal CuN_2O_3 completes its coordination sphere through two nitrogen atoms from bpy ring (Cu−N1: 2.001 Å and Cu−N2: 2.003 Å), two phosphonate oxygen atoms (O5 and O2) from two different H_2L ligands in the basal plane and the apical site is coordinated to oxygen atom from the VO_2OH group.

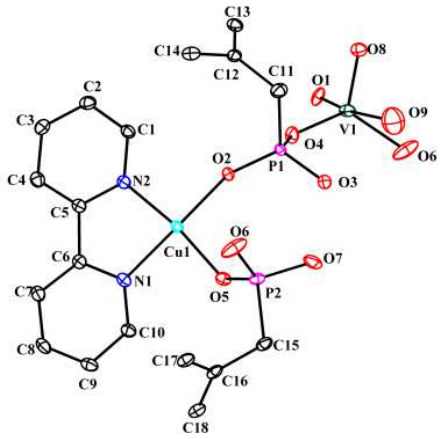

Figure 4.4. A ORTEP view of the basic unit of **2**. Hydrogen atoms are removed for clarity. Thermal ellipsoids are at the 40% probability level.

V(V) atom is also present in square pyramidal VO_4OH geometry in which two phosphonate oxygen atoms (V1−O4: 1.876 Å and V1−O6: 1.874 Å), two terminal oxygen atoms (V1−O8: 1.560 Å and V1−O1: 1.660 Å) and one hydroxyl group (V1−O9: 2.330) complete its coordination sphere. The square pyramidal polyhedra of two metal centers in CuN_2O_3 and VO_4OH connected to each other by the corner sharing oxygen atom O1 as shown in the Figure 4.5a. These double polyhedra are connected to another such set along the axis and along the layer with the aid of bisphosphonate ligand H_2L with a 2.110 coordination mode. Two types of H_2L ligands are present in the crystal structure which differs in the orientation and mode of coordination. Let us consider the phosphonic acid H_2L_A (shown in orange color in Figure 4.5b) links the adjacent of double polyhedra through the phosphonate oxygens O2 and O4 along the *a* axis, to form a 1D chain and the another phosphonic acid H_2L_B

(shown in green color in the Figure 4.5b) chelate the Cu and V atoms of the double polyhedra with the phosphonate oxygens O6 and O5 resulting in the formation of six membered ring. The 1D chains, formed due to connectivity of H_2L_A with the double polyhedra along the crystallographic *a* axis, are extended to 2D layers by the p-xylyl spacers in both H_2L_A and H_2L_B ligands to form a 2D layer with alternate grids as shown in the Figure 4.5c. Due to difference in type of coordination mode, the length of the ligand changes; as a result, the distance between the chains in the layer vary.

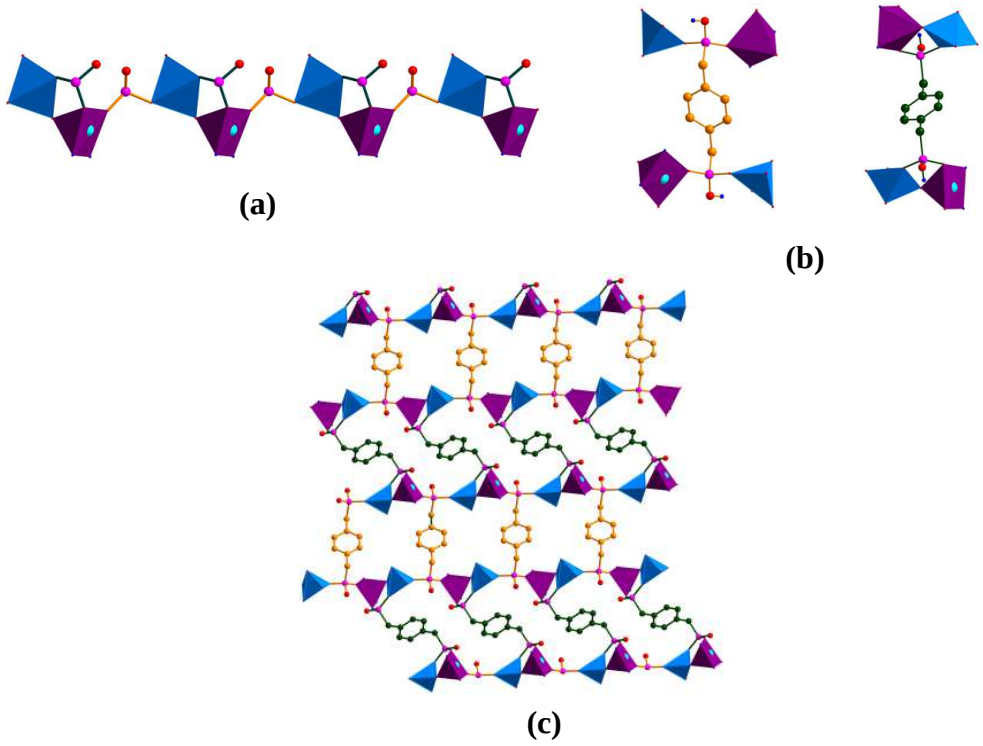

Figure 4.5. (a) 1D chain formed due to connectivity of CuN_2O_3 (purple colored) and VO_4OH (Blue colored) polyhedra with H_2L ligand, (b) Connectivity of H_2L_A and H_2L_B ligands, (c) 2D network formed in the compound **2**. (2,2´-bpy units are removed for the clarity.

4.1.3.3. Comparison among the structures involving metal oxides and metal phosphonate complexes

In our previous chapter, we discussed the mechanistic aspects in the formation and stabilization of eight membered Cu-dimer ring in the coordination matrix and extended the dimensionality of the Cu-dimer by organic and inorganic linkers.[25] When we introduce sodium molybdate in the Cu/p-xylylenebisphosphinic acid/2,2´-bipyridine system, it results in the formation of 2D network, in which the 1D Cu-dimer chains $[Cu(2,2'\text{-bpy})(L)]_n$, are linked by the inorganic linker tetramolybdate (Mo_4O_{12}). In this process of extending the dimensionality of the Cu dimers by inorganic linkers, we

introduced (in the present study) sodium tungstate and ammonium metavanadate in the Cu/p-xylylenebisphosphonic acid/2,2'-bipyridine system to form compounds **1** and **2**. The plausible mechanism for the formation of compounds **1** and **2** are shown in the following equations and Scheme 4.3.

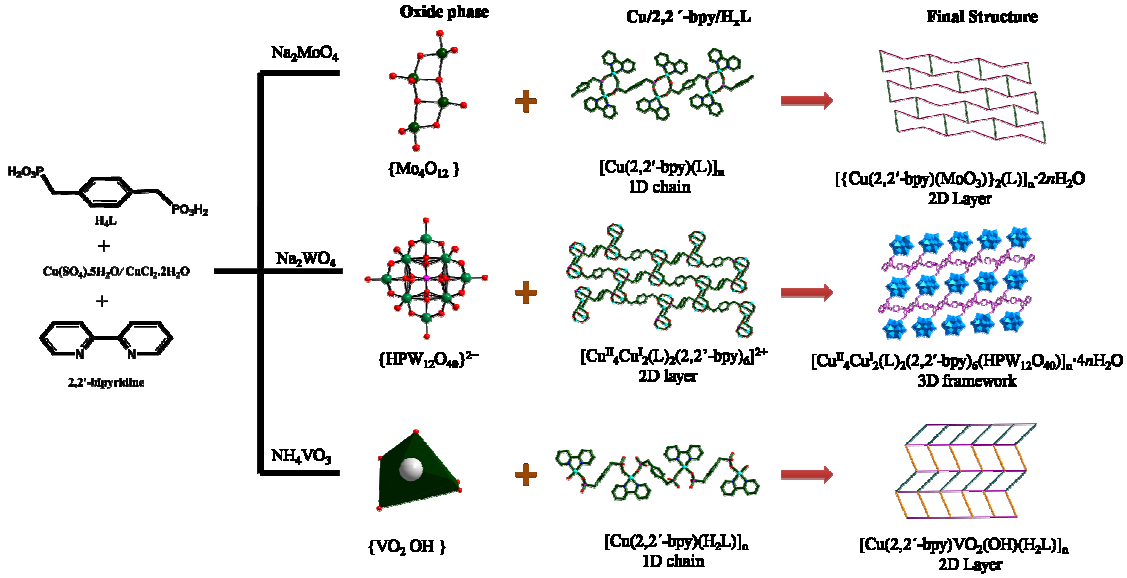

Scheme 4.3. Schematic representation of the self assembly of the polyanions and metal organophosphonate phases

$$CuSO_4.5H_2O \xrightarrow{H_2O} [Cu(H_2O)_6]^{2+}\ SO_4^{2-}$$

$$[Cu(H_2O)_6]^{2+}\ SO_4^{2-} + 2,2'\text{-bpy} \xrightarrow{120\ ^oC} [Cu(2,2'\text{-bpy})(H_2O)_2SO_4]_n$$

$$12WO_4^{2-} + PO_4^{3-} + 25H^+ \xrightarrow{pH=4.20} \{HPW_{12}O_{40}\}^{2-} + 12H_2O$$

$$6[Cu(2,2'\text{-bpy})(H_2O)_2SO_4]_n + 2nH_4L \xrightarrow{180\ ^oC} [Cu^{II}_4Cu^{I}_2(2,2'\text{-bpy})_6(L)_2]_n^{2n+} + 6nSO_4^{2-} + 12nH_2O + 8nH^+ - 2ne^-$$

$$[Cu^{II}_4Cu^{I}_2(2,2'\text{-bpy})_6(L)_2]_n^{2n+} + n\{HPW_{12}O_{40}\}^{2-} + 4\ H_2O \xrightarrow{180\ ^oC} [Cu^{II}_4Cu^{I}_2(2,2'\text{-bpy})_6L_2(PW_{12}O_{40})]_n\cdot 4nH_2O\ (1)$$

$$[Cu(2,2'\text{-bpy})(H_2O)_2SO_4]_n + nH_4L \xrightarrow{180\ ^oC} [Cu(2,2'\text{-bpy})H_2L]_n + nSO_4^{2-} + 2nH_2O + 2nH^+$$

$$VO_3^- + H^+ \xrightarrow{pH=2.70} VO_2OH$$

$$[Cu(2,2'\text{-bpy})H_2L]_n + nVO_2OH \xrightarrow{180\ ^oC} [Cu(2,2'\text{-bpy})VO_2OH(H_2L)]_n\ (2)$$

As shown in Scheme 4.3, the tungstate WO_4^{2-} ions in presence of H_3PO_4, undergo self assembly process to form a α-disordered keggin and the metal/organoamine/phosphonate favors the formation of 2D $[Cu^{II}_4Cu^{I}_2(L)_2(2,2'\text{-bpy})_6]$ layers consisting the mixed valent hexa nuclear assemblies. The overall assembly of

the polyanion keggin with the metal phosphonate layers result in the formation of 3D architecture, in which the 2D metal phosphonate layers are linked by the Keggin anions. In a similar way, the employment of ammonium metavandate in the synthesis result in the formation of VO_2OH and 1D $[Cu(2,2'\text{-bpy})\ H_2L)]_n$ chains, and the connectivity of these subunits gives a 2D layers. In this compound the Cu/p-xylylenebisphosphinic acid/2,2′-bipyridine system does not form dimer or hexamer as described in the above compounds. The phosphonate oxygen atoms, which are accountable for the formation of the dimer, are connected to the VO_2OH group and there by prevents the formation of the dimer.

As shown in the Scheme 4.3, different POMs favor the different metal phosphonates phases. In all the compounds, POMs increase the dimensionality of the metal phosphonates by linking them in different directions.

4.1.4. Conclusion

Inorganic oxides represent the most important class of materials as far as stability and application aspects are concerned. In order to investigate the self assembly process of bimetallic inorganic oxides involving metal organophosphonates, herein, we have identified three dimensional covalently linked material $[Cu^{II}_4Cu^{I}_2(L)_2(2,2'\text{-bpy})_6(HPW_{12}O_{40})]_n \cdot 4nH_2O$ (**1**) and two dimensional compound $[Cu(2,2'\text{-bpy})VO_2(OH)(H_2L)]_n$ (**2**). The attractive feature of this article is that in the compound **1**, hexa-nuclear assemblies of Cu metal phosphonates layers are extended by the inorganic linker PW_{12}. Compound **1** is a distinctive example that features the existence of Cu-hexamer in the 3D coordination matrix. The formation of VO_2OH in compound **2** prevents the formation of the eight membered Cu dimer rings. The magnetic studies and the isolation of different phases involving the hexameric assemblies are under progress. The isolation of the different metal phosphonate phases under different polyanions reveals the mechanistic aspects in the self assembly process of MOP oxide materials.

Table 4.1. Crystal data and structural refinement parameters for compounds **1** and **2**.

	1	**2**
Empirical formula	$C_{76}H_{73}Cu_6N_{12}O_{56}P_5W_{12}$	$C_{18}H_{19}CuN_2O_9P_2V$
Formula weight	4792.69	583.78
T [K]	100	100
λ [Å]	0.71073	0.71073
Crystal system	Triclinic	Triclinic
Space group	*P*-1	*P*-1
a [Å]	12.784(17)	8.006(7)
b [Å]	12.392(18)	10.619(9)
c [Å]	17.908(2)	12.539(11)
α[deg]	77.94(2)	83.59(10)
β [deg]	79.05(2)	75.42(10)
γ [deg]	66.86(2)	88.44(10)
V [Å^3]	2737.5(6)	1025.3(15)
Z	1	2
D_{calc} [Mg m^{-3}]	2.907	1.891
μ [mm^{-1}]	13.856	1.707
F[000]	2197	590
Crystal size [mm^3]	0.12 x 0.08 x 0.08	0.40x 0.30 x 0.18
θ range for data collection [deg]	1.67 to 25.00	1.69 to 26.39
Reflections collected/unique	26015 / 9587	10844 / 4168
R (int)	0.0682	0.0225
Data/restraints /parameters	9587 / 0 / 767	4168 / 0 / 299
Goodness-of-fit on F^2	1.128	1.067
R_1/wR_2 [I > 2σ(I)]	0.0761/ 0.1582	0.0371/0.0985
R_1/wR_2 (all data)	0.1035/ 0.1699	0.0410/0.1012
Largest diff. Peak /hole [e Å^{-3}]	2.911 and –3.014	0.748 and -0.874

Table 4.2. Selected bond lengths [Å] for compounds **1** and **2.**

Compound 1			
W(1)−O(1)	1.672(15)	W(1)−O(7)	1.893(17)
W(1)−O(8)	1.87(2)	W(1) −O(9)	1.927(12)
W(1) −O(10)	1.858(17)	W(1) −O(19A)	2.36(2)
W(1) −O(20B)	2.53(2)	W(2)−O(2)	1.684(13)
W(2)− O(10)	1.881(18)	W(2)− O(11)	1.90(2)
W(2)− O(12)	1.85(2)	W(2)−O(19A)	2.39(2)
W(2)−O(15)#1	1.872(19)	W(2) −O(19B)#1	2.50(2)
W(3)−O(3)	1.677(16)	W(3)−O(8)	1.874(18)
W(3)−O(12)	1.889(17)	W(3)−O(13)	1.886(14)
W(3)−O(19A)	2.29(2)	W(3)-O(17)#1	1.886(15)
W(3)−O(20A)	2.550(21)	W(4)−O(4)	1.673(15)
W(4)− O(13)	1.877(14)	W(4)− O(14)	1.903(18)
W(4)−O(20A)	2.424(19)	W(4)−O(19B)	2.29(2)
W(4) −O(18)#1	1.868(15)	W(4)−O(11)#1	1.898(16)
W(5)− O(5)	1.676(15)	W(5)− O(9)	1.827(13)
W(5)−O(14)	1.840(19)	W(5)−O(15)	1.883(17)
W(5)−O(16)	1.904(16)	W(5)−O(19B)	2.39(2)
W(5)−O(20B)	2.41(2)	W(6)− O(7)	1.880(18)
W(6)− O(16)	1.854(13)	W(6)− O(17)	1.894(14)
W(6)− O(18)	1.919(15)	W(6)− O(20B)	2.27(2)
W(6)−O(20A)#1	2.38(2)		
Cu(1)-O(26)	1.926(13)	Cu(1)-O(23)	1.939(11)
Cu(1)-N(1)	2.008(18)	Cu(1)-N(2)	2.020(16)
Cu(1)-O(2)	2.235(13)	Cu(2)-O(25)	1.928(12)
Cu(2)-O(22)	1.964(12)	Cu(2)-N(3)	2.005(14)
Cu(2)-N(4)	2.015(14)	Cu(2)-O(22)#2	2.264(11)
Cu(3)-O(21)	1.901(12)	Cu(3)-O(24)	1.907(12)
Cu(3)-N(5)	1.983(16)	Cu(3)-N(6)	2.014(15)
P(1)-O(20A)	1.52(2)	P(1)-O(20B)	1.62(2)
P(1)-O(19B)	1.63(2)	P(1)-O(19A)	1.70(2)
P(2)–O(21)	1.503(12)	P(2)−O(22)	1.515(11)
P(2)−O(23)	1.498(12)	P(2)−O(24)	1.503(13)
P(2)−O(25)	1.518(13)	P(2)−O(26)	1.511(13)
Compound-2			
Cu(1)-O(2)	1.915(2)	Cu(1)-O(5)	1.935(2)
Cu(1)-N(1)	2.001(2)	Cu(1)-N(2)	2.003(2)
Cu(1)-O(1B)#3	2.228(5)	Cu(1)-O(1C)#3	2.292(5)
O(2)-P(1)	1.497(2)	O(3)-P(1)	1.517(2)
O(4)-P(1)	1.548(2)	O(4)-V(1)	1.876(2)
O(5)-P(2)	1.515(2)	O(6)-P(2)	1.535(2)
O(6)-V(1)#3	1.874(3)	O(7)-P(2)	1.534(2)
O(8A)-O(8B)	0.595(6)	O(8A)-V(1)	1.622(7)
V(1)-O(8B)	1.551(7)	V(1)-O(1B)	1.585(5)
V(1)-O(1C)	1.728(5)	V(1)-O(6)#4	1.874(3)
V(1)-O(9)	2.331(4)	O(1B)-O(1C)	0.654(5)
O(1B)-Cu(1)#4	2.228(5)	O(1C)-Cu(1)#4	2.292(5)

Symmetry transformations used to generate equivalent atoms: #1 -x+1,-y,-z#1, #2 -x,-y+1,-z+1, #3 -x,-y,-z; #2, #4 -x,-y+1, z+1

4.1.5. References

[1] *(a)* W. Buchner, R. Schliebs, G. Winter and K. H. Buchel, Industrial Inorganic Chemistry VCH: New York, 1989; *(b)* R. K. Grasselli, *Appl. Catal*., 1985, **15**, 127-139; *(c)* D. W. Bruce, D. O'Hare, Inorganic Materials, Wiley: Chichester, 1992; *(d)* P. A. Cox, Transition Metal Oxides; Clarendon Press: Oxford, England, 1995.

[2] *(a)* A. J. Cheetham, *Science,* 1996, **264**, 794; (b) B. Cockayne and D. W. James, Eds. Modern Oxide Materials, Academic Press: NewYork, 1972.

[3] A. Clearfield, *Chem. Rev*., 1988, **88**, 125-148.

[4] *(a)* T. Sawaki and Y. AoyamaE, *J. Am. Chem. Soc.*, 1999, **121**, 4793–4798; *(b)* H. K. Chae, M. Eddaoudi, J. Kim, S. I. Hauck, J. F. Hartwig, M. O'Keeffe, and O. M. Yaghi, *J. Am. Chem. Soc.*, 2001, **123**, 11482–11483.

[5] *(a)* H. Zhao, R. A. Heintz, X. Ouyang, K. R. Dunbar, C. F. Campana, and R. D. Rogers, *Chem. Mater.*, 1999, **11**, 736–746. *(b)* J. A. Swift and M. D. Ward, *Chem. Mater.*, 2000, **12**, 1501–1504.

[6] S. I. Stupp, P. V. Braun, *Science*, 1997, **277,** 1242.

[7] M. I. Khan and J. Zubieta, *Prog. Inorg. Chem*. 1995, **43**, 1.

[8] Y. Zhang, J. R. D. DeBord, C. J. O'Connor, R. C. Haushalter, A. Clearfield, and J. Zubieta, *Angew. Chem. Int. Ed*., 1996, **35**, 989-991.

[9] *(a)* T. Arumuganathan, A. S. Rao, and S. K. Das, *Cryst Growth Des.*, 2010, **10** 4272–4284; *(b)* V. Shivaiah, M. Nagaraju, and S. K. Das, *Inorg. Chem.*, 2003, **42**, 6604–6606; *(c)* V. Shivaiah and S. K. Das, *Inorg. Chem.*, 2005**, 44**, 7313–7315; *(d)* V. Shivaiah and S. K. Das, *Inorg. Chem.*, 2005, **44**, 8846–8854; *(e)* T. Arumuganathan and S. K. Das *Inorg. Chem.*, 2009, **48**, 496–507.

[10] *(a)* R. S. Rarig, Jr., R. Lam, P. Y. Zavalij, J. K. Ngala, R. L. LaDuca, Jr., J. E. Greedan and J. Zubieta, *Inorg chem*., 2002, **41**, 2124-2133; *(b)* R. C. Finn and J. Zubieta, *Inorg chem*., 2001, **40**, 2466-2467; *(c)* P. J. Hagrman and J. Zubieta, *Inorg.Chem.*, 2000, **39**, 5218-5224; *(d)* R. L. LaDuca, Jr., M. Desciak, M. Laskoski, R. S. Rarig, Jr. and J. Zubieta, *J. Chem. Soc., Dalton Trans.*, 2000, 2255–2257.

[11] *(a)* E. Burkholder, V. Golub, C. J. O'Connor and J. Zubieta, *Inorg.Chem.*, 2004, **43**, 7014−7029; *(b)* P. DeBurgomaster, A. Aldous, H. Liu, C. J. O'Connor, and J. Zubieta, *Cryst. Growth Des.*, 2010, **10**, 2209–2218; *(c)* N.

Calin and S. C. Sevov, *Inorg.Chem.*, 2003, **42**,7304−7308; *(d)* E. Dumas, C. Sassoye, K. D. Smith and S. C. Sevov, *Inorg.Chem.*, 2002, **41**, 4029−4032.

[12] *(a)* K. Maeda, Y. Kiyozumi and F. Mizukami, *J. Phys. Chem. B.*, 1997, **101**, 4402-4412; *(b)* F. Odobel, B. Bujoli and D. Massiot, *Chem. Mater.,* 2001, **13**, 163-173; *(c)* G. Alberti, M. Casciola, U. Costantino, A. Peraio and E. Montoneri, *Solid State Ionics,* 1992, **50**, 315-322; *(d)* G. Alberti and M. Casciola, *Solid State Ionics***,** 1997, **97**, 177-186; *(e)* L. A. Vermeulen and M. E. Thompson, *Nature* 1992, **358**, 656; *(f)* D. Deniaud, B. Schollorn, D. Mansuy, J. Rouxel, P. Battioni and B. Bujoli, *Chem. Mater*. 1995, **7**, 995-1000.

[13] *(a)* P. Yin, S. Gao, Z -M. Wang, C-H. Yan, L-M. Zheng and X-Q. Xin, *Inorg. Chem.*, 2005, **44**, 2761-2765; *(b)* V. Chandrasekhar, T. Senapati, A. Dey and E. C. Sanudo, *Inorg. Chem*., 2011, **50**, 1420-1428; *(c)* S-Z. Hou, D-K. Cao, Y-Z. Li and L-M. Zheng, *Inorg. Chem*., 2008, **47**, 10211-10213; *(d)* D. Papoutsakis, J. E. Jackson and D. G. Nocera, *Inorg. Chem*. 1996, **35**, 800-801.

[14] *(a)* E. V. Bakhmutova, X. Ouyang, D. G. Medvedev and A. Clearfield, *Inorg. Chem.*, 2003, **42**, 7046-7051; (b) S. Drumel, P. Janvier, P. Barboux, M. B. Doeuff and B. Bujoli, *Inorg. Chem*., 1995, **34**, 148-156; *(c)* J. L. Bideau, C. Payen, P. Palvadeau and B. Bujoli, *Inorg. Chem.*, 1994, **33**, 4885-4890; *(d)* S. Y. Song, J. F. Ma, J. Yang, M. H. Cao, H. J. Zhang, H. S. Wang and K. Y. Yang, *Inorg. Chem.*, 2006, **45**, 1201-1207; *(e)* G. Cao, H. Lee, V. M. Lynch and T. E. Mallouk, *Inorg. Chem.*, 1988, **27**, 2781-2785.

[15] *(a)* M. Mehring and *M.* Schurmann, *Chem. Commun.*, 2001, 2354-2355; *(b)* V. Baskar, M. Shanmugam, E. C. Sanudo, M. Shanmugam, D. Collison, E. J. L. McInnes, Q. Wei and R. E. P. Winpenny, *Chem. Commun*., 2007, 37-39; *(c)* C. R. Samanamu, M. M. Olmstead, J. L. Montchamp and A. F. Richards, *Inorg. Chem.*, 200**8, 47**, 3879-3887; *(d)* R. Murugavel, and S. Shanmugan, *Chem. Commun.*, 2007, 1257-1259.

[16] *(a)* V. Chandrasekhar, R. Azhakar, T. Senapati, P. Thilagar, S. Ghosh, S. Verma, R. Boomishankar, A. Steiner and P. K¨ogerle, *Dalton Trans.*, 2008, 1150-1160; *(b)* V. Chandrasekhar, L. Nagarajan, R. Cle´rac, S. Ghosh, and S. Verma, *Inorg. Chem.*, 2008, **47**, 1067-1073; *(c)* R. P. Doyle, P. E. Kruger, B. Moubaraki, K. S. Murray and M. Nieuwenhuyzen, *Dalton Trans.*, 2003, 4230-4237

[17] *(a)* J. M. Taylor, A. M. Mahmoudkhani and G. K. H. Shimizu, *Angew. Chem. Int. Ed.*, 2007, **46**, 795-798; *(b)* D. Kong, J. Zon, J. MacBee, and A. Clearfield, *Inorg. Chem*., 2006, **45**, 977-986; *(c)* O. R. Evans, H. L. Ngo and W. Lin, *J. Am. Chem. Soc.*, 2001, **123**, 10395-10396; *(d)* J. Liang and G. K. H. Shimizu, *Inorg. Chem*. 2007, **46**, 10449-10451.

[18] *(a)* F. A. Almeida Paz, J. Rocha, J. Klinowski, T. Trindade, F-N. Shi and L. Mafra, *Prog. Solid State Chem*., 2005, **33**, 113-125; *(b)* J. Y. Lu, *Coord. Chem. Rev*. 2003, **246**, 327-347.

[19] *(a)* N. G. Armatas, D. G. Allis, A. Prosvirin, G. Carnutu, C. J. O'Connor, K. Dunbar, and J. Zubieta, *Inorg.Chem*., 2008, **47**, 832−854; *(b)* E. Burkholder, V. Golub, C. J. O'Connor, and J. Zubieta, *Inorg.Chem*., 2004, **43**, 7014−7029.

[20] *(a)* R. C. Finn, R. S. Rarig, Jr. and J. Zubieta, *Inorg.Chem*., 2002, **41**, 2109−2123; *(b)* C. Peloux, A. Dolbecq, P. Mialane, J. Marrot and F. Sécheresse, *Dalton Trans*., 2004, 1259–1263.

[21] *(a)* P. DeBurgomaster, W. Ouellette, H. Liu, C. J. O'Connor and J. Zubieta, *CrystEngComm*, 2010, **12**, 446–469; *(b)* G. Yucesan, M. H. Yu, W. Ouellette, C. J. O'Connor and J. Zubieta, *CrystEngComm*, 2005, **7**,480–490; *(c)* W. Ouellette, G. Wang, H. Liu, G. T. Yee, C. J. O'Connor and J. Zubieta, *Inorg.Chem*., 2009, **48**, 953-963.

[22] *(a)* U. Kortz, C. Marquer, R. Thouvenot and M. Nierlich, *Inorg.Chem*., 2003, **42**,1158−1162; *(b)* C. R. Mayer, J. Marrot and F. Secheresse, J. Mol. Struct., 2004, **704**, 59–62; *(c)* P. Mialane, A. Dolbecq and F. Secheresse, *Chem.Commun*., 2006, 3477–3485.

[23] U. Kortz, J. Vaissermann, R. Thouvenot, and P. Gouzerh, *Inorg.Chem*., 2003, **42**,1135−1139.

[24] M. Yuan, Y. Li, E. Wang, Y. Lu, C. Hu, N. Hu, H. Jia, *J. Chem. Soc., Dalton Trans*., **2002**, 2916–2920.

[25] *(a)* B. K. Tripuramallu, S. Ghosh and S. K. Das, unpublished results; *(b)* B. K. Tripuramallu, R. Kishore and S. K. Das, *Polyhedron,* 2010, **29**, 2985-2990.

[26] *(a)* V. Chandrasekhar, T. Senapati and E. C. Sanudo, *Inorg.Chem*., 2008, **47**, 9553-9560; *(b)* A. Fernández-Botello, A. Escuer, X. Solans, M. Font-Bardía, A. Holý, H. Sigel and V. Moreno, *Eur. J. Inorg. Chem*., 2007, 1867-1873.

[27] C. R. Mayer, M. Herve, H. Lavanant, J. C. Blais and F. Secheresse, *Eur. J.*

Inorg. Chem., 2004, **5**, 973.

[28] *(a) SAINT: Software for the CCD Detector System*; Bruker Analytical X-ray Systems, Inc.: Madison, WI, **1998**; *(b) SADABS: Program for Absorption Correction;* G. M. Sheldrick University of Gottingen: Gottingen, Germany, **1997**; *(c) SHELXS-97: Program for Structure Solution;* G. M. Sheldrick, University of Gottingen: Gottingen, Germany, **1997**; *(d) SHELXL-97: Program for Crystal Structure Analysis;* G. M. Sheldrick University of Gottingen: Gottingen, Germany, **1997**.

[29] *(a)* M.-g. Liu, P.-p. Zhang, J. Peng, H.-x. Meng, X. Wang, M.Zhu, D. -d. Wang, C.-l. M. and K. Alimaje, *Cryst.Growth Des*., 2012, **12**, 1273−1281;*(b)* H. Yang, S. Guo, J. Tao, J. Lin and R. Cao, *Cryst.Growth Des*., 2009, **9**, 4735-4744; *(c)* Y. Wang, Y. Peng, L.-N. Xiao, Y.-Y. Hu, L.-M. Wang, Z.-M. Gao, T.-G. Wang, F.-Q. Wu, X.-B. Cui and J.-Q. Xu, *CrystEngComm*, 2012, **14**, 1049–1056; *(d)* P.-P. Zhang, J. Peng, H.-j. Pang, J.-q. Sha, M. Zhu, D. d. Wanga and M.-g. Liu, *CrystEngComm*, 2011, **13**, 3832–3841; *(e)* Y. Wang, L. Ye, T.-g. Wang, X.-B. Cui, S.-Y. Shi, G.-W. Wang and J.-Q. Xu, *Dalton Trans*., 2010, **39**, 1916-1919; *(f)* G. Hou, L. Bi, B. Li, and L. Wu, *Inorg. Chem*., 2010, **49**, 6474-6483; *(g)* H. Yang, S. Gao, J. Lu, B. Xu, J. Lin and R. Cao, *Inorg. Chem.*, 2010, **49**, 736–744.

[30] J. M. Maestre, X. Lopez, C. Bo, J.-M. Poblet and N. C. –Pastor, *J. Am .Chem. Soc*. 2001, **123**, 3749 3758.

[31] M. O"Keeffe and N. E. Brese, *J.Am.Chem.Soc*. 1991, **113**, 3226-3229.

[32] B.-Z. Lin, L.-W. He, B.-H. Xu, X.-L. Li, Z. Li, and P.-D. Liu *Cryst.Growth Des*., 2009, **9**, 273-281.

[33] *(a)* A. Yokoyama, T. Kojim, K. Ohkubo and S. Fukuzumi, *Inorg. Chem.*, 2010, **49**, 11190-11198; *(b)* H.-J. Pang, H. Y. Ma, J. Peng, C.-J. Zhang, P.-P. Zhang and Z.-M. Su, *CrystEngComm* 2011, **13**, 7079-7085.

4.2. Understanding the Formation of Metal-oxide Based Inorganic Solids: Assessing the Influence of Tetrazole Molecule

4.2.1. Introduction

Metal oxide-based solids form an important class of materials showing their promising applications in the contemporary research areas during past several years. A significant research in this area have been directed partly due to interest in their chemistry as well as its applications.[1] Molybdenum oxides containing transition metals are good candidates of the catalytic applications owing to their structural rigidity. For example, transition metal molybdates of composition $MMoO_4$ (M=Mn, Co, Cu and Zn) catalyze the oxidative dehydrogenation of the propane,[2] and magnesia supported molybdates are used for anaerobic oxidation of butane to butadiene.[3] $MnMoO_4$ is used for high capacity anode material of lithium battery.[4] In general there is a correlation between the complexity of the structure and functionality of the material.[5] The constant evolution of complexity of molybdenum oxides in the terms of functionality requires more knowledge on synthetic strategies to understand the oxide structures.[6] One such strategy for the modification of oxide structures involves introduction of organic molecules as structure directors. Zeolites,[7] biomineralized materials,[8] mesoporous oxides,[9] and transition metal phosphates[10] are the examples in which an organic constituent acts as structure-directing role in the constitution of the oxide microstructures. By exploiting the structure-directing role of polyfunctional organic molecules (for example, organoamine ligands), a wide variety of bimetallic oxides were isolated.[11] Typically hydrothermal methods have been commonly used to synthesize the molybdenum oxide-based materials; the technique offers an excellent route to isolate metastable phases and stabilizes the reliability of the structure.[12] There are two major classes in the M/Mo/O/Ligand family of oxides: (i) poloxomolybdate anion clusters, together with secondary metal/ligand components as complexes or cationic networks, constituting metal-oxide-based solids;[13] (ii) solids constituting oxide microstructures rather than anionic clusters to which secondary metal/ligand components are attached to the peripherals of these oxide microstructures. In the later class of inorganic oxides there are many reports representing $[M(org)_nMo_xO_y]$ (M= transition metals) in which these bimetallic oxide MMo_xO_y components are 1-D chains,[14] 2-D sheets[15] or 3-D frameworks[16] to which organoamines are attached *via* coordination through secondary metals as peripheral moieties or bridging subunits. Among these, 3-D frameworks constituted by bimetallic oxides are quite interesting in terms of

both functionality as well as self assembly processes. Zubieta and co-workers have studied structure directing role of the organoamine ligands in the self assembly of bimetallic oxides with the ligands bipyridylamine (bpa), pyrazine (pyz), pyrimidine (pyrd),[16] and 3,4´-bipy, 3,3´-bipy, 4,4´-bipy.[17] Ramanan and his group investigated the influence of 2-Amino pyridine on the formation of copper molybdates.[18]

As shown in Scheme 4.4, the pyrazine and pyrimidine have two nitrogen donors, triazole has three nitrogen donors and tetrazole has four nitrogen donors. From the previous reports, it is known that pyrazine and pyrimidine form complex 3-D bimetallic oxides CUMO-5 & CUMO-6 with well-defined channels occupied by the pyrazine and pyrimidine units respectively.[16] These two are rare examples, in which bimetallic oxide forms a 3-D framework and organoamines support the frameworks. As the donor to donor distance is less in both the ligands (pyrazine and pyrimidine), this allows the secondary metal polyhedron of a layer / chain to connect the adjacent layer / chain at shortest distances (through the metal-oxo group) resulting a 3-D bimetallic oxide framework. But in the cases, where the donor to donor distance is more (eg. 4,4 bipy , dpe, dpa, average N–N distance is 6.52 to 8.62 Å),[17] these ligands separate the metal polyhedron layers at largest distances, thereby forming of pillared-layered structures. Interestingly, the ligands pyradazine and triazole (Scheme 4.4) having adjacent donor sites do not form a 3-D bimetallic oxide frameworks, rather, these ligands form a cationic networks in which the oxide clusters are embedded.[19]

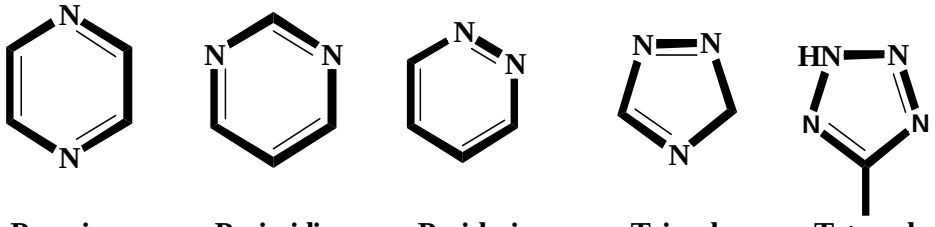

Scheme 4.4. Various polyazaheteroaromatic organic molecules as structure directing roles in the self assembly process of metal oxide based solids.

Among these polyazaheteroaromatic compounds (Scheme 4.4), tetrazoles are of special interest because they consist of all possible bridging fashions for coordinating the adjacent metal centers. The versatility of a tetrazole molecule lies in the availability of more number of donor sites (nitrogen donors). The geometry of these donor sites can act as bridging as well as chelating ligands leading to the desirable networks.[20] Due to an availability of four donor sites; it has opportunity to bridge the surrounding secondary

metal polyhedron; thus tetrazole molecule with more donor sites can template the formation of oxide network. The only report of tetrazole involving poloxomolybdates, reported by Zubieta and co-workers, has described cationic networks of copper and tetrazoles, in which anionic octamolybdates have been shown to be encapsulated in the channels or voids of the cationic frameworks.[21] In the present study, we have chosen a tetrazole, namely '4-ptz' [5-(4-pyridyl) tetrazole], a tetradentate ligand, to study the influence of the tetrazole molecule on the formation of bimetallic oxide-based new solids, which exploits the geometry of the tetrazole molecule in understanding the self assembly of the bimetallic oxides. We wish to report here the synthesis and structural characterization of two compounds $[Cu(4\text{-}Hptz)(Mo_2O_7)]$ (**3**) and $[Cu(4\text{-}Hptz)_2(H_2O)_3]_2[Mo_8O_{26}]$ (**4**). In compound **3**, 5-(4-pyridyl) tetrazole (4-ptz) templates the formation of $Cu_4Mo_6O_{10}$ rings through the all four donor sites, and these rings stack to each other to form a 3-D bimetallic oxides, whereas, in compound (**4**) tetrazole forms complex cation $[Cu(4\text{-}Hptz)_2(H_2O)_3]^{2+}$ using only one donor N atom, which in turn, is stabilized by the supramolecular interactions with one-dimensional octamolybdate chains $[Mo_8O_{26}]_n^{4n-}$.

4.2.2. Experimental Section

4.2.2.1. Materials and Methods

All the chemicals were received as reagent grade and used without any further purification. 5-(4-pyridyl) tetrazole (4-ptz) was prepared according to the reported procedure.[22] Elemental analyses were determined by FLASH EA series 1112 CHNS analyzer. Infrared spectra of solid samples were recorded on a JASCO – 5300 FT – IR spectrophotometer as KBr pellets. Thermo gravimetric analyses were carried out on a STA 409 PC analyzer and corresponding masses were analyzed by QMS 403 C mass analyzer, under the flow of N_2 gas with a heating rate of 5 °C min^{-1}, in the temperature range of 30–900 ^oC.

4.2.2.2. Synthesis

Synthesis of the compound $[Cu(4\text{-}Hptz)(Mo_2O_7)]$ (3)

A mixture of ammonium heptamolybdate tetrahydrate (0.10 mmol, 0.125 g), copper nitrate trihydrate (0.51 mmol, 0.123 g), 4-ptz (0.50 mmol, 0.074 g), and water (555.5 mmol 10.0 g) in the mole ratio 1:5.1:5:5555 was taken; to the resulting reaction mixture, 0.1 mL Et_3N

was added and stirred for 30 min. Then the pH of the reaction mixture was adjusted to 1.7 by adding 0.5 M HNO_3. The solution was then transferred to 23 mL Teflon lined autoclave in the stainless steel vessel and heated at 180 °C for 72 hr and cooled to room temperature over two days to give red block crystals of **3**. Yield: 0.10 g (38%, based on copper) Anal. Calc. for $C_6H_5N_5CuMo_2O_7$ (514.56): C, 14.00; H, 0.97; N, 13.61. Found: C, 14.78; H, 1.01; N, 13.78. IR (KBr pellet) (υ/cm^{-1}): 3458, 3082, 2920, 2240, 1637, 1516, 1437, 1195, 1022, 850, 760, 634.

Synthesis of the compound $[Cu(4\text{-}Hptz)(H_2O)_3]_2[Mo_8O_{26}]$ (4)

A mixture of ammonium heptamolybdate tetrahydrate (0.20 mmol, 0.247 g), copper nitrate trihydrate (0.09 mmol, 0.023 g), 4-ptz (0.19 mmol, 0.028 g), and water (555.5 mmol 10.0 g) in the mole ratio 2.22:1:2.11:6172 was taken followed by the addition of Et_3N (0.1 mL) and the resulting reaction mixture were stirred for 30 min. The pH of the reaction mixture was then adjusted to 2.0 by the 0.5 M HNO_3. The solution was then transferred to 23 mL Teflon lined autoclave in the stainless steel vessel and heated at 120 °C for 72 hr and cooled to room temperature over two days to give blue block crystals of **4**. Yield: 0.04g (22%, based on copper) Anal. Calc. for $C_{24}H_{32}Cu_2Mo_8N_{20}O_{32}$ (2007.32): C, 14.36; H, 1.60; N, 13.95. Found: C, 13.84; H, 1.42; N, 13.68. IR (KBr pellet) (υ/cm^{-1}): 3354, 3099, 2096, 1637, 1520, 1385, 1199, 1047, 956, 906, 841, 814, 754, 707, 596, 516, 480.

4.2.2.3. X-ray Crystallography

Data were measured on a Bruker SMART APEX CCD area detector system [λ(Mo Kα) = 0.71073 Å], graphite monochromator, 2400 frames were recorded with an ω scan width of 0.3°, each for 8 seconds, a crystal detector distance of 60 mm, and a collimator of 0.5 mm. The data were reduced using SAINTPLUS,[23] the structures were solved using SHELXS-97[24] and refined using SHELXL-97.[25] All non hydrogen atoms were refined anisotropically. We tried to locate the hydrogen atom on the nitrogen atom of the pyridine ring in compound **3** through differential Fourier maps, but did not succeed. Crystal data, structure refinement parameters for both the compounds are summarized in Table 4.3

4.2.3. Results and Discussion

4.2.3.1. Synthesis

In the previous report dealing with 5-(4-pyridyl) tetrazole (4-ptz), a cationic network has been shown to be formed by utilizing only two nitrogen's of tetrazole ring and one nitrogen atom of pyridine ring, in which octamolybdates are encapsulated in the voids or

channels reminiscent to triazole.[21] In this case, the nitrogen atoms of the pyridine ring of the ligand 4-ptz, can also form coordinate covalent bond with the metal centre and alters the formation of oxide structure. The profound influence of the geometry of the 4-ptz ligand can be shown in the oxide structure only by blocking the coordination of the pyridine-nitrogen atom and making availability of the four nitrogens in the tetrazole ring for its coordination (Scheme 4.5). In the course of our investigation on the synthetic conditions to fulfill these necessities, we have deprotonated the tetrazole ring by adding a base, whereby the negative charge is delocalized in the ring making all the nitrogens available simultaneously for their coordination. To block the coordination of the pyridine nitrogen atom, the concerned reactions were performed at relatively acidic (low) pH, and then pyridine nitrogen gets protonated and blocks its coordination to metal center. This deprotonation–protonation event of the tetrazole ring has profound influence on the formation of oxide structures.

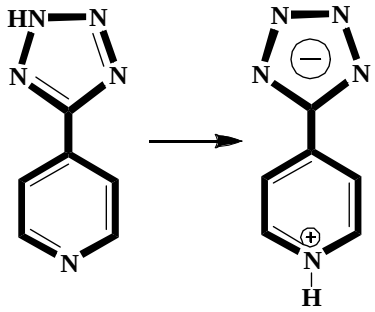

4-ptz **4-Hptz**

ptz = [5-(4-pyridyl) tetrazole]

Scheme 4.5. Scheme showing the modification of the ligand to meet the synthetic conditions.

In a typical synthesis of compound $[Cu(4\text{-}Hptz)Mo_2O_7]$ (**3**), a mixture of ammonium heptamolybdate, copper nitrate, 5-(4-pyridyl) tetrazole (4-ptz) and water in the mole ratio 1:5.1:5:5555 was taken and 0.1 mL of Et_3N was added to deprotonate the tetrazole ring. Subsequently, the pH of the mixture was adjusted to 1.7 by addition of 0.5 M HNO_3 and heated at 180 °C for 72 hr to give a deep red color block crystals. Compound $[Cu(4\text{-}Hptz)_2(H_2O)_3]_2[Mo_8O_{26}]$ (**4)** was also prepared from the same reactants in the similar synthetic manner, but the mole ratio was changed to 2.22:1:2.11:6172 and temperature to 120 °C. Thus, the important variation in the synthesis of compounds **3** and **4** was the variation of mole ratios of the reactants and temperature. In the synthesis of compound **3**, the concentration of ammonium heptamolybdate is less than Cu source and 4-ptz, while in

the compound **4**, the molybdate concentration is more. This concentration variation leads to a drastic change in the self assembly process of metal oxides resulting in two completely different structures (namely, compounds **3** and **4**). Finally, the temperature has also remarkable role in stabilizing the structures, for example, compound **3** was prepared at high temperature 180 °C, while **4** was prepared at relatively low temperature (120 °C). Detailed synthesis and mode of tetrazole binding are shown in Scheme 4.6. The replacement of base Et_3N with other bases does not give the compounds in the desired yields.

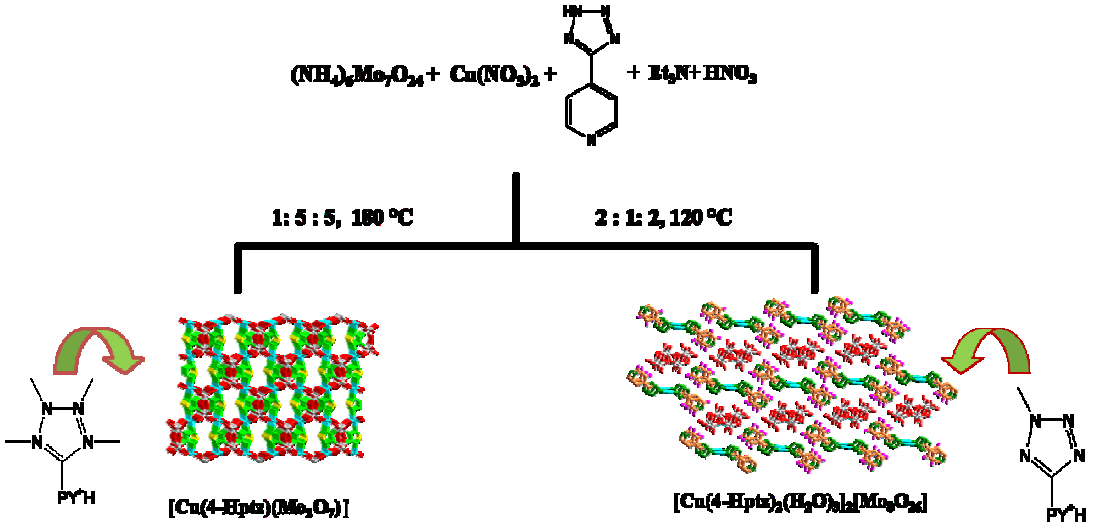

Scheme 4.6. Syntheses of compounds $[Cu(4\text{-}Hptz)Mo_2O_7]$ (**3**) and $[Cu(4\text{-}Hptz)_2(H_2O)_3]_2[Mo_8O_{26}]$ (**4**)

4.2.3.2. Description of the Crystal Structures

Structural description of $[Cu(4\text{-}Hptz)Mo_2O_7]$ (3)

Compound **3** crystallizes in orthorhombic space group *Pnma*; the relevant crystal data and structural refinement for compound **3** are presented in Table 4.3. As shown in Figure 4.6, compound **3** consists of a bimetallic $\{CuMo_2O_7\}$ three dimensional network supported by the nitrogen atoms of the tetrazole ring of 4-Hptz. The relevant asymmetric unit consists of one independent Mo atom to which four oxygen atoms are attached (among these, one oxygen is in special position), one Cu atom in special position and half of the 4-Hptz ligand. The molecular formula of the compound from the asymmetric unit is thus described as $[Cu(4\text{-}Hptz)Mo_2O_7]$, in which the charge of the dianion $[Mo_2O_7]^{2-}$ is compensated by the Cu^{2+} cation. In the ligand 4-ptz, the proton on the nitrogen atom of tetrazole ring is deprotonated, the resulting negative charge is delocalized throughout the ring, while the nitrogen atom of the pyridine ring gets protonated to give a positive charge. Thus, the ligand can be depicted as a neutral ligand, $[5\text{-}(4\text{-}C_5H_4N^+H)CN_4^-](4\text{-}Hptz)$. The

dimer $[Mo_2O_7]^{2-}$ consists of two corner sharing $\{MoO_4\}$ polyhedron with three terminal oxygens of bond lengths 1.763, 1.800 and 1.721 Å respectively and one bridging μ-oxo with bond length of 1.952 Å.

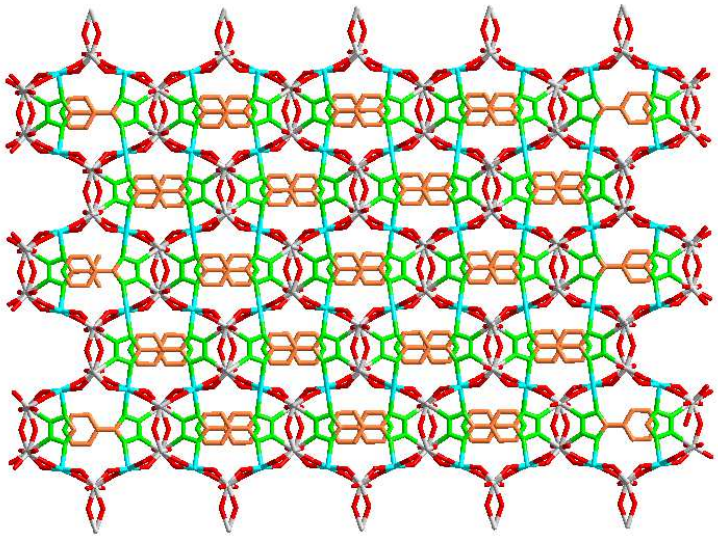

Figure 4.6. 3D packing diagram in the crystal structure of the compound **3** (view along *a*- axis)**.**

The Mo–O–Mo bridge has a bent configuration with bond angle 142.0°. The anion $[Mo_2O_7]^{2-}$ extends its dimensionality to 3D by sharing all the three terminal oxygens with another $[Mo_2O_7]^{2-}$ subunit and $\{CuN_2O_4\}$ octahedron. The two Mo atoms of $[Mo_2O_7]^{2-}$ linked to another unit by the terminal oxygen O1 *via* corner sharing with a distance of 2.202 Å to form a one dimensional square grid running through crystallographic *a* axis (Figure 4.7a).

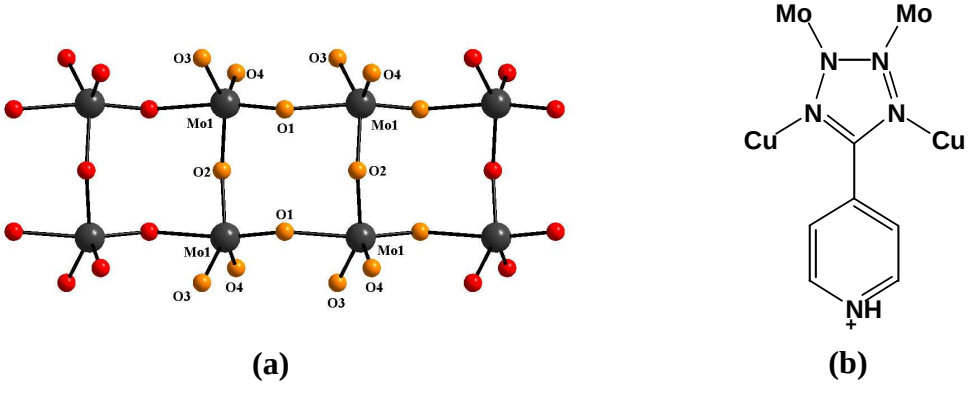

Figure 4.7. (a) One dimensional chainlike arrangement of square grids running through crystallographic *a* axis, (b) coordination of 4-Hptz to the metal centres.

Each molybdenum atom in the dianion $[Mo_2O_7]^{2-}$ is in $\{MoO_5N\}$ octahedron constructed from the nitrogen atom of the tetrazole ring, three terminal oxygens, one bridging μ-oxo and one oxygen atom form the other $[Mo_2O_7]^{2-}$ subunit. Each $\{MoO_5N\}$ octahedron

corner-shares with three $\{MoO_5N\}$ octahedra and two $\{CuN_2O_4\}$ octahedra. The coordination geometry around Cu(II) atom is defined by the two nitrogen atoms (N2) of two tetrazole rings with bond length of 2.230 Å and four corner sharing oxygen atoms (two O3 and two O4) from two dianions $[Mo_2O_7]^{2-}$ with bond lengths 1.897 and 2.252 Å, respectively. Each $\{CuN_2O_4\}$ octahedron corner shares with four $\{MoO_5N\}$ octahedra. From the tetrazole point of view, 4-Hptz is a neutral molecule $[5\text{-}(4\text{-}C_5H_4N^+H)CN_4^-](4\text{-}$Hptz), acting as a tetradentate ligand in which two nitrogen atoms (N1) bind / chelate to one $[Mo_2O_7]^{2-}$ anion and two nitrogen atoms bind / bridge to two copper atoms. The plausible modes of binding with different types of pairs of nitrogen atoms are shown in the Table 4.4. Each tetrazole connects to two Cu octahedra and one $[Mo_2O_7]^{2-}$ anion through four nitrogen donors (Figure 4.7b). There are only few instances in which tetrazole exhibits coordination mode of IX,[26] in which all the nitrogen atoms of the tetrazole ring are involved in the bonding. In order to meet the available coordination requirements, the ligand 4-Hptz adopts slightly bend conformation from the plane. The covalent connectivity in the $\{CuMo_2O_7\}$ network brings about a large 20-membered $\{Cu_4Mo_6O_{10}\}$ ring. Each ring is formed by the two 4-Hptz ligands, whereby the pyridine moiety of each 4-Hptz occupies the cavity of the rings (Figure 4.8a).

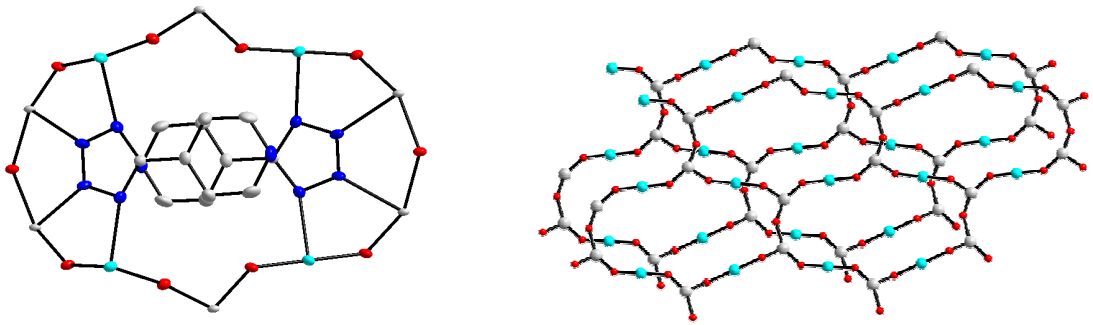

(a) **(b)**

Figure 4.8. (a) 20 Membered $\{Cu_4Mo_6O_{10}\}$ ring, template by two 4-Hptz ligands, (b) stacking of the bimetallic layers formed from the rings.

These rings form sheets and these sheets stacked *via* connection through terminal oxygens to form a 3-D bimetallic oxide network (Figure 4.8b). Two 4-Hptz ligands act as a template in the formation of the $\{Cu_4Mo_6O_{10}\}$ rings through its coordination *via* nitrogen atom to both Cu and Mo octahedra. It is worth mentioning that the coordination from nitrogen to molybdenum is hardly known in inorganic self-assembled structures. The pattern of chains formed with tetrazole rings and the metal centers are shown in Figure

4.9a and the framework of bimetallic oxide $\{CuMo_2O_7\}$ is shown in Figure 4.9b. The arrangement of chains in the framework is shown in Figure 4.9c.

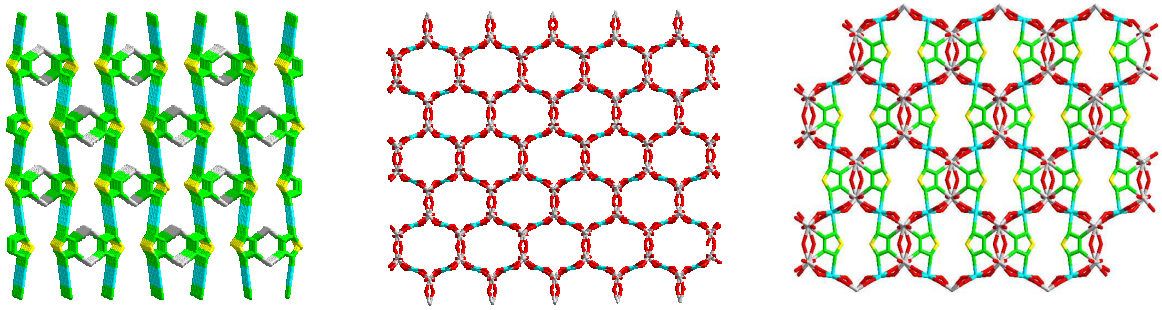

Figure 4.9. (a) Cationic chains, formed from 4-Hptz and metal centers, (b) 3-D framework of $\{CuMo_2O_7\}$ bimetallic oxide, (c) fusion of cationic chains in the 3-D bimetallic oxide.

Structural description of $[Cu(4\text{-}Hptz)_2(H_2O)_3]_2[Mo_8O_{26}]$ (4)

In our investigation of self assembly process of copper molybdates with tetrazole, we isolated compound **4** at different synthetic conditions, with molecular formula $[Cu(4\text{-}Hptz)_2(H_2O)_3]_2[Mo_8O_{26}]$ (**2**). Compound **4** crystallizes in triclinic space group *P-1*; crystal data and structural refinement for compound **4** are presented in Table 4.3. The thermal ellipsoid plot for compound **4** is shown in Figure 4.10.

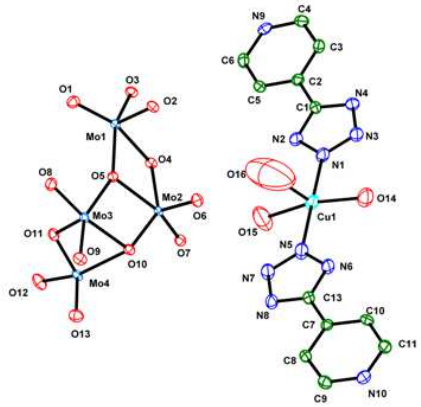

Figure 4.10. Thermal ellipsoidal plot of compound **4,** hydrogen's are not shown for clarity.

The relevant asymmetric unit consists of half of the octamolybdate, $[Mo_4O_{13}]^{2-}$ anion and $[Cu(4\text{-}Hptz)_2(H_2O)_3]^{2+}$ cation. The crystal structure of **4** consists of infinite molybdenum oxide chains constructed from the corner sharing octamolybdate anions $[Mo_8O_{26}]^{4-}$ and discrete Cu(II) cationic complexes $[Cu(4\text{-}Hptz)_2(H_2O)_3]$. Octamolybdate is well characterized and highly explored POM with α-η isomers[27] and has been isolated with different range of organic cations,[28] and inorganic metal complexes.[29] In the present study,

the octamolybdate chains formed in the compound **4** are almost similar with the chains, reported in the compound $[(Me\text{-}NC_5H_5)_4Mo_8O_{26}]$.[30] The monomeric octamolybdate $[Mo_8O_{26}]^{4-}$ unit in the compound **4** comprises of eight edge sharing MoO_6 octahedra. The mode of connectivity of these monomeric octamolybdates gives different types of oxide chains.[30] Each octamolybdate unit in compound **4** consists of four μ^2–oxo groups, in which each oxo group acts as a linker between two molybdenum atoms from the adjacent subunits to form an infinite oxide chains.

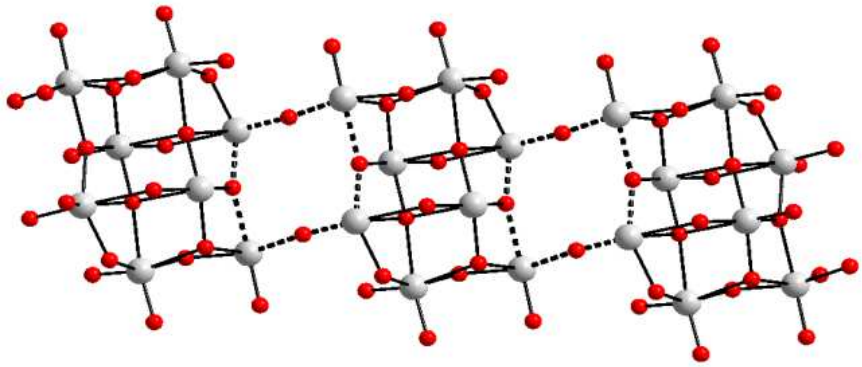

Figure 4.11. Infinite octamolybdate chains with rectangular cavities

The connectivity of a pair of octahedra of one subunit with a pair of octahedra from another subunit through corner sharing (*via* μ^2–oxo) results in an infinite 1-D oxide chains with the formation of rectangular voids of dimension 3.828 Å X 3.862 Å in the linking region (Figure 4.11). The Mo–O–Mo bridges between two subunits are almost linear with an angle of 171.3° whereas the Mo–O–Mo bridge in the compound **3** is bent with an angle of 142.0°. The cation in the compound **4** consists of Cu(II) centers in $\{CuO_3N_2\}$ square pyramids. The geometry at each Cu(II) centre is defined by one oxygen atom (O16) from one coordinated water molecule in apical position and two oxygen atoms (O14 and O15) from two more coordinated water molecules and two nitrogen atoms from the two 4-Hptz ligands in the basal plane. In the crystal structure of compound **4**, O14 and O15 atoms suffer from significant disorder problem and they have been splitted over two positons after fixing their occupancies to 0.5 and 0.5 for O14 and 0.75 and 0.33 for O15. We collected crystal data for compound **4** at liquid nitrogen temperature; however this low temperature data also did not improve the situation of disorder problem.

The pyridine nitrogen atom is protonated and does not involve in the bonding as mentioned previously (Scheme 4.5). Only one nitrogen atom of the tetrazole ring

coordinates to the Cu atom (Mode-II)[26] whereas in **3** all the four nitrogen atoms are bonded to metal centers.

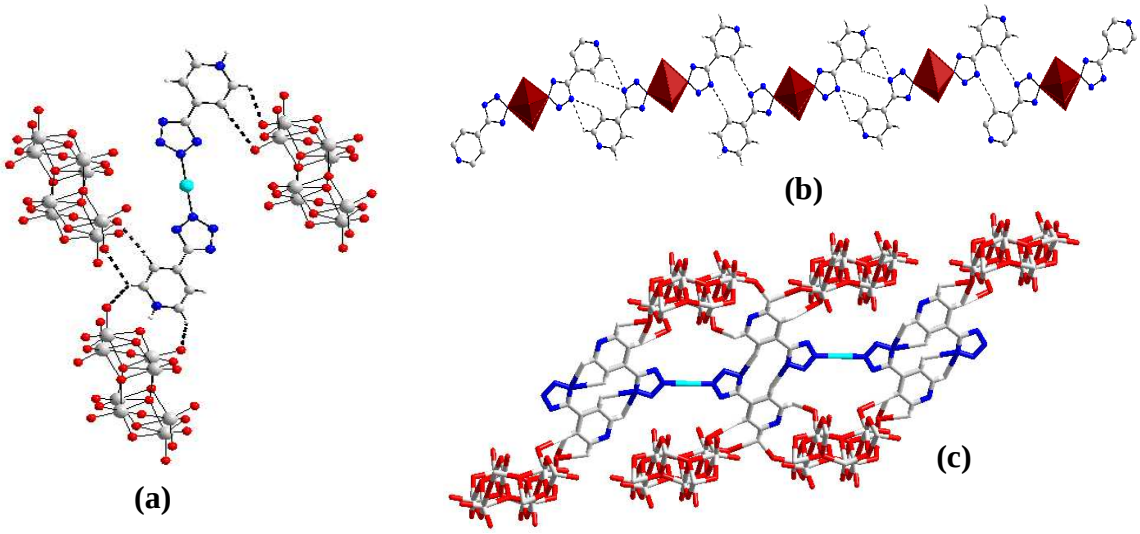

Figure 4.12. (a) C–H···O interactions between the 4-Hptz and octamolybdate chains, (b) C–H···N interactions between the two 4-Hptz ligands, (c) overall C–H···O and C-H···N interactions leading to a 3-D supramolecular frame work.

The void space created by the oxide chains are occupied by the Cu(II) cationic complexes. The oxygen atoms of the octamolybdate chains involves in hydrogen bonding interactions with hydrogen atoms of the pyridine ring. Each cation $[Cu(4\text{-}Hptz)_2(H_2O)_3]$ is connected to three oxide chains *via* C–H···O weak interactions as shown in Figure 4.12a. Also there exists a weak C–H···N supramolecular interactions between two $[Cu(4Hptz)_2(H_2O)_3]$ cations to form a one dimensional chain as shown in the Figure 4.12b. Overall the C–H···N interactions form a one dimensional chainlike structure of $[Cu(4\text{-}Hptz)_2(H_2O)_3]$ cations, which in turn, forms 3-D framework with oxide chains through C–H···O interactions (Figure 4.12c). The relevant hydrogen bonding distances and angles with symmetry operations are listed in the Table 4.5.

4.2.3.3. How a tetrazole molecule influences the self-assembly process of the inorganic oxides

The availability of more number of donor sites and the geometry of the donor sites in the tetrazole ring allows showing an important role in the self assembly process of the inorganic oxides. The higher reacting ability and higher oxidation state of molybdenum tend to form the mononuclear, polynuclear or oligomeric anionic cluster anions such as $[MoO_4]^{2-}$, $[Mo_2O_7]^{2-}$ and $[Mo_8O_{26}]^{4-}$. The formation of these anionic clusters in the self assembly process of inorganic oxides is mainly dependent on the secondary metal

coordination preferences, geometry and availability of the donor sites in the organoamine ligands, and synthetic conditions like pH, temperature and concentration of the reactants. Tetrazoles are known to adopt at least nine distinct types of coordination modes with metal ions in the formation of metal-organic frameworks (see Scheme 4.7).[26]

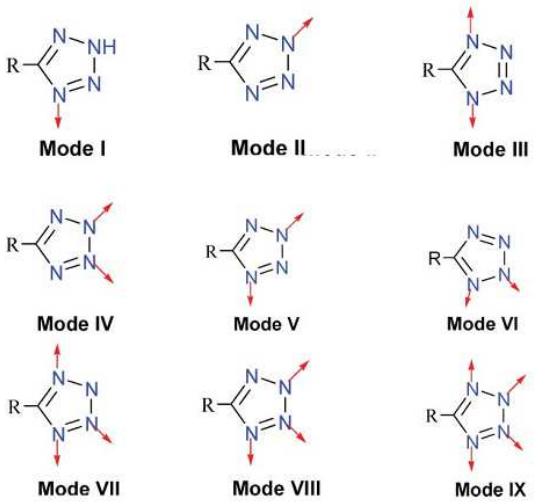

Scheme 4.7. Different coordination modes of the tetrazole ring.

The geometry of tetrazole ring is unique in the sense that the nitrogen atoms can act as both chelated and bridging components (Table 4.4). N-containing ligands involve in the self assembly process of inorganic oxides only through the coordination to the secondary metal ions but not to the Mo metal centre. The delocalization of negative charge in the ring of tetrazole, gives the ring an aromatic sextet (see Scheme 4.8),[31] thereby enhances the coordination ability of the nitrogen atoms of the tetrazole ring. Due to more coordination ability of the nitrogen atoms in the tetrazole ring allows to coordinate to both secondary metal and molybdenum metal centers. This factor makes a tetrazole molecule different from the other nitrogen containing ligands in the self assembly process. As a result, in the compound **3**, tetrazole ring coordinates to two molybdenum centers and thereby prevents the formation of oligomeric anionic clusters from $[Mo_2O_7]^{2-}$ anion. However, in the case of compound **4**, due to more concentration of heptamolybdate (see synthesis section), tetrazole ring does not prevent the formation of the oligomeric anionic clusters and thereby tetrazole acts as monodentate ligand. The formation of the octamolybdate chains in compound **4** is not purely dependent on the influence of the tetrazole ring, but the formation of copper complex cation with tetrazole is an important factor, responsible for the formation of the oxide phase.

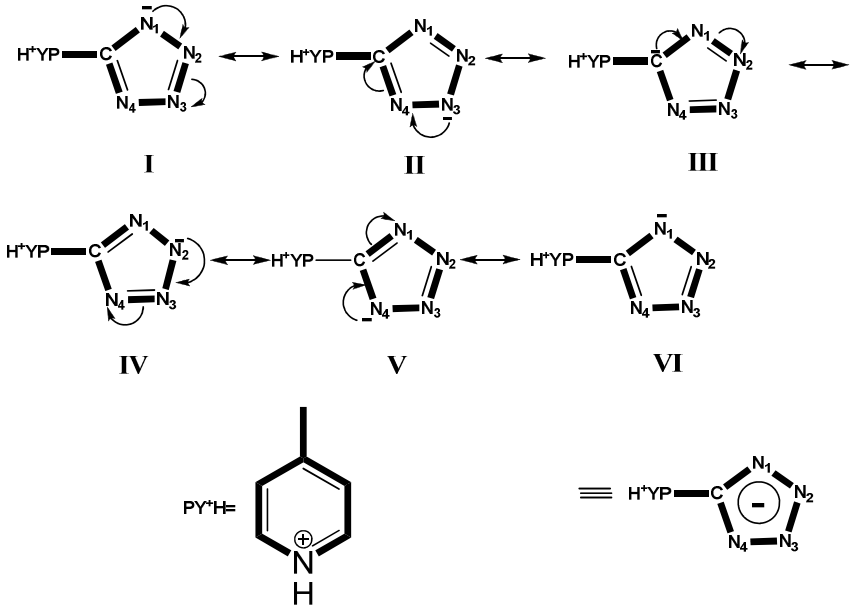

Scheme 4.8. Delocalization of negative charge in the tetrazole ring to give an aromatic sextet

The coordination modes of the tetrazole ring to the metal centers in both the compounds have been shown in Scheme 4.7. This profound influence of tetrazole ring in the formation of oxide phases is only possible when the entire donor sites are available for binding. The mode of the tetrazole ring and the corresponding oxide phase in the compounds synthesized/reported are shown in Table 4.6.

4.2.3.4. Thermogravimetric studies

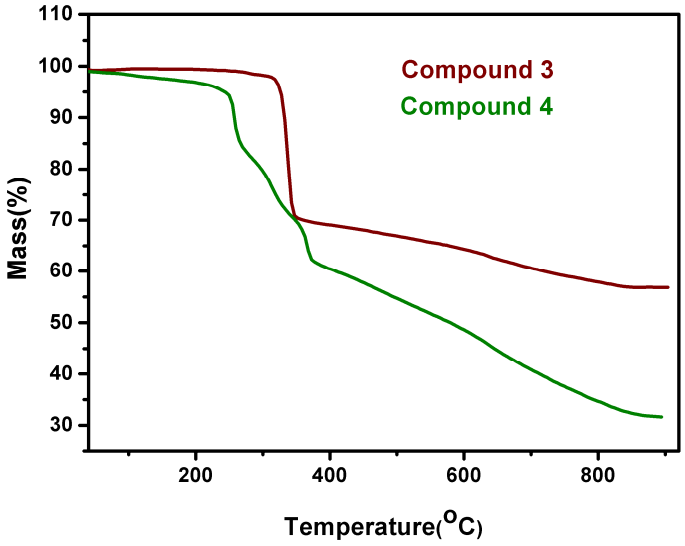

Figure 4.13. Thermogravimetric curves of compounds **3** and **4**

Thermal analyses of both the compounds were performed under nitrogen atmosphere (Figure 4.13). Compound **3** shows a thermal stability up to 320 °C and exhibits a weight loss of 28.20% (theoretical: 28.56%) corresponding to the loss of 4-Hptz. A continuous weight loss occurs in the region 352 °C to 838 °C to produce an amorphous gray powder. On the other hand, compound **4** shows a thermal stability up to 215 °C and exhibits a weight loss of 35% (theoretical : 34.6%) corresponding to the loss of six water molecules and four 4-Hptz moieties. Compound **3** exhibit more thermal stability than compound **4** due to strong coordination of tetrazole to the inorganic oxide phase leading to a three-dimensional network in compound **3**. The continuous weight loses after the exclusion of 4-Hptz in both the compounds give unknown oxide phases.

4.2.4. Conclusion

Inorganic oxides represent the most important class of materials as far as stability and application aspects are concerned. In order to investigate the self assembly process of bimetallic inorganic oxides involving tetrazole, herein, we have identified three dimensional covalently linked material [Cu(4-Hptz)Mo_2O_7] (**3**) and one dimensional compound [Cu(4-Hptz)$(H_2O)_3]_2[Mo_8O_{26}$] (**4**). The attractive feature of this article is that in the compound **3**, tetrazole ring with the aid of four donor sites templates the formation of the {$Cu_4Mo_6O_{10}$} rings, which stacks further to give a 3-D bimetallic oxide frame work of {$CuMo_2O_7$}$_n$. The coordination ability of the nitrogen atoms in the tetrazole ring to coordinate with both transition metal and molybdenum metal centre in compound **3** favors the formation of the 3-D bimetallic oxide. Whereas, in the compound **4** due to more heptamolybdate concentration, tetrazole ring does not play any role to control the oxide phase, and acts as only monodentate ligand. By tuning the synthetic conditions, tetrazole tends to exhibit different coordination modes which can alters the formation of oxide phase. This system not only proves to be a good example to investigate self assembly process and provides more information of the directional syntheses of the inorganic oxide phases, but also offers a fundamental approach of how a nitrogen donor containing organic molecule (tetrazole) influences the self assembly process of the inorganic oxides. Introducing the tetrazole derivatives into the poloxomolybdate (POM) matrix adds a new dimension to the POM based materials in terms of designing solids with specific properties.

Table 4.3. Crystal data and structural refinement for compounds **3** and **4**

	3	**4**
Formula	$C_6H_5N_5CuMo_2O_7$	$C_{24}H_{32}Cu_2Mo_8N_{20}O_{32}$
Molecular Mass	514.57	2007.32
Crystal system	Orthorhombic	Triclinic
Space group	*Pnma*	*P-1*
a(Å)	7.466(2)	7.9321(6)
b (Å)	13.030(4)	12.8279(10)
c (Å)	10.910(3)	12.8668(10)
α (°)	90.00	100.11(10)
β (°)	90.00	105.69(10)
γ (°)	90.00	96.69(10)
T (K)	298	100
Volume ($Å^3$)	1061.3(5)	1222.11(16)
Z	4	1
$D_{calcd.}$ (gcm^{-3})	3.220	2.727
Absorption coefficient	4.363	2.953
F(000)	980	965
λ(Å)	0.71073	0.71073
Crystal size (mm^3)	0.20 x 0.14 x 0.10	0.34 x 0.16 x 0.08
Theta range (°)	2.43 to 24.97	1.64 to 25.99
Reflections collected/unique	8993 / 969	12556 / 4754
R_{int}	0.1332	0.0216
Data/restraints/parameters	969 / 0 / 103	4754 / 0 / 416
Goodness-of-fit on F^2	1.059	1.187
R_1/wR_2 [I>2σ(I)]	0.0426/ 0.1084	0.0264/ 0.0729
R_1/wR_2 (all data)	0.0449/ 0.1122	0.0270/0.0734
Largestdiff.peak/ hole ($eÅ^{-3}$)	2.067 and -1.296	0.859 and -1.411

Table 4.4. Different types of binding modes of nitrogen atom pairs in the [5-(4-pyridyl) tetrazole]

Types of N···N pairs in tetrazole ring	Distance(Å)	Plausible Mode of Binding	4-ptz
N1–N1*	1.303	Chelating/Bridging	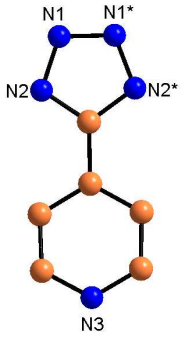
N1–N2	1.329	Chelating/Bridging	
N1–N2*	2.151	Bridging	
N1*–N2	2.151	Bridging	
N1*–N2*	1.329	Chelating/Bridging	
N2–N2*	2.194	Bridging	
N2,N2*–N3	5.049	Pillaring	
N1,N1*–N3	6.190	Pillaring	

Table 4.5. Geometrical parameters of the C–H···O and C-H···N hydrogen bonds (Å,°) involved in supramolecular network of compound **2**. D=donor; A=acceptor.

D-H...A	d(D-H)	d(H...A)	d(D...A)	<(DHA)
C(3)-H(3)...O(3)#5	0.93	2.47	3.377(4)	164.0
C(4)-H(4)...O(4)#5	0.93	2.68	3.319(4)	127.0
C(4)-H(4)...O(1)#6	0.93	2.55	3.281(4)	136.1
C(6)-H(6)...O(10)#6	0.93	2.47	3.110(4)	126.3
C(11)-H(11)...O(5)#7	0.93	2.60	3.466(4)	154.6
C(11)-H(11)...O(2)#8	0.93	2.37	2.958(4)	121.0
C(12)-H(12)...O(2)#8	0.93	2.53	3.037(4)	114.3
C(5)-H(5)...N(7)#9	0.93	2.44	3.336(4)	162.5
C(10)-H(10)...N(3)#10	0.93	2.71	3.294(5)	121.5
C(9)-H(9)...N(3)#10	0.93	2.78	3.324(4)	118.3
N(10)-H(10A)...O(12)#11	0.85(5)	1.80(4)	2.634(4)	165(4)
N(9)-H(9A)...O(7)#6	0.86(5)	1.84(5)	2.698(4)	177(4)

Symmetry transformations used to generate equivalent atoms:
#5 -x+1,-y,-z+1 #6 x-1, y, z-1 #7 x, y+1, z #8 x+1, y+1, z #9 -x+1,-y+1,-z
#10 -x+2,-y+1,-z+2 #11 -x+3,-y+1,-z+2

Table 4.6. Coordination modes of tetrazole and corresponding oxide phases formed in the compounds synthesized/ reported.

Coordination mode of Tetrazole[a]	Oxide phase	Description of structure
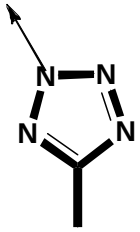	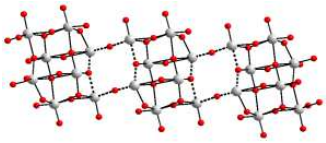 Infinite β-octamolybdate chains	Ion pair compound.
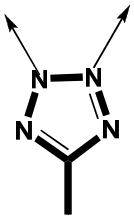	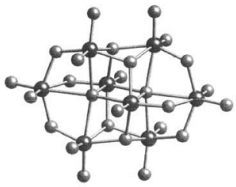 β-octamolybdate anions	2-D, 3-D networks in which octamolybdate anions are encapsulated. [21]
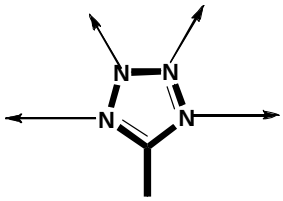	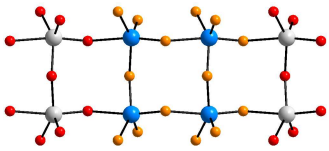	3-D bimetallic oxides to which tetrazoles are attached via nitrogen atoms

[a] *Pyridine moieties are not shown*

4.2.5. References

[1] (a) Buchner, W.; Schliebs, R.; Winter, G.; Buchel, K. H. *Industrial Inorganic Chemistry*; VCH: NewYork, 1989 (b) Grasselli, R. K. *Appl.Catal*. **1985**, 15, 127. (c) Bruce, D. W., O'Hare, D., Eds.; Wiley: Chichester, 1992. (d) Cox, P.A. *Transition Metal Oxides*; Clarendon Press: Oxford, England, 1995. (e) Cheetham, A. J. Science **1996**, 264, 794. (f) Gardner, G. B.; Kiang, Y.-H.; Lu, S.; Asgaonker, A.; Venketaraman, D. *J. Am. Chem. Soc*. **1996**, 118, 6946.

[2] Palacio, L. A.; Echavarria, A.; Sierra, L.; Lombardo, E. A. *Catal. Today* **2005**, 338.

[3] Vrieland, G. E.; Murchison, C. B. *Appl. Catal. A* **1996**, 134, 101.

[4] Kim, S.-S.; Ogura, S.; Ikuta, H.; Uchimoto, Y.; Wakihara, M. *Solid state Ionics* **2002**, 146, 249.

[5] Stupp, S. I.; Braun, P. V. *Science* **1997,** 277, 1242.

[6] (a) Zhang, Y.; DeBord, J. R. D.; O'Connor, C. J.; Haushalter, R. C.; Clearfield, G.; Zubieta, J. *Angew. Chem. Int. Ed.* **1996**, 35, 989. (b) Davis, M. E.; Katz, A.; Ahamad, W. R. *Chem. Mater*. **1996**, 8, 1820.

[7] (a) Smith, J. V. *Chem. Rev.* **1988**, 88, 149. (b) Cundy, C. S.; Cox, P. A. *Chem. Rev.* **2003**, 103, 663.

[8] Mann, S.; Burkett, S. L.; Davis, S. A.; Fowler, C. E.; Mendelson, N. H.; Seins, S. D.; Walsh, D.; Whilton, N. T. *Chem. Mater*. **1997**, 9, 2300.

[9] (a) Chen, J.; Burger, C.; Krishnan, C. V.; Chu, B. *J. Am. Chem. Soc.* **2005**, 127, 14140. (b) Kresge, C. T.; Leonowicz, M. E.; Roth, W. J.; Vartuli, J. C.; Beck, J. S. *Nature* **1992**, 359, 710.

[10] Murugavel, R.; Choudhury, A.; Walawalkar, M. G.; Pothiraja, R.; Rao, C. N. R. *Chem. Rev.* **2008**, 108, 3549.

[11] (a) Hagrman, P. J.; Hagrman, D.; Zubieta, J. *Angew. Chem. Int. Ed.* **1999**, 38, 2638. (b) Hagrman, D.; Hagrman, P. J.; Zubieta, J. *Comments Inorg. Chem.* **1999**, 21, 225. (c) Khan, M. I.; Nome, R. C.; Deb, S.; McNeely, J. H.; Cage, B.; Doedens, R. J. *Cryst. Growth Des.* **2009**, 9, 2848.

[12] (a) Yoshimura, M.; Byrappa, K. *J. Mater. Sci*. **2008**, 43, 2085. (b) Khan, M. I.; Deb, S.; Doedens, R. J. *Inorg. Chem. Comm.* **2009**, 12, 1104.

[13] (a) LaDuca, R. L., Jr.; Rarig, R. S., Jr.; Zapf, P. J.; Zubieta, J. *Inorg. Chim. Acta.* **1999**, 292, 13. (b) Hagrman, D.; Zapf, P. J.; Zubieta, J. *Chem. Comm.* **1998**, 1283.

[14] Zapf, P. J.; Warren, C. J.; Haushalter, R. C.; Zubieta, J. *Chem. Comm.* **1997**, 1543.

[15] (a) Pavani, K.; Singh, M.; Ramanan, A.; Lofland, S. E.; Ramanujachary, K. V. *J. Mol. Struct.* **2009**, 933, 156. (b) Hagrman, D.; Haushalter, R. C.; Zubieta, J. *Chem. Mater.* **1998**, 10, 361. (c) Fang, R.-Q.; Zhao, Y.-F.; Zhang, X.-M. *Inorg. Chim. Acta.* **2006**, 359, 2023.

[16] Hagrman, D.; Warren, C. J.; Haushalter, R. C.; Seip, C.; O'Connor, C. J.; Rarig, R. S.; Johnson, K. M.; LaDuca, R. L., Jr.; Zubieta, J. *Chem. Mater.* **1998**, 10, 3294.

[17] Rarig, R. S.; Lam, R.; Zavalij, P. Y.; Ngala, J. K.; LaDuca, R. L., Jr.; Greedan, J. E.; Zubieta, J. *Inorg. Chem*. **2002**, 41, 2124.

[18] Pavani, K.; Ramanan, A. *Eur. J. Inorg. Chem*. **2005**, 3080.

[19] (a) Hagrman, D.; Zubieta, J. *Chem. Comm*. **1998**, 2005. (b) Hagrman, D.; Sangregorio, C.; O'Connor, C. J.; Zubieta, J. *J. Chem. Soc., Dalton Trans*. **1998**, 3707.

[20] (a) Lin, P.; Clegg, W.; Harrington, R. W.; Henderson, R. A. *Dalton trans*. **2005**, 2388. (b) Dinca, M.; Long, J. R. *J. Am. Chem. Soc.* **2007**, 129, 11172. (c) Pachfule, P.; Das, R.; Poddar, P.; Banerjee, R. *Cryst. Growth Des*. **2010**, 10, 2475.

[21] Jones, S.; Liu, H.; O'Connor, C. C.; Zubieta, J. *Inorg. Chem. Comm*. **2010**, 13, 412.

[22] Ouellette, W.; Liu, H.; O'Connor, C. J.; Zubieta, J. *Inorg. Chem.* **2009**, 48, 4655.

[23] *SAINT: Software for the CCD Detector System*; Bruker Analytical X-ray Systems, Inc.: Madison, WI, 1998.

[24] G. M. Sheldrick, *SHELXS-97, Program for Structure Solution*; University of Göttingen, Göttingen, Germany, **1997**.

[25] G. M. Sheldrick, *SHELXL-97, Program for Crystal Structure Analysis*; University of Göttingen, Göttingen, Germany, **1997**.

[26] Zhao, H.; Qu, Z.-R.; Ye, H.-Y.; Xiong, R.-G. *Chem. Soc. Rev.* **2008**, 37, 84.

[27] (a) α-molybdate Day, V. W.; Fredrich, M. F.; Klemperer, W. G.; Shum, W. *J. Am. Chem. Soc*. **1977**, 99, 952. (b) β-molybdate Kitamura, A.; Ozeki, T.; Yagasaki, A. *Inorg.Chem*. **1997**, 36, 4275. (c) γ-molybdate Niven, M. C.; Cruywagen, J. J.; Heyns, J. B. B. *J. Chem. Soc., Dalton Trans*. **1991**, 2007. (d) δ-Molybdate Xi, R.; Wang, B.; Isobe, K.; Nishioka, T.; Toriumi, K.; Ozawa, Y. *Inorg. Chem*. **1994**, 33, 833. (e) ε-molybdate Hagrman, D.; Zubieta, C.; Rose, D. J.; Zubieta, J.; Haushalter, R. C. *Angew. Chem. Int. Ed*. **1997**, 36, 873. (f) ζ-molybdate Allis, D. G.; Rarig, R. S.; Burkholder, E.; Zubieta, J. *J. Mol. Struct*. **2004**, 688, 11. (g) η-molybdate Rarig, R. S.; Bewley, L.; Burkholder, E.; Zubieta, J. *Ind. J. Chem*. **2003**, 42A, 2235.

[28] Harrison, W. T. A.; Dussack, L. L.; Jacobson, A. J. *Acta crystallogr., Sect. C* **1996**, 52, 1075.

[29] Han, Z.; Gao, Y.; Hu, C. *Cryst. Growth Des*. **2008**, 8, 1261.

[30] Modec, B.; Brencic, J. V.; Zubieta, J. *Inorg.Chem.Commun*. **2003**, 6, 506.

[31] John, E. O.; Willett, R. D.; Scott, B.; Kirchmeier, R. L.; Shreeve, J. M. *Inorg. Chem*. **1989**, 28, 893-897.

Factors Affecting the Conformational Modulation of Flexible Ligands in the Self-Assembly Process of Coordination Polymers: Synthesis, Structural Characterization, Magnetic Properties and Theoretical Studies

5

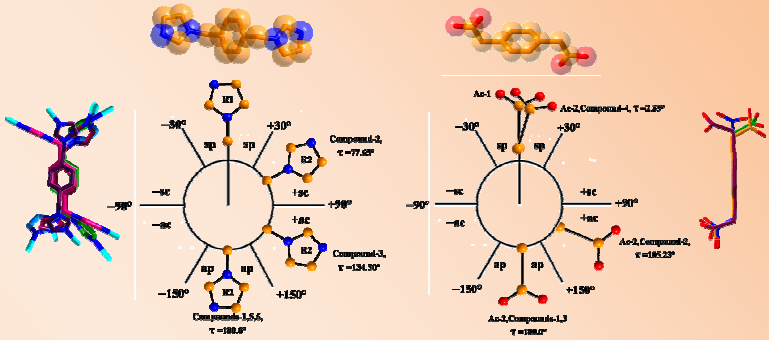

*Six new metal complexes with the formulae, $[Co(pda)(bix)]_n$(**1**), $[Ni(pda)(bix)(H_2O)]_n$ (**2**), $[Cu(pda)(bix)_2(H_2O)_2]_n \cdot 8nH_2O$ (**3**), $[Co_2(\mu\text{-}OH)(pda)(ptz)]_n \cdot nH_2O$ (**4**), $[Co(hfipbb)(bix)_{0.5}]_n$ (**5**), $[Co(2,6\text{-}pydc)(bix)_{1.5}]_n \cdot 4nH_2O$ (**6**) have been synthesized by the reactions of Co(II) , Ni(II), and Cu(II) salts with two flexible ligands 1,4–phenylenediaceticacid (H_2pda), and 1,4-bis (imidazole-1-ylmethyl)-benzene (bix) in presence of co-ligands 5-(4-Pyridyl) tetrazole (4-ptz), 4,4'(hexa-fluoroisopropylidene)bis(benzoicacid) ($H_2hfipbb$), and 2, 6-pyridine dicarboxylic acid (2, 6–H_2pydc), and characterized by single crystal X-ray diffraction analysis, IR spectroscopy and thermogravimetric (TG) analysis. Because of the coordination geometry around the metal ions, and the diverse coordination modes of the flexible ligands in combination with the rigid and flexible co-ligands, the obtained complexes show diverse structures from one dimensional (1D) chain to three dimensional (3D) coordination polymers. **1, 4, 5,** and **6** are Co(II) complexes in which Co(II) ions show tetrahedral coordination in **1,** trigonal bipyrimidal coordination in **4**, and octahedral coordination in **5** and **6.** Complexes **2** and **3** are respectively Ni(II) and Cu(II) complexes in which the metal ions present in octahedral coordination geometries. Factors affecting the conformational change of the flexible ligands in the self assembly process of coordination polymers, such as, coordination geometry around the metal ions, and geometry of the co-ligands have been systematically studied. The rotation of the bonds $C(sp^3)$—$C(sp^2)$ and $C(sp^3)$—$N(sp^3)$ in H_2pda, and bix ligands causes different conformations (cis, trans, gauche); these conformations have been studied by measuring the torsion angle. A comparative study between the torsion angle of the particular conformation of the ligands and coordination geometry of metal ion/geometry of the co-ligand has been undertaken. All the possible cis, trans, and gauche conformations of the flexible ligands have been obtained / observed in our complexes. Theoretical calculations were performed to determine the energies of the different conformations of the flexible ligands. The electronic properties of these complexes have also been investigated in the solid state at room temperature. Finally the temperature dependent magnetic studies for compounds **4** and **5** are described.*

5.1. Introduction

Exploring the chemistry of micro- and meso-porous coordination polymers (CPs) or metal organic frameworks (MOFs), based on the self assembly processes, is of great interest in modern inorganic chemistry because of their potential applications in the gas storage, catalysis, nonlinear optics, separation, and sensing etc.[1] The designing of coordination polymers with specified property remains intriguing challenge to the synthetic chemists, in terms of choosing both organic building units (OBUs) as well as metal ions.[2] A vast literature has been reported in the judicious selection of organic ligands in attaining the desirable topologies.[3] MOFs, based on the rigid carboxylate linkers, have been widely studied and highly explored extensively by Yaghi and co-workers.[4] The combinations of carboxylate linkers along with N-donor linkers were also used to construct a wide variety of 3D open framework materials with interesting sorption properties.[5] In contrast to the rigid ligands, the rational design of coordination polymers based on flexible ligands are quite interesting in terms of self assembly process and structure property relationship.[6] Due to the conformational freedom of the flexible ligands, it results in formation of both discrete macrocylces and infinite polymeric structures; conversion between these two types of structures (discrete and polymer) could also be achieved by the ring-opening isomerism.[7] Cao and his group studied and reviewed the coordination polymers based on flexible ligands.[8] The conformational freedom of the flexible ligands offers the possibility to construct the unpredictable and interesting coordination networks with useful properties. The final structures, based on flexible ligands, are subjected to several factors, such as, synthetic conditions (temp, pH, pressure, and solvents), coordination geometry of metal ions, geometrical disposition of donor sites, template molecules and so on.[9] Thus an investigation on the correlation between the subtle conformation of a flexible ligand and the topology of the coordination network formed is a challenging task for inorganic chemists and it is necessary to check some properties of the resulting coordination polymers.

We have been focusing on the study of the coordination polymers to evaluate the necessary concepts in the self assembly process. Recently we have demonstrated the effect of solvent molecules in directing the dimensionality of coordination networks from 1D to 3D.[10] These studies give us a practical experience in studying the assembly of coordination networks. 1,4-benzenedicarboxylate (H_2bdc) is a well known example of principle rigid system among the carboxylates, and a similar analogue in the N-donor organic ligand is

1,4-bis(1-imidazolyl)benzene) (1,4-bdx); numerous coordination polymers have been reported to explore the binding modes of these ligands in the self assembly processes.[11,12] The study of flexible analogues of these rigid systems would elute the basic principles in the self assembly process of coordination polymers compared to the rigid ligands. 1,4–phenylenediaceticacid (H_2pda), and 1,4-bis (imidazole-1-ylmethyl)-benzene (bix) are such examples of flexible ligands that resemble the corresponding rigid ligands. Recently we have reported both *cis* and *trans* conformations of the flexible phosphonate analogue (*p*-xylylenediphosphonic acid) with cobalt ion.[13] There are several reports on H_2pda with all the possible conformations of the ligand with and without using co-ligands.[14] Cao and co-workers demonstrated the conformation control of flexible H_2pda from *trans* to *cis* conformation by introducing a rigid auxiliary ligand 4,4′-bipyridine.[15] Shi and group reported the series of Zn(II) coordination complexes from isomeric phenylenediacetic acid (1,4-, 1,3-, 1,2-H_2pda) and dipyridyl ligands.[16] On the other hand bix is an another versatile flexible ligand, through which a wide variety of coordination polymers have been constructed, of which some of them exhibit unusual types of entanglement (e.g., rotaxane - like catenation).[17] The deviation and rotation of $C(sp^3)-C(sp^2)$ bond in H_2pda with respect to benzene ring causes disposition of (−COOH) groups in different directions. In the same way $C(sp^3)-N(sp^3)$ bond in bix causes disposition of imidazole rings in different directions. Apart from the typical *cis* and *trans* conformations of the above said flexible ligands, there are some other conformations lying between these *cis* and *trans* conformations. These conformations can be described on the basis of torsion angle measurement of the rotation of the bonds $C(sp^3)-C(sp^2)$ and $C(sp^3)-N(sp^3)$ in H_2pda and bix respectively.[18] Based on aforementioned considerations, we have chosen the flexible ligands H_2pda, and bix to study the effect of coordination geometry of the metal ions and geometry of secondary ligands in modulating the conformations of the flexible ligands. Herein we report the synthesis and characterization of six coordination polymers $[Co(pda)(bix)]_n$(**1**), $[Ni(pda)(bix)(H_2O)]_n$ (**2**), $[Cu(pda)(bix)_2(H_2O)_2]_n\cdot 8nH_2O$ (**3**), $[Co_2$ (μ-OH)(pda)(ptz) $]_n\cdot nH_2O$ (**4**), $[Co(hfipbb)(bix)_{0.5}]_n$ (**5**), $[Co(2,6\text{-}pydc)(bix)_{1.5}]_n\cdot 4nH_2O$ (**6**). The conformational freedoms of these flexible ligands play a crucial role in the construction of the coordination networks varying from 1D to 3D. We have described the temperature dependent magnetic studies for compounds **4** and **5**, considering the Co–Co distance in their crystal structures.

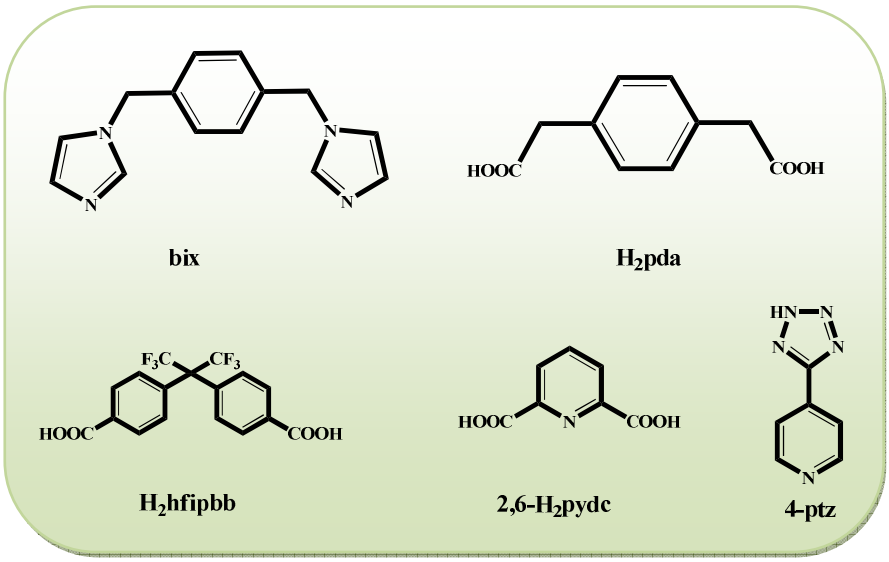

Scheme 5.1. Ligands used in this work

5.2. Experimental Section

5.2.1. Materials and Methods

All the chemicals were received as reagent grade and used without any further purification. The ligands bix and 4-ptz were prepared according to the literature procedures.[19] Elemental analyses were determined by FLASH EA series 1112 CHNS analyzer. Infrared spectra of solid samples obtained as KBr pellets on a JASCO – 5300 FT – IR spectrophotometer. Thermogravimetric analyses were carried out on a STA 409 PC analyzer and corresponding masses were analyzed by QMS 403 C mass analyzer, under flow of N_2 gas with a heating rate of 5 ^oC min^{-1}, in the temperature range of 30-1000 ^oC. Powder X-ray diffraction patterns were recorded on a Bruker D8-Advance diffractometer using graphite monochromated $CuK_{\alpha1}$ (1.5406 Å) and $K_{\alpha2}$ (1.54439 Å) radiations. The electronic absorption spectra have been recorded on a Cary 100 Bio UV-visible spectrophotometer at room temperature. Magnetic susceptibilities were measured in the temperature range 2–300 K on a Quantum Design VSM-SQUID. The energy calculations for the bix and pda^{2-} in the crystal structures have been performed by the single point energy calculations using B3LYP with 6-311g** basis set from the XMol (*.xyz) files of the compounds . All the compounds were synthesized in 23 mL Teflon-lined stainless vessels (Thermocon, India).

5.2.2. Synthesis

Synthesis of $[Co(pda)(bix)]_n$(1)

A mixture of $CoCl_2 \cdot 6H_2O$ (0.12 g, 0.5 mmol), H_2pda (0.097g, 0.5mmol), and bix (0.12g, 0.5 mmol) was dissolved in 10.0 mL of distilled water. The pH of the reaction mixture was adjusted to 6.0 by addition of 1M NaOH solution. Consequently the resulting mixture was stirred for 30 min and transferred to a 23mL Teflon-lined stainless vessel, which was sealed and heated at 180 °C for 72 h and the reaction system was cooled to room temperature over 48 h to obtain purple crystals. Yield: 49% (based on Co) Anal. Calcd. for $C_{24}H_{22}CoN_4O_4$: C, 58.90; H, 4.53; N, 11.44. Found: C, 59.10; H, 4.25; N, 11.68. IR (KBr pellet, cm^{-1}): 3792, 3126, 2916, 1618, 1585, 1523, 1365, 1275, 1086, 1024, 932, 788, 740.

Synthesis of $[Ni(pda)(bix)(H_2O)]_n$ (2)

The same synthetic procedure was used to synthesize **2** as that for **1** except $Ni(NO_3)_2 \cdot 6H_2O$ (0.14 g, 0.5 mmol), was used instead of $CoCl_2 \cdot 6H_2O$ to obtain light green crystals. Yield: 45% (based on Ni) Anal. Calcd. for $C_{24}H_{24}NiN_4O_5$: C, 56.84; H, 4.76; N, 11.04. Found: C, 56.70; H, 4.84; N, 11.21. IR (KBr pellet, cm^{-1}): 3393, 2966, 1558, 1518, 1375, 1261, 1232, 1086, 1024, 941, 800, 721.

Synthesis of $[Cu(pda)(bix)_2(H_2O)_2]_n \cdot 8nH_2O$ (3)

The same synthetic procedure was used to synthesize **3** as that for **1** except $CuCl_2 \cdot 2H_2O$ (0.085g, 0.5 mmol) was used instead of $CoCl_2 \cdot 6H_2O$ to obtain blue block crystals. Yield: 48% (based on Cu) Anal. Calcd. for $C_{38}H_{56}Cu\ N_8O_{14}$: C, 50.02; H, 6.18; N, 12.28. Found: C, 50.25; H, 6.02; N, 12.10. IR (KBr pellet, cm^{-1}): 3400, 3113, 1651, 1574, 1521, 1450, 1358, 1251, 1138, 1109, 1024, 947,850.

Synthesis of $[Co_2(\mu\text{-}OH)(pda)(ptz)]_n \cdot nH_2O$ (4)

A mixture of $Co(OAc)_2 \cdot 4H_2O$ (0.099 g, 0.4 mmol), H_2pda (0.038 g, 0.2 mmol) and 4-ptz (0.029 g, 0.2 mmol) was dissolved in 10.0 mL of distilled water and the pH of the reaction mixture was adjusted to 4.72 by 0.5 M NaOH. Then the resulting mixture was stirred for 30 min and transferred to 23mL Teflon-lined stain less vessel, sealed and heated at 180 °C for 72 h and then cooled to room temperature over 48 h to obtain red block crystals. Yield: 63% (based on Co) Anal. Calcd. for $C_{16}H_{13}Co_2N_5O_6$: C, 39.28; H, 2.67; N, 14.31. Found: C, 39.12; H, 2.38; N, 14.72. IR (KBr pellet, cm^{-1}): 3568, 2916, 2845, 1591, 1412, 976, 760, 717, 555.

Synthesis of $[Co(hfipbb)(bix)_{0.5}]_n$ (5)

To a mixture of $CoCl_2 \cdot 6H_2O$ (0.12 g, 0.5 mmol), bix (0.12g, 0.5 mmol) and H_2hfipbb (0.19 g, 0.5 mmol), 10.0mL of distilled water and 1.0 mL of MeOH were added and the pH was adjusted to 5.2 by adding 0.5 M NaOH. The resulting reaction mixture was stirred for more than 2 h and transferred to 23 mL Teflon-lined stain less vessel, sealed and heated at 180 °C for 72 h and then cooled to room temperature over 48 h to obtain red block crystals. Yield: 59% (based on Co) Anal. Calcd. for $C_{24}H_{15}CoN_2F_6O_4$: C, 50.72; H, 2.66; N, 4.92. Found: C, 50.98; H, 2.42; N, 5.01. IR (KBr pellet, cm^{-1}): 3454, 3140, 2924, 1626, 1523, 1410, 1253, 1172, 1105, 1020, 929, 842, 781, 723, 652.

Synthesis of $[Co(2,6\text{-}pydc)(bix)_{1.5}]_n \cdot 4nH_2O$ (6)

To the mixture of $CoCl_2 \cdot 6H_2O$ (0.12 g, 0.5 mmol), bix(0.12g, 0.5 mmol) and 2,6-H_2pydc (0.083 g, 0.5 mmol), 10.0mL of distilled water and 1.0 mL of MeOH were added and the pH was adjusted to 6.0 by adding 0.5 M NaOH. The resulting reaction mixture was stirred for more than 2 h and the clear solution was transferred to 23 mL Teflon lined stainless vessel, sealed and then heated to 160 °C for 72 h and cooled to room temperature over 48 h to obtain red plate like crystals. Yield: 65% (based on Co) Anal. Calcd. for $C_{28}H_{32}CoN_7O_8$: C, 51.46; H, 4.93; N, 15.00. Found: C, 51.20; H, 5.10; N, 14.75. IR (KBr pellet, cm^{-1}): 3441, 3121, 2199, 1628, 1587, 1521, 1444, 1425, 1359, 1284, 1234, 1182, 1086, 1028, 941, 844.

5.2.3. Single crystal X-ray structure determination of the compounds 1-6

Single-crystals suitable for structural determination of all the compounds (**1–6**) were mounted on a three circle Bruker SMARTAPEX CCD area detector system under Mo-Kα (λ=0.71073A) graphite monochromated X-ray beam, crystal to detector distance 60mm, and a collimator of 0.5 mm. The scans were recorded with an ω scan width of 0.3º. Data reduction performed by SAINTPLUS,[20a] empirical absorption corrections using equivalent reflections performed by program SADABS,[20b] structure solution using SHELXS-97[20c] and full-matrix least-squares refinement using SHELXL-97[20d] for above compounds. All the non-hydrogen atoms were refined anisotropically. Hydrogen atoms on the C atoms were introduced on calculated positions and were included in the refinement riding on the irrespective parent atoms. Attempts to locate the hydrogen atoms for the solvent water molecules in the crystal structure of compounds **3**, **4** and **6** failed. However, no attempts were made to fix these atoms on their parents. Co atoms in the crystal structure of **4** are

refined with occupancy each 0.95, several attempts were made to improve the occupancy and the best value is taken considering the convergence of the refinement. Crystal data, structure refinement parameters for all the compounds (**1–6**) are summarized in Table 5.3 and hydrogen bonding parameters in Table 5.4. Topological analysis of the compound **1** were performed by using the TOPOS software.[20e]

5.3. Results and discussion

5.3.1. Synthesis

All the compounds **1–6** were synthesized by conventional hydrothermal procedures by employing divalent metal salts and the appropriate ligands mentioned in the Scheme 5.1. The infrared spectra of all the compounds are consistent with their single crystal structures. The aromatic ring stretching frequencies of the pda^{2-} and bix ligands are present in the range of ~1600 to 1200 cm^{-1}. The asymmetric and symmetric stretching frequencies of the C–O stretching modes of the dicarboxylate ligands were present as strong bands at 1585 and 1523 cm^{-1} (**1**), 1558 and 1518 cm^{-1} (**2**), 1574 and 1521 cm^{-1} (**3**), 1591 and 1412 cm^{-1} (**4**), 1523 and 1410 cm^{-1} (**5**) and 1587 and 1521 cm^{-1} (**6**). The aliphatic C–H stretchings of the $–CH_2$ group in all the compounds are present in the range of 2800 to 3000 cm^{-1}. The bands arising from the O–H stretching modes of the coordinated and uncoordinated water molecules are observed in the range of 3300 cm^{-1}. The identities of the compounds **1-6** are further confirmed by structure solution from single crystal X-ray diffraction. The rotation of the $C(sp^3)—C(sp^2)$ and $C(sp^3)—N(sp^3)$ bonds in the pda^{2-} and bix ligands respectively are explained on the basis of the torsion angle as described below.

5.3.2. Definition of torsion angle

Torsion angle (τ) in the chain of the vectors (atoms) *i, j, k, l* can be defined as the dihedral angle between the plane of vectors containing *i, j, k* and the plane containing *j, k, l* (Scheme 5.2). In a Newman projection the torsion angle is the angle (having an absolute value between 0° and 180°) between the bonds of two specified groups, one from the atom nearer (proximal) to the observer and the other from the further (distal) atom. The torsion angle between the atoms *i* and *l* is then considered to be positive if the bond *i – j* is rotated in a clockwise direction through less than 180° in order that it may eclipse the bond *k – l*; a negative torsion angle requires rotation in the opposite sense. Stereochemical

arrangements corresponding to torsion angles between 0° and 180° based on the direction of the rotation are shown in the Scheme 5.2.

By locating the *i, j, k, l* atoms in the dipodal flexible ligands pda^{2-} and bix at the flexible group (–CH_2–), the torsion angels are measured and the conformations of the ligands have been explained. Three different types of the torsion angles for both pda^{2-} and bix ligands are considered to measure the skewing of the acetate and imidazole groups. In which τ_1(ijkl), τ_2(l'k'j'i'), are calculated to measure the twist of acetate and imidazole groups from the mean phenyl ring plane. τ_3(ijj'i') and τ_3(jkk'j') are calculated to measure the twist with respect each other acetate and imidazole rings respectively. Torsion angle τ_3 gives the information of the particular conformation of the ligand (such as *cis*, *trans*, and *guache* or *skew*) as shown in the Scheme 5.2.

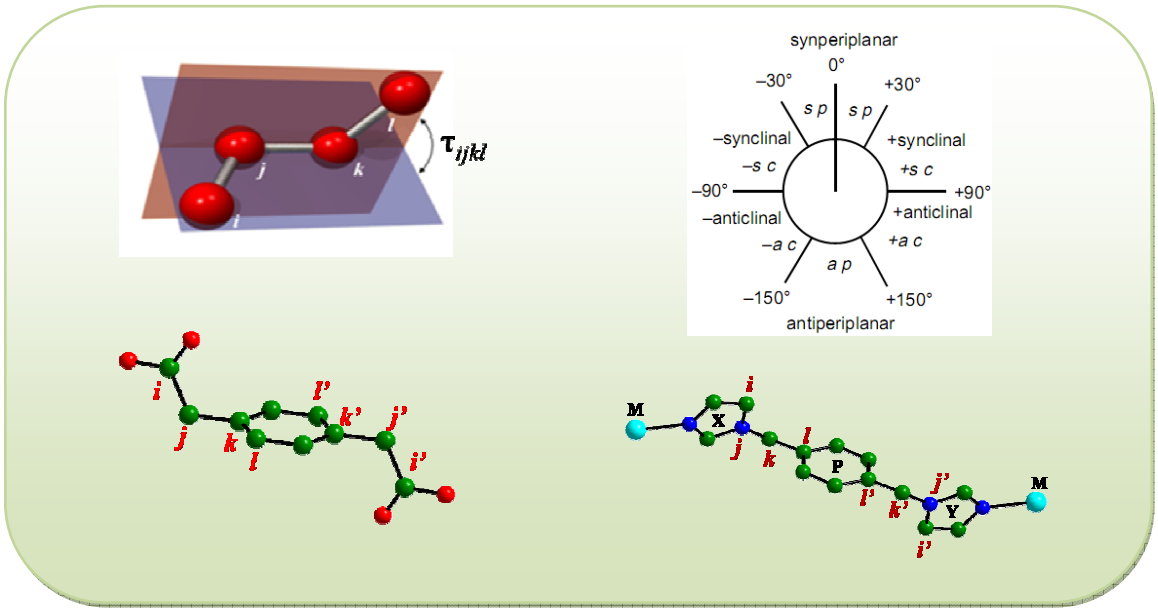

Scheme 5.2. Pictorial representation of the torsion angle

5.3.3. Description of crystal structures

Structural description of $[Co(pda)(bix)]_n$(1)

Compound **1** crystallizes in triclinic space symmetry P-1. The asymmetric unit of **1** consists of one independent Co(II) ion, one pda^{2-} anion, and one bix ligand. As shown in Figure 5.1a each Co(II) ion in **1** is four coordinated with distorted tetrahedral geometry composed of two carboxylic oxygen atoms from two pda^{2-} anions (Co–O = 2.001(3) and 1.996(3) Å) and two nitrogen atoms from two bix ligands (Co–N= 2.061(3) and 2.024 (3) Å). pda^{2-} acts as a bidentate ligand with coordination mode μ_1-η^1: η^0, and coordinates to two cobalt atoms in a well-known *trans* configuration, with anti-periplanar torsion angle

of 180° and a separation of 12.80 Å between two cobalt atoms. A bidentate bix ligand coordinates to two cobalt atoms in a usual *trans* configuration (τ=180°) and connects the cobalt atoms with a separation of 15.09 Å. The connectivity of the pda^{2-} and the bix ligands through the Co-tetrahedra forms meso-helices as shown in the Figure 5.1b. The overall structure is composed by tetrahedral Co polyhedra linked by the linkers bix and pda^{2-} to form a 3D interpenetrated structure with uniform pore size.

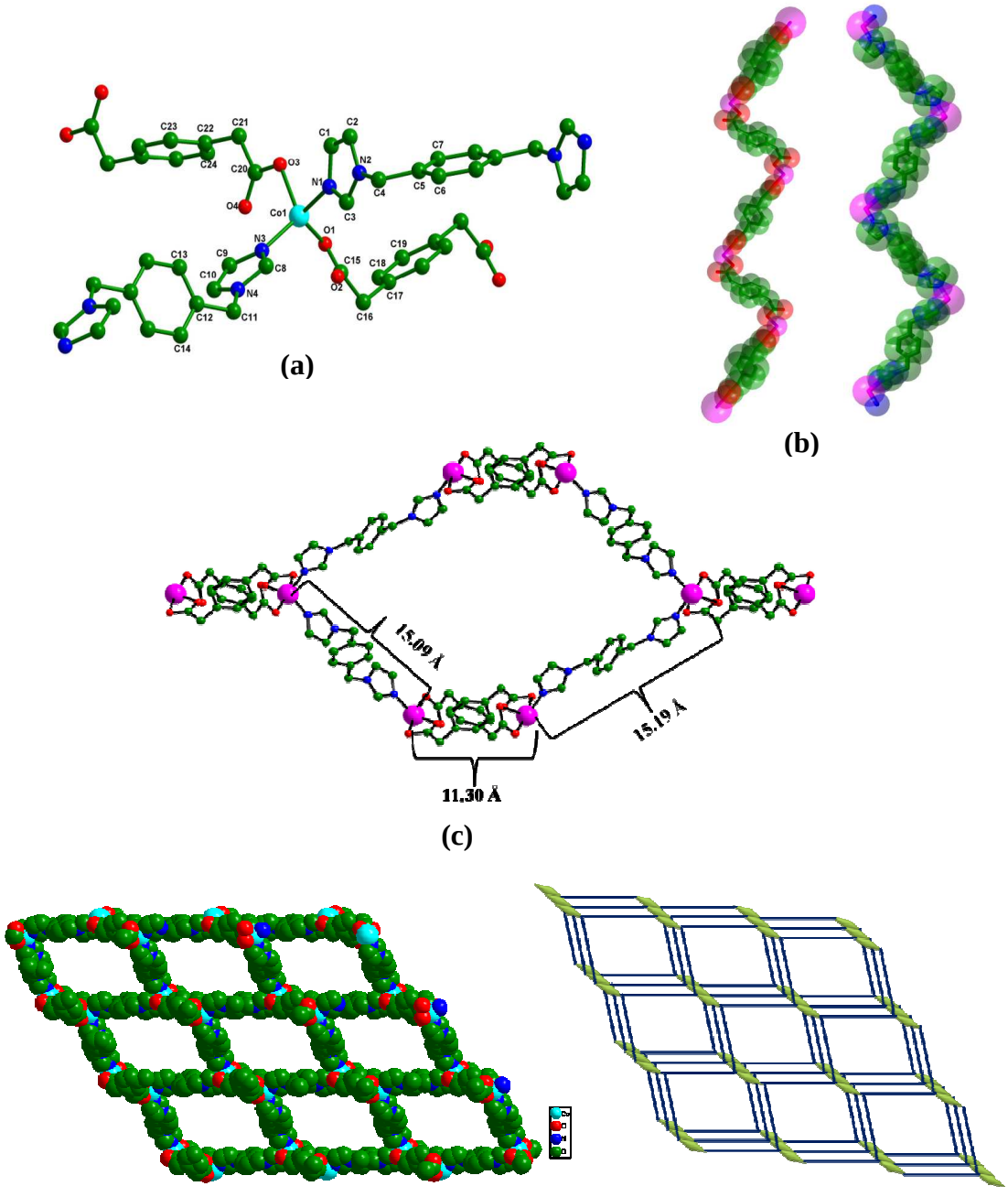

Figure 5.1. (a) Coordination environment around the Co^{II} ion in **1** with hydrogen atoms omitted for clarity. (b) meso helices constructed by the pda^{2-} and bix ligands (c) 3D frame work of **1** illustrating the dimensions of the pore sizes (d) 4-fold interpenetrated diamond net and its schematic representation.

In the duel ligand system containing carboxylate and N-donor ligands, various combinations involving flexible and rigid analogues based on phenylene spacers have been reported .Among those well known combinations such as rigid carboxylate, rigid N-donor (1,4-H_2bdc, 1,4-bdx),[21] rigid carboxylate, flexible N-donor (1,4-H_2bdc, bix)[22] are studied. In the present system, the combination flexible carboxylate and flexible N-donor (H_2pda, bix) has been studied. Thus, the combination of flexible carboxylate and flexible N-donor ligand gives rise to a 3D porous coordination polymer with approximate pore size of 15 x 15 Å (Figure 5.1c). Usually, long, rigid, ligands result in interpenetration and decrease the pore sizes to large extent.[23] In compound **1**, the combination of long flexible ligands results in a 3D framework; the flexibility of the ligands minimizes the interpenetration to give a considerable uniform pore sizes.

To better understand the 3D structure of **1**, Co(II) ion in the tetrahedral coordination can be described as a four connected node, since it links two pda^{2-} ligands and two bix ligands. Each pda^{2-} / bix ligand is considered as a connector between two metal ions. Topological analysis of this framework with TOPOS software reveals a 4-fold interpenetrated diamond-type (dia 6^6 topology) structure. Such connectivity repeats infinitely to give the 3D framework of **1** as schematically shown in Figure 5.1d.

Structural description of $[Ni(pda)(bix)(H_2O)]_n$ (2)

X-ray diffraction analysis of compound **2** reveals that the asymmetric unit consists of one crystallographically independent Ni(II) center. As shown in Figure 5.2a, the six-coordinated Ni(II) center [NiN_2O_4] shows a distorted octahedral geometry with three carboxylate oxygen donors (O1, O2, O3) from two different pda^{2-} ligands, one oxygen donor O5 from water molecule and two nitrogen donors (N2, N3) from two different bix ligands. Complex **2** is an extended one- dimensional chainlike structure consists of two meso chains: chain-A, constituted by pda^{2-} ligands and chain-B, constituted by bix ligands as shown in Figure 5.2b. Each pda^{2-} ligand in chain-A is bidentate ligand which adopts μ_2-bridging mode with one carboxylate group in a μ_1-η^1: η^1 chelating mode and the other in μ_1-η^1: η^0 monodentate mode. Furthermore the acetate side chains are twisted with respect to the aromatic ring by various extents, in which arm-A (denoted by C16–C15) shows antiperiplanar torsion angle of 174.63° (through C22–C17–C16–C15) and arm-B (denoted by C24–C23) exhibits a anticlinal torsion angle of –70.30°(through C19–C20–C24–C23). The two acetate groups twisted with respect to each other by an anticlinal torsion angle of

105.23° (through C16–C15–C24–C23), which is a *gauche* conformation of pda^{2-}ligand (Table 5.1). The pda^{2-} along the chain separates the two Ni(II) centers with a distance of 12.03 Å and Ni–Ni–Ni angle through the pda^{2-} ligand is almost 180°. In chain-B the exo-bidentate ligand bix coordinates to Ni centers through nitrogen donor, and the bix ligand twists their imidazole rings to different extents, in order to meet the coordination requirements imposed by the pda^{2-} ligand at Ni octahedron. The dihedral angles between the imidazole ring planes and the least-squares plane of phenyl group are 82.72° and 83.32° respectively, and the two imidazole groups twisted each other by an synclinal torsion angle of 77.65° (through N1–C4–C14–N4).

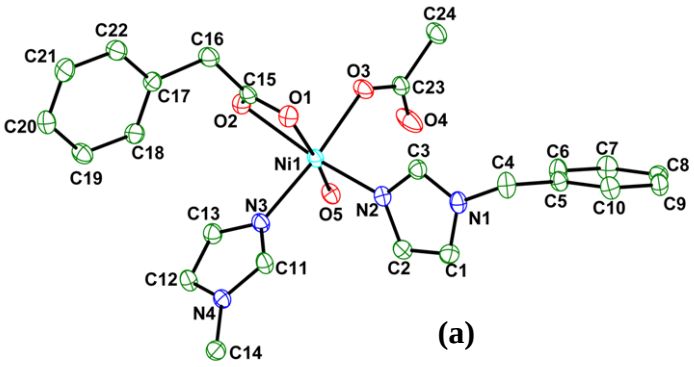

(a)

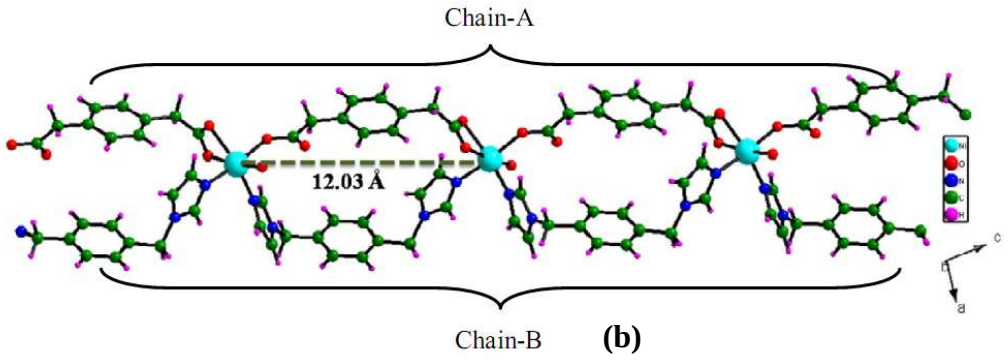

(b)

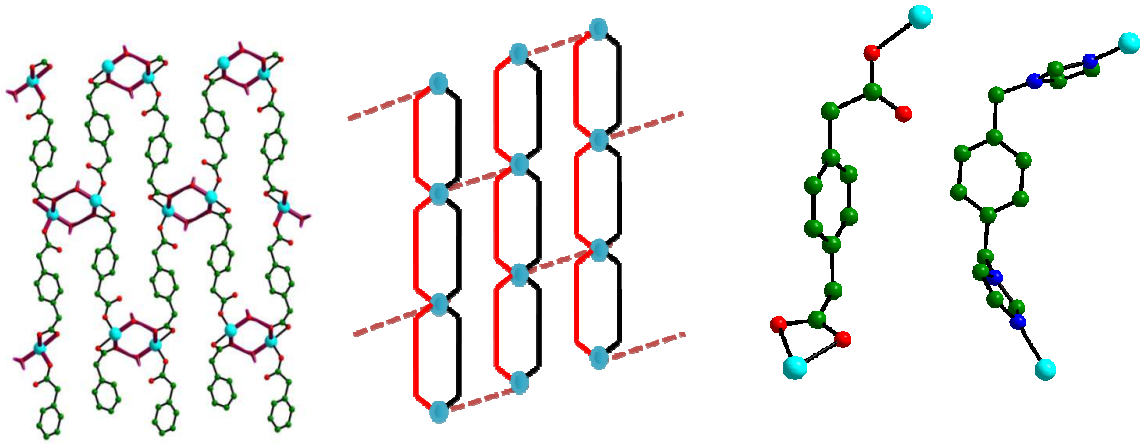

(c) **(d)**

Figure 5.2. (a) Thermal ellipsoid plot diagram of **2** (b) 1D double chains constituted by pda^{2-} and bix ligands (c) 2D supramolecular network formed due to hydrogen bonding and its schematic representation. (d) *gauche* conformations of pda^{2-} and bix ligands

The bidentate bix molecules twist their imidazole rings to 77.65° to establish a physical bridge between Ni centers with a separation of 12.03 Å (Table 5.2), as imposed by the pda^{2-} ligand through chain-A. The two chains A and B constitute a 1D double-chain structure with a 25-membered ring between two metal centers. Due to coordination of aqua ligand on the apical site of the Ni-octahedra, pda^{2-}, bix ligands modulate their conformations in order to meet the coordination requirements at the Ni(II)–octahedra. The adjacent double chains are linked *via* hydrogen bonding interactions with the aid of the water molecule and the carboxylate oxygen (O2) to form an eight membered ring (Table 5.4) resulting in a 2D network (Figure 5.2c). It must be remarked that in the crystal structure of **2**, both flexible ligands (pda^{2-} and bix) adopt *gauche* conformations apart from the regular *trans* and *cis* conformations to meet the coordination requirements of the metal atom (Figure 5.2d).

Structural description of $[Cu(pda)(bix)_2(H_2O)_2]_n \cdot 8nH_2O$ (3)

Compound **3** crystallizes in triclinic space group P–1. The repeating unit consists of one $[Cu(bix)_2(H_2O)_2]^{2+}$ cation, one pda^{2-} anion and four lattice water molecules. The Cu(II) ion locates on a symmetry center and is coordinated by four nitrogen atoms from four different bix ligands in a basal plane and two oxygen atoms from two aqua ligands arranged *trans* to each other on the apical coordination sites to furnish an octahedral geometry (Figure 5.3a). The repeating unit $[Cu(bix)_2(H_2O)_2]^{2+}$ extends to 1D double chain structure, in which the anion pda^{2-} occupies the void space created between two metal centers in the double chain (Figure 5.3b). Each constituent chain of the double chain is constructed by linking the two Cu(II) ions with the bidentate bix ligands with a separation of 13.03 Å. The bix ligand twists its imidazolyl moieties with respect to each other to an anticlinal torsion angle of 134.50°(through N2–C4–C8–N4), and the angles between the planes of the imidazole rings and the plane of phenylene group are 83.65° and 77.0° respectively (Table 5.2). In the anion pda^{2-}, both the acetate side chains are twisted with respect to each other by an antiperiplanar torsion angle of 180.0° (donated by C15–C16–C16–C15) exhibiting a typical *trans* conformation (Table 5.1). The existence of isolated pda^{2-} ligand as anion, apart from the Cu(II)–octahedron, is probably the factor for the bix ligand to adopt the *gauche* conformation with anticlinal torsion angle apart from the

regular *trans* and *cis* conformations. From the crystal packing diagram, it can be seen that the cationic chains and pda^{2-} anions are connected by the classical hydrogen bonds between the coordinated aqua ligands of cation, the carboxylate oxygen atoms of anion, and the lattice water molecules (Table 5.4). A hydrogen bonded 8-membered ring of type $R^4_2(8)$ has been formed with the assistance of the two coordinated aqua ligands (O3) and two carboxylate oxygen atoms (O2). This synthon $R^4_2(8)$ connects the two adjacent cationic chains along *ac* plane and two pda^{2-} anions along the *b*-axis resulting in the 2D supramolecular network.

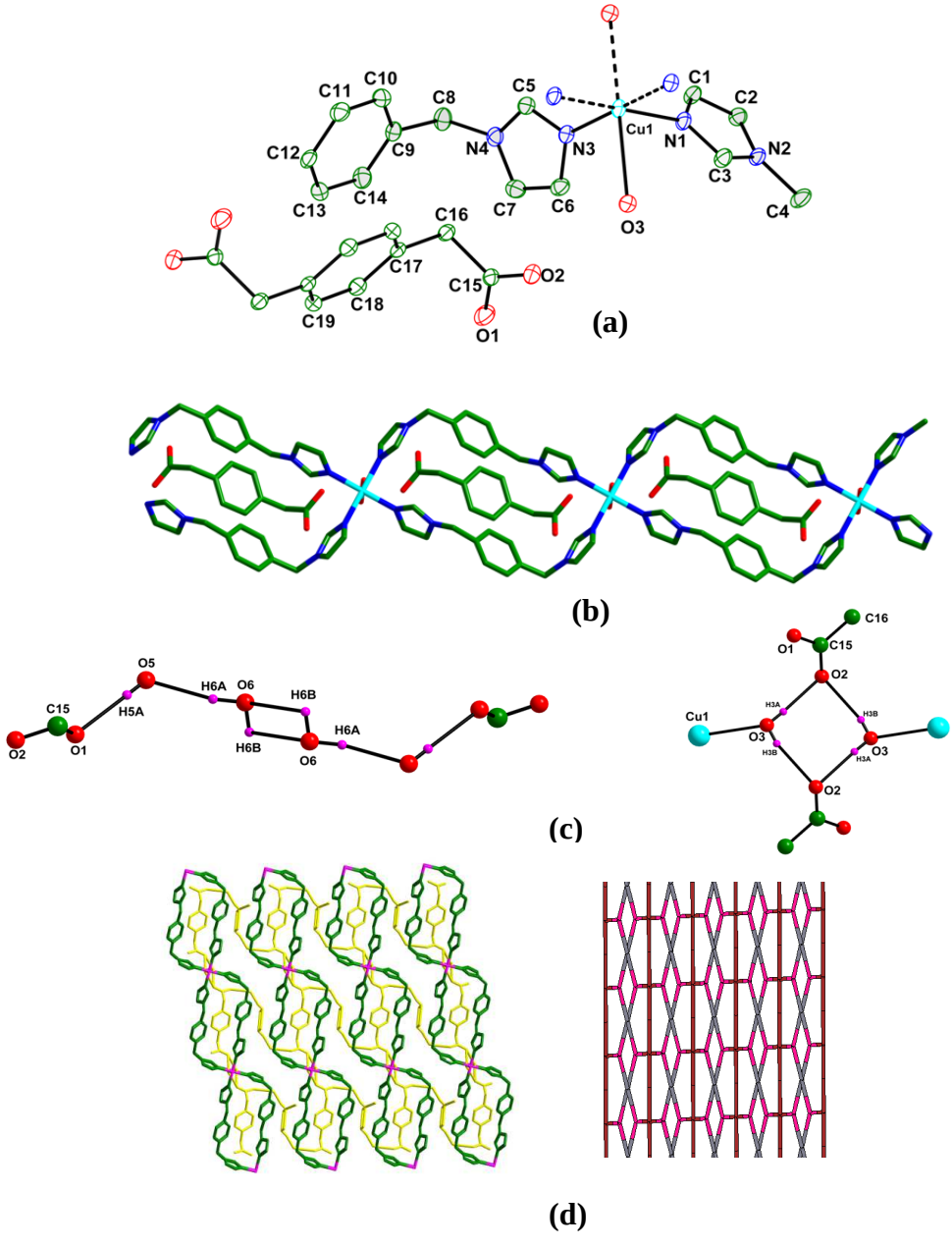

Figure 5.3. (a) ORTEP diagram of **3** (b) 1D double chains constituted by bix ligands incorporating pda^{2-} ligands (c) hydrogen bonded ring motifs constituted by water molecules and carboxylate oxygen's (d) 3D supramolecular structure formed due to hydrogen bondings and schematic representation.

Another ring of type $R^2_2(4)$ has been formed with the assistance of two water molecules (O6); this synthon connects the two pda^{2-} anions along the crystallographic *ac* plane with the help of lattice water molecule (O5) and carboxylate oxygen (O1) (Fig. 5.3c).The overall supramolecular interactions result in a 3D supramolecular network as shown in the Figure 5.3d (Green color network due to bix & yellow color network due to pda^{2-}). Interestingly in the crystal structure of complex **3**, the anion pda^{2-} templates the formation of cationic chains of $[Cu(bix)_2(H_2O)_2]_n^{2n+}$ without involving in the coordination to the metal ion. The conformational freedom of the ligand bix allows to twist its imidazole rings in order to meet the geometrical requirements imposed by the pda^{2-} anion.

Structural description of $[Co_2(\mu\text{-}OH)(pda)(ptz)]_n \cdot nH_2O$ (4)

As shown in the Figure 4a, the asymmetric unit in the crystal structure of compound **4** (space group P2(1)/*n*) consists of two crystallographically independent Co(II) ions bridged by hydroxyl group, one pda^{2-} anion, ptz^{1-} anion, and a lattice water molecule. Co1 is present in tbp geometry, defined by two oxygen atoms (O2, O5) from two different pda^{2-} anions, one μ_2–OH (O1) in the basal plane and two nitrogen donors (N2,N5) from two different ptz^{1-} anions (one from tetrazole ring and another from pyridine ring of ptz) in the apical positions. Another cobalt atom Co2 is also present in tbp geometry defined by two oxygen atoms (O3, O4) from two different pda^{2-} anions, one μ_2–OH (O1) in the basal plane and two nitrogen donors (N1, N4) from two different ptz^{1-} anions (both from the tetrazole rings). Each pda^{2-} anion coordinates to four Co(II) atoms with μ_2-η^1: η^1 bridging mode on either side in a typical *cis* conformation to form a molecular box (Figure 4b). Both acetate side chains in the pda^{2-} twist with respect to each other with synperiplanar torsion angle of 2.30° (slight deviation of torsion angle for *cis* conformation) viewed through C1–C2–C9–C10. Furthermore the acetate chains twist with respect to phenylene ring to various extents, in which arm-A (denoted by C1–C2) shows anticlinal torsion angle of −77.27° (through C1–C2–C3–C4) and arm-B (denoted by C10–C9) exhibits a anticlinal torsion angle of 101.92°(through C10–C9–C6–C7) (Table 5.1). The pda^{2-} coordination constitutes an 8-membered cobalt-dimer ring (with Co–Co distance of 3.711 Å) through the acetate side chains on either side, and the *cis* conformation of the pda^{2-} forms a 22-membered metallocycle by linking these cobalt dimer rings (Figure 4b). The metallocycle

acts as a four connector and extends into two dimensions with another four metallocycles through the bridging hydroxyl group (μ_2–OH) with Co–Co distances of 3.476 Å through crystallographic *bc* plane (Figure 4c). This 2D network is again, in turn, connected by the co-ligand ptz in a μ_4 coordination mode (μ_3 from the tetrazole ring and μ_1 from the pyridine ring of the ptz).

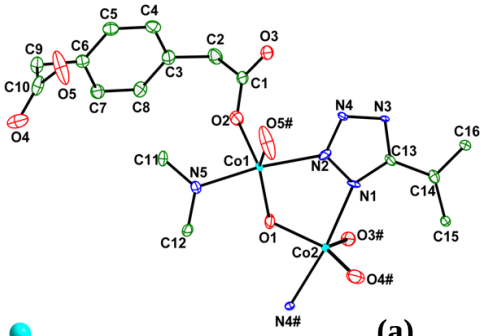

(a)

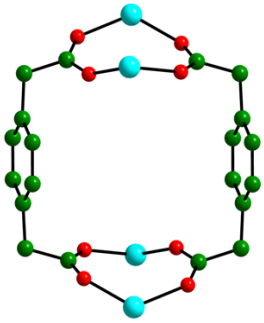

(b)

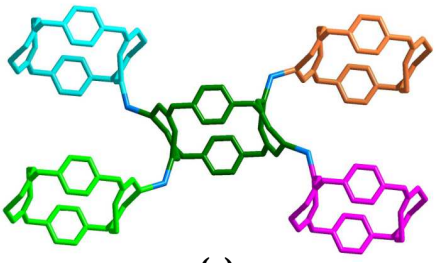

(c)

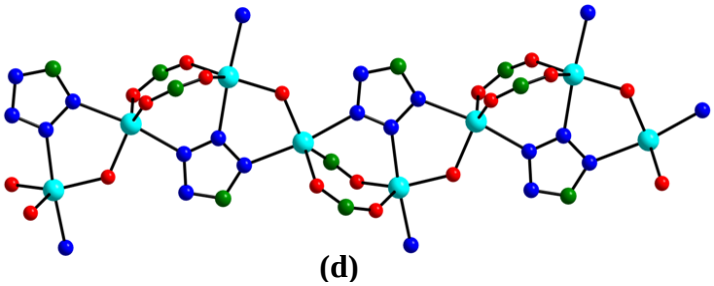

(d)

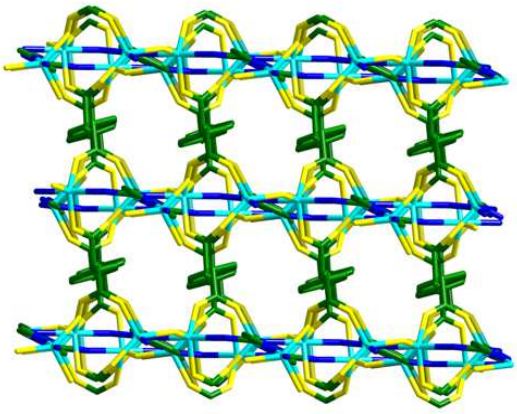

(e)

Figure 5.4. (a) Thermal ellipsoidal plot diagram of **4** (b) Molecular box formed due to *cis* conformation of the pda^{2-} ligand (c) extension of molecular boxes chain through μ_2–OH group (d) 1D chain formed chain formed *via* tetrazole nitrogen's, cobalt atoms and carboxylate oxygen atoms (e) the overall 2D framework of compound **4**

The co-ligand ptz^{1-} again links the Co dimer ring with the nitrogen donors by linking N5 atom from pyridine ring and N3 atom of tetrazole ring to Co atoms (which resemble the coordination mode of 4.4′-bipyridine). Due to availability of more number of donor sites in the tetrazole moieties, they are known to adopt at least nine distinct types of coordination modes and the geometry of the donor sites allow to coordinate the surrounding metal polyhedra at shortest distances.[24] In the present system the tetrazole ring coordinates to three Co atoms through the three nitrogen atoms (N1, N2, N4), i.e two Co atoms from the one Co dimer ring and one Co atom from another dimer thereby forming 1D chain in which the Co atoms are bridged by tetrazole rings and μ_2–OH groups (Figure 5.4d). Due to the *cis* conformation of the pda^{2-} anion a metallocycle ring has been formed which further extends by the bridging with μ_2–OH group and tetrazole ring to form 2D layers as shown in the Figure 5.4e.

Structural description of $[Co(hfipbb)(bix)_{0.5}]_n$ (5)

The asymmetric unit in the crystal structure of compound **5** consists of one cobalt atom, one $hfipbb^{2-}$ ligand and half of the bix ligand. Compound **5** crystallizes in a monoclinic space group *C2/c*. Crystallographic analysis reveals the 2D interpenetrated metal-acid layers which are connected by the bix ligand giving rise to a 3D pillared layered framework. The 2D interpenetrated metal acid layers are composed of SBUs (secondary building units) of dimetallic tetracarboxylate paddle-wheel clusters bridged by the $hfipbb^{2-}$ moieties (Figure 5.5a).[25] As displayed in the Figure 5.5a, the coordination geometry of each cobalt atom in the paddle wheel is in distorted octahedron, the equatorial plane of which comprises of four oxygen atoms from carboxylate groups of four $hfipbb^{2-}$ ligands, the apical coordination sites are filled by one nitrogen atom from the bix ligand with Co–N distance of 2.044 Å and another Co atom of the paddlewheel. The Co–O bond lengths in the SBUs vary in the range of 2.026 – 2.092 Å and the intra-dimer Co–Co separation is 2.858 Å. The dihedral angle between the bent rings of the $hfipbb^{2-}$ ligand is 81.79 °, these bent $hfipbb^{2-}$ moieties link four other neighboring paddle-wheels resulting a 2D net with dimensions 14.38 Å X 14.35Å. The skeleton of these 2D layers can also be viewed as the unique helical tubular double layer, which are similar to the previously reported Co-hfipbb sheets in the compound $[Co(hfipbb)(py)]_n$ (Figure 5.5b).[25] These helical interpenetrated

double layers are extended to 3D framework with the aid of flexible exobidentate bix ligand. bix ligand connects the two paddle wheels of two different double layers with a separation of 14.81Å in a regular *trans* fashion. The connectivity pattern of linker bix forms 1D chains through the crystallographic *c* axis connecting the double layers in the *ab* plane (Figure 5c). The imidazole rings twist with respect to each other by an antiperiplanar torsion angle of 180º through (N2–C21–C21–N2) indicating *trans* conformation (Table 5. 4). The two imidazole rings in the bix ligand twist from the phenyl ring plane by a torsion angle of 76.86° through (C18–N2–C20–C21), and the angles between the planes of the imidazole rings and the plane of phenylene group are 67.57° (Table 5.2).

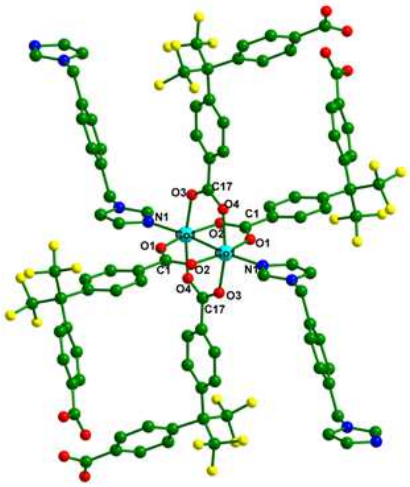

(a)

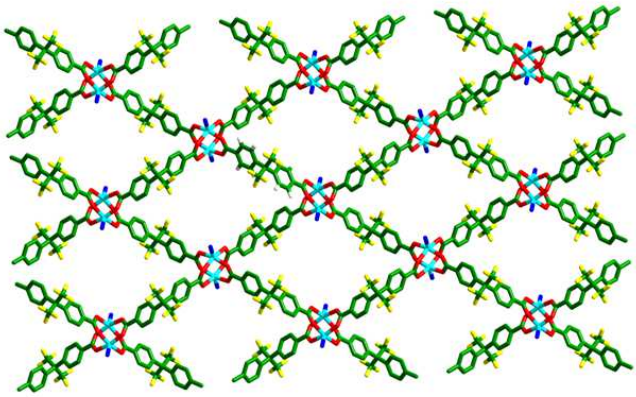

(b)

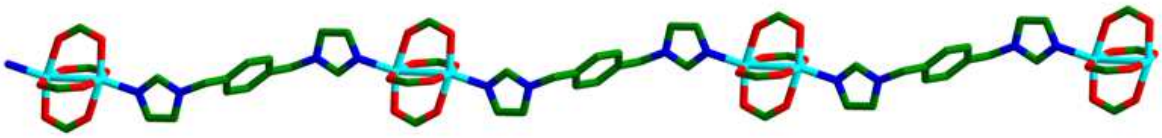

(c)

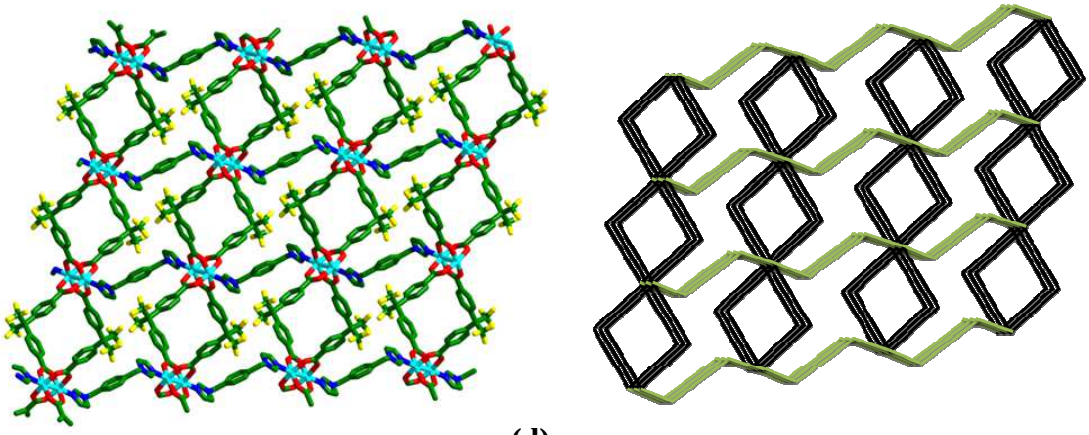

(d)

Figure 5.5. (a) The coordination environment to the Co atoms in the paddle wheel (b) 2D helical double layer formed *via* paddle wheels (c) 1D chain formed by connecting the paddle wheels by the bix ligands (d) The overall 3D framework of compound **5** and its Schematic representation of the 3D framework.

Paddle wheels are considered as six connected nodes and $hfipbb^{2-}$ as linkers to form 2D unique helical double layers, and these layers are pillared by the bix ligand as linker resulting in the formation of a 3D framework as shown in the Figure 5.5d.

Structural description of $[Co(2,6\text{-pydc})(bix)_{1.5}]_n \cdot 4nH_2O$ (6)

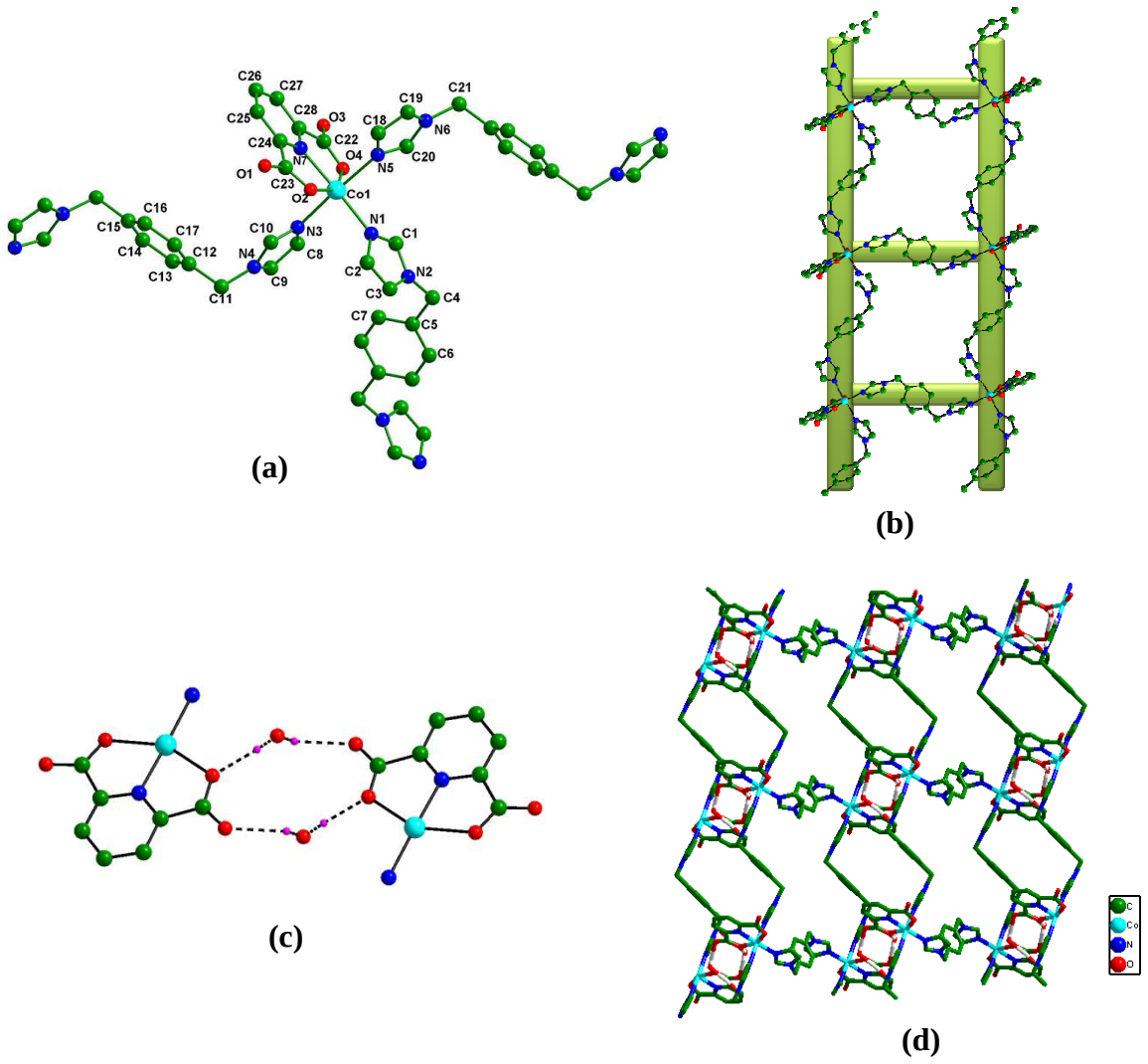

Figure 5.6. (a) The immediate coordination environment of Co atom in the compound **6** (b) 1D ladder running though *a* axis (c) 12 membered hydrogen bonded ring formed by the assistance of water molecule and carboxylate oxygen atoms (d) 2D supramolecular network formed due to classical hydrogen bondings.

A single crystal X-ray diffraction study reveals that compound **6** is a 1D ladder-like structure that crystallizes in triclinic space group P-1. As shown in the Figure 5.6a the Co(II) is in distorted octahedral coordination sphere that is defined by the two nitrogen donors from two different bix ligands in apical positions, and two carboxylate oxygens

and one nitrogen donor from one 2,6–pydc and one bix nitrogen atom in the basal plane. 2,6–pydc[26] blocks the three coordination sites of the Co(II) octahedron and leaves the three coordination sites for the bix nitrogen atoms. The three bix ligands attached to the Co(II)–octahedron connects to three other cobalt atoms with a separation of 13.96 Å and 14.02Å to form a square box with Co(II)-2,6–pydc complex as corner and bix ligands as edges; it extends to a 1D ladder structure (Figure 5.6b). Two types of bix ligands are involved in the formation of 1D ladder based on different conformations. The bix ligand represented by {N3N4N6N5} connects two cobalt atoms with a separation of 14.02Å, and the bix ligand represented by {N1N2N2N1} creates a separation of 13.96Å between the two cobalt atoms. The imidazole rings in the bix {N3N4N6N5} twist with respect to each other by an antiperiplanar torsion angle of 174.50°(through N6–C21–C11–N4) and the imidazole rings with twist with respect to the phenyl ring by 94.73 (through C12–C11–N4–C9) –105.17°(through C12–C11–N4–C9). In the other bix ligand {N1N2N2N1}, the imidazole rings twist with respect to each other by an antiperiplanar torsion angle of 180° and twist with respect to phenyl ring by 72.76° (Table 5.2).The bix ligand does not show any unusual conformation to meet the coordination requirements imposed by the Co(II)–octahedron and confines to a typical *trans* conformation of antiperiplanar torsion angles of 174.50° (a slight deviation from the regular *trans* conformation of 180°) and 180°. As anticipated, classical hydrogen bonding between lattice water molecules and carboxylate oxygens were observed with O···O distances varying from 2.774(5) to 2.935(7) Å; and non classical hydrogen bonds were observed between C–H moieties and carboxylate oxygens as well as lattice water molecules (Table 5.4). With the assistance of the lattice water molecule (O8) and the carboxylate oxygens (O3 and O4), a twelve membered hydrogen bonded ring $R^4_4(12)$ has been formed between the two 1D ladders (Figure 5.6c). The connectivity pattern of these rings to connect the 1D ladders extends to form a 2D supramolecular network (Figure 5.6d).

5.3.4. Factors effecting the conformations of the flexible ligands in the self-assembly of coordination networks

The conformational rotations of the flexible ligands H_2pda and bix in all the six compounds (**1** to **6**) has been studied under three different schemes to rationalize the effects of (i) Coordination geometries of different metal ions in modulating the conformations of the flexible ligands, (ii) Conformational modulation of the pda^{2-} by

increasing the number of donor sites and rigidity in the N-donor co-ligand. (iii) Geometry of the carboxylate ligands in the conformational changes of the N-donor ligand bix.

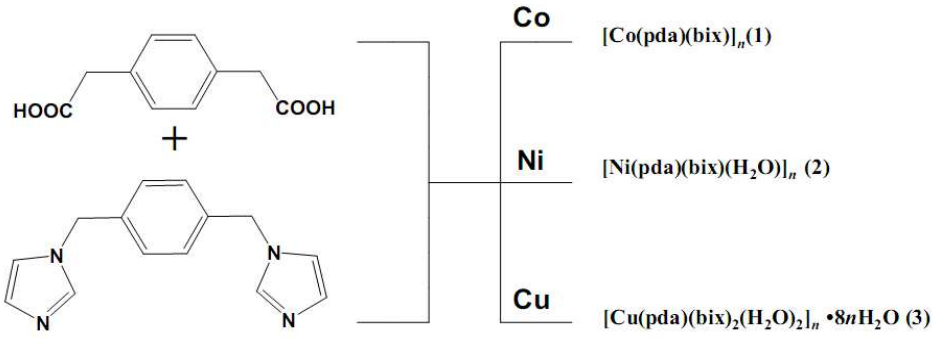

Scheme 5.3. Scheme showing the coordination geometries of different metal ions in modulating the conformations of the flexible ligands

As shown in the Scheme 5.3, three structurally different compounds **1** to **3** have been prepared by varying the metal ions. The cobalt atom in the compound **1** is present in the distorted tetrahedral environment (two carboxylate oxygens from two pda^{2-} ligands, two nitrogens from bix ligands), and both the flexible ligands pda^{2-} and bix in the structure adopt a regular *trans* conformation with a predicted antiperiplanar torsion angle of 180° (Table 5.2) to give a 3D framework. Whereas in compound **2**, nickel atom is present in distorted octahedron (three carboxylate oxygens from two carboxylic acids, two nitrogens from different bix ligands and one aqua ligand) and the two imidazole rings in the bix ligand exhibits a synclinal torsion angle of 77.65°, and the two acetate groups in the pda^{2-} shows anticlinal torsion angle of 105.23° to meet the coordination requirements imposed by the metal ions. In the compound **3**, in which Cu(II) atom present in slightly distorted octahedron (four nitrogens from different bix ligands and two aqua ligands) and the two imidazole rings in the bix exhibits a anticlinal torsion angle of 134.50°, but the two acetate groups in the pda^{2-} shows a typical *trans* conformation of antiperiplanar torsion angle of 180°. A careful analysis of these three structures reveals that the coordination of aqua ligands (one in **2,** two in 3), to metal polyhedra restricts the coordination sites for the ligands to coordinate to the metal thereby these flexible ligands modulate their conformations in order to meet the coordination geometry at the metal polyhedra. Thus it can be say that, the blocking at the coordination sites of the metal polyhedra allows to regulate the conformations of the flexible ligand. This approach of blocking the coordination sites has worked out in our previous report[13] to achieve the *cis* conformation

of the *p*-xylylenediphosphonic acid along with the *trans* conformation. bix ligand exists in three conformations with torsion angles antiperiplanar (*trans*), synclinal (towards *cis*), anticlinal (towards *trans*) in compounds **1**, **2**, and **3** respectively. In a similar fashion pda^{2-} exists in two conformations: antiperiplanar (*trans*) in compounds **1** and **3**; anticlinal (towards *trans*) in **2**. From the previous reports,[27] the *trans* conformations always lead to formation of higher dimensional frameworks and the *cis* conformations leads to closed rings. In compound **1** cobalt with coordination number 4 adopt the *trans* conformation of both the ligands to form a 3D framework whereas the Ni and Cu in the compounds **2** and **3** with coordination number six adopts the anticlinal and synclinal conformations of the ligands thereby forming a 1D extended ring structures. The thermodynamically more stable *trans* forms dominates in almost all the complexes of the previous reports, [28] as a result the factors governing the conformational control of these ligands are of particular interest in assembling the coordination networks involving flexible ligands . In view of these factors the compounds **1** to **3** represents a classical example in which the coordination geometry of the metal ions plays an important role in modulating the conformations of the flexible ligands.

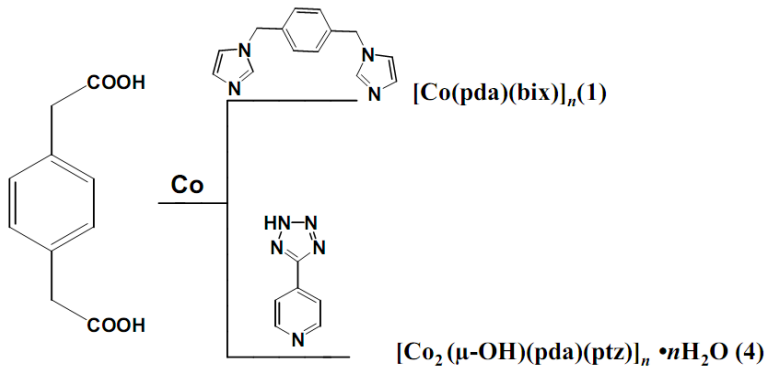

Scheme 5.4. Scheme illustrating the conformational modulation of the pda^{2-} by increasing the number of donor sites and rigidity in the N-donor co-ligand.

The factors that modulate the conformations of the flexible ligand pda^{2-} have been studied by varying the N-donor ligands from flexible bidentate to rigid multidentate ligand (Scheme 5.4). From the previous report[15] in the M(II)–pda^{2-} system, pda^{2-} exists in the *trans* conformation. In compound **1** pda^{2-} confines to typical *trans* conformation by employing flexible bidentate ligand bix, whereas pda^{2-} adopts a *cis* conformation with a synperiplanar torsion angle of 2.35° by using a rigid pentadentate ligand 4-ptz. In a duel ligand system the conformational changes in one of the ligands is strongly influenced by

the coordination pattern of the other ligand. By changing the flexible coligand to rigid ligand the thermodynamically favored *trans* conformation has been changed to *cis* conformation. This type of rigidity modulated conformation of pda^{2-} has been demonstrated by the Cao and co-workers by introducing the rigid 4,4-Bipyridine to metal-carboxylate system.[15] Rigid co-ligand has more ability to modulate the conformation of the flexible ligand than flexible co-ligand.

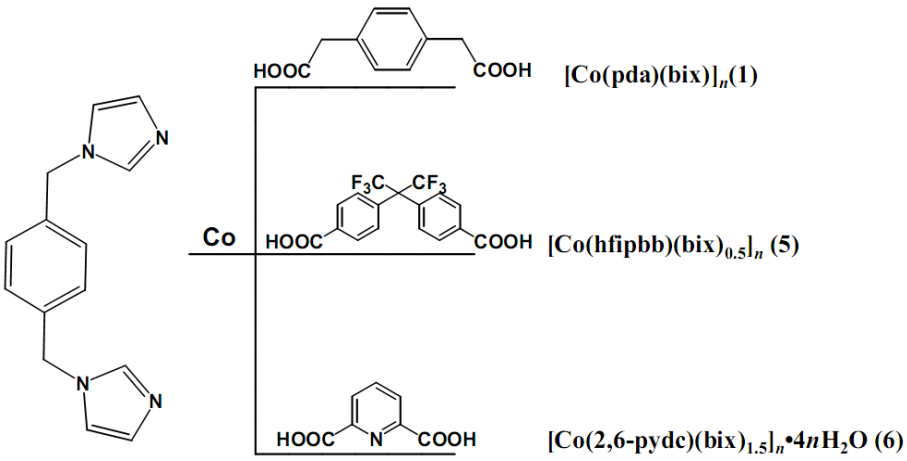

Scheme 5.5. Geometry of the carboxylate ligands in the conformational changes of the N-donor ligand bix

As shown in the Scheme 5.5, in order to study the different conformations of the bix ligand, we have employed three carboxylic acids with different geometrical dispositions of carboxylate group to synthesize the compounds **1**, **5** and **6**.

Table 5.1. Geometrical parameters describing the conformations of pda^{2-} ligand in compounds **1–4** (see also Scheme 5.2).

C.No	Torsion Angle τ (°)			Separation between Metal atoms(Å)
	τ_3(ijj'i')	τ_1(ijkl)	τ_2(l'k'j'i')	
1	180.0	90.08	–90.08	12.80
2	105.23	174.63	–70.30	12.03
3	180.0	101.92	–101.92	Uncoordinated
4	2.35	100.17	–77.27	8.10

A flexible carboxylic acid H_2pda, bent carboxylic acid H_2hfipbb, and rigid blocking carboxylic acid 2, 6–pydc, employed impose the same conformations to the bix ligand, in a typical *trans* conformation in all the three compounds **1**, **5** and **6**. The three carboxylic acids used do not modulate the thermodynamically stable *trans* conformation to other

conformations. But the steric requirements imposed by the carboxylate groups on the metal polyhedra allow the bix ligands to twist their imidazole rings with respect to phenyl group to certain extents *i.e* 51.29° in **1**, 76.86° in **5** and 94.73° in **6** (Table 5.2). In compound **6** there is a slight deviation from the *trans* conformation and exhibits a antiperiplanar torsion angle of 174.50°.

Table 5.2. Geometrical parameters describing the conformations of bix ligands in the compounds **1-3, 5, 6** (see also Scheme 5.2).

C.No	Torsion angle τ(°)			Angle between the aromatic rings(°)			Separation between metal atoms(Å)
	τ_3(jkk'j')	τ_1(ijkl)	τ_2(l'k'j'i')	X-Y	X-P	P-Y	
1	180.0	51.29	-51.29	0.00	71.62	71.62	15.19
2	77.65	51.02	-102.59	73.05	81.5	82.69	12.03
3	134.58	163.53	-78.75	82.32	80.39	70.89	13.03
5	180.0	76.86	-76.86	0.00	67.57	67.57	14.81
6	A- 180.0 B- 174.50	72.76 94.73	-72.76 -105.17	0.00 9.36	88.61 69.18	88.61 73.37	14.02 13.96

The conformational control of the bix ligand solely depends on the coordination requirements imposed by the metal octahedron, which in turn depends on the steric requirements created by the carboxylate ligands. By changing the geometry of carboxylate group the imidazole rings in the bix ligand twist with respect to phenyl ring to certain extent maintaining twist with respect to each other by same angle. The Newman projection of the bix and pda^{2-} ligands with the observed torsion angles in the compounds **1–6** has been shown in Figure 5.7. Different conformations of the flexible ligands change the length of the ligand through various extents, which in turn varies the separation between the metal atoms. Usually the length of the *trans* conformer is more than the *cis* and the *guache* conformer have intermediate lengths (Figure 5.8).

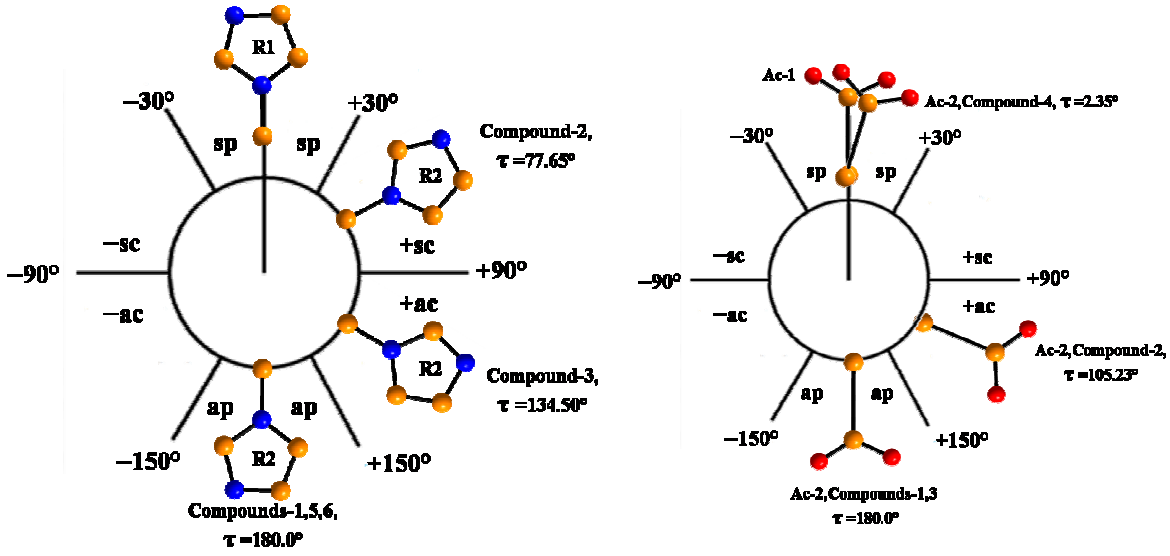

Figure 5.7. Newmann projection representation of the bix (left) and pda^{2-} (right) ligands; R1, R2 represent the imidazole rings in the bix ligand. Ac-1, Ac-2 represents the acetate groups in the pda^{2-} ligands. The angle is measured with respect to each other imidazole rings or acetate groups, not with respect to phenyl ring. So R1, Ac-1 have taken at the mean position and the orientation of the other rings/groups has been shown

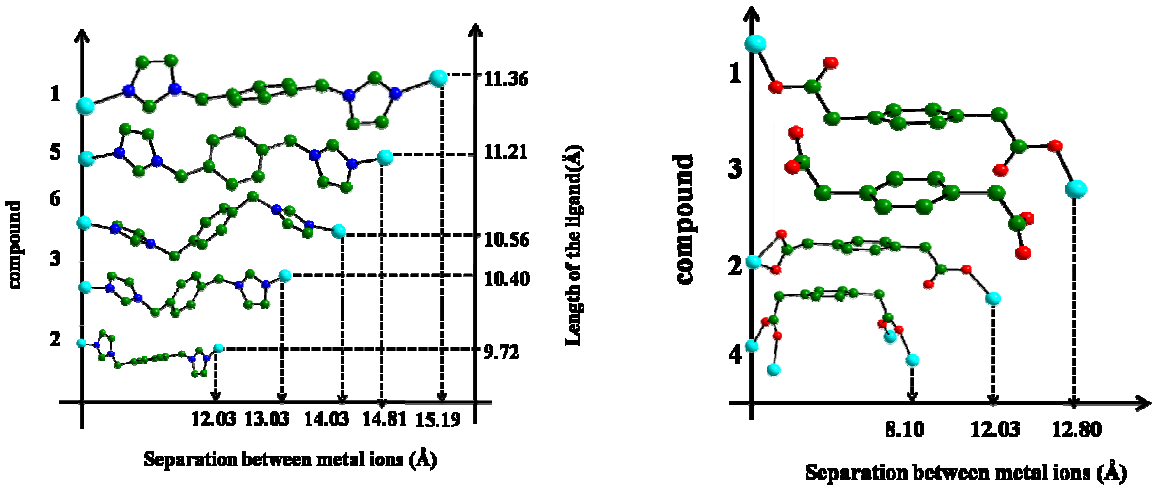

Figure 5.8. Projections of the bix (left) and pda^{2-} (right) ligands on the scale viewing the length of the ligands and separation created between the metal atoms

5.3.5. Theoretical Calculations

To determine the stability of the bix and pda^{2-} ligands in their different conformations in the title compounds, theoretical calculations have been performed. The molecular geometries of only the ligands were taken from the CIF files of the compounds, and the single point, optimized energy calculations have been carried out by using B3LYP with 6-311g** basis set. From the literature, the energy calculations have been performed by optimizing the crystal structures through various optimization methods (Dreiding force

field) using DFT (Density Functional Theory) methods.[29] In the present case the calculations were performed by DFT methods by optimizing only the ligand geometries.

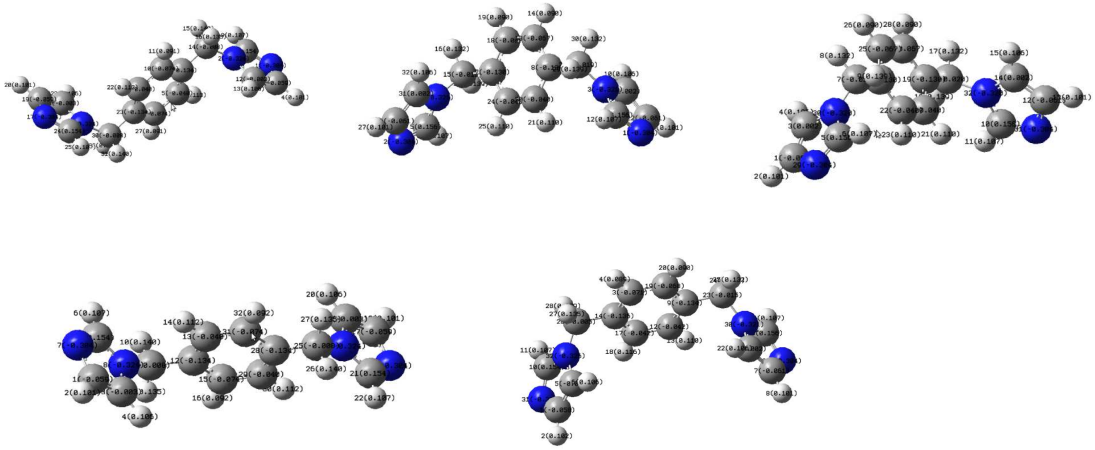

Figure 5.9a. b3lyp/6-3111g** optimized geometrical structures of conformers of bix ligands in the compounds **1**, **2**, **3**, **5**, **6** with the atom labeling scheme and Mulliken charges (in parenthesis).

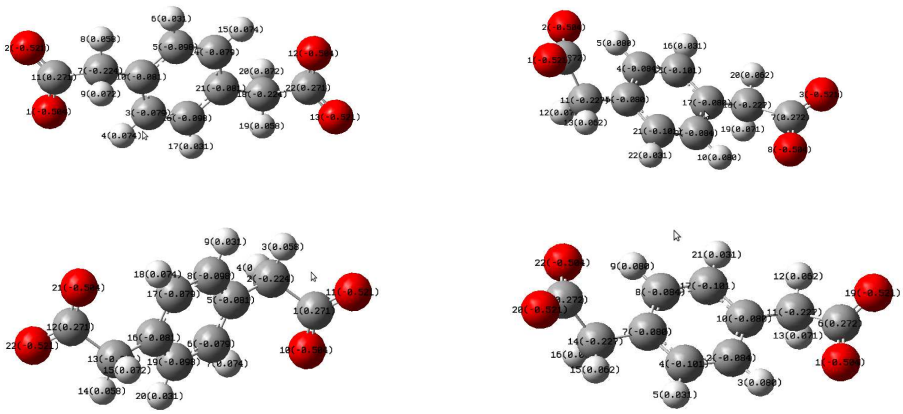

Figure 5.9b. b3lyp/6-3111g** optimized geometrical structures of conformers of pda^{2-} with the atom labeling scheme and Mulliken charges (in parenthesis).

The optimized energy of the bix ligand in all the compounds show almost same energy (Kcal/mole) in all its conformers, -477592.9776 (-477426.575) for **1**, -477592.8070 (-477427.367) for **2**, -477592.9776 (-477423.600) for **3**, -477592.9887 (-477426.574) for **5**, -477592.7359 (-477421.693) for **6**. The optimized energy of pda^{2-} ligand in all the compounds also show almost same energy (Kcal/mole) in all its conformers -431100.09311 (-431003.7712) for **1**, -431099.4490 (-431004.0174) for **2**, -431100.0836 (-431008.4104) for **3**, -431099.4490 (-431014.2817) for **4**. The values in the parenthesis indicates single point energies From the optimized energy values, all the conformations of the bix ligand converge almost to same energy in the potential energy surface, similarly in the case of pda^{2-} also. These results indicate that the bix and pda^{2-} ligands can show stable

cis, *trans* and *gauche* conformations. The theoretical calculations shows that the energy barrier to transform from one conformation to another is very less, so that the ligand can exist in different conformations depending upon the coordination requirements (Figure 5.9).

5.3.6. XRPD and Thermogravimetric analysis

TGA curves are made under flowing N_2 for crystalline samples **1–6** in the temperature range 30–1000 °C (Figure 5.10). Compound **1** exhibit a thermal stability up to 254 °C and undergoes continues weight loss attributed to the decomposition of bix and pda^{2-} ligands. Compounds **2** and **3** shows continuous weight loses of the lattice and coordinated aqua ligands followed by the decomposition of organic parts. For compound **4** a continuous weight loss of 7.78% (calcd, 7.15%) in the region 40–360 °C corresponds to complete loss of lattice water molecule and –OH group and then the framework belongs to collapse. Compound **5** exhibits a thermal stability up to 220 °C and then the framework collapses in two steps. Compound **6** shows a weight loss of 11.65 % (Calcd, 11.02%) in the region 65 – 122 °C corresponds to the loss of four lattice water molecules. Among all the compounds **4** exhibits a high thermal stability up to 360 °C in which pda^{2-} exists in *cis* conformation.

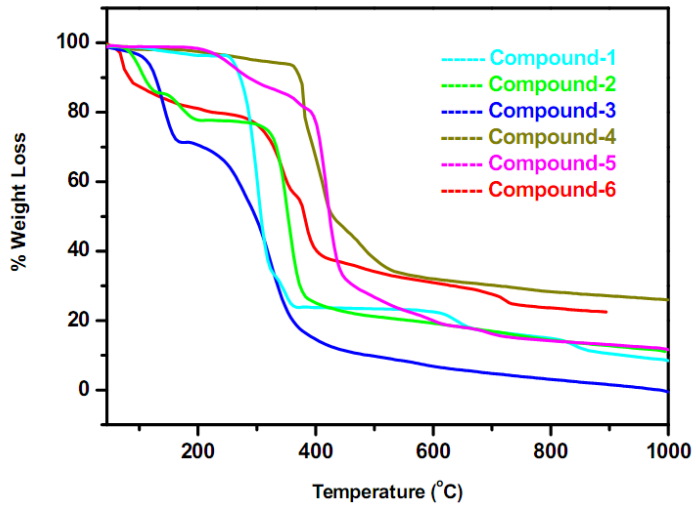

Figure 5.10. Thermogravimetric curves of the compounds **1–6.**

The thermal stability of the compound constructed by the *cis* pda^{2-} (which is thermally less stable) is more stable than the compound constructed by the *trans* pda^{2-} (which is thermally more stable) is due to presence of rigid multidentate co-ligand in **4** , and flexible bidentate co-ligand in **1.** In the remaining compounds containing bix ligands with

trans conformation shows high thermal stability than compounds containing bix ligands with other conformations.

To ensure the phase purity of the products X-ray powder diffraction data for all the compounds have been recorded. Similar diffraction patterns for the simulated data (calculated from single crystal data) and observed data prove the bulk homogeneity of the crystalline solids (Figure 5.11). Although the experimental patterns have a few un-indexed diffraction peaks and some are slightly broadened and shifted in comparison to those simulated from the single-crystal data, it can still be regarded that the bulk as-synthesized materials represent compounds. From the TGA curves, the weight of compounds **2**, **3** and **6** are lost in the beginning due to the losses of solvated water molecules. The slight inconsistencies in the patterns are due to the loosely bonded solvent molecules in the crystal structures.

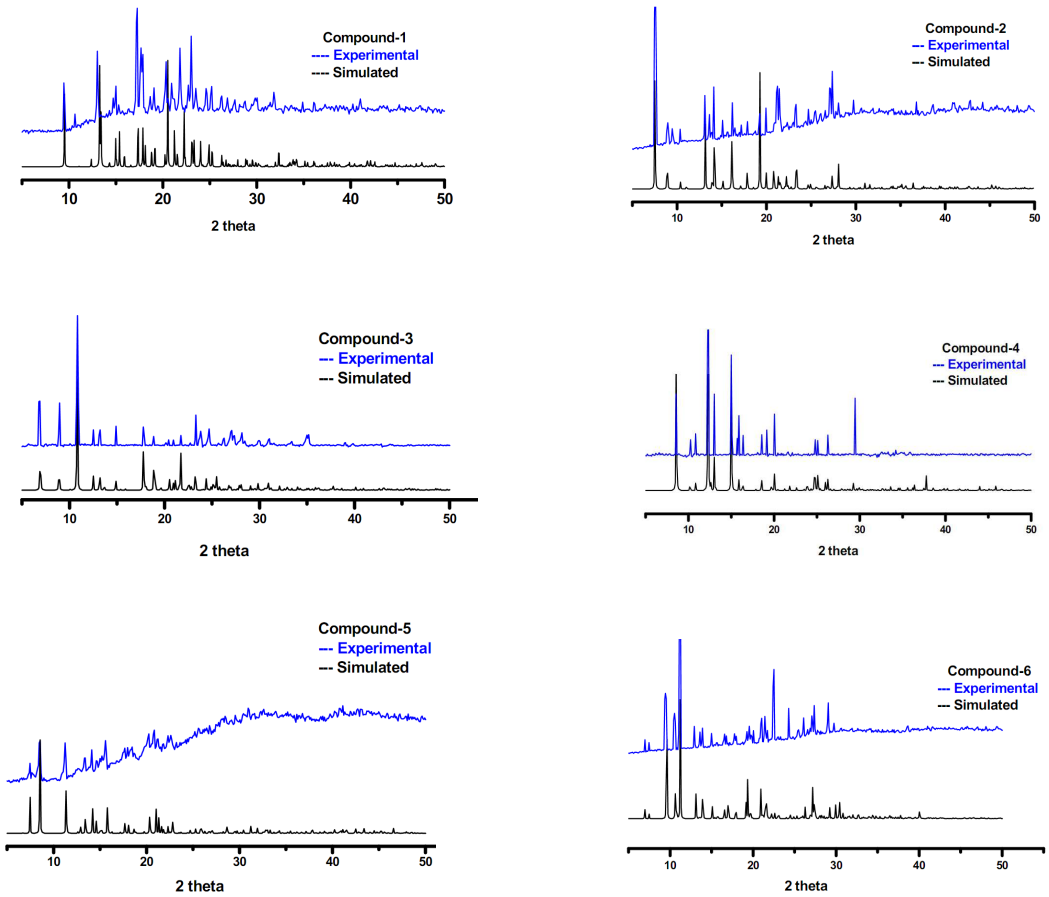

Figure 5.11. Powder X-ray patterns of the compounds **1**-**6**.

5.3.7. Electronic Properties

Solid state diffuse reflectance (electronic absorption) spectra for the compounds **1-6** are presented in Figure 5.12. The absorption peaks at 576, 332, 270 nm (compound **1),** 332, 264 nm (Compound **2**), 584, 260 nm (Compound **3**) 576, 278nm (Compound **4**), 572, 274, 236 nm (Compound **5**), and 520, 344, 270 nm (Compound **6**) are observed in the respective spectra. In all the spectra, the lowest energy bands are assigned due to d-d transitions of metal ions Co(II) (**1**, **4**, **5 & 6**) and Cu(II) (**3**) present in the title compounds, and the highest energy bands are due to Π–Π* and n–Π* transitions from phenyl group and imidazolyl moieties. The conformational changes of the flexible ligands do not affect the absorption peaks in the compounds.

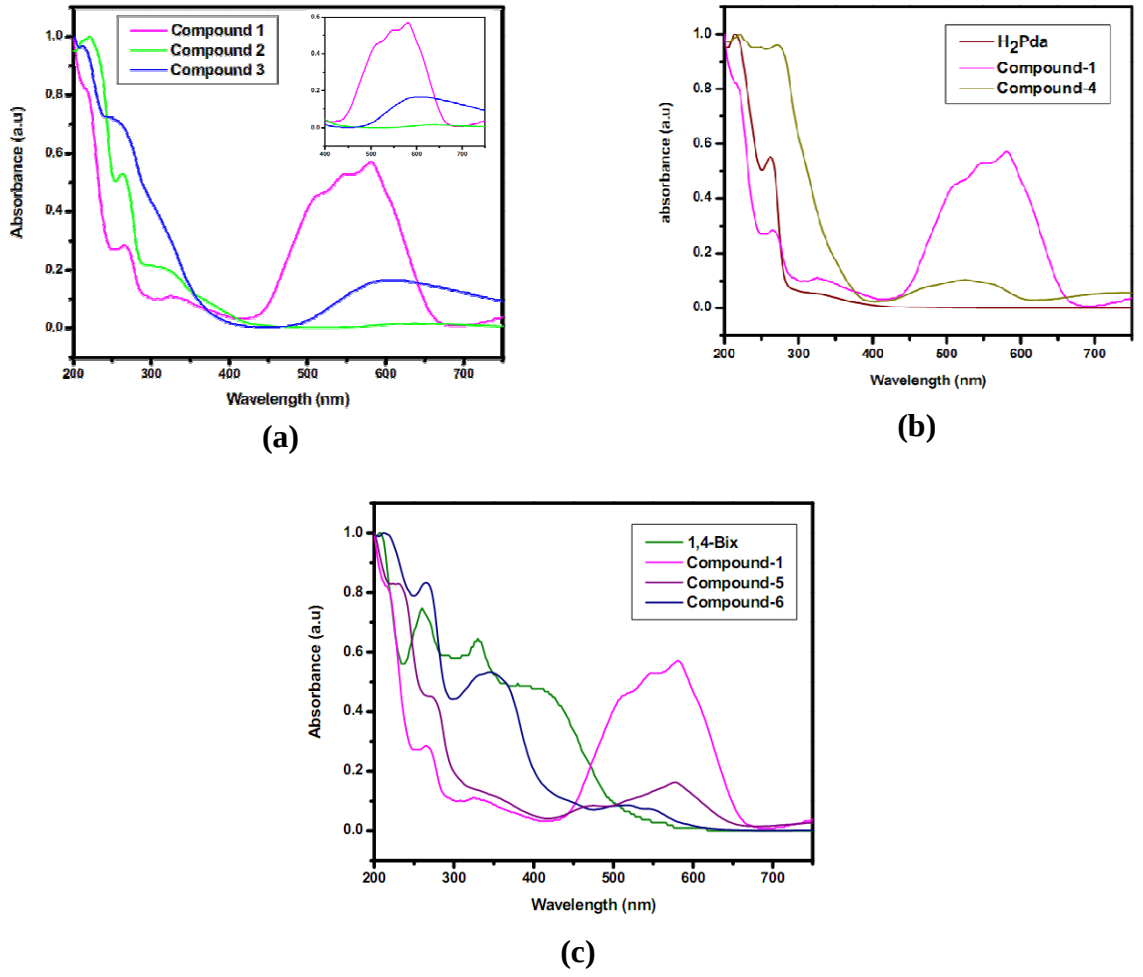

Figure 5.12. (a) Compounds **1**, **2**, **3** in which conformational modulation of the ligands influenced by the coordination geometry (b) Compounds **1** and **4** in comparison with the H_2pda (c) Compounds **1**, **5**, **6** in comparison with the bix ligand

5.3.8. Magnetic Properties

Temperature dependent magnetic susceptibility χ_m of **4** was measured in an applied dc field of 1 K0e in the temperature range 2–300K (Figure 5.13). The $\chi_m T$ value at the room temperature is 4.45 cm^3 K mol^{-1} for per Co(II) ion, which is much higher than the calculated spin-only value (1.87 cm^3 K mol^{-1}) for an uncoupled high-spin Co(II) ion (S=3/2, g=2) with octahedral geometry, indicating the orbital contribution of Co(II) ions.[29] Upon cooling the $\chi_m T$ value decreases smoothly to reach a value of 1.070 cm^3 K mol^{-1} at 22K and slightly shifted the curve and then decreases to minimum value of 0.220 cm^3 K mol^{-1} at 2K. The presence of round peak at 6K in the χ_m vs T indicates a low dimensional antiferromagnetic ordering. The Neel temperature T_N=6K was determined from the sharp peak in d $\chi_m T/dt$.[30] Due to paramagnetic impurities the χ_m value increases below 4k. The results show that the compound shows an overall antiferromagnetic interactions and also spin-orbit coupling interactions between the adjacent Co(II) ions.

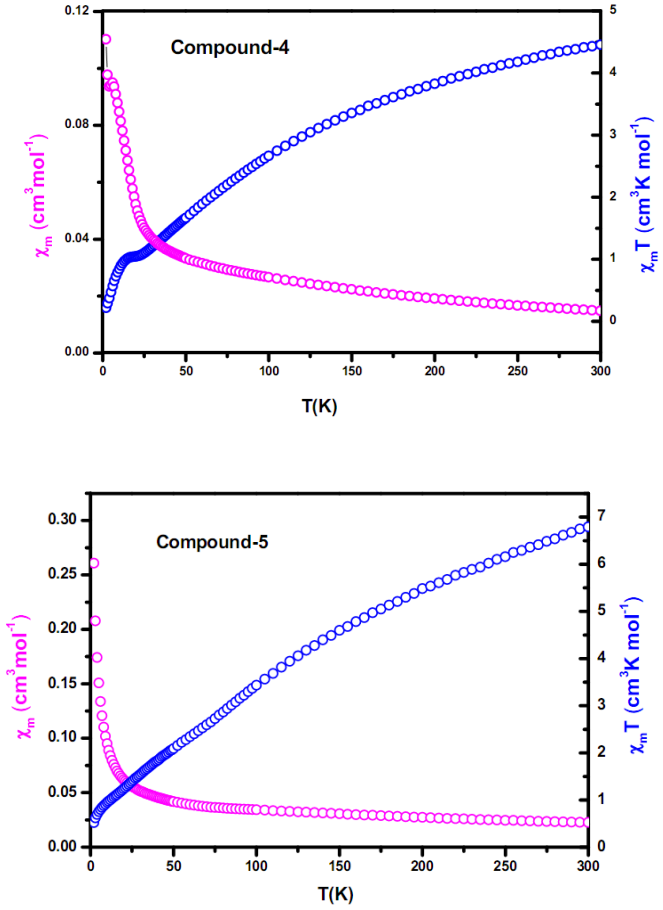

Figure 5.13. Plots of χ_m, $\chi_m T$ versus T for the compounds **4** and **5**

The magnetic susceptibility of compound **5** was measured in an applied dc field of 1T in the temperature range of 2–300 K (Figure 5.12). Compound **5**, which is essentially a Co-

dimer with four carboxyl ligands coordinating to two Co(II) ions, that form a typical paddle wheel SBU, which is further connected through the axial site by the bix ligand. The $\chi_m T$ value at the room temperature is 6.79 cm^3 K mol^{-1}, which is much higher than the calculated spin-only value 3.87 cm^3 K mol^{-1} for two Co(II) ion (S=3/2), with octahedral geometry. This indicates the orbital contribution of Co(II) ions to the observed $\chi_m T$ value. The curve indicates the typical antiferromagnetic and spin-orbit coupling interactions, present in the compound.

5.4. Conclusion

In summary, we report here the six new coordination polymers (**1–6**), based on flexible ligands (H_2pda, bix) by employing the different co-ligands (4-ptz, H_2hfipbb, 2, 6-H_2pydc) to rationalize the factors that modulate the conformational changes of the flexible ligands. Compounds **1 – 3** represent the example in which the coordination geometry of the metal ion plays an important role in modulating the different conformations, such as *trans*, *cis* and *guache* forms of the pda^{2-} and bix ligands. The availability of the coordination sites around the metal polyhedra is responsible to regulate the degree of flexibility to adopt various conformations to maximize the intra- and intermolecular forces in the crystal structure. Compound **4** represents an example in which the *cis* conformation of the pda^{2-} ligand is stabilized by the rigid pentadentate ligand 4-ptz. Conformational modulation of the flexible acid ligand under the influence of the rigid and flexible co-ligands has been studied and the rigid co-ligand is preferred as best selection in achieving the modulation. The effect of the dicarboxylate ligands with different geometrical dispositions of carboxylate groups on the conformations of the neutral flexible co-ligand bix has been demonstrated. The variations in the deviations of the imidazole rings with respect to the phenyl rings in the bix ligand have been observed by employing these different carboxylic acids. In the self assembly process of duel ligand containing coordination polymers, the geometry of one of the ligand (such as flexibility, geometry of the coordinating atoms etc.) transmits to the metal polyhedra and the metal polyhedra influences the geometry in the other ligand and so on. The compounds, reported in this article, represent classic examples to study the new perspectives in the mechanism of self assembly process of coordination polymers. Many more systematic studies are needed to rationalize the factors discussed in affecting the conformational modulation of the flexible ligands. Theoretical studies confirm that the stability of the ligands does not alter by adopting different conformations.

Table 5.3. Crystal data and structural refinement parameters for compounds **1–6**.

	1	**2**	**3**
Empirical formula	$C_{24}H_{22}N_4O_4Co$	$C_{24}H_{24}N_4O_5Ni$	$C_{38}H_{56}N_8O_{14}Cu$
Formula weight	494.01	507.18	912.46
T(K) / λ(Å)	298(2), 0.71073	298(2), 0.71073	298(2), 0.71073
Crystal system/Space group	triclinic/ *P-1*	monoclinic/ $P2_1/n$	triclinic/*P-1*
a (Å)	6.892 (6)	8.655(4)	8.370(4)
b (Å)	8.561 (7)	10.949(6)	10.357(5)
c (Å)	18.950 (16)	23.799(12)	13.037(6)
α (°)	96.295 (10)	90.00	101.575(6)
β (°)	98.064 (10)	100.017(7)	90.785(6)
γ (°)	103.275 (10)	90.00	101.798(7)
Volume (Å^3)	1065.80(16)	2221.0(19)	1082.0(9)
Z, ρ_{calcd} (g cm^{-3})	2, 1.539	4, 1.517	1, 1.400
μ (mm^{-1}), *F*(000)	0.846/510	0.919/1056	0.579/481
goodness-of-fit on F^2	1.132	1.069	1.083
R1/ wR2 [I > 2σ (I)]	0.0565/0.1341	0.0331/0.0835	0.0433/0.1031
R1/ wR2 (all data)	0.0635/0.1392	0.0385/0.0865	0.0475/0.1057
Largest diff peak/hole(e Å^{-3})	0.621/–0.579	0.479/–0.176	0.272/–0.201

	3	**4**	**5**
Empirical formula	$C_{16}H_{13}N_5O_6Co_2$	$C_{24}H_{15}F_6N_2O_4Co$	$C_{28}H_{32}N_7O_8Co$
Formula weight	489.17	568.31	653.54
T(K)/ λ(Å)	298(2), 0.71073	298(2), 0.71073	298(2),0.71073
Crystal system/Space group	monoclinic/ $P2_1/n$	monoclinic/ *C*2/*c*	triclinic/ *P*-1
a (Å)	9.0096(9)	27.375(6)	10.122(3)
b (Å)	20.558 (2)	7.277(15)	12.159(4)
c (Å)	9.7353(10)	24.644(5)	13.553(4)
α (°)	90.00	90.00	91.707(5)
β (°)	100.547(2)	106.240(2)	109.504(5)
γ (°)	90.00	90.00	102.552(5)
Volume (Å^3)	1772.7(3)	4731.4(16)	1525.2(8)
Z, ρ_{calcd} (g cm^{-3})	4, 1.833	8, 1.602	2, 1.423
μ (mm^{-1}), *F*(000)	1.919, 984	0.810, 2288	0.623, 680
R1/ wR2 [I > 2σ (I)]	0.0729/ 0.189	0.0372/ 0.0912	0.0651/0.1456
R1/ wR2 (all data)	0.0182/0.1930	0.0447/0.0942	0.0804/0.1543
Largest diff peak/hole (e Å^{-3})	2.259/ –0.712	0.802/ –0.297	0.610/ –0.266

Table 5.4. Geometrical parameters of the C–H···O and C-H···N hydrogen bonds (Å, °) involved in supramolecular networks of compounds **2**, **3** and **6**.[a] D=donor; A=acceptor.

D-H...A	d(D-H)	d(H...A)	d(D...A)	<(DHA)
		Compound-2		
C(14)-H(14B)...O(4)#1	0.97	2.32	3.236(3)	156.6
C(4)-H(4A)...O(1)#2	0.97	2.34	3.259(3)	158.6
C(10)-H(10)...O(1)#2	0.93	2.78	3.542(3)	139.5
O(5)-H(5A)...O(2)#3	0.87(3)	1.86(3)	2.721(2)	172(3)
		Compound-3		
O(3)-H(3A)...O(2)#1	0.82(3)	1.95(3)	2.770(3)	174(3)
O(6)-H(6A)...O(5)#4	0.90(9)	1.90(9)	2.781(7)	166(8)
C(2)-H(2)...O(6)#5	0.93	2.61	3.388(6)	140.9
C(5)-H(5)...O(1)#6	0.93	2.43	3.323(3)	162.0
		Compound-6		
C(13)-H(13)...O(1)# 6	0.93	2.68	3.515(6)	149.7
C(14)-H(14)...O(7)# 7	0.93	2.46	3.306(7)	150.6
C(10)-H(10)...O(5)# 4	0.93	2.53	3.384(7)	152.5
C(8)-H(8)...O(8)# 8	0.93	2.65	3.556(6)	163.6
C(19)-H(19)...O(8)# 9	0.93	2.49	3.344(6)	153.2
C(20)-H(20)...O(7)# 8	0.93	2.45	3.282(8)	149.4
C(4)-H(4B)...O(6)# 8	0.97	2.53	3.447(7)	158.7
C(1)-H(1)...O(6)# 8	0.93	2.77	3.524(6)	138.6
O(6)-H(6A)...O(1)# 4	0.95(6)	2.20(7)	2.851(6)	125(5)
O(8)-H(8B)...O(4)# 8	0.92(7)	1.86(7)	2.774(5)	171(6)
O(8)-H(8A)...O(3)# 10	0.74(6)	2.15(6)	2.822(5)	152(6)
O(7)-H(7A)...O(8)# 3	0.89(6)	2.05(7)	2.935(7)	172(6)

[a]*Symmetry transformations used to generate equivalent atoms*
#1 -x+1,-y+1,-z #2 -x+1,-y,-z #3 -x,-y+1,-z #4 -x+1,-y,-z+1 #5 x-1,y,z-1 #6 x-1,y,z #7 -x,-y,-z+1 #8 -x+1,-y+1,-z+1 #9 -x+2,-y+1,-z+1 #10 x,y,z-1

5.5. References

[1] (a) Halper, S. R.; Do, L.; Stork, J. R.; Cohen, S. M. *J. Am. Chem. Soc*. **2006**, *128*, 15255. (b) Hasegawa, S.; Horike, S.; Matsuda, R.; Furukawa, S.; Mochizuki, K.; Kinoshita, Y.; Kitagawa, S. *J. Am. Chem. Soc*. **2007**, *129*, 2607. (c) Kitagawa, S.; Matsuda, R. *Coord. Chem. Rev*. **2007**, *251*, 2490. (d) Yaghi, O. M.; O'Keeffe, M.; Ockwig, N. W.; Chae, H. K.; Eddaoudi, M.; Kim, J. *Nature* **2003**, *423*, 705. (e) Luo, F.; Zheng, J. M.; Batten, S. R. *Chem. Commun*. **2007**, 3744. (f) Moulton, B.; Zaworotko, M.J. *Chemical Reviews*, **2001**, *101*, 1629. (g) Rao,V. K.; Chakrabarti, S.; Natarajan. S. *Inorg. Chem*. **2007**, *46*, 10781.

[2] (a) Kitura, R.; Fujimoto, K; Noro, S.; Kondo, M; Kitagawo, S. *Angew. Chem. Int. Ed*. **2002**, *41*, 133. (b) Shin, D. M.; Lee, I. S.; Chung, Y. K. *Inorg. Chem*. **2003**, *42*, 8838. (c)Ayappan, P; Evans, O, R.; Cui, Y.; Wheeler, K. A.; Lin, W. B. *Inorg. Chem*. **2002**, *41*, 4978. (d) Dinca, M.; Long, J. R. *J. Am. Chem. Soc*. **2005**, *127*, 9376. (e) Yoon, J. W.; Jung, S. H; Hwang, Y. K.; Humphrey, S. M.; Wood, P.T.; Chang, J. S. *Adv. Mater*. **2007**, *19*, 1830. (f) Han, S. S.; Deng, W, Q.; Goddard, W. A. *Angew. Chem. Int. Ed*. **2007**, *46*, 6289. (g) Bar, A. K.; Chakrabarty, R.; Chi, K-W.; Batten, S. R.; Mukherjee, P. S. *Dalton Trans*., **2009**, 3222.

[3] (a) Ma, B. Q.; Mulfrot, K. L.; Hupp, J. T. *Inorg. Chem*. **2005**, *44*, 4912. (b) Custelcean, R.; Gorbunova, M. G. A. *J. Am. Chem. Soc*. **2005**, *127*, 16362. (c) Doble, D. M. J.; Benison, C. H.; Blake, A. J.; Fenske, D.; Jackson, M. S.; Kay, R. D.; Li, W.-S.; Schroder, M. *Angew. Chem. Int. Ed*. **1999**, *38*, 1915. (d) Zhang, H.; Wang, X. M.; Zhang, K. C.; Teo, B. K. *J. Am. Chem .Soc*. **1996**, *118*, 11813.

[4] (a) Li, H.; Eddaoudi, M.; Groy, T. L.; yaghi, O. M. *J. Am .Chem. Soc*. **1998**, *120*, 8571. (b) Chen, B.; Eddaoudi, M.; Hyde, S. T.; O'Keeffe, M.; Yaghi, O. M. *Science*, **2001**, *291*, 1021. (c) Eddaoudi, M.; Kim, J.; Rosi, N.; Vodak, D.; Wachter, J.; O'Keeffe, M.; Yaghi, O. M. *Science*, **2002**, *43*, 2334. (d) Yaghi, O. M.; O'Keeffe, M.; Ockwig, N.; Chae, H.; Eddaoudi, M.; Kim, J. *Nature* **2003**, *423*, 705.

[5] (a) Schaate, A.; Klingelhofer, S.; Behrens, P.; Wiebcke, M. *Cryst. Growth Des*. **2008**, *8*, 3200. (b) Liu, Y.; Qi, Y.; Lv. Y. Y.; Che, Y. X.; Zheng, J. M. *Cryst. Growth Des*. **2009**, *9*, 4797. (c) Li, Z. X.; Hu, T. L.; Ma, H.; Zeng, Y. F.; Li, C. J.; Tong, M. L.; Bu, X. H. *Cryst. Growth Des*. **2010**, *10*, 1138. (d) Yang, J.; Ma, J. F.; Battern, S. R.; Su, Z. M. *Chem. Commun*. **2008**, 2223. (e) Pachfule, P.; Dey, C.; Panda, T.; Banarjee, R. *CrystEngcomm* **2010**, *12*, 1600.

[6] (a) Dai, F.; Dou, J.; He, H.; Zhao, X.; Sun, D. *Inorg. Chem.*, **2010**, *49*, 4117 (b) Willans, C. E.; French, S.; Barbour, L. J.; Gertenbach, J. A.; Junk, P. C.; Lloyd, G. O.; Steed, J. W. *Dalton Trans*., **2009**, 6480. (c) Dong, Y. B.; Jiang, Y. Y.; Li, J.; Ma, J. P; Liu, F. L.; Tang, B.; Huang, R. Q.; Batten, S. R. *J. Am .Chem. Soc*., **2007**, *129*, 4520. (d) Li, L. L.; Liu, L. L.; Zheng, A. X.; Chang, Y. Z.; Dai, M.; Ren, Z. G.; Li, H. X.; Lang, J. P. *Dalton Trans*., **2010**, *39*, 7659.

[7] (a) Su, C. Y.; Goforth, A. M.; Smith, M. D.; zurLoye, H. C. *Inorg. Chem*. **2003**, *42*, 5685. (b) Cai, Y. P.; Su, C. Y.; Chen, C. L.; Li, Y. M.; Kang, B. S.; Chan, A. S. C.; Kaim, W. *Inorg. Chem.* **2003**, *42*, 163.

[8] (a) Li, G.; Lu, J.; Li, X.; Yang, H.; Cao, R. *CrystEngComm*, **2010**, *12*, 3780. (b) Liu, T. F.; Lu, J.; Lin, X.; Cao, R. *Chem. Commun*., **2010**, *46*, 8439. (c) Li, X.; Weng, X.; Tang, R.; Lin, Y.; Ke, Z.; Zhou, W.; Cao, R. *Cryst. Growth Des*. **2010**, *10*, 3228. (d) Liu, T. F.; Lu, J.; Cao, R. *CrystEngComm*, **2010**, *12*, 660.

[9] (a) Tanake, D.; Kitagawa, S. *Chem. Mater*., **2008**, 922. (b) Carlucci, L.; Ciani, G.; Proserpio, D. M.; Rizzato, S. *Chem. Commun.*, **2000**, 1319. (c) Tong, X. L.; Wang, D. Z.; Hu, T. L.; Song, W. C.; Tao, Y.; Bu, X. H. *Cryst. Growth Des*. **2009**, *9*, 2280.

[10] Bolligarla, R.; Das, S.K. *CrystEngComm*, **2010**, 3409.

[11] (a) Koner, R.; Goldberg, I. *CrystEngComm*, **2009**, 1217. (b) Qin, C.; Wang, X.; Carlucci, L.; Tong, M.; Wang, E.; Hua, C.; Xua, L. *Chem. Commun.*, **2004**, 1876. (c) Liang, X. Q.; Zhou, X. H.; Chen, C.; Xiao, H. P.; Li, Y. Z.; Zuo, J. L; You, X. Z. *Cryst. Growth Des*. **2009**, *9*, 1041. (d) H. Y. Bai, J. F. Ma, J. Yang, Y. Y. Liu, H. Wu, J. C. Ma, *Cryst. Growth Des*. **2010**, *10*, 995.

[12] (a) Li, Z. X.; Zeng, Y. F.; Ma, H.; Bu, X. H. *Chem. Commun*., **2010**, *46*, 8540. (b) Fan, J.; Yee. G. T.; Wang, G.; Hanson, B. E. *Inorg. Chem.*, **2006**, *45*, 599. (c) Li, Z. X.; Xu, Y.; Zuo, Y.; Li, L.; Pan, Q.; Hu, T. L.; Bu, X. H. *Cryst. Growth Des*., **2009**, *9*, 3904.

[13] Tripuramallu, B. K.; Kishore, R.; Das, S. K. *Polyhedron*, **2010**, *29*, 2985.

[14] (a) Pan, L.; Adams, K. M.; Hernandez, H. E.; Wang, X.; Zheng, C.; Hattori, Y.; Kaneko, K. *J. Am .Chem. Soc.*, **2003**, *125*, 3062. (b) Fabelo, O.; Delgado, L. C.; Pasan, J.; Delgado, F. S.; Lloret, F.; Cano, J.; Julve, M.; Perez, C. R. *Inorg. Chem.*, **2009**, *48*, 11342. (c) Carpanese, C.; Ferlay, S.; Kyritsakas, N.; Henry, M.; Hosseini, M. W. *Chem. Commun.*, **2009**, 6786. (d) Su, Z.; Chen, S. S.; Fan, J.; Chen, M. S.; Zhao, Y.; Sun, W. Y. *Cryst. Growth Des*., **2010**, *10*, 3675.

[15] Liu, T.; Lu, J.; Shi, L.; Guo, Z.; Cao, R. *CrystEngComm* **2009**, *11*, 583.

[16] Yang, G. P.; Wang, Y. Y.; Zhang, W. H.; Fu, A. Y.; Liu, R. T.; Lermontava, E.; Shi, Q. Z. *CrystEngComm*, **2010**, *12*, 1509.

[17] (a) Imaz, I. Maspoch, D.; Blanco, C. R.; Falcon, J. M. P.; Campo, J.; Molina, D. R. *Angew. Chem. Int. Ed.*, **2008**, *47*, 1857. (b) Yang, J.; Ma, J. F.; Batten, S. R.; Su, Z. M. *Chem.Commun*., **2008**, 2233. (c) Sathiyendiran, M.; Wu, J. Y.; Velayudham, M.; Lee, G. H.; Peng, S. M.; Lu, K. L. *Chem. Commun*., **2009**, 3795. (d) Su, C. Y.; Cai, Y. P.; Chen, C. L.; Smith, M. D.; Kaim, W.; ZurLoye, H. C. *J. Am. Chem. Soc*., **2003**, *125*, 8595. (e) Lan, Y. Q.; Li, S. L.; Qin, J. S.; Du, D. Y.; Wang, X. L.; Su, Z. M.; Fu, Q. *Inorg. Chem*., **2008**, 10600.

[18] Li, R. Y.; Wang, B. W.; Wang, X. Y.; Wang, X. T.; Wang, Z. M.; Gao, S.; *Inorg. Chem.*, **2009**, *48*, 7174.

[19] (a) (b) Dhal, P. K.; Arnold, F. H. *Macromolecules*, **1992**, *25***,** 7051 (c) Ouellette, W.; Liu, H.; O'Connor, C. J.; Zubieta, J.; *Inorg. Chem.*, **2009**, *48*, 4655..

[20] (a) *SAINT: Software for the CCD Detector System*; Bruker Analytical X-ray Systems, Inc.: Madison, WI, **1998** (b) *SADABS: Program for Absorption Correction;* G. M. Sheldrick University of Gottingen: Gottingen, Germany, **1997**. (c) *SHELXS-97: Program for Structure Solution;* G. M. Sheldrick, University of Gottingen: Gottingen, Germany, **1997**. (d) *SHELXL-97: Program for Crystal Structure Analysis;* G. M. Sheldrick University of Gottingen: Gottingen, Germany, **1997**. (e) Blatov, V. A.; Shevchenko, A. P.; Serezhkin, V. N. J. Appl.Crystallogr. 2000, *33*, 1193. TOPOS software is available for download at http://www.topos.ssu.samara.ru.

[21] Li, Z. X.; Chu, X.; Cui, G. H.; Liu, Y.; Li, L.; Xue, G. L. *CrystEngComm*., **2011,** *13*, 1984

[22] Liu, M.; Li, X.; Li, J.; Sun, W.; Yang, Z.; Gang, F.; Chen, J.; Ma, J.; Yang, G. *Transition met Chem.*, **2009**, *34*, 185.

[23] (a) Wu, B.; Liang, J.; Zhao, Y.; Li, M.; Li, S.; Liu, Y.; Zhang, Y.; Yang, X-J. *CrystEngComm*, **2010**, *12*, 2129. (b) Zhang, L.; Yao, Y-L.; Che, Y-X.; Zheng, J-M. *Cryst. Growth Des*., **2009**, *10*, 528.

[24] (a) Tripuramallu, B. K.; Kishore, R.; Das, S. K. *Inorganica Chim Acta*, **2011**, 368, 132. (b) Lin, P.; Clegg, W.; Harrington, R. W.; Henderson, R. A. *Dalton trans.* **2005**, 2388. (c) Zhao, H.; Qu, Z. R.; Ye, H. Y.; Xiong, R. G.; *Chem. Soc. Rev.*, **2008**, *37*, 84.

[25] (a) Han, L.; Zhao, Y.; Zhao, W. N.; Li, X.; Liang, Y. X. *Cryst. Growth Des*., **2009**, *9*, 660.(b) Pachfule, P.; Dey, C.; Panda, T.; Banarjee, R. *CrystEngComm*., **2010**, *12*, 1600. (c) Ji, C. C.; Qin, L.; Li, Y. Z.; Guo, Z. J.; Zheng, H. G. *Cryst. Growth Des*., **2011**, 11, 480.

[26] (a) Wen, L.; Li, Y.; Lu, Z.; Lin, J.; Duan, C.; Meng, Q. *Cryst. Growth Des*., **2006**, *6*, 530. (b) Wen, L. L.; Dang, D. B.; Duan, C. Y.; Li, Y. Z.; Tian, Z. F.; Meng, Q. J. *Inorg. Chem.*, **2005**, *44*, 7161.

[27] (a) Su, C. Y.; Cai, Y. P.; Chen, C. L.; Zhang, H. X.; Kang, B. S. *J. Chem. Soc. ,Dalton Trans*. **2001**, 359. (b) Su, C. Y.; Cai, Y. P.; Chen, C. L.; Kang, B. S. *Inorg.Chem.* **2001**, *40*, 2210.

[28] (a) Modrow, A.; Zargarani, D.; Herges. R.; Stock, N. *Dalton trans.* **2011**, *40*, 4217.

[29] (a) Carlin, R. L. *Magnetochemistry*; Springer-Verlag: Berlin, Heidelberg, 1986. (b) Kahn,O. *Molecular Magnetism*; VCH: Weinheim,1993.

[30] Zhao, J. P.; Hu, B. W.; Yang, Q.; Zhang, X. F.; Hu, T. L.; Bu, X. H. *Dalton trans.* **2010**, *39*, 56.

Synthesis, Structural Characterization and Magnetic Properties of a Series of Coordination Polymers: Importance of Linker Coordination Angle in Tuning the Dimensionality

6

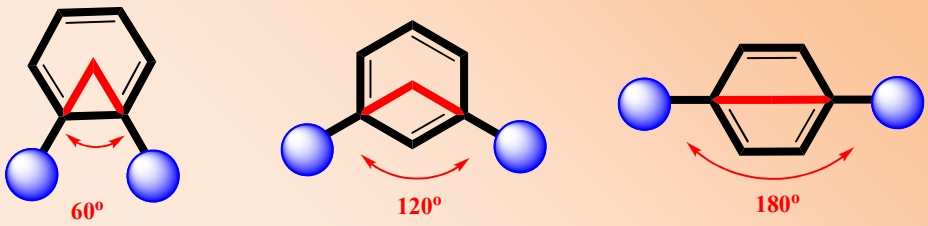

The chapter describes the synthesis and structural characterization of a series of coordination polymers emphasizing the role of angle between the coordinating groups in the linker. Here in we report the six new compounds $[Co(hfipbb)(1,2\text{-}bix)]_n \cdot nH_2O$ (**1**) $[Co(hfipbb)(1,3\text{-}bix)_{0.5}]_n$ (**2**) $[Co(1,2\text{-}pda)(1,2\text{-}bix)]_n$ (**4**) $[Co_2(\mu\text{-}OH)(1,3\text{-}pda)(4\text{-}ptz)]_n$ (**7**) $[Co(2\text{-}pztz)(1,4\text{-}pda)_2]_2[Co(H_2O)_6] \cdot 2nH_2O$ (**8**) $[Mn(2\text{-}pztz)(1,4\text{-}pda)_2]_2[Mn(H_2O)_6] \cdot 2nH_2O$ (**9**) *based on the flexible carboxylate ligands, namely, 1,2−phenylenediaceticacid (1,2−*H_2*pda), 1,3−phenylenediaceticacid (1,3−*H_2*pda), 4,4'-(hexa-fluoroisopropylidene)bis(benzoicacid) (*H_2*hfipbb) and secondary N-donor ligands 1,3−bis (imidazole-1-ylmethyl)-benzene (1,3−bix), 1,2−bis (imidazole-1-ylmethyl)-benzene (1,2−bix), 5-(4-Pyridyl) tetrazole (4−ptz) and 2-(2H-tetrazol-5-yl)pyrazine (2−pztz). The position of the coordinating groups in the linker is explained based on the linker coordination angles (LCA). A systematic comparison between the compounds **1**, **2**, with* $[Co(hfipbb)(1,4\text{−}bix)_{0.5}]_n$ (**3**), *4 with* $[Co(1,4\text{−}pda)(1,4\text{−}bix)]_n$ (**5**) *and* **7**-**9** *with* $[Co_2(\mu\text{-}OH)(1,4\text{-}pda)(4\text{-}ptz)]_n \cdot nH_2O$ (**6**) *reveals the role of LCA in tuning the dimensionality. When the coordinating groups in the linker are closer to each other i.e. having minimum LCA, the length of the ligand decreases and as a result low dimensional structures are observed in the crystals of compounds* **1**−**5** *. In the system containing flexible carboxylate and rigid tetrazole, if the flexible carboxylate adopts cis conformation, then the dimensionality of the structure solely depends upon the LCA of the tetrazole moiety as observed in the case of compounds* **6**−**9**. *Finally the temperature dependent magnetic susceptibility measurements of the compounds* **1**, **2** *and* **8** *are described demonstrating the antiferromagnetic interactions between the metal centers.*

6.1. Introduction

The design and synthesis of metal organic frameworks (MOFs) and coordination polymers (CPs) have become a focus of a great deal of interest in recent years due to not only their undisputed structural beauty and entangled architectures but also potential application in areas such as catalysis, gas storage, separation, magnetism, luminescence, nonlinear optics, sensing and so on.[1] The choice of linker plays an influential role in designing the target polymers depending on the geometry and properties, such as, position of the coordinating groups, flexibility or rigidity of the ligand and also the various coordination modes of the ligand.[2] Among those factors, the position of the coordinating groups on the linker plays an important role in fine tuning of the dimensionality. In case of designing the coordination polymers by using the mixed linkers, the position of the coordinating groups on the linker often plays a major role in directing the dimensionality.[3] The general position of the coordinating groups in the simple phenyl linker are ortho-, meta-, and para-bidentate modes. The angle between the coordinating groups in the linker, which is known as linker coordination angle (LCA), varies as the length and geometry of the spacer changes; as a result the overall skeleton geometry of the linker changes *i.e.* bent, V-shaped, linear etc. Zhou and co-workers reported the application of mixture of bridging linkers with different LCAs in coordination-driven self assembly process.[4] The coordination networks, based on rigid ligands exploiting the LCA, are extensively studied due to their regular and well defined coordination modes.[5] In contrast, flexible ligands are less explored in the rational design of coordination polymers, because it is difficult to predict the final architectures owing to their more number of degrees of freedom and hence few conformational restraints.[6]

Currently considerable effect is devoted to enriching the structural library of coordination networks based on the flexible ligands. The major parameters to be considered in designing the ditopic flexible ligand based-coordination networks are secondary ligand, coordination availability at the metal coordination sphere, length of the spacer and position of the coordinating groups etc. All these factors have tendency to modulate the conformations of the flexible ligands which is primarily responsible for obtaining the higher dimensional structures. Cao *et al*. reported a series of coordination polymers based on the flexible ligands and used these compounds as functional materials for potential applications[7]. In the previous chapter, we discuss the factors affecting the conformational modulation of flexible ligands by exploring the above mentioned factors. Wang et al.

reported a series of Zn^{2+} coordination polymers based on the position of the coordination groups in isomeric phenylene diacetates with rigid ligand, 4,4′-bipyridine and 1,2-dpe.[8] The literature reports of the mixed linker coordination networks, based on the flexible linkers, are very rare in exploiting the position of the coordinating groups in the linker. This concept prompted us to study the affect of the linker coordination angles of the various flexible ligands in designing the coordination networks.

We have chosen the phenylene diacetates,[9] bisimidazolyl nitrogen donors,[10] and rigid tetrazoles[11] in exploring the library of coordination networks by tuning linker coordination angles. We have described the synthesis, structural characterization of a series of coordination polymer containing compounds $[Co(hfipbb)(1,2-bix)]_n \cdot nH_2O$ (**1**) $[Co(hfipbb)(1,3-bix)_{0.5}]_n$ (**2**) $[Co(1,2-pda)(1,2-bix)]_n$ (**4**) $[Co_2(\mu\text{-}OH)(1,3-pda)(4-ptz)]_n$ (**7**) $[Co(2-pztz)(1,4-pda)_2]_2[Co(H_2O)_6] \cdot 2nH_2O$ (**8**) $[Mn(2-pztz)(1,4-pda)_2]_2[Mn(H_2O)_6] \cdot 2nH_2O$ (**9**). These compounds are compared with the compounds, that are reported in the previous chapter, namely, $[Co(hfipbb)(1,4-bix)_{0.5}]_n$ (**3**) $[Co(1,4-pda)(1,4-bix)]_n$ (**5**) and $[Co_2(\mu-OH)(1,4-pda)(4-ptz)]_n \cdot nH_2O$ (**6**) in exploring the effect of the LCA.

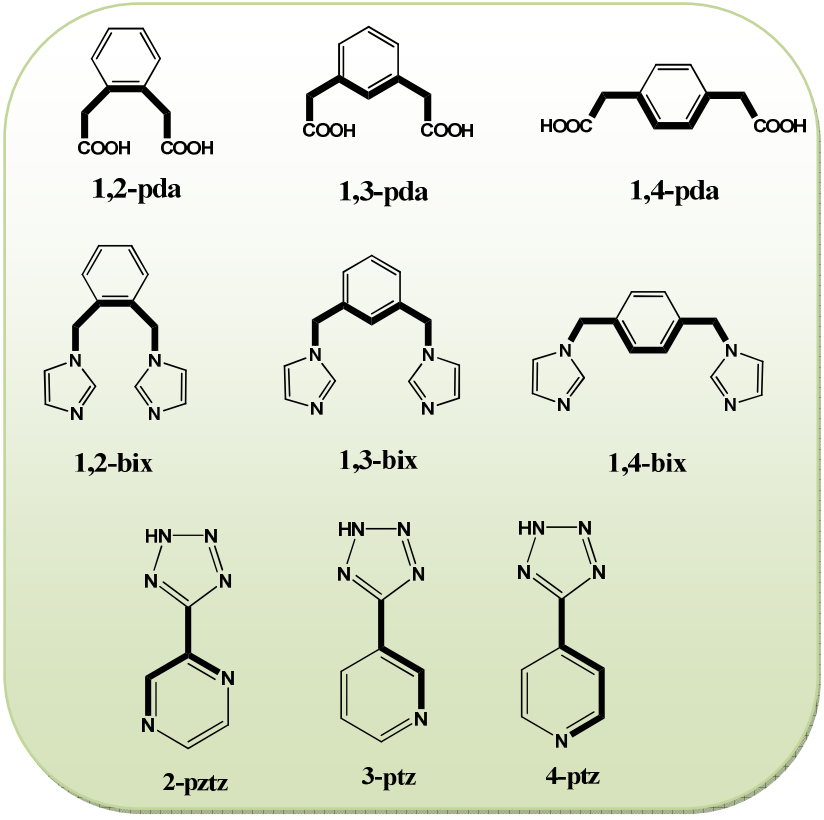

Scheme 6.1. Different class of linkers with possible linker coordination angles employed in this work.

6.2. Experimental Section

6.2.1. Materials and methods

All the chemicals were received as reagent grade and used without any further purification. The ligands 1,4−bix, 1,3−bix, 1,2−bix, 4−ptz, 2−tzpyz were prepared according to the literature procedures.[12] Elemental analyses were determined by FLASH EA series 1112 CHNS analyzer. Infrared spectra of solid samples obtained as KBr pellets on a JASCO – 5300 FT – IR spectrophotometer. Thermogravimetric analyses were carried out on a STA 409 PC analyzer and corresponding masses were analyzed by QMS 403 C mass analyzer, under flow of N_2 gas with a heating rate of 5 ^oC min^{-1}, in the temperature range of 30-1000 ^oC. Powder X-ray diffraction patterns were recorded on a Bruker D8-advance diffractometer using graphite monochromated $CuK_{\alpha1}$ (1.5406 Å) and $K_{\alpha2}$ (1.54439 Å) radiations. The electronic absorption spectra have been recorded on a Cary 100 Bio UV-visible spectrophotometer at room temperature. Magnetic susceptibilities were measured in the temperature range 2–300 K on a Quantum Design VSM-SQUID. All the compounds were synthesized in 23 mL Teflon-lined stainless vessels (Thermocon, India). Synthesis of the compounds **3**, **5** and **6** are described in the previous chapter.

6.2.2. Synthesis

Synthesis of $[Co(hfipbb)(1,2-bix)]_n \cdot nH_2O$ (1)

A mixture of $CoCl_2 \cdot 6H_2O$ (0.25 mmol, 59.5 mg), H_2hfipbb (0.25 mmol, 98.0 mg) and 1,2−bix (0.25 mmol, 60.0 mg) was dissolved in assorted solvent mixture of H_2O (10.0 mL) + DMF (1.0 mL) and stirred for 30 min. The pH of the reaction mixture was adjusted to 6.10 by adding 5M NaOH and placed in a 23 mL Teflon-lined stainless steel autoclave, which was sealed and heated at 160 °C for 72 h. The autoclave was allowed to cool to room temperature for 48 h. Deep red block crystals of compound **1** were obtained in 65.5% yield (based on Co). Anal. Calcd. (%) for $C_{31}H_{22}N_4F_6O_5Co$ (M_r = 703.46): C, 52.93; H, 3.15; N, 7.96. Found: C, 52.6; H, 2.98 N, 7.48. IR (KBr pellet, cm^{-1}): 3516, 3138, 3015, 1699, 1612, 1556, 1518, 1462, 1244, 1170, 1091, 968, 949, 777, 717, 653.

Synthesis of $[Co(hfipbb)(1,3-bix)_{0.5}]_n$ (2)

Compound **2** was prepared by the same procedure as that for compound **1** except that ligand 1,3−bix was used in place of 1,2−bix. The resulting purple block crystals were collected by filtration in 80.2% yield (based on Co). Anal. Calcd. (%) for $C_{24}H_{15}CoN_2F_6O_4$

(M_r = 568.31): C, 50.72; H, 2.66; N, 4.92. Found: C, 50.34; H, 2.28; N, 4.68. IR (KBr pellet, cm^{-1}): 3425, 3126, 3015, 2858, 1693, 1518, 1410, 1240, 1170, 1020, 945, 929, 779, 652.

Synthesis of $[Co(1,2-pda)(1,2-bix)]_n$ (4)

The compound **4** was prepared following the same procedure as mentioned in compound **1** except that 1,2–H_2pda was used instead of H_2hfipbb and the pH was adjusted to 7.35. Red block crystals of **5** were obtained in 60.3% yield (based on Co). Anal. Calcd. (%) for $C_{24}H_{22}CoN_4O_4$ (M_r = 489.39): C, 58.90; H, 4.53; N, 11.44. Found: C, 58.45; H, 4.35; N, 11.01. IR (KBr pellet, cm^{-1}): 3140, 2997, 2916, 1695, 1572, 1520, 1369, 1265, 1226, 1024, 949, 852, 810, 748, 721, 657.

Synthesis of $[Co_2(\mu\text{-}OH)(1,3-pda)(4-ptz)]_n$ (7)

A mixture of $CoCl_2 \cdot 6H_2O$ (0.50 mmol, 119 mg), 1,3−pda (0.25 mmol, 48.5 mg) and 4−ptz (0.25 mmol, 36.65 mg) was dissolved in 10 mL distilled H_2O which was adjusted to pH = 4.20 with 5 M NaOH. The final mixture was sealed in a 23 mL Teflon−lined stainless steel autoclave and heated at 180 °C for 3 days. Dark red block crystals were obtained that were filtered off and collected in 55.2% yield. Anal. Calcd. (%) for $C_{16}H_{12}Co_2N_5O_5$ (M_r = 472.17): C, 40.70; H, 2.56; N, 14.83. Found: C, 40.15; H, 2.02; N, 14.09%. IR (KBr pellet, cm^{-1}): 3574, 1614, 1601, 1442, 1419, 1394, 1290, 1221, 974, 842, 760, 715, 630.

Synthesis of $[Co(2-pztz)(1,4-pda)_2]_2[Co(H_2O)_6]\cdot 2nH_2O$ (8)

A mixture of $CoCl_2 \cdot 6H_2O$ (0.50 mmol, 119.0 mg), 1,4-pda (0.25 mmol, 48.5 mg) and 2-pztz (0.25 mmol, 37 mg) in H_2O (10.0 mL) was stirred for 30 min and the pH of the reaction mixture was adjusted to 5.4 by adding 5M NaOH. The reaction mixture was placed in a 23 mL Teflon-lined stainless steel autoclave it was then sealed and heated at 130 °C for 96 h. The autoclave was allowed to cool to 30 °C for 48 h. Deep red block crystals of compound **8** were obtained in 65.5% yield (based on Co). Anal. Calcd. (%) for $C_{30}H_{38}Co_3N_{12}O_{16}$ (M_r = 999.51): C, 36.05; H, 3.83; N, 16.81. Found: C, 35.15; H, 3.24; N, 16.69. IR (KBr pellet, cm^{-1}): 3362, 3026, 2926, 1684, 1616, 1574, 1523, 1410, 1253, 1170, 972, 935, 842, 746.

Synthesis of $[Mn(2-pztz)(1,4-pda)_2]_2[Mn(H_2O)_6]\cdot 2nH_2O$ (9)

Compound **9** was prepared in the same way as described for compound **8,** by using $MnCl_2\cdot 4H_2O$ (0.50 mmol, 99 mg) in place of $CoCl_2\cdot 6H_2O$; a large quantities of colorless crystals were obtained that were filtered off. The yield of the reaction was 78.9% (based on Mn). Anal. Calcd. (%) for $C_{30}H_{38}Mn_3N_{12}O_{16}$ (M_r = 987.52): C, 36.48; H, 3.87; N, 17.02. Found: C, 36.02; H, 3.17; N, 16.85. IR (KBr pellet, cm^{-1}): 3489, 3290, 1668, 1583, 1514, 1400, 1188, 1151, 1035, 856, 769, 677.

6.2.3. Single crystal X-ray structure determination of the compounds 1, 2, 4, 7-9

Single-crystals, suitable for structural determination of all the compounds (**1, 2 ,4, 7-9**), were mounted on a three circle Bruker SMARTAPEX CCD area detector system under Mo-Kα (λ=0.71073A) graphite monochromated X-ray beam, crystal to detector distance 60 mm, and a collimator of 0.5 mm. The scans were recorded with an ω scan width of 0.3º. Data reduction performed by SAINTPLUS,[13a] empirical absorption corrections using equivalent reflections performed by program SADABS,[13b] structure solution using SHELXS-97[13c] and full-matrix least-squares refinement using SHELXL-97[13d] for above compounds. All the non-hydrogen atoms were refined anisotropically. Hydrogen atoms on the C atoms were introduced on calculated positions and were included in the refinement riding on the irrespective parent atoms. Crystal data, structure refinement parameters for all the compounds **1**, **2**, **4**, **7**−**9** are summarized in Table 6.2. Topological analysis of the compounds were performed by using the TOPOS software.[13e]

6.3. Results and discussion

6.3.1. Synthesis

For a systematic investigation of the effect of linker coordination angles, the flexible phenylendiacetates, bis (imidazole-1-ylmethyl)-benzene, bent carboxylate ligand H_2hfipbb and rigid tetrazoles were used. We adopted the hydrothermal technique, as the high temperature and high pressure during the reaction drastically increase the solubility and the reactivity of the reactants. Many factors such as pH, temperature, metal–ligand stoichiometry, reaction time, versatility of metal coordination geometry are all important in the formation of final products. We have taken the d^7 metal atom Co(II) [$CoCl_2\cdot 6H_2O$] and d^5 metal atom Mn(II) [$MnCl_2\cdot 6H_2O$] as the metal source in the synthesis of the compounds. The syntheses were performed at 180 ºC for compounds **1**, **2**, **4** and **7** and 130°C for **8** and **9** in water. Since H_2hfipbb is highly insoluble in water; assorted solvent

water/DMF (5:1) is used in case of compound **1** and **2** instead of only water. All the complexes are air stable and insoluble in water.

6.3.2. Linker Coordination Angle (LCA)

In ditopic ligands, the coordination angle between the two coordinating groups is called as a linker coordination angle. For a simple phenyl linker, three different linker coordination angles (i.e. 60°, 120°, and 180°) between the two coordinating groups are possible. Different terminologies are used to represent position of the coordinating groups in the linker such as, ortho, meta, para and (1,4)-, (1,3)-, and (1,2)- etc. In case of designing coordination architectures with mixed linkers, the LCAs of both the linkers should be considered in obtaining the desired topologies. The task becomes more difficult in case of flexible ditopic linkers as far as designing and analyzing are concerned. An important point to remember in quantifying the LCA is that it is different from the dihedral angle between the two coordinating groups and angle between two coordinating atoms. It is notable that LCA for a ligand is maintained same even though the conformations, coordination modes and coordinating groups vary; it depends only on the position of the coordinating groups in the linker. The LCAs of the ligands phenylenediacetates, bis (imidazole-1-ylmethyl)-benzene, bent carboxylate ligand H_2hfipbb and rigid tetrazoles, employed in this work, are shown in the following Table 6.1.

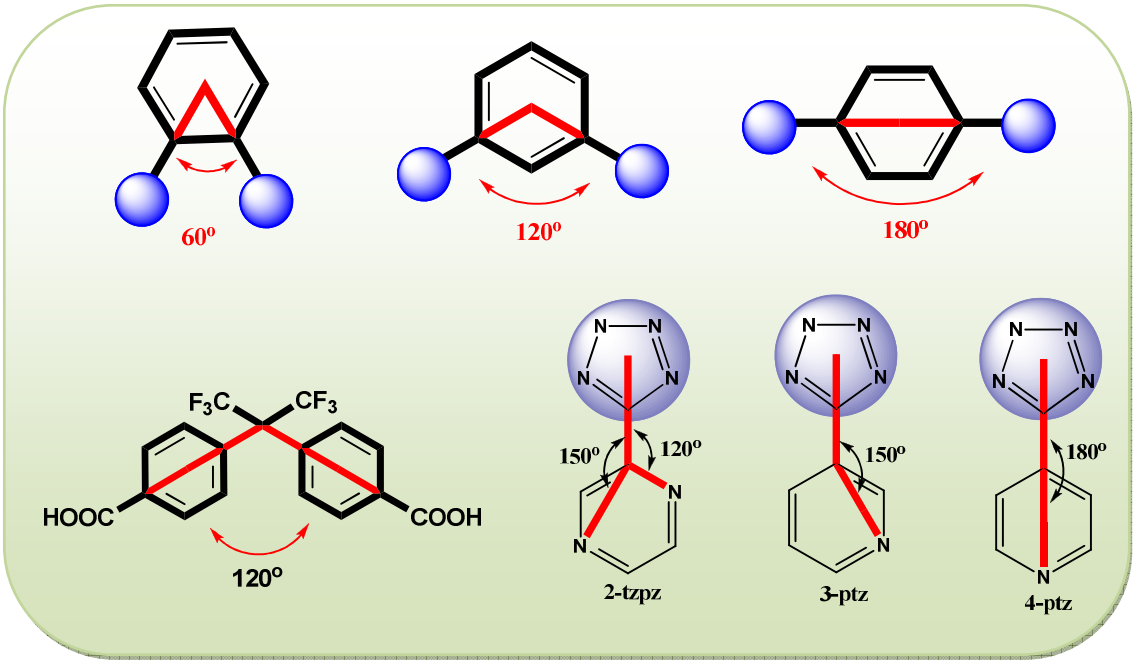

Scheme 6.2. Schematic representation of linker coordination angles of the flexible ligands.

Table 6.1. Linker coordination angles of various linkers employed in this work (see scheme 6.2).

Ligand name	**1,4-**	**1,3-**	**1,2-**
pda	1,4−pda =180°	1,3−pda =120°	1,2−pda =60°
bix	1,4−bix =180°	1,3−bix =120°	1,2−bix =60°
ptz	4−ptz =180°	3−ptz =150°	2−ptz =120° 2−pztz =120°,150°
hfipbb	4,4′−hfipbb =120°		

In case of tetrazole ligands, as shown in the scheme 6.2, the LCA is measured between the tetrazole core ring and the position of the nitrogen atom in the pyridine ring.

6.3.3. Description of crystal structures

Structural description of $[Co(hfipbb)(1,2\text{-}bix)]_n \cdot nH_2O$ (1)

Compound **1** is a 2D extended coordination polymer that crystallizes in orthorhombic space group *ccca*. The crystal structure consists of Co(II) atom in a tetrahedral $\{CoN_2O_4\}$ center constituted by the oxygen atoms from two different $hfipbb^{2-}$ units, and nitrogen atoms from two different 1,2−bix ligands and one lattice water molecule as shown in the Figure 6.1a. Both the carboxylate groups in the $hfipbb^{2-}$ coordinates to the metal center in μ_1-η_1,η_0 coordination mode. The dihedral angle between the two benzene rings in the $hfipbb^{2-}$ anion is 74.77°, which is larger than that of 68.57° in the neutral H_2hfipbb ligand. The connectivity of $hfipbb^{2-}$ anions with the metal centers result in the formation of 1D metal acid zig-zag chains along the crystallographic *b* axis as shown in the Figure 6.1b. The metal-hfipbb systems are very well known in the literature for the formation of paddle-wheel structures containing open coordination site at the metal apical position, which is used to extend the dimensionality by the N-donor ligands.[14]

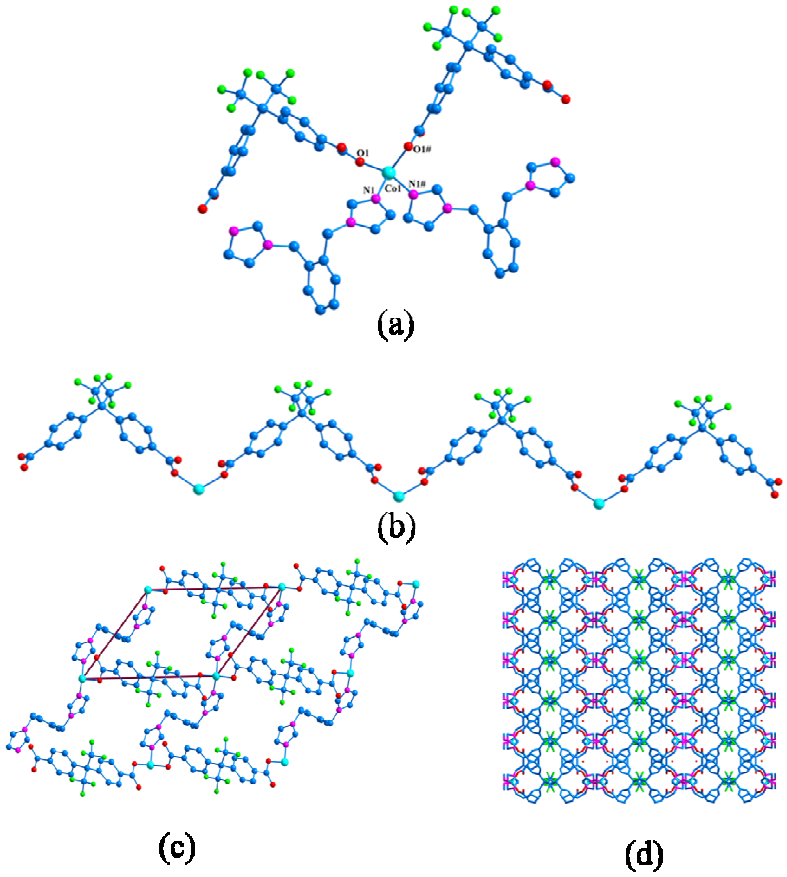

Figure 6.1. (a) Molecular diagram of compound **1** in atom labeling scheme at coordination sphere, (b) 1D Co-hfipbb zig-zag chains. (c) 2D (4,4) connected topology viewing the square grid, (d) 3D stacking of 2D layers showing the two different types of cavities.

In the crystal structure of compound **1**, metal-hfipbb forms 1D chains; these chains are extended to form a 2D (4,4) connected sheets with the aid of 1,2-bix ligands.[15] 1,2-bix ligand connects the Co(II) atoms of the adjacent 1D chains in a typical *trans* conformation with antiperiplanar torsion angle of 151.84 ° (viewed through N2−C13−C13−N2) and creates a separation of 10.236 Å between the two chains. The overall connectivity of 1,2−bix ligands with the metal acid chains result in the formation of (4,4) corrugated sheets with dimensions of 13.177 X 10.236 Å (Figure 6.1c). The 2D layers of compound **1** are stacked along each other to form two different types of cavities *i.e* fluorinated cavities and non fluorinated cavities in which lattice water molecules are presented as shown in the Figure 6.1d.

Structural description of $[Co(hfipbb)(1,3\text{-}bix)_{0.5}]_n$ (2) and $[Co(hfipbb)(1,4\text{-}bix)_{0.5}]_n$ (3)

Both the compounds **2** and **3** are isostructural and crystallize in monoclinic space group $P2_1/c$. The secondary ligand 1,4−bix in the compound **3** is replaced by the 1,3−bix[16] to

form a compound **2**. The dimensionality and topology of both the structures are similar except the structural parameter allied to the secondary ligand that varies. In compound **3** the separation created by the 1,4−bix ligand between the metal acid layers is 14.81 Å, and the separation created by the 1,3−bix in compound **2** is almost similar i.e.14.63 Å. 1,3−bix ligand in compound **2** exists in typical *trans* conformation with anticlinal torsion angle of 136.75° and the dihedral angles between the imidazole rings with the least squares plane of phenyl ring are 66.51° and 64.67°.

Structural description of $[Co(1,2-pda)(1,2-bix)]_n$ (4) and $[Co(1,4-pda)(1,4-bix)]_n$ (5).

Compound **5** is a 3D coordination polymer and the structural details are previously reported whereas, compound **4** is 2D coordination polymer that crystallizes in monoclinic space group $P2_1/c$. The asymmetric unit consists of one crystallographic independent Co(II) atom in tetrahedral geometry, one 1,2−pda^{2-} and one 1,2−bix ligands. The tetrahedral geometry around Co(II) atom is constituted by two oxygen atoms from two different 1,2−pda^{2-} ligands and two nitrogen atoms from two different 1,2−bix ligands (Figure 6.2a). The carboxylate 1,2−pda^{2-} coordinates to the Co(II) center in μ_1-η_1,η_0 coordination mode on either sides and connects the adjacent Co(II) tetrahedra in a typical *trans* conformation with anticlinal torsion angle of 132.64° (viewed through N4-C24-C14-N2). The acetate side chains twisted with respect to phenyl through various extents *i.e*. 101.46° (through C4−C3−C2−C1) and 96.92° (through C7−C8−C9−C10). 1,2-pda^{2-} separates the two Co(II) centers with a distance of 8.512 Å to form a 1D metal-acid chains along the crystallographic *a* axis (Figure 6.2b). These chains are connected to each other with the aid of 1,2−bix ligands along the *b* axis to form a 2D layer in the *ab* plane. 1,2−bix connects the Co(II) atoms of the adjacent chains in a typical *trans* conformation with antiperiplanar torsion angle of 151.22° (viewed through N4−C24−C14−N2) and creates of separation of 12.114 Å between the two metal centers. The dihedral angles between the imidazole ring planes and the least-squares plane of phenyl group are 74.01° and 77.50° respectively. The connectivity of the 1,2−bix to the metal acid chains result in the formation of 2D (4,4) connected sheets with dimensions of 12.114 X 8.512 Å (Figure 6.2c). The presence of flexibility in the ligands, employed, result in the formation of wave like layers with crest and troughs at metal acid chains. These layers are stacked along the *c* axis and the adjacent layers are tilted to ~ 7 Å and the alternate layers are arranged in back-to-back fashion as shown in the Figure 6.2d.

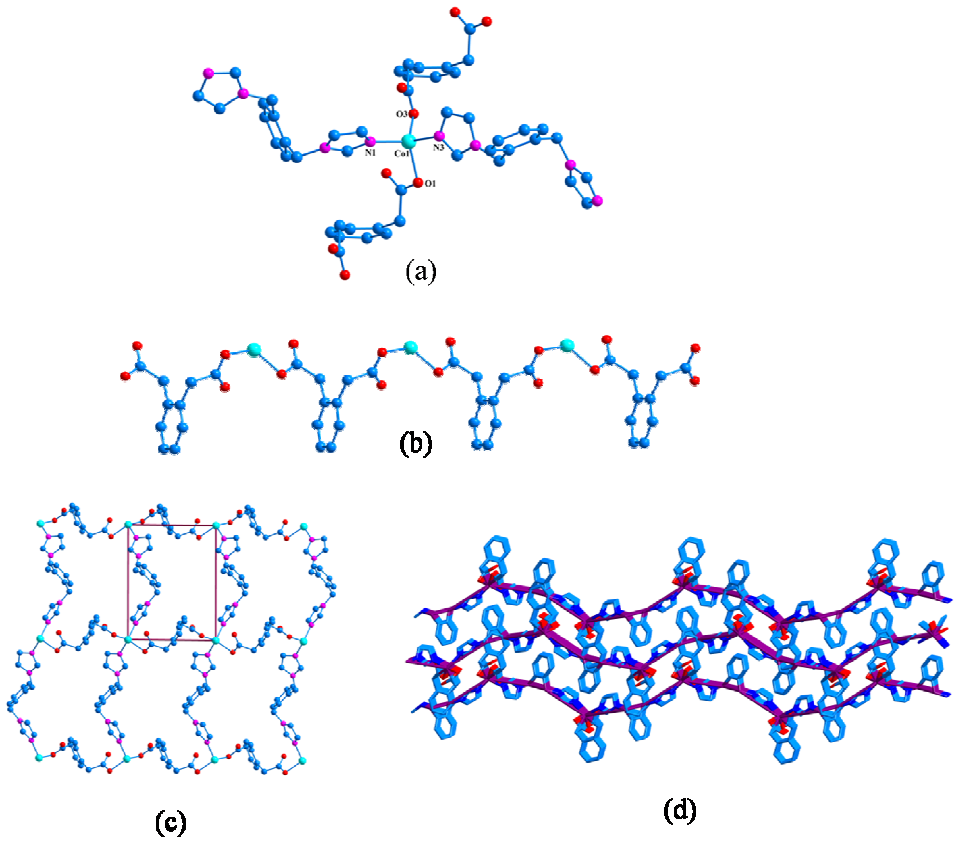

Figure 6.2. (a) Molecular diagram of compound **2** in atom labeling scheme at coordination sphere, (b) 1D Co−1,2-pda zig-zag chains, (c) 2D (4,4) connected topology viewing the square grid, (d) 3D stacking of 2D layers showing the tilting between two layers.

Structural description of $[Co_2(\mu\text{-}OH)(1,4\text{−}pda)(4\text{−}ptz)]_n \cdot nH_2O$ (6) and $[Co_2(\mu\text{-}OH)(1,3\text{−}pda)(4\text{−}ptz)]_n$ (7)

Both the compounds are crystallized in monoclinic space group $P2_1/n$. The compounds **6** & **7** are isostructural except the carboxylate ligand 1,4−pda in **6** is replaced by the 1,3-pda in **7** and a lattice water molecule present in the compound **6**, which is absent in compound **7**. The structural description of the compound **6** was elucidated in previous chapter; herein, we describe the structural consequences obtained by replacing 1,4−H_2pda with 1,3−H_2pda in terms of torsion angles and length of the ligand etc. The asymmetric unit of compound **7** consists of two Co(II) atoms in tbp geometry connected by the μ_2-hydroxy group and one 1,3−pda^{2-} and 4−ptz^{1-} anion. Both the acetate groups in the 1,3−pda^{2-} anion adopts μ_2-η_1,η_1 coordination mode in a typical *cis* conformation with synclinal torsion angle of 29.84° (viewed through C8−C7−C9−C10), whereas the torsion angle exhibited by the acetate side chains of 1,4−pda^{2-} in compound **6** is 2.30 Å. A very slight structural changes observed in the metallocycles formed due to *cis* connectivity of the carboxylate ligands *i.e.* 22-membered macrocycle with dimensions of 7.531 X 8.109 Å was observed in case of

1,4-pda^{2-} in compound **6** whereas, 20-membered macrocycle with dimensions of 8.322 X 7.946 Å was formed in case of 1,3−pda^{2-} in compound **7**. Also the benzene rings in the metallocycle formed in compound **6** are faced parallel to each other due to 1,4−connectivity in the pda^{2-} ligand, but the benzene rings are not faced parallel to each other in compound **7** due to 1,3−connectivity in the pda^{2-} ligand (Figure 6.3). The connectivity of the metallocycles and tetrazole rings in compound **7** is almost similar to compound **6** to form 2D sheets. The lattice water molecule present in the void space created by the metallocycles in the compound **6** is not presented in the compound **7**. The increase in size of the metallocycle due to 1,3−pda^{2-}, increases the cell volume to ~5.01 % when compared to compound **6**.

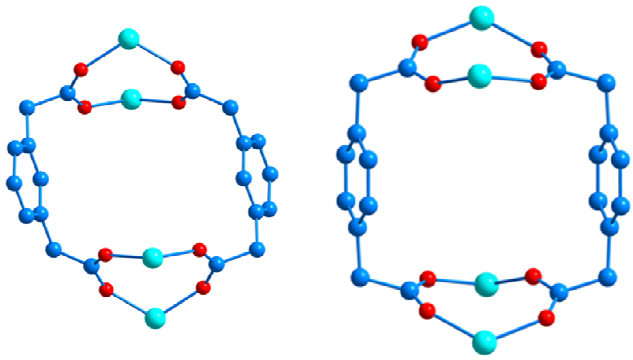

Figure 6.3. Metallocycles formed due to cis connectivity of 1,3−pda^{2-} and 1,4−pda^{2-} in compound **7** (left) and compound **6** (right) respectively.

Structural description of [Co(2-pztz)(1,4-pda)$_2$]$_2$[Co(H$_2$O)$_6$]·2*n*H$_2$O (8) and [Mn(2-pztz)(1,4-pda)$_2$]$_2$[Mn(H$_2$O)$_6$]·2*n*H$_2$O (9)

Both the compounds **8** and **9** are isomorphous, so, here we describe only the structural description of compound **8**. Compound **8** is 1D ion pair compound that crystallizes in triclinic space group *P-1*. The molecular diagram consists of 1D anionic chain [Co(2−pztz)(1,4−pda)$_2$]$^{2-}$ whereby the charge is compensated by cationic [Co(H$_2$O)$_6$]$^{2+}$ units. The repeating unit in the 1D chain consists of two crystallographic independent Co(II) atoms in tbp geometry bridged by the two 2−pztz^{1-} ligands[17] and connected to four 1,4−pda^{2-} ligands (Figure 6.4a). The tbp geometry of each Co(II) atom in the anionic chain is furnished by three nitrogen atoms from two different 2−pztz^{1-} ligands in the basal plane and two 1,4−pda^{2-} ligands in the apical positions. The tetrazole rings of two 2−pztz^{1-} ligands bridges the two Co(II) atoms (through the adjacent nitrogen atoms N3 and N4) to form a six membered dimer ring with 4.179 Å of Co−Co separation, also the pyrazine nitrogen atom N1 of 2−pztz^{1-} ligand coordinates to the Co(II) atoms. The overall

connectivity of 2−pztz^{1-} ligands to metal centers result in the formation of the Co-dimer {Co_2(2−pztz)$_2$} rings as shown in the Figure 6.4b. The 2−pztz^{1-} in the crystal structure exhibits a μ_3 coordination mode (μ_2 from tetrazole ring and μ_1 from pyrazine ring) and the other nitrogen atom N2 in the pyrazine ring remains uncoordinated. The {Co_2(2−pztz)$_2$} dimer connects to other dimer through a two pairs of 1,4−pda^{2-} ligands in a typical *cis* conformation. Each 1,4−pda^{2-} coordinates to the metal center through μ_1 coordination mode and the acetate side chains in the skeleton are twisted with respect to each other through a synclinal torsion angle of 49.06 Å (viewed through C11−C12−C17−C18) indicating typical *cis* conformation. The presence of 1,4−pda^{2-} in the *cis* conformation results in the formation of {Co_2(1,4−pda)$_2$} molecular loops as shown in the Figure 6.4c; overall, the connectivity of these loops with the dimers result in the formation of 1D extended chain along the crystallographic *c* axis as shown in the Figure 6.4d. The hexa aqua cobalt(II) cations compensate the charge of the anionic chains and stays as a lattice component. From the crystal packing diagram [Co(H_2O)$_6$]$^{2+}$ cations are located between the two adjacent chains along the plane and nearly sandwiched between the two {Co_2(1,4−pda)$_2$} loops along with the lattice water molecules (Figure 6.4e). As anticipated, due to presence of lattice water molecules and coordinated water molecules in the hexa aqua cationic complex, strong hydrogen bonding were expected.

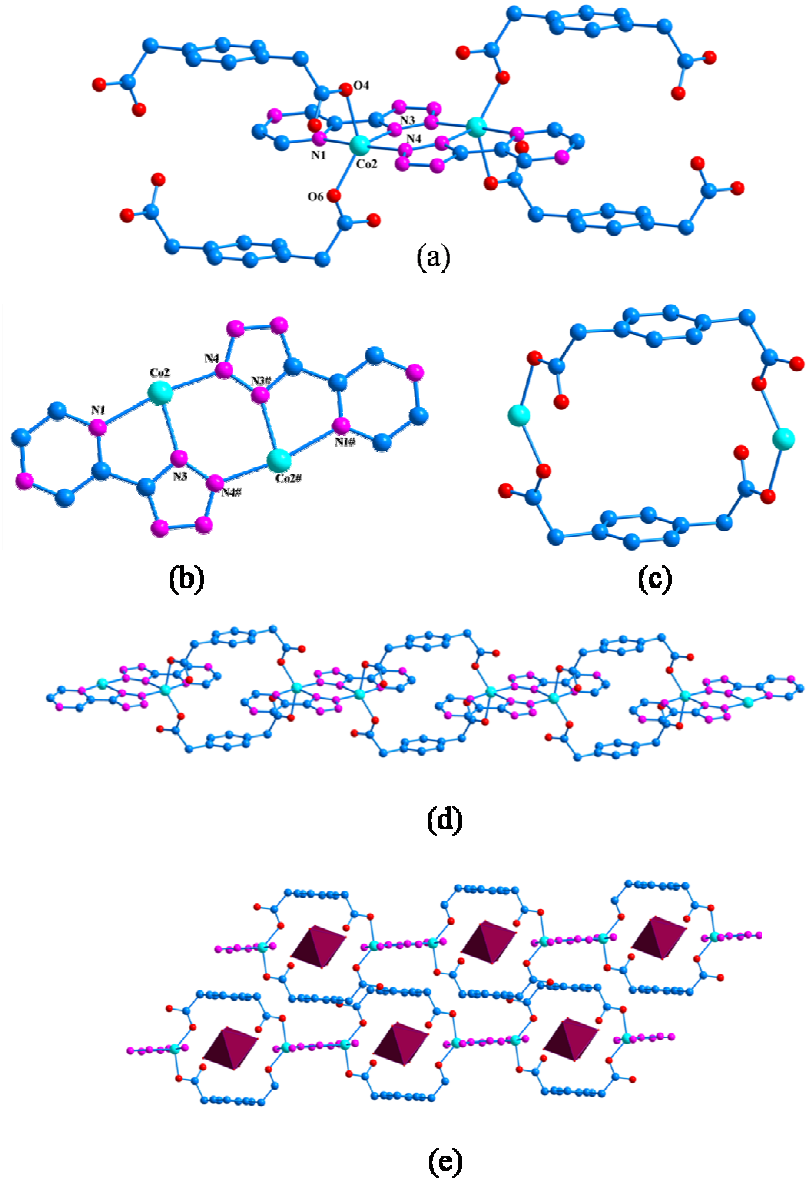

Figure 6.4. (a) Molecular diagram of compound **7** in atom labeling scheme at coordination sphere.(hexaaquacobaltate ion has been now shown), (b) Six-membered Co-dimer ring formed due to tetrazole coordination, (c) Molecular loop formed due to cis connectivity of the 1,4-pda^{2-} ligand,(d) 1D extended chain formed due to connectivity of 2-pztz and 1,4-pda ligands, (e) 2D packing diagram illustrating the position of cationic species in the cavities.

Affect of linker coordination angle (LCA) in tuning the dimensionality of the coordination architecture

Scheme 6.1, displays the possible LCAs of the phenylenediacetates bis (imidazole-1-ylmethyl)-benzene, bent carboxylate ligand hfipbb and rigid tetrazoles. The combination of these linkers in constructing the mixed linker coordination networks will often lead to intriguing dimensionalities. The compounds presented in the study are present under three different schemes (Schemes 6.3-6.5) to visualize the rational affect of the linker coordination angle.

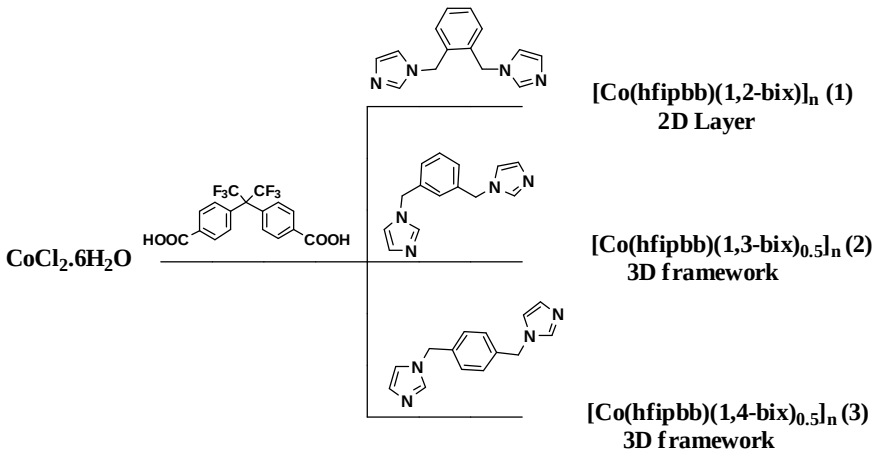

Scheme 6.3. Affect of dimensionality by changing the linker coordination angle of the isomeric bis (imidazole-1-ylmethyl)-benzene (bix) ligands with the metal-hfipbb system.

As shown in the Scheme 6.3, the compounds **1**, **2** and **3** are constituted by the Co-hfipbb−(1,n)-bix (n=2,3,4) composition matrix. Compound **1** is a 2D structure and compounds **2**, **3** are 3D layered-pillared isostructural frameworks. All the compounds contain metal-hfipbb networks which are extended by the bix ligands. In compound **1** metal-hfipbb form a 1D chains which are connected by the 1,2−bix ligands to form 2D layers. But, in compounds **2** and **3** metal-hfipbb form a 2D helical double layers which are connected by the 1,3−bix (for **2**) and 1,4−bix (for **3**) to form a 3D layered-pillared frameworks. The linker coordination angles of 1,3−bix and 1,4−bix are 120° and 180° respectively; as a result the length of the ligands in the crystal structures are 10.75 Å and 11.21 Å respectively. The linker coordination angle of 1,2−bix is 60°, as a result the length of the ligand in the *trans* conformation is 7.75 Å. The longer ligands 1,3−bix and 1,4−bix favor the formation of metal-carboxylate paddlewheel layers in compounds **2** and **3**, since the length of the secondary ligand (1,4−bix or 1,3−bix) can separate these layers with definite distance to reduce the intermolecular repulsions. But the shorter secondary ligand 1,2−bix does not favor the formation of metal-carboxylate layers; as a result the metal-hfipbb forms a 1D chain.

In all the three compounds the secondary bix ligand adopts a *trans* conformation with variable torsion angles (151.84° for **1**, 136.75° for **2** and 180° for **3**). Even though, the torsional displacement of imidazole rings in 1,3−bix ligand in **2** is less compared to **3** but the length of the 1,3−bix ligand is similar to 1,4−bix in **3** (14.81 for 1,4−bix and 14.63 for 1,3−bix), as a result 1,3−bix and 1,4−bix assisted compounds are isostructural.

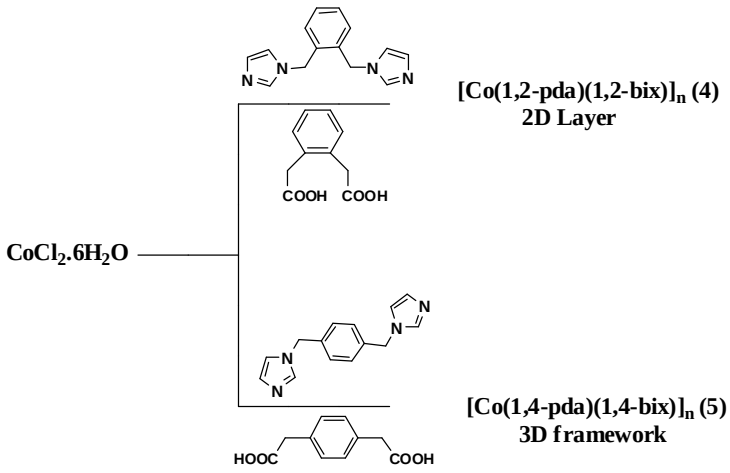

Scheme 6.4. Affect of dimensionality by changing the linker coordination angle of the isomeric bis (imidazole-1-ylmethyl)-benzene (bix) ligands and phenylene diacetate ligands.

As shown in the Scheme 6.4, the connectivity of 1,2−pda and 1,2−bix result in the formation of 2D layers in compound **4** and 1,4−pda and 1,4−bix result in the formation of 3D framework in compound **5**. In both the compounds, the Co(II) atom is presented in the same $\{CoN_2O_4\}$ tetrahedral geometry, but the linker coordination angle (LCA) changes the dimensionality of the compounds. In compound **4** the LCA's of both the ligands are 60° whereas, the LCA's of the ligands in compound **5** are 180°. The difference in these angles changes the length of the ligand as a result the annex of the ligand changes. The ligand with least LCAs generally creates the minimum separation between the metal polyhedra. The separation created by the 1,2−pda and 1,2−bix ligands in compound **4** is 8.512 Å and 12.114 Å respectively, while the separation created by the 1,4−pda and 1,4−bix ligands in compound **5** is 12.80 Å and 15.09 Å. Due to more length, the ligands protrude outside the layer to form a 3D framework, whereas, the short ligand connects to the metal centers in the same layer.

In both the compounds **4** and **5**, the carboxylate ligands (1,2−pda and 1,4−pda) and N-donor secondary ligands (1,2−bix and 1,4−bix) adopt a *trans* conformation. The flexibility of the ligands is one among the reason for the longer ligands to protrude outside the 2D plane to form 3D structure (**5**) and for shorter ligands to hang about in the same plane (**4**). Compounds **4** and **5** are mixed linker coordination networks in which both the linkers exhibit same LCA values *i.e* either 60° and 60° in **4** and 180° and 180° in **5**. Perhaps in this system the lower LCAs form 2D structures and higher LCAs form 3D structures and the linkers with mixed LCAs form either 2D or 3D only.

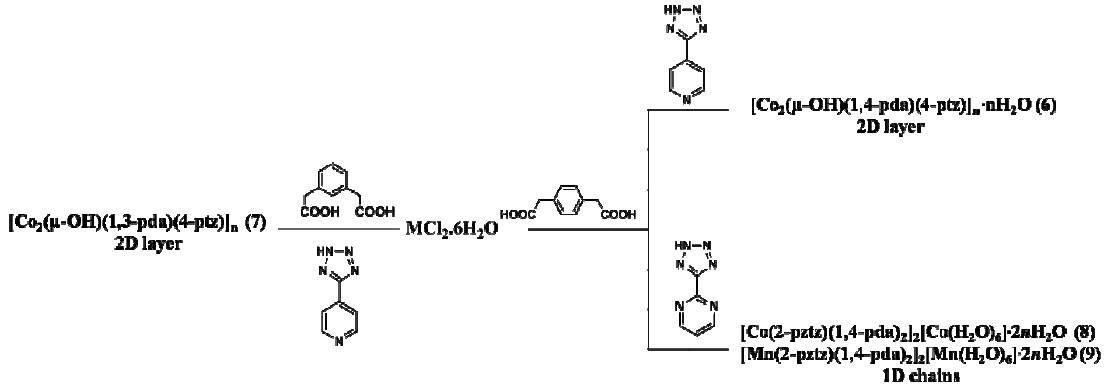

Scheme 6.5. Affect of dimensionality by changing the linker coordination angle of the isomeric phenylene-diacetate ligands with different rigid tetrazole ligands.

As shown in the Scheme 6.5, both the compounds **6** and **7** are isostructural even though the LCAs of the carboxylate ligands are 180° in **6** and 120° in **7**. In the case of compounds **6** and **7**, the flexible carboxylate ligands adopt the *cis* conformation which primarily decreases the dimensionality. Usually *cis* conformations form low dimensional structures whereas *trans* conformations form high dimensional structures. In this scenario, the other factor *i.e* LCA of secondary ligand plays an important role in tuning the dimensionality. In compounds **6** and **7**, the secondary ligand is 4-ptz with LCA of 180° as a result these compounds are 2D structures. Whereas, in compounds **8** and **9**, 1,4-pda adopts *cis* conformation and the dimensionality of the compounds is one, this is because the secondary ligand 2-tzpz has an LCA of 60°. As a result in the compounds where flexible ligands adopt *cis* conformation the LCA of secondary ligand plays an important role in modifying the dimensionality of the final architectures.

6.3.5. XRPD and Thermogravimetric analysis

To ensure the phase purity of the products, X-ray powder diffraction data for all the compounds have been recorded. Similar diffraction patterns for the simulated data (calculated from single crystal data) and observed data prove the bulk homogeneity of the crystalline solids (Figure 6.5). Although the experimental patterns have a few un-indexed diffraction peaks and some are slightly broadened and shifted in comparison to those simulated from the single-crystal data, it can still be regarded that the bulk as-synthesized materials represent compounds.

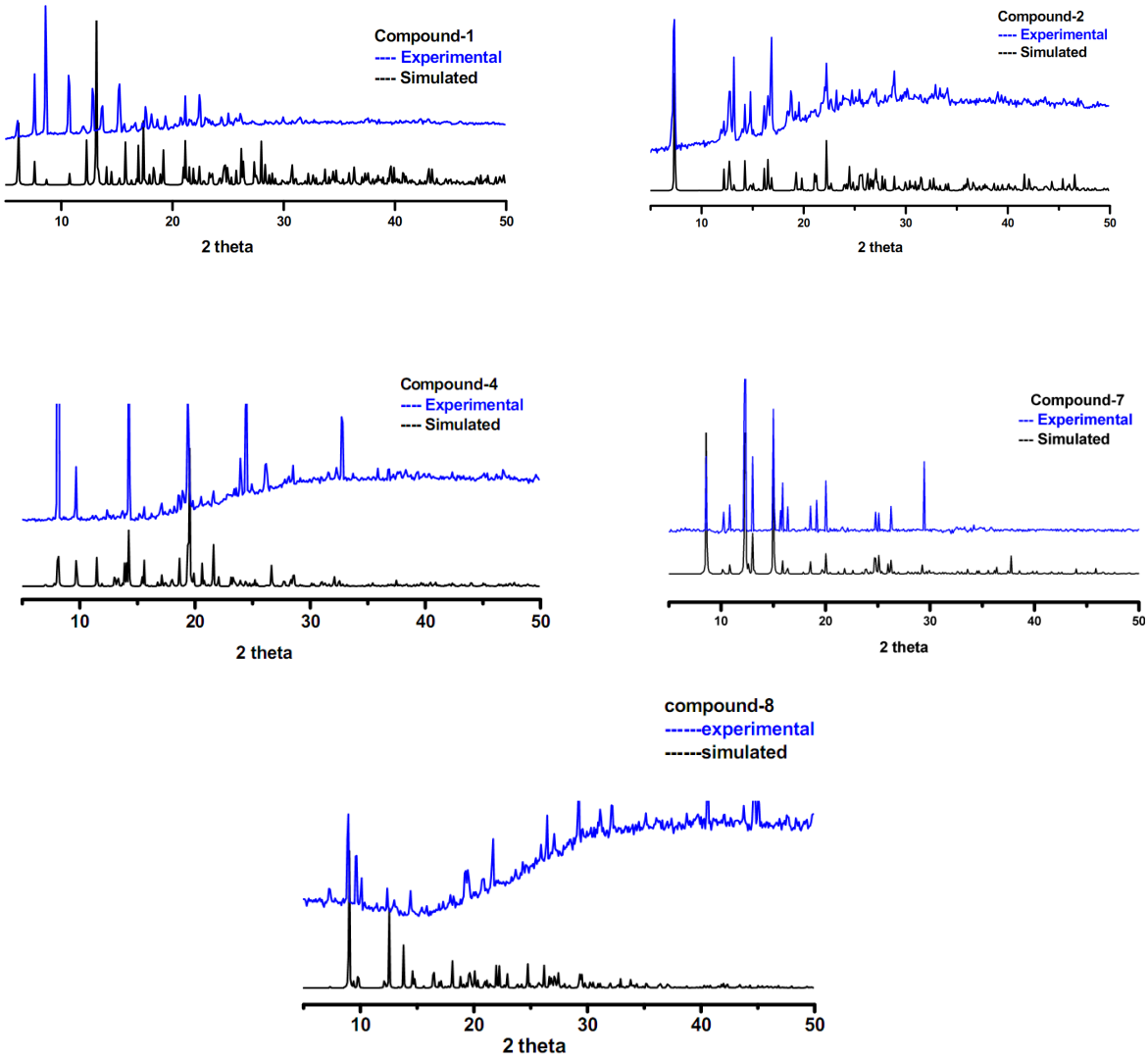

Figure 6.5. Powder X-ray patterns of the compounds **1**, **2**, **4**, **7** and **8.**

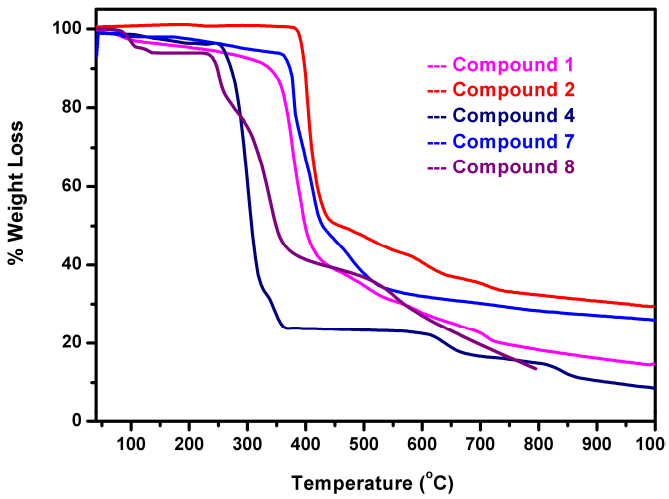

Figure 6.6. Thermogravimetric curves of the compounds **1**, **2**, **4**, **7** and **8.**

TGA curves are made under flowing N_2 for crystalline samples in the temperature range 30–1000 °C (Figure 6.). The compounds **1**, **2**, and **7** exhibit high thermal stability up to 400 °C and undergo continued weight loss which is attributed to decomposition of organic ligands. But compound **4** shows less thermal stability up to 250 °C and undergoes continuous weight loss due to decomposition of organic ligands. Compound **8** shows initial weight loss due to coordinated water molecules in the cation $[Co(H_2O)_6]^{2+}$ and lattice water molecules with weight loss of 13.50% (Theoretical 14.44%) and under goes continuous weight losses owing to organic ligands.

6.3.6. Magnetic Properties

Compound 1

The plots of both χ_M *vs T* and $\chi_M T$ *vs T* for compound **1** are shown in Figure 6.7a. Room temperature $\chi_M T_{300}$ value of 2.40 cm^3 K mol^{-1} is much higher than the expected value for isolated Co^{II} ion ($\chi_M T$ = 1.875 cm^3 K mol^{-1} for a S=3/2 ion). As the temperature is lowered, the $\chi_M T$ decreases smoothly to 1.31 cm^3 K mol^{-1} at 2K. $1/\chi_M$ *vs T* plot follows the Curie–Weiss law at the high temperature with negative Weiss constant θ= –5.23 K.

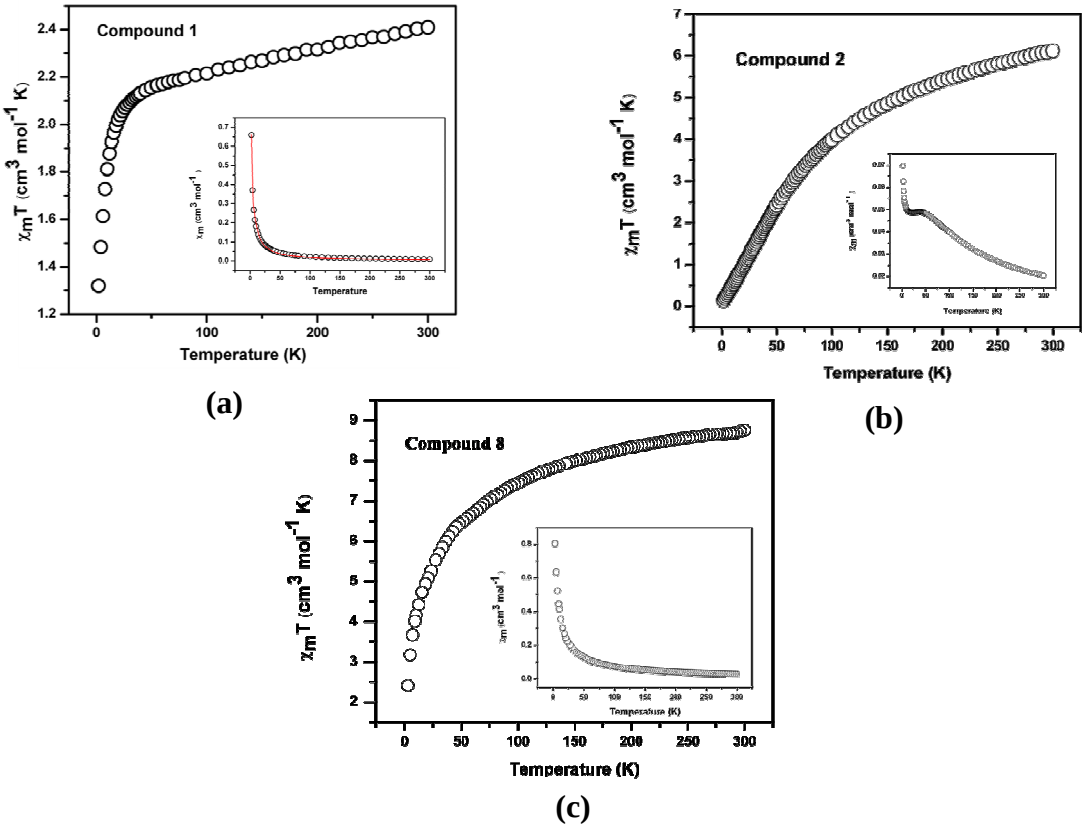

Figure 6.7. Plots of χ_M *vs T* and $\chi_M T$ *vs T* (inset) for the compounds **1**, **2**, and **8** in the temperature range of 2–300K.The red line indicates the fitting using theoretical model (see text).

In this compound, the higher value of $\chi_M T$ than the expected spin-only value indicates the orbital contribution of the octahedral Co(II) ion. The observed spin-orbit coupling in compound **1** can be calculated by the expression for S=3/2 systems with dominant zero field splitting effects, D,[18] (eqs. 1–4)

$$\chi_{\parallel} = (Ng^2\beta^2/KT)[A/B] \qquad (1)$$

$$\text{Where } A=[1+ 9\exp(-2D/KT)] \text{ and}$$

$$B=[4(1+ \exp(-2D/KT)]$$

$$\chi_{\perp} = (Ng^2\beta^2/KT)[C/D] \qquad (2)$$

$$\text{Where } C = [4 + (3KT/D) (1- \exp(-2D/KT)] \text{ and}$$

$$D=[4(1+ \exp(-2D/KT)]$$

$$\chi_M' = [(\chi_{\parallel} + \chi_{\perp})/3] \qquad (3)$$

$$\chi_M = \chi_M'/\{1- \chi_M'(2zJ'/Ng^2\beta^2)\} \qquad (4)$$

*The parameters **N**, β and K have their normal meanings. The best fit obtained from 2–300 K with g= 2.27 (2) D= –6.07 (1) cm^{-1} and zJ'= 2.49 (6) with agreement factor of 1.82 X 10^{-4}. The value of D calculated from the above expressions is in the range expected for tetrahedral metal center (i.e. D = –36 to +13 cm^{-1})[18b].*

Compound 2

The temperature dependent of magnetic susceptibility is presented as a χ_M *vs T* and $\chi_M T$ *vs T* plots in Figure 6.7b. The magnetic susceptibility (χ_M value) of compound **2** increase with decreasing temperature and a broad maximum has been observed at around 100 K and then after 16 K sharply increases up to 2K. The nature of the χ_M *vs T* curve observed for compound **2** is similar to that observed for compound Co(endi)$(N3)_2$ in the literature.[23] At room temperature (300K), $\chi_M T$ value is 6.121 cm^3 K mol^{-1} which is far higher than the spin-only value for two isolated Co(II) atoms (3.75 cm^3 K mol^{-1}, g =2.0). Upon cooling, the $\chi_M T$ value decreases continuously to 0.139 cm^3 K mol^{-1} at 2K. The nature of the $\chi_M T$ *vs T* plot suggests a dominant antiferromagnetic exchange between the two Co^{II} ions and the strong spin–orbital coupling through the ^4T_g state of the octahedral Co(II) center. The structure of the compound **1** reveals that the antiferromagnetic exchange between the two Co^{2+} ions is transmitted through the –O–C–O– bridges in the Co-paddle wheels. We tried to fit the susceptibility curve with the simple isolated dimer equation but we could not succeed due to large hump observed in the susceptibility curve.

Compound 8

Both χ_M *vs T* and $\chi_M T$ *vs T* plots of the compound **8** is presented in the Figure 6.7c. The room temperature $\chi_M T$ value of compound **8** is 8.76 cm^3 K mol^{-1} which is much higher than the spin only value of 5.625 cm^3 K mol^{-1} for three Co(II) ions indicating the unquenched orbital contribution Co(II) ion. By lowering the temperature, the $\chi_M T$ value continuously decreases up to 2.41 cm^3 K mol^{-1} at 2K. In compound 8 two Co(II) ions are bridged by the nitrogen atoms of the tetrazole ring and the remaining Co(II) atom is in lattice position in perfect octahedron. This factor make difficult in analyzing the exchange phenomenon through the bridge.

6.4. Conclusion

In designing coordination polymers, based on the flexible linkers, several factors influence the self-assembly process; among those the angle between the coordinating groups *i.e.* linker coordination angle (LCA) alters the dimensionality of the coordination networks. This concept has been discussed in this chapter with a series of compounds **1**–**9**. The self-assembly of the Co–hfipbb matrix with secondary N–donor bis (imidazole-1-ylmethyl)-benzene (bix) linkers having LCAs of 60° (for **1**), 120° (for **2**) and 180° (for **3**) reveals the amendment of dimensionality according to the intermolecular repulsions and length of the ligand. Compound **4** is 2D and **5** is 3D mixed linker coordination networks in which the LCAs of the linkers are 60°, 60° in case of **4** and 180°,180° in case of **5** demonstrate the effect of length of the ligand depending upon the LCA. Compounds **6**–**9** are coordination networks based on the {M-pda-tz} constituents, in which the flexible carboxylates 1,4–pda in **6**, **8** and **9** and 1,3–pda in **7** adopts a *cis* conformation which have same structural consequences on the dimensionality. In this situation the LCA of the tetrazole directs the dimensionality in obtaining 2D structures of **6** and **7** with tetrazole LCA of 180° and 1D structures of **8** and **9** with tetrazole LCA of 60°. All the compounds presented in the study are series of examples to enrich the structural library of the coordination networks based on flexible linkers with possible linker coordination angles. Finally the temperature dependent magnetic susceptibility measurement of the compounds **1**, **2**, **7**, **8** and **9** divulge the antiferromagnetic exchange between the metal centers.

Table 6.2 Crystal data and structural refinement parameters for compounds **1, 2, 4, 7-9**.

	1	**2**	**4**
Empirical formula	$C_{31}H_{22}N_4F_6O_5Co$	$C_{24}H_{15}F_6N_2O_4Co$	$C_{24}H_{22}CoN_4O_4$
Formula weight	703.46	568.07	489.39
T(K) / λ(Å)	298(2), 0.71073	298(2), 0.71073	298(2), 0.71073
Crystal system	Orthorhombic	monoclinic	monoclinic
Space group	*Ccca*	*C*2/*c*	$P2_1/c$
a (Å)	13.177(8)	27.073(2)	8.5118(7)
b (Å)	15.668(8)	7.5096(4)	22.703(2
c (Å)	18.950 (16)	24.255(2)	11.3906(8)
α (°)	90.00	90.00	90.00
β (°)	90.00	104.317(10)	105.401(7)
γ (°)	90.00	90.00	90.00
Volume (Å^3)	5977(5)	4778.2(7)	2122.1(3)
Z, ρ_{calcd} (g cm^{-3})	8, 1.563	8, 1.678	4, 1.532
μ (mm^{-1}), F(000)	0.660/2856	0.919/1598	0.850 /1012
goodness-of-fit on F^2	1.248	1.069	1.034
R1/ wR2 [I > 2σ (I)]	0.0687/0.1377	0.0435/0.1035	0.0535 / 0.0934
R1/ wR2 (all data)	0.0867/0.1440	0.0545/0.1435	0.0875 /0.1061
Largest diff peak/hole(e Å^{-3})	0.618/–0.307	0.679/–0.376	0.401 /–0.313
	7	**8**	**9**
Empirical formula	$C_{16}H_{12}N_5O_5Co_2$	$C_{30}H_{38}Co_3N_{12}O_{16}$	$C_{30}H_{38}Mn_3N_{12}O_{16}$
Formula weight	472.17	999.51	987.54
T(K)/ λ(Å)	298(2), 0.71073	298(2), 0.71073	298(2), 0.71073
Crystal system	monoclinic	triclinic	triclinic
Space group	$P2_1/n$	*P-1*	*P*-1
a (Å)	8.9732(4)	9.3717(8)	9.4961(6)
b (Å)	20.4712(9)	10.1843(9)	10.0739(6)
c (Å)	10.4084(5)	11.7377(11)	11.7102(8)
α (°)	90.00	112.9560(10)	112.3640(10)
β (°)	102.998(5)	106.240(2)	108.6290(10)
γ (°)	90.00	90.6960(10)	90.0830(10)
Volume (Å^3)	1862.95(15)	967.32(15)	971.98(11)
Z, ρ_{calcd} (g cm^{-3})	4, 1.683	1, 1.716	2, 1.687
μ (mm^{-1}), F(000)	1.819, 948	1.360, 511	1.048, 505
R1/ wR2 [I > 2σ (I)]	0.0517/ 0.1153	0.0322/ 0.0767	0.0463/0.1243
R1/ wR2 (all data)	0.0715/0.1254	0.0385/0.0802	0.0493/0.1266
Largest diff peak/hole (e Å^{-3})	0.840/ –0.416	0.357/ –0.229	1.280/ –0.87

6.5 References.

[1] (a) Halper, S. R.; Do, L.; Stork, J. R.; Cohen, S. M. *J. Am. Chem. Soc*. **2006**, *128*, 15255. (b) Hasegawa, S.; Horike, S.; Matsuda, R.; Furukawa, S.; Mochizuki, K.; Kinoshita, Y.; Kitagawa, S. *J. Am. Chem. Soc*. **2007**, *129*, 2607. (c) Kitagawa, S.; Matsuda, R. *Coord. Chem. Rev*. **2007**, *251*, 2490. (d) Yaghi, O. M.; O'Keeffe, M.; Ockwig, N. W.; Chae, H. K.; Eddaoudi, M.; Kim, J. *Nature* **2003**, *423*, 705. (e) Luo, F.; Zheng, J. M.; Batten, S. R. *Chem. Commun*. **2007**, 3744. (f) Moulton, B.; Zaworotko, M. J. *Chemical Reviews,* **2001**, *101*, 1629. (g) Rao, V. K.; Chakrabarti, S.; Natarajan. S. *Inorg. Chem*. **2007**, *46*, 10781.

[2] (a) Kitura, R.; Fujimoto, K; Noro, S.; Kondo, M; Kitagawo, S. *Angew. Chem. Int. Ed*. **2002**, *41*, 133. (b) Shin, D. M.; Lee, I. S.; Chung, Y. K. *Inorg. Chem*. **2003**, *42*, 8838. (c) Ayappan, P; Evans, O, R.; Cui, Y.; Wheeler, K. A.; Lin, W. B. *Inorg. Chem*. **2002**, *41*, 4978. (d) Dinca, M.; Long, J. R. *J. Am. Chem. Soc*. **2005**, *127*, 9376. (e) Yoon, J. W.; Jung, S. H; Hwang, Y. K.; Humphrey, S. M.; Wood, P.T.; Chang, J. S. *Adv. Mater*. **2007**, *19*, 1830. (f) Han, S. S.; Deng, W, Q.; Goddard, W. A. *Angew. Chem. Int. Ed*. **2007**, *46*, 6289. (g) Bar, A. K.; Chakrabarty, R.; Chi, K-W.; Batten, S. R.; Mukherjee, P. S. *Dalton Trans*., **2009**, 3222.

[3] (a) Schaate, A.; Klingelhofer, S.; Behrens, P.; Wiebcke, M. *Cryst. Growth Des*. **2008**, *8*, 3200. (b) Liu, Y.; Qi, Y.; Lv, Y. Y.; Che, Y. X.; Zheng, J. M. *Cryst. Growth Des*. **2009**, *9*, 4797. (c) Li, Z. X.; Hu, T. L.; Ma, H.; Zeng, Y. F.; Li, C. J.; Tong, M. L.; Bu, X. H. *Cryst. Growth Des*. **2010**, *10*, 1138. (d) Yang, J.; Ma, J. F.; Battern, S. R.; Su, Z. M. *Chem. Commun*. **2008**, 2223. (e) Pachfule, P.; Dey, C.; Panda, T.; Banarjee, R. *CrystEngcomm* **2010**, *12*, 1600

[4] Li, J.-R.; Zhou, H.-C. *Angew. Chem. Int. Ed.* **2009**, *48*, 8465.

[5] a) Blake, A. J.; Champness, N. R.; Chung, S. S. M.; Li, W. S.; Schro¨ der, M. *Chem. Commun.* **1997**, 1005. (b) Maekawa, M.; Konaka, H.; Suenaga, Y.; Sowa, T. K.; Munakata, M. *Dalton Trans*. **2000**, 4160. (c) Wu, H. C.; Thanasekaran, P.; Tsai, C. H.; Wu, J. Y.; Huang, S. M.; Wen, Y. S.; Lu, K. L. *Inorg. Chem*. **2006**, *45*, 295. (d) Cho, B. Y.; Min, D.; Lee, S. W. *Cryst. Growth Des*. **2006,** *6*, 342. (e) Gao, E. Q.; Cheng, A. L.; Xu, Y. X.; Yan, C. H.; He, M. Y. *Cryst. Growth Des*. **2005,** *5*, 1005. (f) Halder, G. J.; Neville, S. M.; Kepert, C. J. *CrystEngComm* **2005**, *7*, 266. (g) Dybtsev, D. N.; Chun, H.; Kim, K. *Chem. Commun*. **2004**, 1594. (h) Liu, G. F.; Zhang, W. H.; Chen, Y.; Liu, D.; Lang, J. P. *Inorg. Chem. Commun*. **2007**, *10*, 1049.

[6] Blake, A. J.; Brooks, N. R.; Champness, N. R.; Crew, M.; Deveson, A.; Fenske, D.; Gregory, D. H.; Hanton, L. R.; Hubberstey, P.; Schroder, M. *Chem. Commun*. **2001**, 1432.

[7] (a) Li, G.; Lu, J.; Li, X.; Yang, H.; Cao, R. CrystEngComm, **2010**, 12, 3780. (b) Liu, T. F.; Lu, J.; Lin, X.; Cao, R. Chem. Commun., **2010**, *46*, 8439. (c) Li, X.; Weng, X.; Tang, R.; Lin, Y.; Ke, Z.; Zhou, W.; Cao, R. *Cryst. Growth Des*. **2010**, *10*, 3228. (d) Liu, T. F.; Lu, J.; Cao, R. CrystEngComm, **2010**, *12*, 660.

[8] Yang, G. P.; Wang, Y. Y.; Zhang, W. H.; Fu, A. Y.; Liu, R. T.; Lermontava, E.; Shi, Q. Z. CrystEngComm, **2010**, *12*, 1509.

[9] (a) Pan, L.; Adams, K. M.; Hernandez, H. E.; Wang, X.; Zheng, C.; Hattori, Y.; Kaneko, K. *J. Am .Chem. Soc*., **2003**, *125*, 3062. (b) Fabelo, O.; Delgado, L. C.; Pasan, J.; Delgado, F. S.; Lloret, F.; Cano, J.; Julve, M.; Perez, C. R. Inorg. Chem., **2009**, *48*, 11342. (c) Carpanese, C.; Ferlay, S.; Kyritsakas, N.; Henry, M.; Hosseini, M. W. Chem. Commun., **2009**, 6786. (d) Su, Z.; Chen, S. S.; Fan, J.; Chen, M. S.; Zhao, Y.; Sun, W. Y. *Cryst. Growth Des*., **2010**, *10*, 3675.

[10] (a) Imaz, I. Maspoch, D.; Blanco, C. R.; Falcon, J. M. P.; Campo, J.; Molina, D. R. *Angew. Chem. Int. Ed.*, **2008**, *47*, 1857. (b) Yang, J.; Ma, J. F.; Batten, S. R.; Su, Z. M. Chem.Commun., **2008**, 2233. (c) Sathiyendiran, M.; Wu, J. Y.; Velayudham, M.; Lee, G. H.; Peng, S. M.; Lu, K. L. Chem. Commun., **2009**, 3795. (d) Su, C. Y.; Cai, Y. P.; Chen, C. L.; Smith, M. D.; Kaim, W.; ZurLoye, H. C. *J. Am. Chem. Soc*., **2003**, *125*, 8595.

[11] (a) Tripuramallu, B. K.; Kishore, R.; Das, S. K. *Inorg. Chim Acta*, **2011**, *368*, 132. (b) Lin, P.; Clegg, W.; Harrington, R. W.; Henderson, R. A. *Dalton trans.* **2005**, 2388. (c) Zhao, H.; Qu, Z. R.; Ye, H. Y.; Xiong, R. G.; *Chem. Soc. Rev.*, **2008**, *37*, 84.

[12] (a) Dhal, P. K.; Arnold, F. H. *Macromolecules*, **1992**, *25***,** 7051 (c) Ouellette, W.; Liu, H.; O'Connor, C. J.; Zubieta, J.; *Inorg. Chem.*, **2009**, *48*, 4655.

[13] (a) *SAINT: Software for the CCD Detector System*; Bruker Analytical X-ray Systems, Inc.: Madison, WI, **1998** (b) SADABS: Program for Absorption Correction; G. M. Sheldrick University of Gottingen: Gottingen, Germany, **1997**. (c) SHELXS-97: Program for Structure Solution; G. M. Sheldrick, University of Gottingen: Gottingen, Germany, **1997**. (d) SHELXL-97: Program for Crystal Structure Analysis; G. M. Sheldrick University of Gottingen: Gottingen, Germany, **1997**. (e) Blatov, V.

A.; Shevchenko, A. P.; Serezhkin, V. N. J. *Appl.Crystallogr*. **2000**, 33, 1193. TOPOS software is available for download at http://www.topos.ssu.samara.ru.

[14] (a) Han, L.; Zhao, Y.; Zhao, W. N.; Li, X.; Liang, Y. X. *Cryst. Growth Des*. **2009**, *9*, 660. (b) Pachfule, P.; Dey, C.; Panda, T.; Banarjee, R. *CrystEngComm* **2010**, *12*, 1600. (c) Ji, C. C.; Qin, L.; Li, Y. Z.; Guo, Z. J.; Zheng, H. G. *Cryst. Growth Des*. **2011**, *11*, 480.

[15] (a) Yang, J.; Ma, J.-F.; Batten, S. R.; Ng, S. W.; Liu, Y.-Y. *CrystEngComm*, **2011**, *13*, 5296. (b) Lee, H.-J.; Cheng, P.-Y.; Chen, C.-Y.; Shen, J.-S.; Nandi, D.; Lee, H. M. *CrystEngComm*, **2011**, *13*, 4814.

[16] (a) Li, B.; Yang, F.; Zhang, Y.; Li, G.; Zhou, Q.; Hua, J.; Shi, Z.; Feng, S.; *Dalton Trans.*, **2012**, *41*, 2677. (b) Zang, S.-Q.; Fan, Y.-J.; Li, J.-B.; Hou, H.-W.; Mak, T. C. W. *Cryst. Growth Des.*, **2011**, *11*, 3395.

[17] (a) Darling, K.; Ouellette, W.; Prosvirin, A.; Freund, S.; Dunbar, K. R.; Zubieta, J. *Cryst. Growth Des.*, **2012**, *12*, 2662. (b) Li, Z.; Li, M.; Zhou, X. -P.; Wu, T.; Li, D.; Ng, S. W. *Cryst. Growth Des.*, **2007**, *7*, 1992.

[18] (a) Marshall, S. R.; Rheingold, A. L.; Dawe, L. N.; Shum, W. W.; Kitamura, C.; Miller,J. S. *Inorg. Chem.*, **2002**, *41*, 3599. (b) Makinen, M. W.; Kuo, L. C.; Yim, M. B.; Wells,G. B.; Fukuyama, J. M.; Kim, J. E. *J. Am. Chem. Soc*. **1985**, *107*, 5245

Concluding Remarks and Future Scope of the Present Work

Concluding Remarks

The thesis describes the mechanistic aspects in the self-assembly of the coordination networks based on the rigidity and flexibility of the linkers.

Chapter 2 illustrates the novel class of eight membered simple building unit (SBU), Cu-dimer in terms of the formation and stability under hydrothermal conditions. The dimensionality of eight membered Cu-dimers has been extended by employing organic and inorganic linkers. The void space created in the 2D layers constructed by the Cu-dimers has a potential to exploit the host-guest phenomenon, that has been demonstrated with the aid of variable temperature PXRD studies. Magnetic exchange between the two metal centers in the dimmers, based on the conformation, has been explained by measuring the torsion angle of the particular conformation and compared with the theoretical models.

Chapter 3 portrays the role of secondary ligand and the biphenyl spacer in obtaining the 1D coordination polymer containing compounds. By creating the crowdedness at the metal polyhedra using the secondary ligands 2, 2´-bpy, it offers us to regulate the dimensionality of the compounds in case of the flexible ligands. This route has also tendency to stabilize the different conformations of flexible ligands (viz. *cis* and *trans*) in the same crystal structure. The twisting of phenyl rings in the biphenyl spacer appended to the flexible groups alters the coordination modes of the phosphonate groups to form low dimensional structures; this has been demonstrated in comparison with the mono-phenyl spacer.

Self-assembly of the metal oxide materials based on structure directing agents have been illustrated in the chapter 4. In the first section of the chapter 4, the self-assembly of Cu/*p*-xylylenediphosphonic acid/2,2´-bpy in the presence of metal oxides sources Na_2MoO_4, Na_2WO_4, Na_3VO_4 has been studied. In the resulting compounds, metal phosphonate phases are extended by the metal oxides (tetramolybdate in case of Na_2MoO_4, Keggin cluster in case of Na_2WO_4 and VO_2OH in case of Na_3VO_4). In the second part, the assessment of the tetrazole molecule in the self-assembly of the metal oxide materials has been discussed. By tuning the synthetic conditions, tetrazole has a tendency to exhibit different coordination modes which can alter the formation of oxide phase. This system

not only proves to be a good example to investigate self assembly process and provides more information of the directional syntheses of the inorganic oxide phases, but also offers a fundamental approach of how a nitrogen donor containing organic molecule (tetrazole) influences the self assembly process of the inorganic oxides. Introducing the tetrazole derivatives into the poloxomolybdate (POM) matrix adds a new dimension to the POM based materials in terms of designing solids with specific properties.

Factors affecting the conformational modulation of the flexible ligands in the self-assembly of the coordination polymers have been discussed in the chapter 6. The major outcomes of this work are:

(i) The availability of the coordination sites around the metal polyhedra is responsible to regulate the degree of flexibility to adopt various conformations to maximize the intra- and intermolecular forces in the crystal structure.

(ii) Conformational modulation of the flexible acid ligand under the influence of the rigid and flexible co-ligands has been studied and the rigid co-ligand is preferred as best selection in achieving the modulation and

(iii) The effect of the di-carboxylate ligands with different geometrical dispositions of carboxylate groups on the conformations of the neutral flexible co-ligand.

Chapter 6 mainly describes the role of the linker coordination angle in tuning the dimensionality of the coordination networks. A series of flexible ligands with various linker coordination angles reveals the amendment of dimensionality according to the intermolecular repulsions and length of the ligand. All the compounds presented in this study are series of examples to enrich the structural library of the coordination networks based on flexible linkers with possible linker coordination angles.

Future Scope

Higher ordered flexible ligands

Metal-organic frameworks or coordination polymers are of particular interest in the materials chemistry mainly due to their potential in meeting the requirements at the industrial level in the fields of adsorption, catalysis, sensing, and separation principles. To accomplish these materials, the use of crystal engineering tools becomes crucial to achieve the adequate packing of the molecules that may lead to the desired properties.

The overall thesis describes the mechanistic aspects in the self-assembly of the coordination networks based on the flexible ligands. As shown in the Scheme 1, we have used the ligands in which the coordinating groups are separated by the phenyl or biphenyl spacer by flexible (–CH_2–) spacer. We intend to increase the order of flexibility in the ligands by increasing the number of flexible groups in the organic ligands as shown in the following Scheme 1.

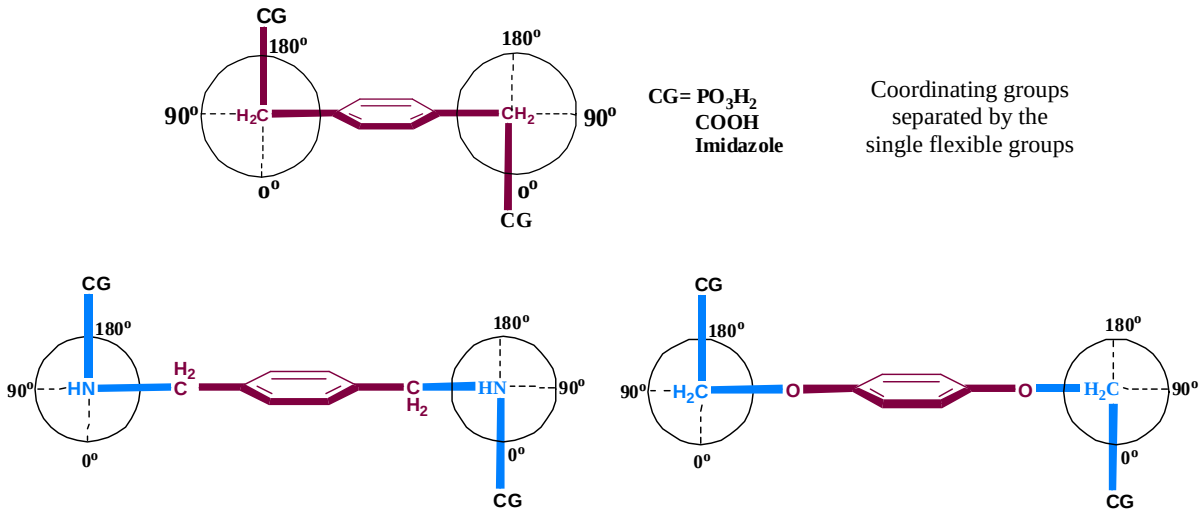

Scheme 1. Schematic representation of the order of flexibilities

In this context, in future, we plan to synthesize the ligands in which the coordinating groups are separated by the phenyl or biphenyl spacer by the (–CH_2–O–) or (–CH_2–NH–) groups. This approach would allow us to construct the coordination networks which have tendency to increase or decrease the potential void space in the frameworks by removing the guest molecules.

Tetrazoles: a new class of multidentate ligands

We have used rigid multidentate tetrazole ligands as a secondary ligands in chapter 5 and 6 to the study their affect in the conformational changes of the flexible carboxylate ligands. Also we have assessed the enhanced coordinating tendency of the nitrogen atoms in the tetrazole molecule in the self-assembly of the metal oxide based solids as described in chapter 4.

Based on these observations we are now planning to design a coordination solids based on the different tetrazole skeletons. Due to the presence of four nitrogen atoms in the tetrazole, it has tendency to connect the metal centers at shortest distances; as a result a prominent magnetic exchange phenomenon should be observed through the nitrogen bridges. Compound **3** in the 4th chapter, compound **4** in the 5th chapter and compounds **7**–**9** in the 6th chapter are the examples of such observation.

Tuning the dimensionality of the polyoxometal-organic frameworks (PMOFs) by the changing the polyanions

Polyoxometal-organic frameworks are class of compounds that are constituted by metal oxides as nodes or linkers. The past era witnessed the different coordination networks based on the polyanions such as Anderson, Keggin, octamolybdate and Dawson.

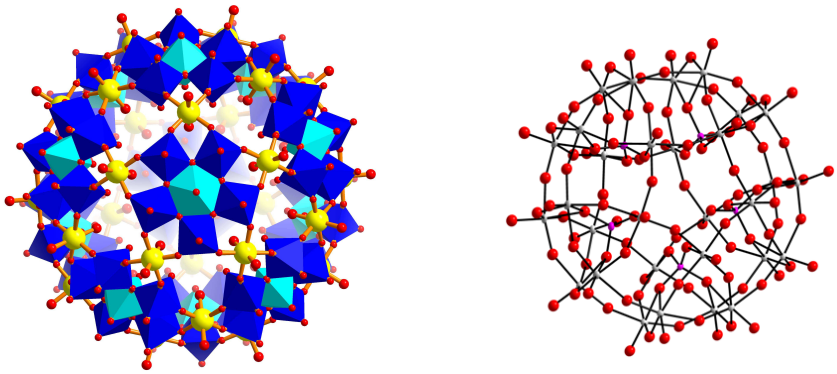

Figure 1. Polyhedral representation of Mo_{132} (Left), ball and stick representation of Pressyler anion (Right).

We wish to synthesize to coordination networks based on the large polyanions such as Mo_{132} and Presslyer anion (Figure 1) with the flexible nitrogen ligands and rigid tetrazole ligands along with the secondary metal atoms. This approach allows us to design the materials with greater pore volumes and high adsorption capacities.

List of Publications

1) Synthesis, structural characterization and properties of one-dimensional coordination polymers of cobalt (II)- and nickel(II)-phosphonate complexes with 2,2´-bipyridine as a secondary ligand component: observation of both cis- and trans- conformations of a diphosphonic acid

Bharat Kumar Tripuramallu, Kishore Ravada, Samar K. Das, ***Polyhedron*** 2010, 29 2985.

2) 2-Aminoanilinium2-chloroacetate

A. Srinivasa Rao, **Bharat Kumar Tripuramallu**, Kishore Ravada, Samar K. Das, ***Acta cryst. Sec. E***, 2010, E-66, o1945.

3) Understanding the formation of metal-oxide based inorganic solids, assessing the influence of tetrazole molecule

Bharat Kumar Tripuramallu, Kishore Ravada and Samar K. Das, ***Inorg. Chim. Acta***. 2011, 368, 132.

4) Ion-pair charge transfer complex with near-ir absorption: synthesis, crystal structure and properties of $[Hb]_2[Cu(mnt)_2]$(Hb=1-(4-((1h-imidazol-1-yl) methyl)benzyl)-1h-imidazol-3-ium)

Kishore Ravada, **Bharat Kumar Tripuramallu**, Gummadi Durgaprasad, Samar K. Das, ***J. Mol. Struct***. 2011**,** 37, 990.

5) Synthesis and structural characterization of potassium coordination polymers based on a copper-bis(dithiolato) complex $[Cu(btdt)_2]^1$ ({btdt}^{2} = 2,1,3-benzenethiadiazole-5,6-dithiolate): role of coordinating solvents and counter cation

Ramababu Bolligarla, **Bharat Kumar Tripuramallu**, Vudagandla Sreenivasulu, Samar K. Das, ***Indian Journal of Chemistry Sec*. A** 2011, 50A, 1410.

6) A manganese(II) sandwich-type phosphotungstate complex – synthesis, structural characterization and catalytic activity towards liquid-phase aerobic epoxidation of alkenes

Ketan Patel, **Bharat Kumar Tripuramallu** and Anjali Patel, ***Eur. J. Inorg. Chem***. 2011, 12, 1871.

7) Factors affecting the conformational modulation of flexible ligands in the self assembly process of coordination polymers: synthesis, structural characterization, magnetic properties and theoretical studies of $[Co(pda)(bix)]_n$, $[Ni(pda)(bix)(H_2O)]_n$, $[Cu(pda)(bix)_2(H_2O)_2]_n \cdot 8nH_2O$, $[Co_2(\mu\text{-}OH)(pda)(ptz)]_n \cdot nH_2O$, $[Co(hfipbb)(bix)_{0.5}]_n$, and $[Co(2,6\text{-}pydc)(bix)_{1.5}]_n\ 4nH_2O$

Bharat Kumar Tripuramallu, Paulami Manna**,** Samala Nagaprasad Reddy Samar K. Das, ***Cryst.Growth Des***. 2012, 12, 777.

8) Synthesis, structural, and spectral characterization of keggin-type mono cobalt(ii)-substituted phosphotungstate

Pragati Shringarpure, **Bharat Kumar Tripuramallu**, Ketan Patel and Anjali Patel ***J. Coord. Chem***. 2011, 64, 4016.

9) Synthesis, structural characterization and magnetic properties of a new series of coordination polymers: importance of steric hindrance at the coordination sphere

Paulami Manna, **Bharat Kumar Tripuramallu** and Samar K. Das ***Cryst.Growth Des***. 2012, (In Press)

10) Mechanistic aspects in the formation of copper dimer bridged by phosphonic acid and extending its dimensionality by organic and inorganic linkers: synthesis, structural characterization, magnetic properties and theoretical studies

Bharat Kumar Tripuramallu, Sandip Mukherjee and Samar K. Das (Under Revision).

Posters and Presentations

1) **Bharat Kumar Tripuramallu** and Samar K Das, Hydrothermal synthesis and characterization of multidimensional metal phosphonates Poster presentation at "**Chemfest-2009**" which was held in *University of Hyderabad*, Hyderabad, India on March, 2009

2) **Bharat Kumar Tripuramallu** and Samar K Das, Understanding the Formation of Cu Dimer and Extending its Dimensionality via Organic and Inorganic Linkers: Synthesis, Characterization and Properties Poster presentation at "**MTIC-XIII**" which was held in *IISC Bangalore*, India on December, 2010**.**

3) **Bharat Kumar Tripuramallu and** Samar K Das, Flexibility of a ligand a key factor in the assessment of topology of the structures; Synthesis characterization and properties of coordination polymers. Poster presentation at "**Second International Conference on Multifunctional, Hybrid and Nano-materials"** which was held in Strasbourg, *France* on March 2011.

4) **Bharat Kumar Tripuramallu** and Samar K Das, Study of Mechanistic Aspects in the Self-Assembly of Coordination Polymers in Duel ligand Systems Involving Flexible Ligands Poster presentation at "**MTIC-XIV**" which was held in *University of Hyderbad*, India on December, 2011.

5) **Bharat Kumar Tripuramallu** and Samar K Das, Understanding the Formation of Cu Dimer Bridged by Phosphonic Acid and Extending its Dimensionality By Organic and Inorganic Linkers: Synthesis, Structural Characterization Magnetic Properties and Theoretical Studies

   (i) Poster and Oral presentation at "**Chemfest-2012**" which was held in *University of Hyderabad*, Hyderabad, India on March, 2012.

   (ii) Oral presentation at "**Oxford Diffraction Users Meet**" which was held in *Indore*, India on April, 2012.

सत्यमेव जयते